

**TOWARDS GAS-PHASE ENZYMES: ION CHEMISTRY FOR
INTRODUCING SELECTIVE DISSOCIATION PATHWAYS INTO
BIO-IONS**

by

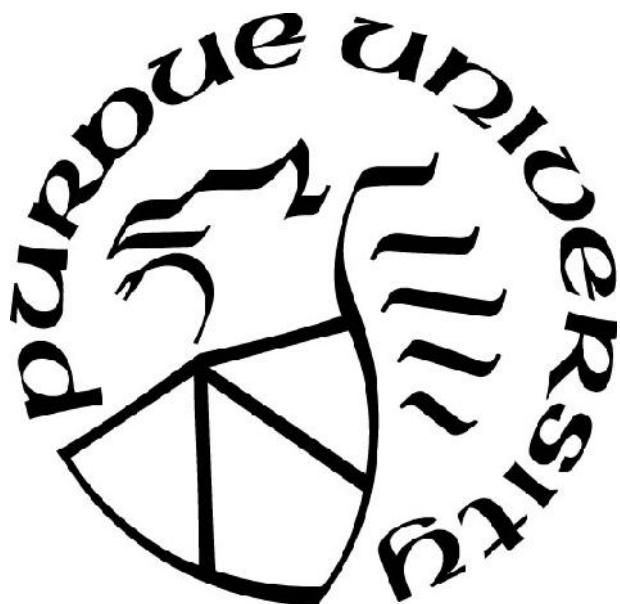
David J. Foreman

A Dissertation

Submitted to the Faculty of Purdue University

In Partial Fulfillment of the Requirements for the degree of

Doctor of Philosophy



Department of Chemistry

West Lafayette, Indiana

May 2020

**THE PURDUE UNIVERSITY GRADUATE SCHOOL
STATEMENT OF COMMITTEE APPROVAL**

Dr. Scott A. McLuckey, Chair

Department of Chemistry

Dr. Mary J. Wirth

Department of Chemistry

Dr. Christopher Uyeda

Department of Chemistry

Dr. Julia Laskin

Department of Chemistry

Approved by:

Dr. Christine Hrycyna

*To my wife, my family, my friends, and my mentors,
with all my love, appreciation, and thanks.*

ACKNOWLEDGMENTS

Since my initial interest in chemistry in high school, I have always viewed my role as a scientist as a lifelong vocation. In that sense, there are many individuals who have contributed to my development into an independent researcher. First, I would like to thank Mr. Knittel, my high school chemistry teacher, for initially sparking my interest in chemistry and I would like to thank my college professors, Dr. Anthony Fernandez and Dr. Cynthia McGowan, for continuing to foster my scientific curiosity. After graduation from Merrimack College, I spent four years in industry and was fortunate to have had so many great colleagues. It would be remiss of me not to mention Rod Cole, a colleague and friend who encouraged me to pursue a doctoral degree.

A special thanks goes out to my mom, my dad, and my sister for their love and support throughout my life, but especially when I moved 1300 miles from home to continue my education. Although my visits back to Massachusetts became less frequent, their support and encouragement never wavered. My friends from home have also been a tremendous support system for me throughout my tenure at Purdue. Several of them made multiple trips to the Midwest to visit and each time I went home I could always count on seeing them over dinner or drinks and it was as if I had not moved away at all. To my wife, Avery, thank you for the love and support throughout this process – I know it has been difficult sometimes with me often setting work as my first priority. Thank you for encouraging me to take time for us. Our weekend trips, small weekday dates, and even just sitting at home by the fire has made my graduate experience and life in Indiana much more enjoyable. You have contributed immensely to my success in graduate school.

It has been a privilege working in Professor Scott McLuckey's group. Scott aspired to knowledge and provided an environment where his philosophy on, and approach to education was evident. I am grateful for his mentorship and for sharing his passion in science with me. Throughout my time in the group, I have had the pleasure of working with extraordinary people. First, to the older students, who paved the way before me, thank you for exemplifying the hard work necessary to excel in Scott's lab. To Josh, Chris, and Elissia, it has been a remarkable journey throughout graduate school together – you were all fantastic classmates. To the younger students, Caitlin, Anthony, John, Kenny, Hsi-Chun, Jay, Abdirahman, Ian, De'Shovan, Nicole, Kim, Alex, and Sarah, I hope that you enjoy the rest of your time in lab and continue to strive for excellence. Thanks must also be given to Jim Hager and Larry Campbell of Sciex. Their patience with my

incessant questions has contributed significantly to my understanding of mass spectrometry instrumentation.

During my time at Purdue, I have forged several amazing friendships, many of which I feel will last a lifetime, namely, Eric and Amy, Ben, and Josh. Eric, Amy, it was an honor being able to stand beside the two of you at your wedding. I often think back to all of the Tuesdays at trivia and Friday and Saturday nights spent playing games – they are some of my fondest memories and I am lucky to have them. Ben, I am elated that you asked me to be the Godfather of Brer. I am looking forward to many more trips to the ballpark with you and your family. Josh, the weekly libations where we talked science, sports, and major life decisions were one of the great perks to our friendship and a healthy distraction from spending time in lab. I also had the distinct pleasure of being involved with many intramural and recreational sports teams. To Space Group, Team Chemistry, and We Like Turtles, there are too many individuals to mention by name, but I truly enjoyed our times together.

Last, but certainly not least, I would like to thank Dr. Mary Wirth, Dr. Chris Uyeda, and Dr. Julia Laskin for serving as my committee members.

TABLE OF CONTENTS

LIST OF TABLES	10
LIST OF SCHEMES.....	11
LIST OF FIGURES	12
LIST OF ABBREVIATIONS.....	19
ABSTRACT.....	22
CHAPTER 1. RECENT DEVELOPMENTS IN GAS-PHASE ION/ION REACTIONS FOR ANALYTICAL MASS SPECTROMETRY	23
1.1 Introduction to Gas-Phase Ion/Ion Reactions	23
1.2 Developments in Ion/Ion Reaction Instrumentation	24
1.2.1 Front-End Ion/Ion Reaction Instrumentation.....	25
1.2.2 <i>In Vacuo</i> Ion/Ion Reaction Instrumentation	26
1.2.3 Analysis of High <i>m/z</i> Product Ions from Ion/Ion Reactions.....	29
1.3 Proton Transfer Ion/Ion Reactions.....	31
1.3.1 Product Ion Analysis.....	31
1.3.2 Precursor Charge State Manipulation	33
1.3.3 Structural Proteomic Studies	37
1.4 Electron Transfer Ion/Ion Reactions.....	37
1.4.1 Electron Transfer Charge Reduction	38
1.4.2 Charge Transfer Dissociation	39
1.5 Reactions That Proceed Through Complex Formation	40
1.5.1 Metal Ion Transfer	40
1.5.2 Charge Inversion.....	41
1.5.3 Oxidation Reactions.....	44
1.5.4 Covalent Chemistry: Bond Formation in the Gas-Phase.....	46
1.6 Reagent Ion Selection	47
1.7 Future Outlook	50
1.8 References.....	51
CHAPTER 2. NOVEL PEPTIDE ION CHEMISTRY ASSOCIATED WITH GOLD (I) CATIONIZATION: PREFERENTIAL CLEAVAGE AT LYSINE RESIDUES.....	67

2.1	Introduction.....	67
2.2	Experimental.....	69
2.2.1	Materials	69
2.2.2	Mass Spectrometry	70
2.3	Results and Discussion	70
2.3.1	Formation of $[M - H - NH_3]^+$: Loss of $H AuNH_3$	70
2.3.2	Reactivity of Basic Residues	73
2.3.3	Influence of Lysine Position on $H AuNH_3$ Loss	75
2.3.4	Proposed Mechanisms for the Formation of $[M - H - NH_3]^+$ Ions	77
2.3.5	MS ³ Fragmentation: Preferential Cleavage N-terminal to Oxidized Lysine Residues..	
	82
2.3.6	Oxidation of Melittin	86
2.4	Conclusions.....	86
2.5	References.....	87
CHAPTER 3. GOLD (I) CATIONIZATION PROMOTES RING OPENING IN LYSINE		
CONTAINING CYCLIC PEPTIDES.....		
		92
3.1	Introduction.....	92
3.2	Experimental.....	94
3.2.1	Materials and Reagents.....	94
3.2.2	Sample Preparation	94
3.2.3	Mass Spectrometry	94
3.3	Results and Discussion	96
3.3.1	Sunflower Trypsin Inhibitor	97
3.3.2	-Loop.....	105
3.4	Conclusions.....	108
3.5	References.....	109
CHAPTER 4. GAS-PHASE SEQUENCING OF CYCLOTIDES: INTRODUCTION OF		
SELECTIVE RING OPENING AT DEHYDROALANINE VIA ION/ION REACTION.....		
		115
4.1	Introduction.....	115
4.2	Experimental.....	118
4.2.1	Materials	118

4.2.2	Sample Preparation	119
4.2.3	Reduction and Alkylation	119
4.2.4	Ion/Ion Mass Spectrometry.....	119
4.2.5	LC-MS/MS Analysis	120
4.3	Results and Discussion	121
4.3.1	Generation of Dehydroalanine via Ion/Ion Reaction.....	121
4.3.2	Opening CyI4 at Dehydroalanine	122
4.3.3	Sequencing Known Cyclotides in a Complex Fraction.....	130
4.3.4	Partial de Novo Sequencing of an Unknown Cyclotide	135
4.4	Conclusions.....	143
4.5	References.....	144
CHAPTER 5. MAXIMIZING SELECTIVE CLEAVAGES AT ASPARTIC ACID AND PROLINE RESIDUES FOR THE IDENTIFICATION OF INTACT PROTEINS		150
5.1	Introduction.....	150
5.2	Experimental	152
5.2.1	Sample Preparation	152
5.2.2	Reduction and Alkylation of Trypsinogen	153
5.2.3	Mass Spectrometry	153
5.2.4	Database Search.....	154
5.3	Results and Discussion	155
5.3.1	Experimental Design and Rationale	155
5.3.2	Protocol Demonstration Using Reduced and Alkylated Trypsinogen.....	159
5.3.3	Identification of Model Proteins	163
5.4	Conclusions.....	171
5.5	References.....	172
CHAPTER 6. VALET PARKING FOR PROTEIN ION CHARGE STATE CONCENTRATION: ION/MOLECULE REACTIONS IN LINEAR ION TRAPS.....		177
6.1	Introduction.....	177
6.2	Experimental	178
6.2.1	Materials and Sample Preparation	178
6.2.2	Mass Spectrometry	179

6.3	Results and Discussion	181
6.3.1	Valet Parking Premise and Theory	181
6.3.2	Demonstration of Valet Parking	182
6.3.3	Valet Parking of a Simple Mixture	188
6.3.4	Potential Improvements	189
6.4	Conclusions.....	191
6.5	References.....	191
VITA.....		195
PUBLICATIONS.....		196

LIST OF TABLES

Table 4.1. List of assignments, measured isotopic masses, theoretical isotopic masses, and mass differences for the cyI4 data of Figure 4.4.....	124
Table 5.1. Summary of Database Search Results.	161
Table 5.2. Summary of the Top Five Proteins Ranked According to P-Score for Ubiquitin MS/MS Data.	165
Table 5.3. Summary of the top five ranked proteins of the ubiquitin MS/MS database search.	166
Table 5.4. Summary of the top five ranked proteins of the apomyoglobin MS/MS database search.	166
Table 5.5. Summary of the top five ranked proteins of the trypsinogen MS/MS database search.	168
Table 5.6. Summary of the top five ranked proteins for carbonic anhydrase without N-terminal acetylation.	168
Table 5.7. Summary of the top five ranked proteins for carbonic anhydrase with N-terminal acetylation.	170

LIST OF SCHEMES

Scheme 2.1. Proposed mechanism for the formation $[M - H - NH_3]^+$ from an N-terminal lysine residue: loss of AuH via hydride abstraction followed by loss of ammonia.	81
Scheme 2.2. Proposed mechanism for the formation $[M - H - NH_3]^+$ from an internal lysine residue: loss of AuH via hydride abstraction followed by loss of ammonia.	81
Scheme 2.3. Fragmentation mechanism for a) $[M + H]^+$ and b) $[M - H - NH_3]^+$	82
Scheme 3.1. General strategy for cyclic peptide analysis via gold (I) cationization utilizing gas-phase ion/ion chemistry.	97
Scheme 3.2. Generation of the dehydroalanine analog of SFTI via the consecutive losses of 91 Da.	103

LIST OF FIGURES

- Figure 1.1. Dual source reactor used to perform ion/ion reactions (a) mounted to the front end of a mass spectrometer and (b) free-standing to be adapted to any mass spectrometer platform. Reprinted from the Supporting Information of Cotham, V. C.; Shaw, J. B.; Brodbelt, J. S. *Anal. Chem.* **2015**, 87, 9396–9402 (ref 16). Copyright 2015 American Chemical Society. 26
- Figure 1.2. a) Schematic of the SLIM boards used for dual polarity ion confinement looking at the x–y plane (left) and z–y plane (right). b) 3-D view of the SLIM device showing the ion conduits. The green line represents the equidistant line between the SLIM surfaces. Reprinted by permission from Springer Nature: Journal of the American Society for Mass Spectrometry, Garimella, S. V. B.; Webb, I. K.; Prabhakaran, A.; Attah, I. K.; Ibrahim, Y. M.; Smith, R. D. *J. Am. Soc. Mass Spectrom.* **2017**, 28, 1442–1449 (ref 32). Copyright 2017..... 29
- Figure 1.3. Schematic of the instrumental setup for the waveform switching experiments. The sine wave is applied to the ring electrode and the square wave is applied to the end-cap electrodes. Reprinted by permission from Springer Nature: Journal of the American Society for Mass Spectrometry, Lee, K. W.; Eakins, G. S.; McLuckey, S. A. *J. Am. Soc. Mass Spectrom.* **2019**, 30, 1126–1132 (ref 33). Copyright 2019..... 30
- Figure 1.4. ETD product ion spectrum of the $[M + 26H]^{26+}$ charge state of apomyoglobin followed by sequential ion/ion proton transfer (IIPT) reaction for a) 0 ms, b) 20 ms, c) 40 ms, d) 80 ms, and e) 160 ms. Reprinted from *Int. J. Mass Spectrom.*, Vol. 377, Anderson, L. C.; English, A. M.; Wang, W.; Bai, D. L.; Shabanowitz, J.; Hunt, D. F. Protein derivatization and sequential ion/ion reactions to enhance sequence coverage produced by electron transfer dissociation mass spectrometry, pp. 617–624 (ref 49). Copyright 2015, with permission from Elsevier..... 33
- Figure 1.5. Mass spectra of SOD/CuZn complexes a) as observed under native MS conditions (top), isolation and 25 ms proton transfer reaction of the 12+/6+ species (middle), and isolation and 25 ms proton transfer reaction of the 11+ species (bottom) with b) a 60 m/z wide zoomed view of the 10+/5+ region. Adapted from Holden, D. D.; Brodbelt, J. S. *Anal. Chem.* **2016**, 88, 12354–12362 (ref 62). Copyright 2016 American Chemical Society. 35
- Figure 1.6. MS/MS analysis scheme of 50S L22 E. coli ribosomal protein. a) Positive electrospray mass spectrum, b) 100 ms proton transfer and parallel ion parking of the 600–1000 m/z isolation window, and c) HCD product ion spectrum of the data-dependently selected 10+ precursor. Reproduced from Ugrin, S. A.; English, A. M.; Syka, J. E. P.; Bai, D. L.; Anderson, L. C.; Shabanowitz, J.; Hunt, D. F. *J. Am. Soc. Mass Spectrom.* **2019**, 30, 2163–2173 (ref 71). Copyright 2019..... 36
- Figure 1.7. Electrospray mass spectrum of a AT/heparin complex is shown in gray. Ion charge state assignment is facilitated by limited electron transfer charge reduction using wide (pink) and narrow (cyan) precursor ion selection windows. The species labeled A, B, and C represent resolved charge-reduced species present in the precursor isolation windows. Reproduced from Zhao, Y.; Abzalimov, R. R.; Kaltashov, I. A. *Anal. Chem.* **2016**, 88, 1711–1718 (ref 91). Copyright 2016 American Chemical Society. 38

Figure 1.8. Product ion spectra of $[18:1 - H + MgPhen]^+$ for the isomeric mixture of 18:1 n-9/n-7 at the molar ratios of a) 5/95 and b) 95/5. Product ions used in the multiple linear regression for relative quantitation are shown in red. Calculated molar ratios (mean \pm standard deviation, n = 3) are shown in green. The lightning bolt corresponds to the species subjected to CID. Adapted from Randolph, C. E.; Foreman D. J.; Blanksby, S. J.; McLuckey, S. A. *Anal. Chem.* **2019**, 91, 9032–9040 (ref 137). Copyright 2019 American Chemical Society. 43

Figure 1.9. Collisional activation of the ion/ion reaction complex formed between the reaction of the periodate anion with a) doubly protonated doubly GYSLGNWVCAAK/CK, b) triply protonated CELAAAMK/GCR, and c) triply protonated WWCNDGR/NLCNIPCSALLSSDITASVNCAK. The degree signs correspond to water losses, and the lightning bolts correspond to the species subjected to CID. Reproduced from Pilo, A. L.; McLuckey, S. A. *Anal. Chem.* **2016**, 88, 8972–8979 (ref 140). Copyright 2016 American Chemical Society..... 45

Figure 1.10. Product ion spectrum from CID of the complex formed between doubly protonated KGAGGKGAGGKL and a) HOAt, b) HOBt, and c) NHS. The m/z region corresponding to proton transfer is shaded in red, the m/z region corresponding to covalent modification is shaded in yellow, and the m/z region corresponding to the complex ion is shaded in green. Reprinted by permission from Springer Nature: Journal of the American Society for Mass Spectrometry, Bu, J.; Peng, Z.; Zhao, F.; McLuckey, S.A. *J. Am. Soc. Mass Spectrom.* **2017**, 28, 1254–1261 (ref 150). Copyright 2017..... 50

Figure 2.1. a) Post-ion/ion reaction spectrum from the reaction between doubly protonated M = KGAILAGAILR and $[AuCl_2]^-$. b) Beam-type CID of the ion/ion reaction product ions. c) Ion trap CID spectrum of the $[M + Au]^+$ ion generated from the process of b). Open circles indicate water loss and the lightning bolt indicates the species subjected to CID. Aurated fragment ions are represented with green diamond superscripts. 72

Figure 2.2. Activation of $[KGAILAGAILR - H - NH_3]^+$ derived from collisional activation of $[M + Au]^+$. Open circles indicate water loss, and the lightning bolt indicates the species subjected to CID. Modified fragment ions are represented with red square superscripts..... 73

Figure 2.3. Activation of a) $[KAKAKAA + Au]^+$, b) $[RARARAA + Au]^+$, and c) $[HAHAHAA + Au]^+$ ions produced via beam-type CID of the ion/ion reaction products formed between the doubly protonated peptide and the gold dichloride reagent anion. Shaded circles indicate ammonia loss, open circles indicate water loss, and the lightning bolts indicate the species subjected to CID. Aurated fragment ions are represented with green diamond superscripts. Modified fragment ions, $[b/y - H - NH_3]^+$, are represented with red square superscripts. 74

Figure 2.4. Activation of $[KAKAKAA - H - NH_3]^+$ derived from collisional activation of $[M + Au]^+$. Shaded circles indicate ammonia loss, open circles indicate water losses, and the lightning bolt indicates the species subjected to CID. Modified fragment ions are represented with red square superscripts. 75

Figure 2.5. Activation of $[K(^{13}C_6, ^{15}N_2)\text{-AFK} + Au]^+$ ion formed via ion/ion reaction. Shaded circles indicate ammonia loss, open circles indicate water loss, and the lightning bolt indicates the species subjected to CID. Aurated fragment ions are represented with green diamond superscripts. 76

Figure 2.6. Activation of a) aurated KGAGGHGAGGHL and b) aurated HAGGGHGAGGKL formed in the gas-phase. Shaded circles indicate ammonia loss, open circles indicate water losses, and the lightning bolt indicates the species subjected to CID. Aurated fragment ions are represented with green diamond superscripts. 77

Figure 2.7. Activation of a) $[KAYK + Au]^+$, b) $[KAYK + Au - NH_3]^+$, c) $[KAYK - H - NH_3]^+$ produced from sequential NH_3 and HAu loss, and d) $[KAYK - H - NH_3]^+$ produced directly from CID of the post ion/ion product $[M + Au]^+$. Shaded circles indicate ammonia loss, open circles indicate water losses, and the lightning bolt indicates the species subjected to CID. Aurated fragment ions are represented with green diamond superscripts. Modified fragment ions are represented with red square superscripts. 78

Figure 2.8. a) Activation of doubly aurated melittin, $[M + 2Au]^{2+}$ derived from the ion/ion reaction between quadruply protonated melittin and two gold dichloride reagent anions. b) Activation of oxidized melittin $[M - H - NH_3 + Au]^{2+}$ after the loss of NH_4Au from $[M + 2Au]^{2+}$. Shaded circles indicate ammonia loss and the lightning bolt indicates the species subjected to CID. Aurated fragment ions are represented with green diamond superscripts. Modified fragment ions are represented with red triangle superscripts. Fragment ions corresponding to cleavages N-terminal to oxidized lysine residues are indicated with blue text. 79

Figure 2.9. a) Q1 isolation of $[melittin - H + Au]^{2+}$. b) q2 CID of $[melittin - H + Au]^{2+}$. The lightning bolt indicates the species subjected to CID. 80

Figure 2.10. Ion trap CID of $[KGAILAGAILR + ^{107}Ag]^+$ (Compare to Figure 2.1c – CID of $[KGAILAGAILR + Au]^+$). Open circles indicate water losses and the lightning bolt indicates the species subjected to CID. Argentinated fragment ions are represented with open diamond superscripts. 82

Figure 2.11. Activation of a) $[YGGKFL - H - NH_3]^+$, b) $[GAILKGAILR - H - NH_3]^+$, and c) $[ARAMAWAKA - H - NH_3]^+$ derived from collisional activation of $[M + Au]^+$. Shaded circles indicate ammonia losses, open circles indicate water losses, and the lightning bolt indicates the species subjected to CID. Modified fragment ions, $[b/y - H - NH_3]^+$, are represented with red square superscripts. Fragment ions corresponding to cleavages N-terminal to oxidized lysine residues are indicated with blue text. 84

Figure 2.12. Activation of $[YGGKFL + H]^+$. Shaded circles indicate ammonia losses, open circles indicate water losses, and the lightning bolt indicates the species subjected to CID. Fragment ions corresponding to cleavages N-terminal to oxidized lysine residues are indicated with blue text. 85

Figure 2.13. Activation of $[GAILKGAILR + H]^+$. Shaded circles indicate ammonia losses, open circles indicate water losses, and the lightning bolt indicates the species subjected to CID. Fragment ions corresponding to cleavages N-terminal to oxidized lysine residues are indicated with blue text. 85

Figure 2.14. Activation of $[ARAMAWAKA + H]^+$. Shaded circles indicate ammonia losses, open circles indicate water losses, and the lightning bolt indicates the species subjected to CID. Fragment ions corresponding to cleavages N-terminal to oxidized lysine residues are indicated with blue text. 86

Figure 3.1. Structures of (a) sunflower trypsin inhibitor and (b) β -loop. Stereochemistry not shown.	95
Figure 3.2. Activation of (a) $[M + Au]^+$ and (b) $[M - H - NH_3]^+$ where M = reduced and alkylated sunflower trypsin inhibitor. Open circles indicate water loss and shaded circles indicate ammonia loss. The lightning bolt indicates the species subjected to CID.	98
Figure 3.3. Activation of (a) $[M + H]^+$ and (b) $[M - H]^-$ where M = reduced and alkylated AACAACAA. Open circles indicate water loss and the lightning bolt indicates the species subjected to CID.	98
Figure 3.4. Activation of $[M + H]^+$ where M is reduced and alkylated KGAILCGAILR using a) iodoacetamide, b) iodoacetic acid, c) acrylamide, or d) N-ethylmaleimide as the alkylating agent. The lightning bolt indicates the species subjected to CID.	99
Figure 3.5. Activation of m/z 1081 formed via a) ion/ion reaction with IO_4^- or b) the loss of 159 from $[KGAILCN\text{-ethylmaleimide}GAILR + H]^+$. Open circles indicate water loss and shaded circles indicate ammonia loss. The lightning bolt indicates the species subjected to CID.	100
Figure 3.6. Activation of a) $[M + Au]^+$, b) $[M + Au - 91]^+$, and c) $[M + Au - 91 - 91]^+$ where M = reduced and alkylated sunflower trypsin inhibitor. Open circles indicate water loss. The lightning bolt indicates the species subjected to CID.	102
Figure 3.7. MS^4 product ion spectrum of $[M - H - NH_3 - 91 - 91]^+$ formed via collisional activation as shown in Figure 3.6c. M = reduced and alkylated sunflower trypsin inhibitor. Open circles indicate water loss and shaded circles indicate ammonia loss. The lightning bolt indicates the species subjected to CID. Product ions corresponding to opening at lysine are highlighted in red. Fragment ions corresponding to opening at dehydroalanine are highlighted in blue and green.	104
Figure 3.8. Linearized structures of SFTI corresponding to ring opening at a) the oxidized lysine residue, b) dehydroalanine at the 11 th position, and c) dehydroalanine at the 3 rd position.	104
Figure 3.9. Activation of a) singly protonated reduced and alkylated sunflower trypsin inhibitor and b) doubly protonated reduced and alkylated sunflower trypsin inhibitor. Open circles indicate water loss. The lightning bolt indicates the species subjected to CID.	105
Figure 3.10. Activation of (a) $[M + Au]^+$ and (b) $[M - H - NH_3]^+$ where M = β -loop. (c) Expanded view of (b) between m/z 500 and m/z 1500. Open circles indicate water loss and shaded circles indicate ammonia loss. The diamond superscript indicates an auroated ion. The lightning bolt indicates the species subjected to CID.	106
Figure 3.11. Activation of (a) $[M + Au]^+$, (b) $[M - H - NH_3]^+$, and (c) y_{10} where M = KGAILPGAILR. Activation of (d) $[GAILPGAILR + H]^+$. Open circles indicate water loss and shaded circles indicate ammonia loss. The lightning bolt indicates the species subjected to CID. Lysine residue loss (i.e., 147 Da lower in mass) is represented with a superscripted “-147.” ..	107
Figure 3.12. Activation of the y_{13GK} fragment ion of Figure 3.7b. Open circles indicate water loss and shaded circles indicate ammonia loss.	108
Figure 4.1. General cyclotide structure showing the head-to-tail cyclic backbone and three disulfide bonds forming the cyclic cysteine knot.	116

Figure 4.2. Ion/ion reaction between triply protonated cyI4 and sulfate radical anion: a) post ion/ion reaction spectrum, b) beam-type CID of $[M + 3H + SO_4]^{2+}$, c) ion trap CID of $[M + H]^{2+}$, and d) DDC-CID of the ion/ion reaction products of panel a.	122
Figure 4.3. Product ion spectrum from the collisional activation of dehydroalanine containing cyI4, $[M + H - 90]^{2+}$. The lightning bolt corresponds to the species CID.	123
Figure 4.4. 500 m/z wide zoomed views from the collisional activation of cyI4 $[M + H - 90]^{2+}$. a) m/z 500-1000, b) m/z 1000-1500, c) m/z 1500-2000, d) m/z 2000-2500, e) m/z 2500-3000, and f) m/z 3000-3500. The lightning bolt corresponds to the species subjected to CID.	124
Figure 4.5. Individual fragmentation maps of cyI4 opened at a) Cys1, b) Cys2, c) Cys3, d) Cys4, e) Cys5, and f) Cys6. g) Cumulative fragmentation map from all ring openings.	129
Figure 4.6. Venn diagram showing the unique and overlapping fragment ions from activation of the cyI4 $[M + H - 90]^{2+}$ ion.	130
Figure 4.7. Positive nESI of a) wild type early LC fraction and b) reduced and alkylated early LC fraction.	131
Figure 4.8. Cumulative fragmentation maps of a) cyO8, b) cyI2, and c) viba11.	132
Figure 4.9. 500 m/z wide zoomed views from the collisional activation of cy08 $[M + H - 90]^{2+}$. a) m/z 500-1000, b) m/z 1000-1500, c) m/z 1500-2000, d) m/z 2000-2500, and e) m/z 2500- 3000. The lightning bolt corresponds to the species subjected to CID.	133
Figure 4.10. 500 m/z wide zoomed views from the collisional activation of cyI2 $[M + H - 90]^{2+}$. a) m/z 500-1000, b) m/z 1000-1500, c) m/z 1500-2000, d) m/z 2000-2500, and e) m/z 2500- 3000. The lightning bolt corresponds to the species subjected to CID.	134
Figure 4.11. 500 m/z wide zoomed views from the collisional activation of viba11 $[M + H - 90]^{2+}$. a) m/z 500-1000, b) m/z 1000-1500, c) m/z 1500-2000, d) m/z 2000-2500, and e) m/z 2500- 3000. The lightning bolt corresponds to the species subjected to CID.	135
Figure 4.12. General procedure for de novo sequencing.	136
Figure 4.13. De novo sequencing of ion series 1.	137
Figure 4.14. De novo sequencing of ion series 2.	137
Figure 4.15. De novo sequencing of ion series 3.	138
Figure 4.16. De novo sequencing of ion series 4.	138
Figure 4.17. De novo sequencing of ion series 5.	138
Figure 4.18. De novo sequencing of ion series 6.	139
Figure 4.19. De novo sequencing of ion series 7.	139
Figure 4.20. De novo sequencing of ion series 8.	139
Figure 4.21. De novo sequencing of ion series 9.	140
Figure 4.22. De novo sequencing of ion series 10.	140

Figure 4.23. All identified ion series overlaid in one spectrum. Ion series are stacked in chronological order, with Ion Series 1 on the bottom and Ion Series 10 on the top.	140
Figure 4.24. Aligned sequences for the ten ion series identified during de novo sequencing....	141
Figure 4.25. LC–MS/MS analysis of reduced and alkylated Glu-C digested [unknown + 4H] ⁴⁺ using a) targeted CID or b) targeted EThcD as an activation method. c) The combined fragmentation maps of panels a and b.....	143
Figure 5.1. Illustration of selective cleavages upon collisional activation.	156
Figure 5.2. Ion trap CID spectrum of ubiquitin for a) [M + 8H] ⁸⁺ , b) [M + 7H] ⁷⁺ , c) [M + 6H] ⁶⁺ , and d) [M + 5H] ⁵⁺ precursor ions. Cleavages C-terminal to aspartic acid residues are labeled in red, cleavages N-terminal to proline residues are labeled in blue, and non-specific cleavages are labeled in black.....	157
Figure 5.3. Ion trap CID spectrum of ubiquitin [M + 4H] ⁴⁺ . Cleavages C-terminal to aspartic acid residues are labeled in red, cleavages N-terminal to proline residues are labeled in blue, and non-specific cleavages are labeled in black.	158
Figure 5.4. a) Scatter plot of arginine count versus protein mass. b) Histogram of mass-to-charge ratios calculated using ± 3 the predicted number of arginine residues.	159
Figure 5.5. a) Nano-electrospray mass spectrum of reduced and alkylated trypsinogen. b) Post ion/ion spectrum from reaction of a with PFO dimer. c) q0 ion parking of the [M + 17H] ¹⁷⁺ ion under the same reaction conditions as b. d) Q1 isolation of c). e) Post ion/ion spectrum and isolation of m/z 1500 to m/z 2500 from the reaction of d) with PFO dimer. ^a a, b, and c are plotted on the same absolute intensity scale while ^b d and e are plotted on a scale of percent relative abundance.	160
Figure 5.6. Simultaneous activation of the [M + 16H] ¹⁶⁺ to [M + 10H] ¹⁰⁺ charge states of reduced and alkylated trypsinogen via DDC collisional activation. Only peaks matched to ± 15 ppm of theoretical b- and y-fragment ions are labeled.....	161
Figure 5.7. Percentage of the total matched fragment area for (red) cleavages C-terminal to aspartic acid residues, (blue) cleavages N-terminal to proline residues, or (green) nonspecific cleavages.	164
Figure 6.1. Ion optics and essential elements of the QTRAP 4000 ion path.	179
Figure 6.2. Schematic of the external manifold used to introduce reagent in q2 for ion/molecule reactions.	180
Figure 6.3. Positive electrospray mass spectrum of ubiquitin with a) no additional storage time in q2 or Q3, b) 400 ms storage in q2 (i.e. 400 ms ion/molecule reaction), and c) 400 ms storage in Q3 prior to mass analysis. The abundance weighted average charge state is represented with the colored dashed line.	183
Figure 6.4. Positive electrospray mass spectrum of ubiquitin a) pre-ion/molecule reaction, b) post ion/molecule reaction, and c) valet parking of the 8+ charge state. The ion/molecule reaction time is 900 ms, the IQ3 barrier was set to 1.5 V, and a valet parking waveform of 1.9 V at 114.367 kHz was used.	184

Figure 6.5. Positive electrospray mass spectrum of cytochrome c a) pre-ion/molecule reaction, b) post ion/molecule reaction, and valet parking of the c) 12+, d) 11+, or e) 10+ charge state. The ion/molecule reaction time is 900 ms, the IQ3 barrier was set to 1.8 V, and a valet parking waveform of 1.8 V at 114.367 kHz was used. 186

Figure 6.6. Positive electrospray mass spectrum of myoglobin a) pre-ion/molecule reaction, b) post ion/molecule reaction, and valet parking of the c) 16+, d) 15+, or e) 14+ charge state. The ion/molecule reaction time is 600 ms, the IQ3 barrier was set to 2.0 V, and a valet parking waveform of 2.0 V at 114.367 kHz was used. 187

Figure 6.7. Positive electrospray mass spectrum of a cytochrome c and myoglobin mixture a) pre-ion/molecule reaction, b) post ion/molecule reaction, and c) valet parking of the myoglobin 13+ charge state. The ion/molecule reaction time is 900 ms, the IQ3 barrier was set to 2.0 V, and a valet parking waveform of 2.0 V at 114.367 kHz was used. 188

Figure 6.8. Calculated ion frequencies and ion frequency dispersion for consecutive charge states of cytochrome c when cytochrome c 12+ is placed at a) $q = 0.4$ and b) $q = 0.8$ 190

LIST OF ABBREVIATIONS

2-D	Two Dimensional
3-D	Three Dimensional
AC	Alternating Current
AGC	Automatic Gain Control
CID	Collision Induced Dissociation
CTD	Charge Transfer Dissociation
Da	Dalton
DAPI	Discontinuous Atmospheric Pressure Interface
DC	Direct Current
DDC	Dipolar Direct Current
DDC-CID	Dipolar Direct Current Collision Induced Dissociation
DFT	Density Functional Theory
Dha	Dehydroalanine
DTT	Dithithreitol
ECD	Electron Capture Dissociation
ESI	Electrospray Ionization
ETD	Electron Transfer Dissociation
EThcD	Electron Transfer/High-Energy Collision Dissociation
ETnoD	Electron Transfer No Dissociation
eV	Electronvolt
FA	Fatty Acid
FBDSA	4-Formyl-1,3-Benzenedisulfonic Acid
FBMSA	2-Formylbenzenemonosulfonic Acid

FTICR	Fourier Transform-Ion Cyclotron Resonance
HCD	High-Energy Collisional Dissociation
HOAt	Sulfo-Benzoyl-1-Hydroxy-7-Azabenzotriazole Ester
HOBt	Sulfo-Benzoyl-1-Hydroxybenzotriazole Ester
HPLC	High Pressure Liquid Chromatography
IPT	Ion/Ion Proton Transfer
IM	Ion Mobility
IT	Ion Trap
LC	Liquid Chromatography
LC-MS	Liquid Chromatography Mass Spectrometry
<i>m/z</i>	Mass-To-Charge Ratio
MS	Mass Spectrometry
MS/MS	Tandem Mass Spectrometry
MSAE	Mass Selective Axial Ejection
MS ⁿ	Tandem Mass Spectrometry
nESI	Nanoelectrospray Ionization
NETD	Negative Electron Transfer Dissociation
NHS	N-Hydroxysuccinimide
NMR	Nuclear Magnetic Resonance
PC	Phosphatidylcholine
PDPA	1,4-Phenylenedipropionic Acid
PE	Phosphatidylethanolamine
PFO	2,2,3,3,4,4,5,5,6,6,7,7,8,8,8-Pentadecafluoro-1-Octanol
Phen	1,10-Phenanthroline
PIP	Parallel Ion Parking

ppm	Parts Per Million
PTCR	Proton Transfer Charge Reduction
PTM	Post Translational Modification
RF	Radio Frequency
SFTI	Sunflower Trypsin Inhibitor
SLIM	Structure For Lossless Ion Manipulation
T	Tesla
TOF	Time-Of-Flight
TW	Traveling Wave
TWIM	Traveling Wave Ion Mobility
UPLC	Ultra Performance Liquid Chromatography
UV	Ultraviolet
UVPD	Ultraviolet Photodissociation

ABSTRACT

Tandem mass spectrometry has long been used as a tool to extract structural information from an analyte ion. However, the information obtained in a tandem mass spectrometry experiment is dependent on both the ion type subjected to activation and the type of dissociation method used. Several activation methods, including electron capture dissociation (ECD), electron transfer dissociation (ETD), and ultraviolet photodissociation (UVPD) have emerged with a common objective to maximize the number of sequence informative product ions. There is merit, though, in mass spectrometry-based approaches which maximize selective cleavages, serving to concentrate product ion signal into relatively few fragmentation channels or to introduce a weak-spot into a peptide or protein. Ion/ion reactions can be used as a means to transform peptide and protein ions to new ion types which demonstrate highly selective fragmentation channels. Here, the utility of introducing selective cleavages via ion/ion reactions is demonstrated. In one example, a series of proton transfer ion/ion reactions are utilized to concentrate and move the precursor ion signal into a mass-to-charge region most likely to maximize cleavages at aspartic acid and proline, aiding in low abundance protein identification. In another example, various types of ion/ion reactions are utilized to unambiguously sequence cyclic peptides in the gas-phase.

CHAPTER 1. RECENT DEVELOPMENTS IN GAS-PHASE ION/ION REACTIONS FOR ANALYTICAL MASS SPECTROMETRY

Adapted with permission from Foreman, D. J.; McLuckey, S. A. *Anal. Chem.* **2020**, 92, 252-266. Copyright 2019 American Chemical Society.

1.1 Introduction to Gas-Phase Ion/Ion Reactions

While the study of reactions between oppositely charged ions has a long history, particularly within the context of plasmas and interstellar chemistry, the exploitation of such reactions for analytical applications was made possible with the advent of electrospray ionization (ESI).^{1,2} ESI provides a means for generating abundant multiply charged ions from a wide variety of molecular classes. It was then possible to use ESI to generate multiply charged analyte or reagent ions for reactions with ions of opposite polarities without resulting in complete neutralization. The first description of ion/ion reaction studies using ESI was given by Loo et al. using a Y-tube reactor leading to the inlet of an atmosphere/vacuum interface coupled with a quadrupole mass filter.^{3,4} This was an early example of ion/ion chemistry being effected prior to sampling ions into a mass spectrometer. The first implementation of ion/ion reactions within the context of an MSⁿ experiment was demonstrated at Oak Ridge National Laboratory.^{5,6} This was accomplished through the use of electrodynamic ion traps, which allow ions of opposite polarity to be stored in overlapping regions of space. Since those early reports, the use of ion/ion reactions, both *in vacuo* and *ex vacuo*, within the context of molecular analysis has expanded significantly. A number of characteristics make ion/ion reactions attractive for analytical mass spectrometry. For example, given the long-range Coulomb attraction associated with oppositely charged ions, the cross sections for ion/ion collisions are very large such that reactions can be driven on the millisecond to sub millisecond time scales, depending upon ion densities and the extents of ion overlap. Another important characteristic is that mutual neutralization is highly exothermic for virtually all combinations of oppositely charged gas-phase ion/ion reactions. Hence, ion/ion reactions are highly efficient and always result in some kind of reaction. Given the diversity of ion types that can be generated by the suite of ionization methods now available, the range of ion/ion reactions that can be effected is extremely large, even larger than that of ion/molecule reactions, which are limited by volatility constraints. In the case of ion/ion reactions that take place within a tandem

mass spectrometer, such as an ion trap or hybrid instrument, the fact that ions are readily manipulated on a time-dependent basis (i.e., they can be selected or ejected either selectively or nonselectively) enables a high degree of control over the identities of the reactants and the times over which they are exposed to one another.

The attractive characteristics of ion/ion reactions for multiple analytical applications have been illustrated in reports going back to the original works described above. Many of these have been reviewed previously.⁷⁻⁹ In this review, we emphasize developments that have taken place largely within the past decade with particular emphasis on the last 5 years. These have included developments in tools used to implement ion/ion reactions for one or more types of mass spectrometry experiments, an expansion in the range of ion/ion reaction types, and the growth in analytical applications of ion/ion chemistry. The review is organized with descriptions of instrument development, proton transfer chemistry, electron transfer chemistry, and reactions that can proceed only through long-lived complexes.

1.2 Developments in Ion/Ion Reaction Instrumentation

Scientific progress is directly related to and dependent on the development of instrumentation. In this respect, the increasing adoption of ion/ion reactions as an analytical tool within the past half-decade stems from the development of novel instrumentation equipped to perform such experiments. The commercialization of electron transfer dissociation (ETD), and more recently proton transfer charge reduction (PTCR), has emerged as, perhaps, the most significant advancement in ion/ion reaction instrumentation, bringing ion/ion reaction capabilities to laboratories around the world. Previously, research in the area of ion/ion reaction chemistry was exclusively limited to home-built instruments or heavily modified commercial instruments. The evolution of such instrumentation has been reviewed.⁷⁻¹⁰ In this section, rather than providing a complete history of ion/ion reaction instrumentation, we focus on the recent developments since the last comprehensive review of instrumentation in 2008.¹⁰ These developments are described in the context of three categories: ion/ion reactions performed outside the mass spectrometer, ion/ion reactions performed in vacuo, and the analysis of high m/z ions.

1.2.1 Front-End Ion/Ion Reaction Instrumentation

Several criteria must be met for a gas-phase ion/ion reaction to occur, chief among them is the temporal and spatial overlap of oppositely charged ions. In the case of reactions proceeding at or near atmospheric pressure, this is accomplished prior to the introduction of the ions into the vacuum system. As such, the modifications required to perform gas-phase ion/ion chemistry at atmospheric pressure are localized to the ionization region, specifically prior to the entrance to the atmosphere/vacuum interface. Recently, there have been several reports of modified or repurposed commercial ionization sources used for front-end ion/ion reactions.^{11–13}

Two reports of instrumentation highly analogous to that described by L. M. Smith and co-workers^{14,15} involved the modification of commercial ionization sources. In one report, the ESI source of an LC–MS platform was outfitted with a polonium-210 (²¹⁰Po) α -particle source.¹¹ The emitted α -particles initiate ion/molecule reactions involving ambient gas and solvent molecules generating ions of both polarities. Subsequent reactions between the α -particle progeny ions and the analyte ions generated via ESI result in charge reduced analyte ions, which are then sampled into the mass spectrometer for mass analysis. In another report, both an ESI and a nanoelectrospray ionization (nESI) source of a traveling wave ion mobility mass spectrometer (TWIM MS) were modified to contain a corona discharge probe.¹² The discharge generates anions from a nitrogen gas supply that is flowed over the platinum wire/discharge plate. Ensuing proton transfer ion/ion reactions result in the charged reduced protein species. The extent of charge reduction can be modulated by varying the flow rate of nitrogen or the applied voltage to the discharge needle. Robb et al. have demonstrated similar charge reduction reactions by simply repurposing a commercial atmospheric pressure electron-capture dissociation (ECD) source.¹³

In addition to modifying commercial ionization sources as described above, commercial sources can be replaced altogether with modular front-end ionization sources designed to perform ion/ion reactions. For example, the Brodbelt group constructed a free-standing dual ionization source reactor that can be mounted to the front-end of any mass spectrometer.¹⁶ The reactor consists of two electrosonic spray ionization sources fixed to a U-shaped rail. Permitting enhanced control, the angle of the two sources relative to one another and relative to the inlet of the mass spectrometer can be adjusted (Figure 1.1). The first source is integrated with the instrument such that the voltage and polarity are controlled with the instrument software. The voltage of the second source is supplied by an external dual polarity high-voltage power supply.

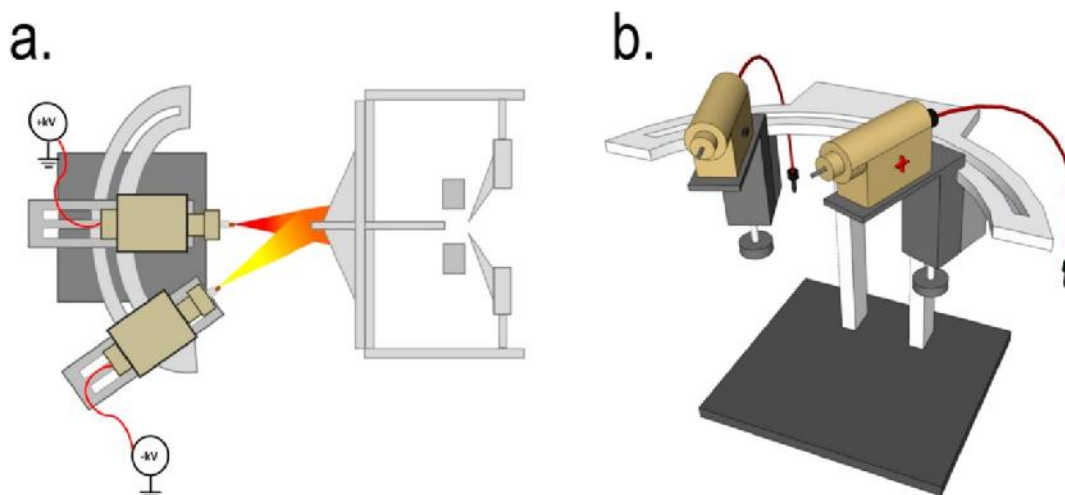


Figure 1.1. Dual source reactor used to perform ion/ion reactions (a) mounted to the front end of a mass spectrometer and (b) free-standing to be adapted to any mass spectrometer platform. Reprinted from the Supporting Information of Cotham, V. C.; Shaw, J. B.; Brodbelt, J. S. *Anal. Chem.* **2015**, 87, 9396–9402 (ref 16). Copyright 2015 American Chemical Society.

With this setup, ion/ion reactions are conducted in dual spray mode where the two sources are operated simultaneously. One source generates a plume of multiply charged peptide cations while the other generates a mixture of singly and doubly charged reagent anions. The two sources are oriented at an angle such that collisions between oppositely charged droplets, pseudodroplets, and gas-phase ions are maximized. Experimental evidence suggests that the reactions proceed exclusively through an ion/ion mediated pathway; the abundance of the peptide/reagent complex is directly related to the anion source voltage. Additionally, when the anion source voltage is zero, reminiscent of an ion/molecule reaction, the peptide/reagent complex is not observed. Stutzman and co-workers have performed similar experiments to demonstrate the charge reduction of synthetic polymers with a bipolar dual spray setup.¹⁷ Despite the setup being highly analogous to the dual spray reactor described above, we note a lack of conclusive evidence suggesting exclusively ion/ion chemistry. Nonetheless, it represents an intriguing avenue for charge state manipulation performed *ex vacuo*.

1.2.2 *In Vacuo* Ion/Ion Reaction Instrumentation

While instrumentation equipped to perform front-end ion/ion reactions offer some advantages (i.e., compatibility with any mass analyzer, simplicity of modifications, etc.), the vast

majority of ion/ion reactions are performed *in vacuo*. There are several distinct advantages to performing experiments within the confines of an electrodynamic trap: (1) independent control/optimization of reactant species, (2) well-defined reaction conditions, and (3) MSⁿ capabilities in conjunction with ion/ion reactions. Ion/ion reactions performed within the mass spectrometer have historically been conducted in either a 3-D quadrupole ion trap or a 2-D linear ion trap. Compared to 3-D traps, linear ion traps have a larger ion capacity and are more efficiently coupled to ionization sources and other devices. Consequently, apart from an IT-IM-TOF instrument which couples a 3-D ion trap with an ion-mobility cell,¹⁸ reactions performed in linear ion traps constitute the bulk of the recent literature.

Much of the work surrounding ion/ion reactions performed in both quadrupolar and hexapolar linear ion traps originates from the development and optimization of the now commercialized ETD instruments. ETD equipped instrumentation has been discussed in detail by Riley and Coon.¹⁹ Therefore, it is outside the scope of this review to thoroughly discuss the instrumentation and methodological developments of ETD. The ion traps in which ETD reactions are performed, however, can serve as reaction regions for any ion/ion reaction. In this context, some of the same instrumentation is mentioned as it pertains to ion/ion reactions other than ETD.

As mentioned above, any electrodynamic ion trap with mutual storage capabilities can be used to perform ion/ion experiments, provided that ions of opposite polarity can be generated and transported to the same trap. This can be accomplished by the generation of oppositely charged ions from two different sources and subsequently introducing ions through two separate orifices or through a common orifice. Instruments of both types have been described in recent years. He et al. described a dual polarity ion trap mass spectrometer of the former type.²⁰ The instrument consists of two ionization sources and two sets of ion optical systems separated by a segmented linear ion trap in the middle. Ions are generated using the two sources and can be transported to the linear ion trap where the reaction proceeds. Application of dipolar DC to one rod set enables the simultaneous detection of positive and negative ions of the same reaction experiment.

Lin et al. also described an instrument in which ions are introduced through separate orifices.²¹ Their home-built mass spectrometer consists of two discontinuous atmospheric pressure interfaces (DAPI) 180° from one another, one rectilinear ion trap, and one detector. Analyte ions are generated by DAPI I, introduced into the trap through its respective orifice and, if desired, isolated using custom waveforms. Reagent anions generated by DAPI II are then introduced into

the trap. Next, the two populations are allowed to react. However, opening the pinch valve of the DAPI results in an increased pressure of the trap which, in turn, could have deleterious effects on the ion/ion reactions. In fact, the proton transfer product ion spectrum shows two low abundance fragment ions which likely originate from the energy deposition by gas flow resulting from the sudden change in pressure from opening of DAPI II. A static higher base pressure is more desirable as it serves to enhance ion/ion reaction efficiency. However, Campbell and Hager have demonstrated ion/ion reactions in a low pressure reaction cell.²² They created an evanescent ion/ion reaction region within the low pressure region of Q3 of a hybrid triple quadrupole/linear ion trap mass spectrometer by adding DC and RF voltages to the optical components surrounding Q3 and by adding a pulsed valve for the addition of a cooling gas. The results of the ion/ion reactions performed in this low-pressure region were similar to that of the higher pressure region.

Early versions of ETD-equipped instrumentation contained a chemical ionization source at the rear of the instrument.^{23,24} Once generated, the reagent radical anions are delivered through the C-trap and into the segmented linear ion trap where the ETD reaction would take place. It was not long before this platform was used for proton transfer reactions.²⁵ In 2013, Hunt and co-workers described a front-end ETD source.²⁶ Here, cations and anions can be generated and introduced through a common orifice at the front of the instrument. Since its inception, the front-end chemical ionization source has been implemented on a number of research grade instruments including the 21 T Fourier transform-ion cyclotron resonance (FTICR) mass spectrometer at the National High Magnetic Field Laboratory.²⁷ Additionally, this source serves as the basis for the newest Orbitrap hybrid systems, including those with PTCR capabilities.

A common characteristic of all the instruments described above is the use of a linear ion trap as the reaction vessel. Ion/ion reactions are not restricted to linear ion traps though. The use of a traveling wave (T-wave) cell as a reaction vessel has been reported.²⁸⁻³¹ Cations and anions are generated at the front of the instrument. The optical polarities are alternately switched, and the quadrupole ion guide is set to transmit either exclusively precursor cations or reagent anions into the T-wave trap cell. The reaction proceeds in this cell as the ion populations are propelled through one another by the T-wave. Similarly, a traveling wave structure for lossless ion manipulation (TW SLIM) devices capable of performing ion/ion reactions has been described.³² Here, one SLIM surface contains four alternating phase RF electrodes interweaved with three traveling wave electrodes (Figure 1.2a). A second SLIM surface contains an identical configuration carrying the

opposite phase on every RF electrode as shown in Figure 1.2b. Simulations suggest ion/ion reactions in this device are feasible but have yet to be demonstrated experimentally.

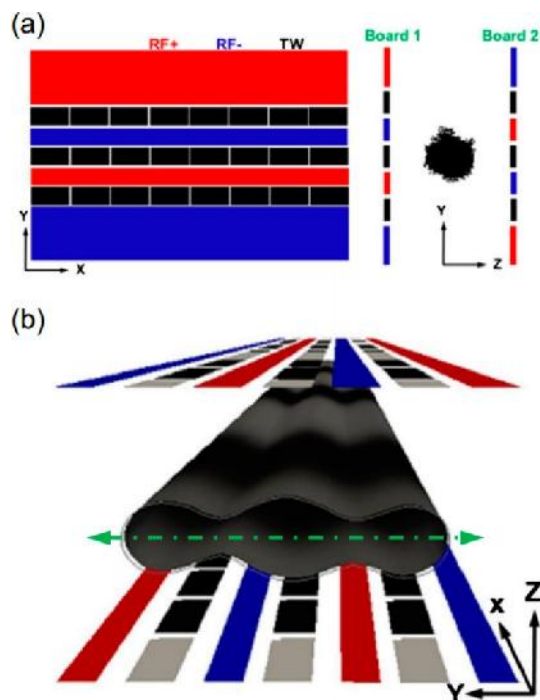


Figure 1.2. a) Schematic of the SLIM boards used for dual polarity ion confinement looking at the x–y plane (left) and z–y plane (right). b) 3-D view of the SLIM device showing the ion conduits. The green line represents the equidistant line between the SLIM surfaces. Reprinted by permission from Springer Nature: *Journal of the American Society for Mass Spectrometry*, Garimella, S. V. B.; Webb, I. K.; Prabhakaran, A.; Attah, I. K.; Ibrahim, Y. M.; Smith, R. D. J. *Am. Soc. Mass Spectrom.* **2017**, 28, 1442–1449 (ref 32). Copyright 2017.

1.2.3 Analysis of High m/z Product Ions from Ion/Ion Reactions

Ion/ion reaction product ions can be one or more orders of magnitude higher in m/z than the reactant ions. This is especially true for proton transfer ion/ion reactions involving proteins of relatively high mass (e.g., >30 kDa). There is, however, a number of challenges associated with generating and analyzing high mass-to-charge ions, both directly from electrospray ionization and from ion/ion proton transfer reactions. In the case of an ion/ion reaction experiment in trapping instruments, the upper m/z limit is dependent on (1) the detector response, (2) the range over which ions of disparate m/z can be mutually stored, and (3) the efficiency in which high m/z ions can be mass selectively ejected toward the detector. Our group has demonstrated a waveform switching

technique that directly addresses the third challenge.³³ A schematic of the instrument is provided in Figure 1.3. A high-frequency sine wave of 1.008 MHz is applied to the ring electrode during ion injection and mutual storage. After the ion/ion reaction period, a low-frequency square wave is applied to the end-cap electrodes, the sine wave is turned off, and product ions are mass selectively ejected via a frequency scan of the square wave. Switching from a high-frequency sine wave operation of the trap to a low-frequency square wave scan during mass analysis eliminates an upper m/z limit associated with voltage constraints. Additionally, the reduction in frequency places the product ions at higher q values, thereby, generating deeper well depths and smaller ion packets despite using lower amplitudes. Using this method, the upper m/z limit of the ion/ion reaction was improved by a factor of 2–3.

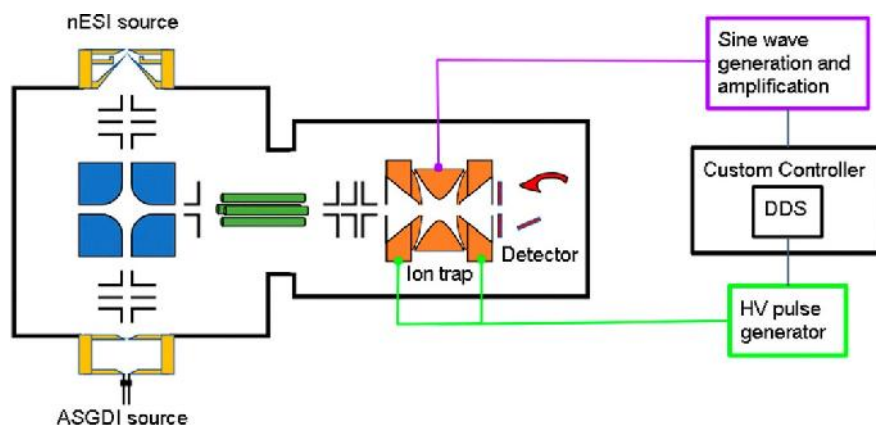


Figure 1.3. Schematic of the instrumental setup for the waveform switching experiments. The sine wave is applied to the ring electrode and the square wave is applied to the end-cap electrodes. Reprinted by permission from Springer Nature: Journal of the American Society for Mass Spectrometry, Lee, K. W.; Eakins, G. S.; McLuckey, S. A. *J. Am. Soc. Mass Spectrom.* **2019**, 30, 1126–1132 (ref 33). Copyright 2019.

In addition to the development in high m/z analysis described above, recent modifications to the Orbitrap mass spectrometer platform have been aimed at increasing the transmission, isolation, fragmentation, and resolution of high m/z ions.^{34–38} Modifications include orthogonal ion injection into the instrument to reduce instrument contamination, insource trapping to facilitate ion desolvation and to minimize the ions' axial momentum, reduction of the RF frequencies applied to the bent flatapole, quadrupole, transfer multipole, C-trap, and HCD-cell, lengthening ion injection times from the C-trap to the Orbitrap mass analyzer, and changes to the image current preamplifier to detect a broader range of ion frequencies. Implementation of these modifications

have enabled the detection of high m/z ions up to m/z 70 000.³⁹ To date, no ion/ion reactions have been performed on this platform. However, it stands to reason these developments can lend themselves to eventually couple ion/ion reactions to high mass-to-charge protein or protein complex ions.

1.3 Proton Transfer Ion/Ion Reactions

The first proton transfer ion/ion reactions were conducted in the early 1990s using the front-end Y-tube reactor.^{3,4} Since then, altering ion charge states via gas-phase proton transfer has developed into a robust and mature technique that has found utility in biological mass spectrometry, primarily in the charge state manipulation of proteins. Much of the early work devoted to proton transfer for protein analysis was performed in 3-D ion traps.^{6,40-43} As the resolution of ion traps is generally limited, identification of ion charges greater than two can be a nontrivial task when adjacent charge states from an analyte of interest are not clearly identifiable. Proton transfer ion/ion reactions, therefore, have historically been used to simplify spectra containing highly charged ions by decreasing ion charges to mostly 1+ or 2+ and by dispersing ions across a wide mass-to-charge range. Increased resolving power can enable charge state determination via measurement of the isotope spacings within a single charge state. Yet, it has been shown that even high-resolution instruments, such as the Orbitrap and FTICR mass spectrometers, can benefit from using proton transfer reactions when complex mixtures of ions are present.⁴⁴ In recent years, as the complexity of protein mixtures subjected to ESI has increased, there has been an extension of proton transfer workflows to high-resolution instruments. Applications of proton transfer ion/ion reactions include MSⁿ product ion analysis, precursor ion charge state manipulation, and precursor ion signal concentration. Additionally, proton transfer reactions are used in structural proteomic studies. The following sections feature recent work describing proton transfer reactions in all these application areas.

1.3.1 Product Ion Analysis

Several activation methods, including electron transfer dissociation and ultraviolet photodissociation (UVPD), have emerged with a common objective to enhance structural characterization by maximizing the number of sequence informative product ions. However,

fragment ions produced using these techniques typically result in a product ion spectrum in which fragments are confined to a relatively narrow m/z range centered about the precursor. When combined with proteins of relatively large size and the multiplicity of fragment ion charge states, the resulting product ion spectrum can be quite complex. In 2005, the Hunt group used sequential ion/ion reactions (i.e., electron transfer dissociation followed by proton transfer reactions) for protein identification.²⁵ ETD of the $[M + 13H]^{13+}$ charge state of ubiquitin performed on a Finnigan LTQ mass spectrometer generated a spectrum that was uninterpretable. However, using proton transfer on the ETD products, approximately 90% of the residues could be sequenced. The utility of this ETD-proton transfer workflow is further demonstrated by the identification of 46 *E. coli* 70S ribosomal proteins.⁴⁵

Expanding upon the work performed in ion trap mass spectrometers,^{25,46–48} Hunt and co-workers have recently coupled the ETD-proton transfer workflow with Orbitrap mass analysis.⁴⁹ In this experiment, a multiply charged protein ion was isolated and fragmented by electron transfer dissociation, resulting in a complex product ion spectrum, as shown in Figure 1.4a. Following ETD, product ions were charge reduced via proton transfer to sulfur hexafluoride radical anions. Figure 1.4b–e shows the resulting charge reduced spectra under identical ETD parameters but increasing proton transfer reaction durations. Interestingly, the most informative reaction duration was observed to be the 20 ms ion/ion proton transfer reaction. ETD followed by proton transfer on the Orbitrap platform has been used in only a few other studies,^{50–52} likely due to the lack of a commercial instrument optimized to perform both types of ion/ion reactions. An increase in the number of applications utilizing ETD followed by proton transfer can be anticipated with the commercialization of PTCR on ETD equipped instruments.

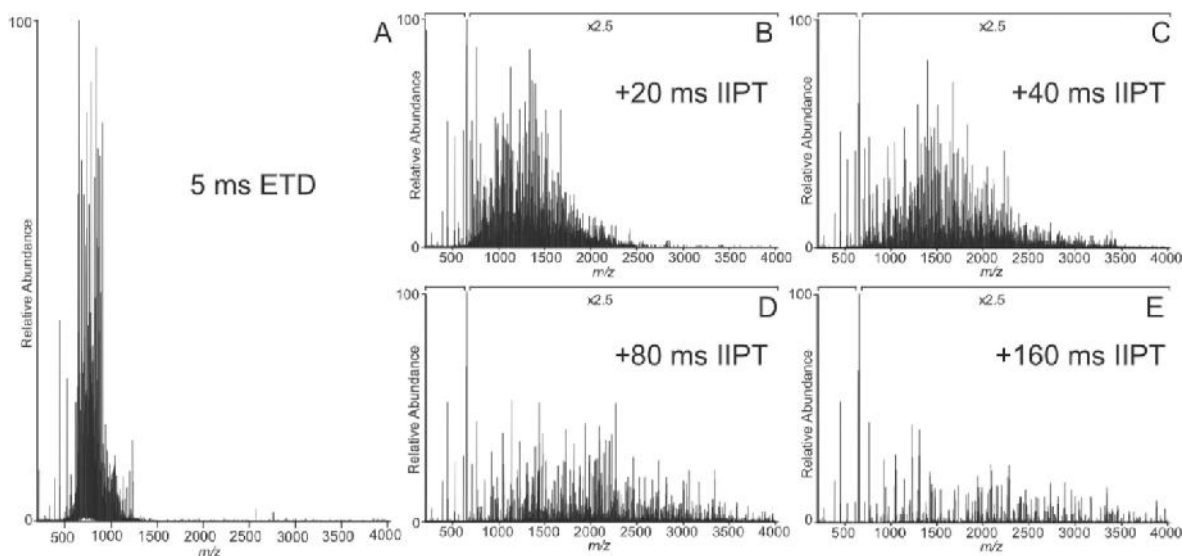


Figure 1.4. ETD product ion spectrum of the $[M + 26H]^{26+}$ charge state of apomyoglobin followed by sequential ion/ion proton transfer (IIPT) reaction for a) 0 ms, b) 20 ms, c) 40 ms, d) 80 ms, and e) 160 ms. Reprinted from *Int. J. Mass Spectrom.*, Vol. 377, Anderson, L. C.; English, A. M.; Wang, W.; Bai, D. L.; Shabanowitz, J.; Hunt, D. F. Protein derivatization and sequential ion/ion reactions to enhance sequence coverage produced by electron transfer dissociation mass spectrometry, pp. 617–624 (ref 49). Copyright 2015, with permission from Elsevier.

1.3.2 Precursor Charge State Manipulation

In addition to reducing spectral complexity during product ion analysis, proton transfer can be used to produce simpler spectra during MS¹ experiments. Laszlo and Bush demonstrate that proton transfer can increase accuracy in assigning charge states of native proteins and protein complexes generated via ESI.⁵³ With ESI under denaturing conditions, as the size of the analyte increases, the propensity for generating multiply charged ions increases potentially creating overlap between charge state distributions of different species even for relatively simple mixtures. For complex mixtures, the overlap can be quite extensive, complicating data interpretation. This problem is exacerbated with polydisperse polymers, where the distributions are broad spanning, in some cases, tens of thousands of Da. Recently, proton transfer ion/ion reactions have been used to alleviate the spectral congestion of large synthetic polymers.^{12,13} In those studies, extensive charge reduction via proton transfer was shown to enable facile data interpretation for polymers up to 40 kDa. Other ion/ion charge reduction strategies have been reported for polymer characterization, though it is unclear if the charge reduction occurs via proton transfer.^{11,17}

Most examples described above (i.e., product ion analysis and polymer analysis) utilize proton transfer reactions to charge reduce analyte ions to mainly the 1+ charge state. However, in some scenarios, it is desirable to perform less extensive charge reduction. For instance, our group has used proton transfer reactions to manipulate precursor ion charge in order to study the charge state dependent collisional activation of proteins.⁵⁴⁻⁵⁹ This technique has been adopted to study the charge state dependent fragmentation of proteins utilizing ETD and UVPD activation methods.⁶⁰⁻⁶³

In 2016, the Brodbelt group reported on the photodissociation patterns of native proteins following gas-phase proton transfer.⁶² While only minor changes in fragmentation were observed, this report demonstrates another attractive application for proton transfer reactions. ESI of bovine superoxide dismutase (SOD)/CuZn complexes under native conditions generates the mass spectrum shown in the top panel of Figure 1.5a. Close examination of the peak at approximately m/z 3140 shows an overlap of 5+ monomers with 10+ dimers (Figure 1.5b, top). This overlap inhibits the independent MS/MS analysis of the monomer or dimer distribution. Proton transfer, on the other hand, can generate purified distributions of monomer and dimer. For example, a clean 5+ monomer distribution and a clean 10+ dimer distribution is generated from proton transfer of the 12+/6+ distribution (Figure 1.5, middle row) and from proton transfer from the 11+ dimer (Figure 1.5, bottom row), respectively. Here, proton transfer is used to purify charge state distributions in the gas-phase. Gas-phase charge state purification via proton transfer reactions involving protein mixtures under denaturing conditions has also been demonstrated,^{41,42} and the Coon group extended this approach to proteomic quantitation with isobaric tagging.^{64,65}

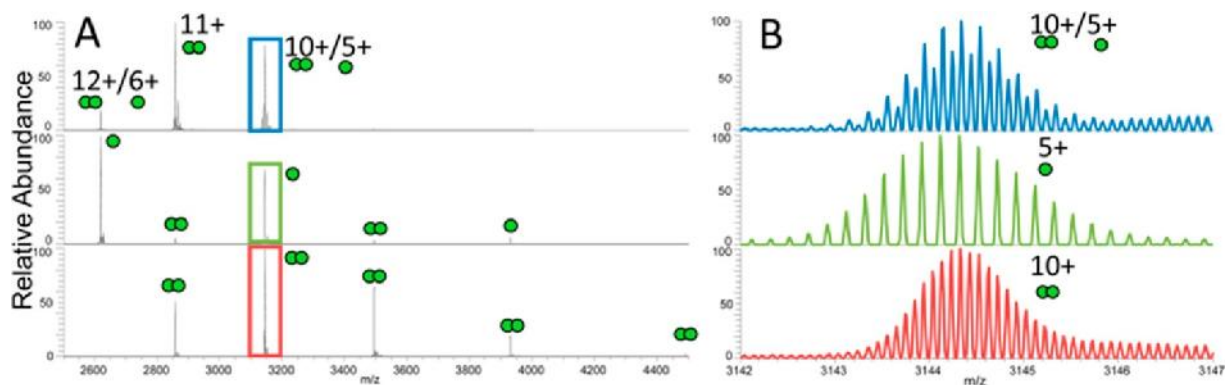


Figure 1.5. Mass spectra of SOD/CuZn complexes a) as observed under native MS conditions (top), isolation and 25 ms proton transfer reaction of the 12+/6+ species (middle), and isolation and 25 ms proton transfer reaction of the 11+ species (bottom) with b) a 60 m/z wide zoomed view of the 10+/5+ region. Adapted from Holden, D. D.; Brodbelt, J. S. *Anal. Chem.* **2016**, 88, 12354–12362 (ref 62). Copyright 2016 American Chemical Society.

The kinetics of ion/ion reactions can play a major role in determining product ion distributions, particularly when mixtures of ions of widely different charges are subjected simultaneously to reaction. Again, using the SOD/CuZn data as an illustrative case, when both the 12+ dimer and 6+ monomer are subjected to proton transfer ion/ion reactions, the resulting spectrum shows only a 5+ monomer distribution with no evidence of the isobaric 10+ dimer species. This follows from the charge squared dependence associated with ion/ion reaction rates.^{40,66} That is to say, the sequential charge reduction reactions of the 12+ dimer react at a faster rate than the 6+ monomer species. Consequently, the entire 10+ population is depleted, having reacted to lower charge states, leaving a relatively enriched purified monomer distribution.

A degree of control over ion/ion reaction kinetics can be effected in a process termed “ion parking.”⁶⁷ This is accomplished by applying a low amplitude auxiliary RF signal at the secular frequency of the desired product ion. The applications of ion parking are numerous. Many of the studies in the past decade involving ion/ion reactions utilized ion parking to enhance sensitivity, including some examples discussed above.^{51,61,62} Recently, we have used ion parking to concentrate precursor ion signal prior to moving the ions to a m/z region likely to maximize cleavage at aspartic acid and proline residues.⁶⁸ The Hunt group implemented “parallel ion parking”^{69,70} during the online high-pressure liquid chromatography (HPLC), data-dependent MS/MS analysis of the *E. coli* ribosome (Figure 1.6).⁷¹ Here, a broadband parallel ion parking waveform is applied to concentrate ion signal without a priori knowledge of the protein (compare

signal intensities of Figure 1.6a,b). Campbell and Le Blanc employed ion parking to impart an additional degree of selectivity during protein quantitation,⁷² and in 2008, L. M. Smith and co-workers combined fixed-charge derivatization and ion parking to generate an abundant precursor at a charge state not generated under conventional electrospray conditions.⁷³ Ion parking provides a high degree of flexibility in mixture analysis applications due both to the concentration of multiple charge states into one or a few charge states, which is attractive for sensitivity, and the simplification of the precursor ion spectrum, which can improve specificity.

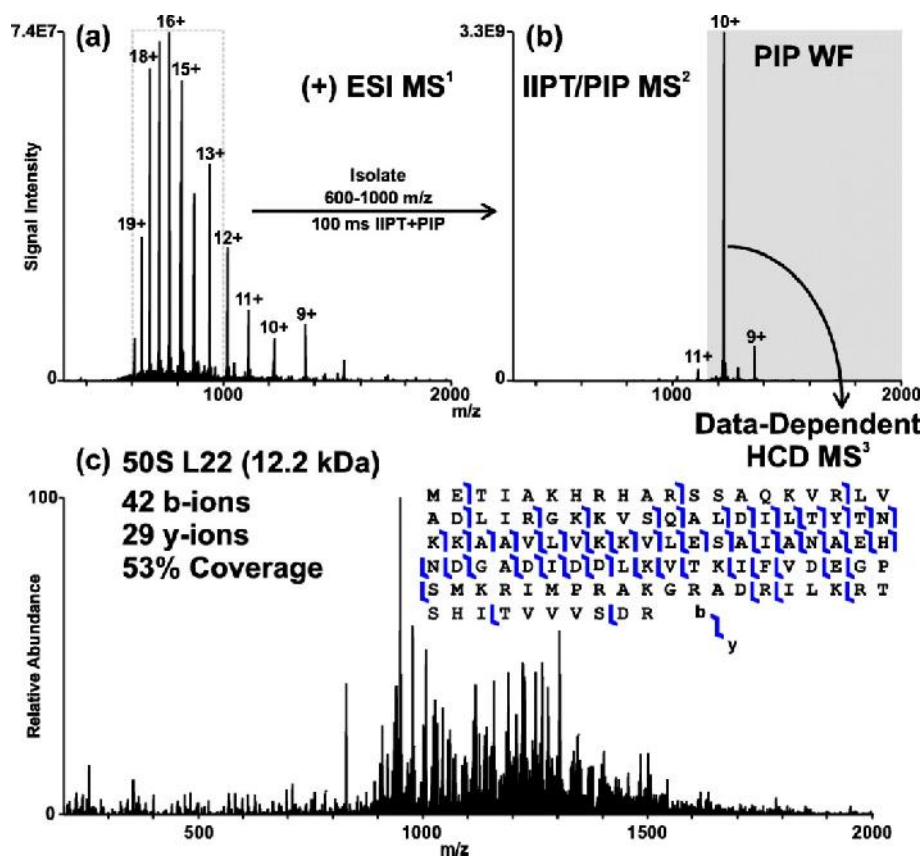


Figure 1.6. MS/MS analysis scheme of 50S L22 E. coli ribosomal protein. a) Positive electrospray mass spectrum, b) 100 ms proton transfer and parallel ion parking of the 600–1000 m/z isolation window, and c) HCD product ion spectrum of the data-dependently selected 10+ precursor. Reproduced from Ugrin, S. A.; English, A. M.; Syka, J. E. P.; Bai, D. L.; Anderson, L. C.; Shabanowitz, J.; Hunt, D. F. *J. Am. Soc. Mass Spectrom.* **2019**, 30, 2163–2173 (ref 71). Copyright 2019.

1.3.3 Structural Proteomic Studies

Native mass spectrometry is increasingly being adopted as a tool for structural biology, allowing researchers to extract more information from a mass spectrometry experiment than simply molecular weight.^{74–77} Coupling ion-mobility with native MS facilitates native protein and protein complex collisional cross section measurements. Those measurements, however, are obtained from the gas-phase structures of the analyte, and unfortunately, there is still a great deal of ambiguity regarding the relation of gas-phase structure with those observed in solution. Expanding upon the early work of Badman and co-workers,^{18,78} the Bush group is combining native mass spectrometry, gas-phase proton transfer, and ion-mobility to study structure/charge relationships and protein folding.^{79–83} Lermyte et al. perform similar experiments but, in their case, an electron transfer reagent anion, 1,4-dicyanobenzene, is used for charge reduction.⁸⁴ Using 1,4-dicyanobenzene leads to a combination of electron transfer and proton transfer.

1.4 Electron Transfer Ion/Ion Reactions

Because of the implementation of ETD across multiple commercially available instrument platforms, electron transfer ion/ion reactions can be considered the most commonly employed type of ion/ion reaction. The ETD process begins with an ion/ion reaction involving the transfer of an electron from a reagent radical anion to a multiply charged analyte cation, viz.,



Fragmentation of the charge-reduced product via radical directed mechanisms results, in the case of multiply charged polypeptide cations, in c- and z• -type fragment ions and extensive primary sequence information.²³ Since its introduction in commercially available instruments, ETD has become a standard approach for the structural characterization of bio-ions. The majority of electron transfer ion/ion reactions are discussed in the context of ETD and negative electron transfer dissociation (NETD). Consequently, ETD and NETD have been extensively reviewed,^{19,85–88} with the latest review being published in 2018.¹⁹ Therefore, ETD is not discussed here. Instead, we highlight other electron transfer ion/ion reactions and their analytical utilities. Specifically, charge reduction via electron transfer and charge transfer dissociation are discussed.

1.4.1 Electron Transfer Charge Reduction

Electron transfer from a reagent radical anion to a multiply charged cation does not always lead to spontaneous dissociation to generate product ions. Nondissociative electron transfer, often referred to as “electron transfer no dissociation” (ETnoD), gives rise to an intact charge reduced product ion. The extent of ETnoD has been shown to be dependent on several factors including protein ion conformation, precursor ion charge state, degree of supplemental activation, etc.^{84,89} This nondissociative channel is undesirable when ETD is the objective, yet several studies exploit the formation of ETnoD products. The Kaltashov group, for example, employ native electrospray ionization in combination with electron transfer^{90–93} or electron capture^{94,95} charge reduction to reduce the spectral complexity of heterogeneous samples. Figure 1.7 shows the native ESI mass spectrum of an antithrombin-III/heparin complex (AT/heparin) in gray. Mass selection of the precursor ion and subsequent electron transfer charge reduction generates the product ion spectra shown in pink and cyan (Figure 1.7). The value of this strategy stems from the ability to correctly assign charges from the resulting mass spectrum that is reduced in spectral complexity. By selecting a narrower population of precursor ions, interpretable mass information can be extracted (compare pink and cyan traces).⁹¹ Lermyte et al. performed similar electron transfer ion/ion reactions, though, in their case, precursor ions were reduced to the 1+ charge state.⁹⁶

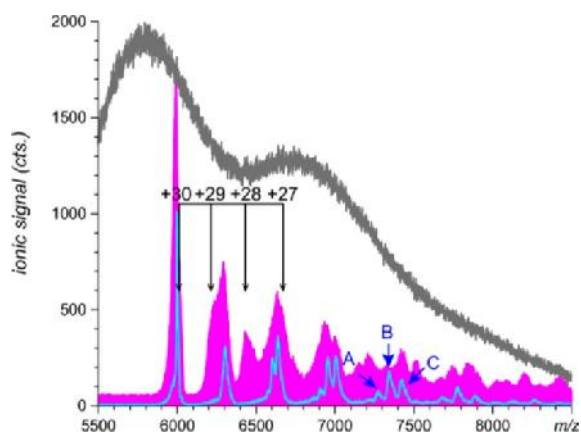


Figure 1.7. Electrospray mass spectrum of a AT/heparin complex is shown in gray. Ion charge state assignment is facilitated by limited electron transfer charge reduction using wide (pink) and narrow (cyan) precursor ion selection windows. The species labeled A, B, and C represent resolved charge-reduced species present in the precursor isolation windows. Reproduced from Zhao, Y.; Abzalimov, R. R.; Kaltashov, I. A. *Anal. Chem.* **2016**, 88, 1711–1718 (ref 91). Copyright 2016 American Chemical Society.

Beyond charge assignment and mass determination, electron transfer charge reduction has proven to be useful in both protein conformational studies and in the generation of metal species in unusual oxidation states. In the former case, the effect of charge reduction on protein conformation has been studied by coupling ETnoD with ion-mobility, providing insights into the importance of net charge in the gas-phase on the extent of protein compaction.^{84,97,98} In the latter case, the transfer of a single electron from a radical anion to a metal–ligand complex, $M(II)L_x$, serves to reduce the metal forming the $M(I)L_x$ complex ion. Gronert first used this technique to study the reactivity of metals in the 1+ oxidation state toward allyl iodide.⁹⁹ Later, Oomens and co-workers used gas-phase reduction via electron transfer to study the coordination environment of several reduced metals and their ligands.^{100,101}

1.4.2 Charge Transfer Dissociation

Charge transfer dissociation (CTD), pioneered by the Jackson lab, is another electron transfer based fragmentation technique. Unlike most ion/ion and ion/electron fragmentation techniques in which reactions proceed through cation/anion interactions, the electron transfer of CTD occurs between two cationic species.¹⁰² Reactions of ions of like charge are characterized by a large Coulomb barrier that must be overcome by a large relative translation. Specifically, analyte cations are irradiated with a beam of 6 keV helium cations, leading to the abstraction of an electron by the helium ion:



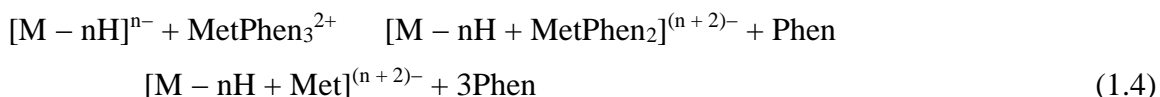
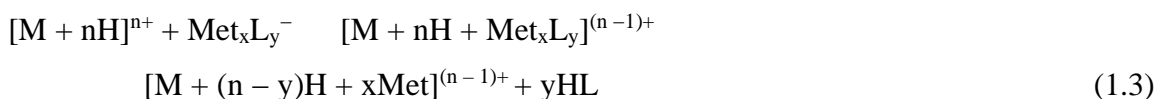
Ultimately, this electron hole initiates radical directed fragmentation. Using cations at 6 keV overcomes the electrostatic repulsive barrier associated with cation/cation collisions. Additionally, helium is intentionally chosen as the cation of choice for CTD due to its adiabatic recombination energy of 24.6 eV, the largest of any 1+ ion, which drives the electron abstraction process from other singly charged cations. In addition to the one-electron oxidation pathway discussed above, experimental evidence exists to suggest a one-step two-electron oxidation pathway.¹⁰³ Compared to ETD, CTD is a unique high-energy dissociation method with the advantage of inducing fragmentation of singly charged precursor ions. To date, CTD has been applied to the analysis of peptides,^{102–104} phospholipids,¹⁰⁵ and oligosaccharides.^{106,107}

1.5 Reactions That Proceed Through Complex Formation

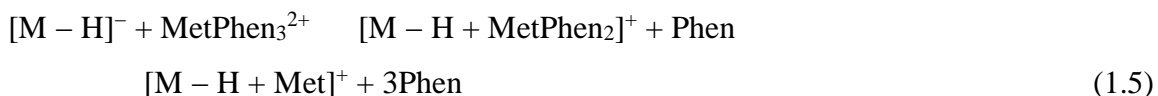
Gas-phase ion/ion reactions between oppositely charged ions proceed through the formation of a Coulombically bound orbit.¹⁰⁸ Initially, the distance between the ions in the orbit can exceed that necessary for chemistry to occur. As translational energy is removed via collisions and/or tidal effects,¹⁰⁹ the size of the orbit decreases until either a small charged particle (i.e., proton or electron) is transferred at a crossing point on the potential energy surface or a physical collision occurs resulting in formation of a collision complex. While all types of ion/ion reactions can take place through complex formation, many reaction types can only take place through complex formation. More so, complex lifetime is largely determined by the strength of the electrostatic interactions, the number of degrees of freedom of the complex, and both the emissive and collisional cooling rates. Examples of ion/ion reactions that can proceed only through a complex include, but are not limited to, metal ion transfer, charge inversion, and covalent chemistries. Recent work from all areas are highlighted below.

1.5.1 Metal Ion Transfer

Ion/ion reactions involving metal-ligand complexes can be used to insert metal cations into analyte ions. These reactions have been demonstrated in both polarities:



where M represents the analyte, Met represents the metal cation, L represents a singly charged anionic ligand, and Phen represents the neutral 1,10-phenanthroline ligand.¹¹⁰⁻¹¹⁵ In the case where the analyte is a singly deprotonated anion, ion/ion reaction with a doubly charged cationic metal phenanthroline complex results in the charge inversion of the analyte:



This case will be discussed in further detail in the Charge Inversion section below.

The reaction presented in eq 1.3, for example, has been used to incorporate gold cations into disulfide containing polypeptides using AuCl_2^- .¹¹⁶⁻¹¹⁸ In all cases, gold cationization showed

a preference for cleavage of disulfide bonds upon collisional activation, in contrast with the collisional activation of the corresponding protonated species. Recently, gold(I) cations have been incorporated into polypeptides lacking disulfide bonds.^{119,120} It was found that gold(I) cationization facilitates peptide oxidation at a neutral lysine residue via the loss of gold hydride and a molecule of ammonia. The resulting structure contains a fixed charge cyclic imine, which weakens the adjacent amide bond. Upon subsequent activation, facile fragmentation N-terminal to the oxidized residue is observed.¹¹⁹ This so-called “weak-spot” at lysine was exploited for cyclic peptide analysis providing a site-specific ring opening pathway. Collisional activation of the oxidized cyclic peptide was shown to lead to unambiguous sequence information.¹²⁰

Whereas metal transfer from a reagent to the analyte is highlighted above, gas-phase ion/ion reactions for selective alkali metal removal have also been demonstrated.^{121,122} Luongo et al. investigated a series of weakly coordinating anions and demonstrated that, of the reagents examined, carborane anions (e.g., $\text{CHB}_{11}\text{Cl}_{11}^-$) were the most selective for the removal of alkali metals.¹²² Later, Betancourt et al. simplified the electrospray mass spectra of Polysorbate 80 via ion/ion reaction with carborane anions.¹²³ ESI of Polysorbate 80 shows overlapping distributions from multiple ion types and multiple charge states below m/z 1400. The ion/ion reaction between Polysorbate 80 cations and carborane anions pushed the charge states to a largely singly charged species. That is to say, doubly charged species adducted one carborane anion and triply charged species adducted two carborane anions. Broadband collisional activation of the product ions results in the removal of the metal cations with carborane. The product ion spectrum is less congested than the electrospray mass spectrum and shows clear distributions of singly charged, metal cationized species.¹²³

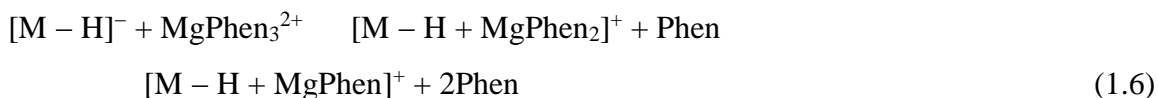
1.5.2 Charge Inversion

Multiple charges (i.e., two or more) can be transferred during a single intimate collision between two ions. For example, ion/ion reaction between a singly protonated phosphatidylethanolamine (PE) and doubly deprotonated 1,4-phenylenedipropionic acid (PDPA) generates the singly deprotonated PE via the transfer of two protons from the PE cation to the PDPA anion.¹²⁴ In this case, the charge of the PE analyte ion is inverted from positive to negative polarity. Charge inversion reactions of both ion polarities have been reported.^{125,126} Our group has been investigating the utility of charge inversion ion/ion reactions and have demonstrated their

applications in sulfo- and phosphopeptide characterization,^{127,128} concentration of multiple cation types to a single anion type,¹²⁹ and reduction of chemical noise.¹³⁰ Sequential charge inversion reactions have been used to increase ion charge.^{131,132}

Charge inversion has proven particularly useful in altering the ion type of fatty acids and glycerophospholipids to yield structurally informative ion types. For example, Stutzman et al. used PDPA dianions to convert phosphatidylcholine (PC) monocations to the structurally informative $[\text{PC} - \text{CH}_3]^-$ anion species. Ion/ion reaction between PC cations and PDPA dianions formed the $[\text{PC} - \text{H} + \text{PDPA}]^-$ complex anion, and subsequent CID of the charge inverted anion resulted in concomitant proton transfer and methyl cation transfer.¹³³ Here, the demethylated PC anions afforded acyl chain information, whereas the PC monocations fragment predominantly to give a choline headgroup product ion. Reactions with PDPA have also been applied to isomeric mixtures of PC and PE lipids. Here, an isomeric mixture of PC and PE cations are reacted in the gas-phase with PDPA dianions, ultimately resulting in the chemical separation of PC and PE upon charge inversion due to the proton/methyl cation transfer unique to PC cations and the double proton transfer pathway undertaken by PE cations.¹²⁴ While a $[\text{PE} - \text{H} + \text{PDPA}]^-$ complex was not directly observed, the $[\text{PE} - \text{H}]^-$ product anion is not likely to be formed from two consecutive single-proton transfer reactions as neutralization would occur after the first reaction and ionization of the neutral from a second encounter is improbable. Rather, two proton transfer reactions within a single collision complex with subsequent dissociation of the complex is far more likely. Combining charge inversion with other techniques, like trimethylation enhancement using ¹³C-diazomethane (¹³C-TrEnDi) or the Paternò–Büchi reaction, can result in enhanced structural characterization of PC and PE phospholipids.^{134,135}

In the above cases, charge inversion was used to convert phospholipid cations to structurally informative anions. Recently, gas-phase charge inversion ion/ion reactions have also been applied to convert fatty acid anions to metalated cations.^{136,137} These reactions have successfully been applied in a shotgun (i.e., direct infusion ESI-MS) approach for fatty acid (FA) profiling, permitting unambiguous FA identification, isomeric distinction, and relative quantitation of isomeric FA. In the special case of magnesium phenanthroline complexes, charge inversion analogous to that of eq 1.5 can be achieved where only two phenanthroline ligands are lost:



Singly deprotonated FA anions, either derived from nonesterified (i.e., free) FA or complex lipid decomposition via solution-based hydrolysis or gas-phase broadband collisional activation, undergo charge inversion when subjected to reactions with tris-phenanthroline magnesium dications to generate $[FA - H + MgPhen]^+$ cations. Subsequent isolation and ion-trap CID of the charge-inverted FA complex cation yields a reproducible, predictable product ion spectrum, that upon spectral matching to a developed FA mass spectral library composed of $[FA - H + MgPhen]^+$ product ion spectra, facilitates localization of carbon-carbon double bond positions and confident FA identification. Furthermore, using multiple linear regression analysis paired with the library data and in conjunction with data derived from FA mixtures, relative abundances of isomeric FA can be sensitively determined (Figure 1.8).¹³⁷ Collectively, this approach provides a relatively rapid and sensitive approach to lipid analysis based entirely on gas-phase chemistries.

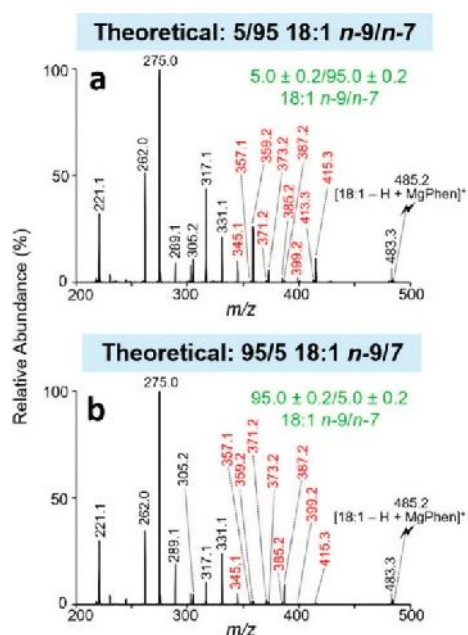


Figure 1.8. Product ion spectra of $[18:1 - H + MgPhen]^+$ for the isomeric mixture of 18:1 n-9/n-7 at the molar ratios of a) 5/95 and b) 95/5. Product ions used in the multiple linear regression for relative quantitation are shown in red. Calculated molar ratios (mean \pm standard deviation, $n = 3$) are shown in green. The lightning bolt corresponds to the species subjected to CID. Adapted from Randolph, C. E.; Foreman D. J.; Blanksby, S. J.; McLuckey, S. A. *Anal. Chem.* **2019**, 91, 9032–9040 (ref 137). Copyright 2019 American Chemical Society.

1.5.3 Oxidation Reactions

Reduction/oxidation reactions in terms of electron transfer have been discussed above. However, oxidation can also be discussed in terms of oxygen transfer (i.e., oxidation is the gain of oxygen) and hydrogen transfer (i.e., oxidation is the loss of hydrogen). The gas-phase oxidation of multiply protonated peptide ions via oxygen transfer has recently been described. The periodate anion, IO_4^- , was used to selectively oxidize methionine residues, and to a lesser extent, tryptophan residues,¹³⁸ alkylated cysteine residues,¹³⁹ and disulfide bonds.¹⁴⁰ Under favorable conditions, the periodate anion can be used to oxidize neutral basic residues in the gasphase.¹⁴¹

In the case of oxygen transfer to disulfide bonds, subsequent activation of the $[\text{M} + \text{H} + \text{O}]^+$ species results in the cleavage of the oxidized disulfide bonds at the $\text{S}(\text{O})\text{-S}$ bond or the $\text{C-S}(\text{O})$ bond, generating a fragmentation pattern indicative of the presence of a disulfide linkage.¹⁴⁰ Tryptic digestion of disulfide intact lysozyme yields a total of three peptides; two peptides contain one intermolecular disulfide bond and one peptide contains one intermolecular and one intramolecular disulfide bond. The product ion spectra from the activation of the three oxidized species are shown in Figure 1.9. In all cases, cleavage of the intermolecular disulfide bond is evidenced by the presence of the A and B chain peptides.

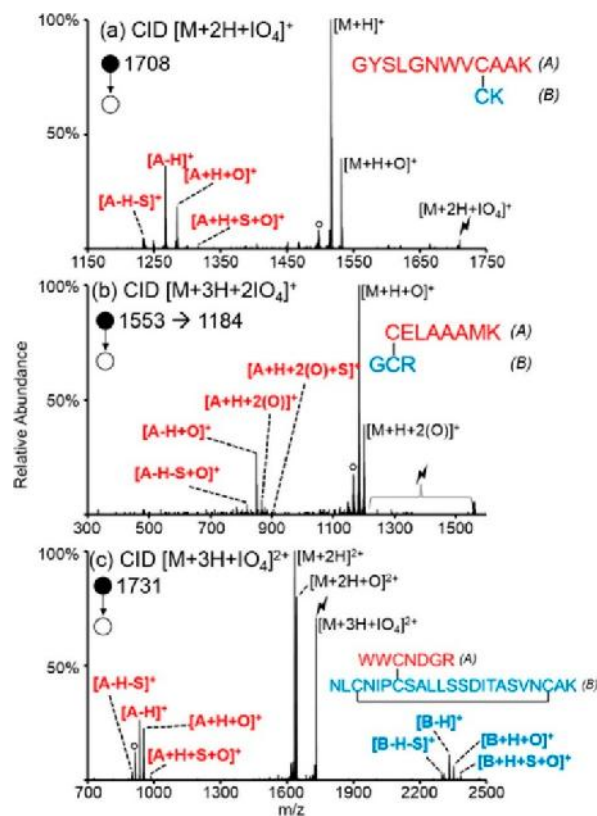


Figure 1.9. Collisional activation of the ion/ion reaction complex formed between the reaction of the periodate anion with a) doubly protonated doubly GYSLGNWVCAAK/CK, b) triply protonated CELAAAMK/GCR, and c) triply protonated WWCNDGR/NLCNIPCSALLSSDITASVNCAK. The degree signs correspond to water losses, and the lightning bolts correspond to the species subjected to CID. Reproduced from Pilo, A. L.; McLuckey, S. A. *Anal. Chem.* **2016**, 88, 8972–8979 (ref 140). Copyright 2016 American Chemical Society.

Similar to the periodate anion, a suite of reagents derived from persulfate can be used to oxidize peptides in the gas-phase; HSO_5^- generates $[\text{M} + \text{H} + \text{O}]^+$, HS_2O_8^- generates $[\text{M} - \text{H}]^+$ and $[\text{M} + \text{H} + \text{O}]^+$, and $\text{SO}_4^{\cdot-}$ generates $[\text{M}]^{+\cdot}$.¹⁴² Notably, the sulfate radical anion, denoted $\text{SO}_4^{\cdot-}$, is used to generate molecular radical cations. For polypeptides/proteins, CID of radical cations can give rise to the loss of radical side chains from several amino acids, forming dehydroalanine.⁸⁷ Fragmentation of peptide ions containing dehydroalanine has been noted to produce abundant c- and/or z-ions N-terminal to dehydroalanine.¹⁴³ In 2017, Peng et al. introduced dehydroalanine into multiply protonated ubiquitin ions via ion/ion reaction with $\text{SO}_4^{\cdot-}$.¹⁴⁴ The so-called “dehydroalanine effect” upon fragmentation led to site specific c-/z-fragment ions. In addition to the sulfate radical anion, other reagent ions have been described to generate radical containing

analyte ions via ion/ion reaction.^{114,115,145} Whatever the reagent, though, introduction of selective cleavage at dehydroalanine may prove useful in several situations. For example, a database search incorporating dehydroalanine fragmentation could provide enhanced specificity in top-down workflows.

1.5.4 Covalent Chemistry: Bond Formation in the Gas-Phase

A relatively new area of ion/ion reaction research involves the formation of covalent bonds in the gas-phase. While some of the examples above (e.g., oxidation via oxygen transfer) involved the formation of new covalent bonds, not all oxidation examples included the formation of new bonds and were therefore not discussed in the context of covalent chemistry. The first selective covalent bond forming ion/ion reaction was reported in 2009 using 4-formyl-1,3-benzenedisulfonic acid (FBDSA) to generate a Schiff base.¹⁴⁶ Much of the early work surrounding Schiff base formation via ion/ion reactions with FBDSA and the monosulfonic acid derivative, 2-formylbenzenemonosulfonic acid (FBMSA) has been previously reviewed.⁹ However, since that review, there have been several reports surrounding Schiff base formation via ion/ion reaction. In one example, Wang et al. identified a rearrangement of Schiff base modified peptide ions that is 19 Da lower in mass than the protonated or deprotonated peptide, which could be mistaken as a water loss.¹⁴⁷ The Brodbelt group has demonstrated how ion/ion Schiff base formation can be used to increase UVPD efficiency compared to the unmodified peptide ions by binding a UV chromophore to the polypeptide.¹⁶ Lastly, the Brodbelt group has also shown how the electrostatic interactions of the sulfonate group of FBDSA with basic residues can be used to retain the phosphate group upon CID of phosphopeptide cations.¹⁴⁸

In the gas-phase, N-hydroxysuccinimide (NHS) ester-based reagents have been utilized to selectively derivatize nucleophilic sites, such as unprotonated arginine residues and unprotonated primary amines, in the gas-phase. Like Schiff base formation, ion/ion reactions involving NHS ester reagents have been reviewed.⁹ Thereafter, Bu and co-workers explored the potential energy surfaces associated with NHS ester reagents and primary amines or guanidine groups.¹⁴⁹ In that work, they explored two scenarios: (1) a case where the transition state barrier to covalent modification is relatively high and (2) a case where the transition state barrier is low and covalent reaction efficiencies are high. Interestingly, the efficiencies of covalent reactions in the former case could be significantly increased by implementing a long, slow-heating activation step prior

to complex dissociation.¹⁴⁹ In later work, Bu and co-workers examined new reagents that exhibited enhanced reactivity toward amines and guanidines, attributed to the lower transition state barrier using triazole ester based reagent ions.¹⁵⁰ In addition to reactivity toward primary amines and guanidines, the gas-phase reactivity of both NHS esters and triazole esters toward carboxylates has been described in recent years.^{151,152} The latter chemistry has proven useful for the identification of carboxylate groups present in salt bridges and/or zwitterions.¹⁵²

A variety of other ion/ion reactions have been described that result in covalent bond formation including alkyl cation transfer,¹⁵³ 1,3-dipolar cycloaddition (i.e., click chemistry),¹⁵⁴ and reactions with Woodward's reagent K (*wrk*).¹⁵⁵ The equivalent solution-phase chemistry of *wrk* was harnessed to prepare a reagent anion for the C-terminal peptide extension via gas-phase ion/ion reactions.¹⁵⁶ Our group also demonstrated the gas-phase N-terminal peptide extension using NHS reagents.¹⁵⁷ In all cases of gas-phase covalent bond formation, reactions were fast and efficient. Additionally, gas-phase ion/ion reactions offer a degree of selectivity that is not obtained with solution-phase reactions. Specifically, reactants can be isolated using a quadrupole mass filter prior to reaction, and the extent of reaction can be controlled.

1.6 Reagent Ion Selection

Mutual storage of oppositely charged ions can result in competitive reaction processes (e.g., proton transfer versus electron transfer) leading to several different product ions, where the major reaction pathways are dependent on both the analyte ion and reagent ion. For example, ETD sequence coverage is influenced by precursor ion charge,^{60,158–160} size,¹⁶¹ and structure.^{162,163} In another example, sodium cationized arginine residues are reactive toward NHS reagent anions while protonated arginine residues are not reactive.¹⁶⁴ In cases where the analyte ion-type is not readily varied, the partitioning of reaction products is determined by the characteristics of the reagent ion. This latter scenario is of particular interest, as the analyte ion-type is determined by the ionization method and, in most cases, the ionization method is selected based on the approach that leads to the greatest analyte ion yield. Thus, it is important to understand the characteristics of reagent ions that influence favored reaction pathways in order to efficiently transform the analyte ion to a product ion-type of interest.¹⁶⁵ Here, several reagent characteristics as they pertain to different reaction types are discussed.

Electron transfer dissociation has been used extensively due to its ability to generate a high degree of structural information from bio-ions. The ideal electron transfer reagent would exclusively transfer an electron to generate fragment ions with minimal formation of nondissociative product ions. However, depending on the nature of the electron transfer reagent ion, proton transfer can compete with electron transfer.^{89,166,167} In fact, a variety of ETD reagents have been explored and, to the best of our knowledge, every ETD anion has shown some degree of proton transfer.^{23,25,166–168} In recognition of the importance of the reagent in ETD, much attention has been devoted to studying ETD reagents.^{48,89,166–169} The likelihood of observing electron transfer is governed largely by the Franck–Condon overlap between the reagent anion and corresponding neutral and the electron affinity of the corresponding neutral.¹⁶⁷ If these parameters are not optimized, that is to say, if the Franck–Condon overlap is minimal and the electron affinity is relatively large, proton transfer will tend to dominate.¹⁶⁷

As highlighted in the above proton transfer section, there are scenarios where proton transfer is highly desirable. In such experiments there should be little contribution from fragmentation. Generally, fragmentation is not observed following proton transfer from a multiply protonated bio-ion to a singly charged reagent anion. Conversely, protonation of a multiply charged anion via ion/ion reaction has been shown to result in fragmentation and the extent of fragmentation was found to be related to the reaction exothermicity.¹⁷⁰ Fragmentation could be minimized by reducing the proton affinity of the cationic reagent.¹⁷⁰ Additionally, for proton transfer, it is often desirable that upon neutralization of the reagent ion, no long-lived complexes survive. Using the experiment performed by Bush and co-workers as an example, proton transfer was used to increase the accuracy of charge state assignment.⁵³ Here, if the reagent was “sticky” and a long-lived complex was formed, the mass of the reagent would be added to the analyte with each reaction. Of course, if every reaction resulted in adduct formation, the mass of the analyte could be readily deduced, yet not all cases result in this ideal scenario. Adduct formation in proton transfer experiments can be especially problematic if the reaction results in a mixture of product ion types (i.e., proton transfer and adduct formation). This situation has been observed with the iodide anion, I⁻.¹⁷¹ When examining a mixture of product ion types, and without a priori knowledge of the analyte, deducing mass information may be challenging.

Several types of gas-phase ion/ion reactions rely on long-lived complex formation. One example is covalent modification in the gas-phase. Han et al. demonstrated the importance of

forming a long-lived complex during Schiff base modification reactions.¹⁴⁶ The sulfonate group of singly deprotonated FBDSA interacts strongly with the doubly protonated peptide ion. This interaction allows enough time for the imine bond formation to occur. When reagents with carboxylate groups were used, which interact less strongly with cations, proton transfer was the sole process observed likely due to a lower barrier from proton transfer relative to that for Schiff base formation.¹⁴⁶ Sulfonate groups and fixed-charge ammonium ions are widely used to promote long-lived complexes. In addition to a sticky group, reagents for covalent modification require a reactive site that undergoes chemical reactions with the analyte ion.

The above examples discussed characteristics crucial to generating the product ion-type of interest. For instance, an electron transfer experiment cannot be successful if the reagent ion results only in proton transfer. Sometimes, there are cases in which multiple reagents lead to comparable results, and selecting a reagent often comes down to subtle, yet important, differences. Sulfo-benzoyl-1-hydroxy-7-azabenzotriazole ester (HOAt), sulfo-benzoyl-1-hydroxybenzotriazole ester (HOBt), and sulfo-benzoyl-N-hydroxysulfosuccinimide ester (NHS) all undergo acyl substitution reactions at primary amines and guanidine in the gas-phase.¹⁵⁰ Figure 1.10 demonstrates that HOAt and HOBt are more reactive toward amines than their NHS counterpart, yet all reagents result in a covalently modified product ion shaded in yellow. The enhanced reactivity results in less selectivity. Choosing triazole ester reagents versus NHS ester reagents will depend on the experiment. In another example, calcium, strontium, barium, and magnesium phenanthroline complexes can be used to charge invert monounsaturated FAs and identify the site of unsaturation.¹³⁶ However, the magnesium phenanthroline complex was the preferred reagent as it showed the lowest degree of water adduction in the collision cell from adventitious water and therefore resulted in more straightforward product ion spectra.¹³⁶ Prentice et al. demonstrated the use of reagent cluster ions for multiple modifications performed in one ion/ion collision.¹⁷² Similar results could be obtained via sequential ion/ion reactions. The difference between the two, however, is the charge “cost.” Using the reagent cluster ion results in the reduction of the analyte charge by only one charge whereas consecutive reactions require a charge for each encounter, thus limiting the extent to which multiple modifications can be performed. It is clear that for a given analyte ion, the identity of the reagent ion is crucial. Therefore, choosing the correct reagent is key for any experiment.

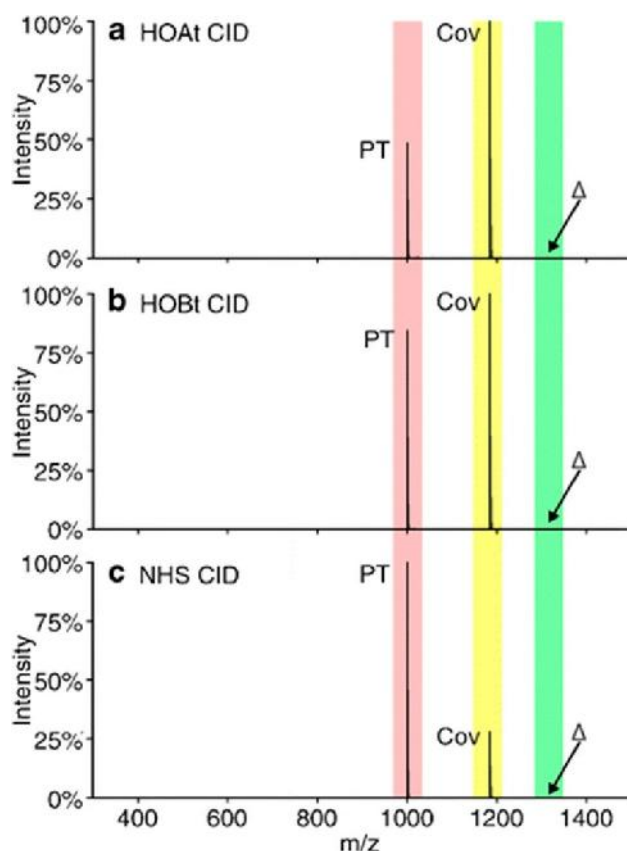


Figure 1.10. Product ion spectrum from CID of the complex formed between doubly protonated KGAGGKGAGGKL and a) HOAt, b) HOBt, and c) NHS. The m/z region corresponding to proton transfer is shaded in red, the m/z region corresponding to covalent modification is shaded in yellow, and the m/z region corresponding to the complex ion is shaded in green. Reprinted by permission from Springer Nature: Journal of the American Society for Mass Spectrometry, Bu, J.; Peng, Z.; Zhao, F.; McLuckey, S.A. *J. Am. Soc. Mass Spectrom.* **2017**, 28, 1254–1261 (ref 150). Copyright 2017.

1.7 Future Outlook

Reactions that are fast and efficient and provide useful information have a long history in analytical chemistry. Over the past 25 years, gas-phase ion/ion reactions have proven to be fast, efficient, and remarkably powerful as means for converting analyte ions into forms that facilitate analysis and/or structural characterization. Single proton transfer applications to simplify mixture analysis, to concentrate charge into a one or a few species, to generate charge states that are not formed directly, etc. were the first to receive extensive attention. Following the discovery of electron transfer reagents by the Hunt group, attention was extended to structural characterization applications analogous to those employing electron capture. The commercial introduction of

products that support ETD experiments greatly expanded the availability of ion/ion reactions to the analytical mass spectrometry community. The commercial availability of instruments that are also optimized for proton transfer ion/ion reactions will likely lead to growing use of charge manipulation applications, particularly in top-down proteomics applications.

Single proton transfer and electron transfer ion/ion reactions are relatively mature in terms of analytical applications. Reactions that require the formation of a long-lived complex, such as charge inversion, metal ion transfer, and selective covalent reaction, on the other hand, are far less explored. However, they illustrate the diversity of reaction types that can be accessed via ion/ion reactions. No instrument vendor currently supports these reaction types as the ion sources generally used to generate proton transfer and electron transfer reagents are not suitable for the generation of reagent ions that lead to these reaction types. Two ESI sources have generally been used to generate the reactants for charge inversion, metal transfer, and covalent reaction. However, commercial platforms that include a separate ion source for mass calibration purposes can, in principle, be adapted for dual-ESI ion/ion reaction experiments, as recently described by Webb et al.³¹ As more laboratories gain access to such capabilities, the range of reactions and applications thereof are likely to grow significantly. As analytical mass spectrometry continues to expand to larger analytes and more complex mixtures, reactions that enhance specificity, simplify mixture analysis, and facilitate structural characterization will find use. Novel gas-phase ion/ion reactions for analytical applications in the future are likely to proceed through long-lived complex formation.

1.8 References

1. Yamashita, M., Fenn, J.B.: Electrospray Ion Source. Another Variation on the Free-Jet Theme. *J. Phys. Chem.* **1984**, 88, 4451-4459.
2. Fenn, J.B., Mann, M., Meng, C.K., Wong, S.F., Whitehouse, C.M.: Electrospray Ionization for Mass Spectrometry of Large Biomolecules. *Science*. **1989**, 246, 64.
3. Loo, R.R.O., Udseth, H.R., Smith, R.D.: Evidence of Charge Inversion in the Reaction of Singly Charged Anions with Multiply Charged Macroions. *J. Phys. Chem.* **1991**, 95, 6412-6415.
4. Ogorzalek Loo, R.R., Udseth, H.R., Smith, R.D.: A New Approach for the Study of Gas-Phase Ion-Ion Reactions Using Electrospray Ionization. *J. Am. Soc. Mass. Spectrom.* **1992**, 3, 695-705.

5. Herron, W.J., Goeringer, D.E., McLuckey, S.A.: Product Ion Charge State Determination via Ion/Ion Proton Transfer Reactions. *Anal. Chem.* **1996**, 68, 257-262.
6. Stephenson, J.L., McLuckey, S.A.: Simplification of Product Ion Spectra Derived from Multiply Charged Parent Ions via Ion/Ion Chemistry. *Anal. Chem.* **1998**, 70, 3533-3544.
7. McLuckey, S.A., Stephenson, J.L.: Ion/Ion Chemistry of High-Mass Multiply Charged Ions. *Mass Spectrom. Rev.* **1998**, 17, 369-407.
8. Pitteri, S.J., McLuckey, S.A.: Recent Developments in the Ion/Ion Chemistry of High-Mass Multiply Charged Ions. *Mass Spectrom. Rev.* **2005**, 24, 931-958.
9. Prentice, B.M., McLuckey, S.A.: Gas-Phase Ion/Ion Reactions of Peptides And Proteins: Acid/Base, Redox, and Covalent Chemistries. *Chem. Commun.* **2013**, 49, 947-965.
10. Xia, Y., McLuckey, S.A.: Evolution of Instrumentation for the Study of Gas-Phase Ion/Ion Chemistry via Mass Spectrometry. *J. Am. Soc. Mass. Spectrom.* **2008**, 19, 173-189.
11. Stutzman, J.R., Crowe, M.C., Alexander, J.N., Bell, B.M., Dunkle, M.N.: Coupling Charge Reduction Mass Spectrometry to Liquid Chromatography for Complex Mixture Analysis. *Anal. Chem.* **2016**, 88, 4130-4139.
12. Campuzano, I.D.G., Schnier, P.D.: Coupling Electrospray Corona Discharge, Charge Reduction and Ion Mobility Mass Spectrometry: From Peptides to Large Macromolecular Protein Complexes. *Int. J. Ion Mobil. Spec.* **2013**, 16, 51-60.
13. Robb, D.B., Brown, J.M., Morris, M., Blades, M.W.: Method of Atmospheric Pressure Charge Stripping for Electrospray Ionization Mass Spectrometry and Its Application for the Analysis of Large Poly(Ethylene Glycol)s. *Anal. Chem.* **2014**, 86, 9644-9652.
14. Scalf, M., Westphall, M.S., Krause, J., Kaufman, S.L., Smith, L.M.: Controlling Charge States of Large Ions. *Science.* **1999**, 283, 194.
15. Scalf, M., Westphall, M.S., Smith, L.M.: Charge Reduction Electrospray Mass Spectrometry. *Anal. Chem.* **2000**, 72, 52-60.
16. Cotham, V.C., Shaw, J.B., Brodbelt, J.S.: High-Throughput Bioconjugation for Enhanced 193 nm Photodissociation via Droplet Phase Initiated Ion/Ion Chemistry Using a Front-End Dual Spray Reactor. *Anal. Chem.* **2015**, 87, 9396-9402.
17. Stutzman, J.R., Bain, R.M., Hagenhoff, S., Woodward, W.H., O'Brien, J.P., Lesniak, M.: Microdroplet Fusion Chemistry for Charge State Reduction of Synthetic Polymers via Bipolar Dual Spray with Anionic Reagents. *J. Am. Soc. Mass. Spectrom.* **2019**, 30, 1742-1749.

18. Zhao, Q., Soyk, M.W., Schieffer, G.M., Fuhrer, K., Gonin, M.M., Houk, R.S., Badman, E.R.: An ion trap-ion mobility-time of flight mass spectrometer with three ion sources for ion/ion reactions. *J. Am. Soc. Mass. Spectrom.* **2009**, 20, 1549-1561.
19. Riley, N.M., Coon, J.J.: The Role of Electron Transfer Dissociation in Modern Proteomics. *Anal. Chem.* **2018**, 90, 40-64.
20. He, M., Jiang, Y., Guo, D., Xiong, X., Fang, X., Xu, W.: Dual-Polarity Ion Trap Mass Spectrometry: Dynamic Monitoring and Controlling Gas-phase Ion-Ion Reactions. *J. Am. Soc. Mass. Spectrom.* **2017**, 28, 1262-1270.
21. Lin, Z., Tan, L., Garimella, S., Li, L., Chen, T.-C., Xu, W., Xia, Y., Ouyang, Z.: Characterization of a DAPI-RIT-DAPI System for Gas-Phase Ion/Molecule and Ion/Ion Reactions. *J. Am. Soc. Mass. Spectrom.* **2014**, 25, 48-56.
22. Campbell, J.L., Hager, J.W.: Creating an Evanescent Ion/Ion Reaction Region Within a Low-Pressure Linear Ion Trap. *Int. J. Mass Spectrom.* **2012**, 323-324, 14-20.
23. Syka, J.E.P., Coon, J.J., Schroeder, M.J., Shabanowitz, J., Hunt, D.F.: Peptide and Protein Sequence Analysis by Electron Transfer Dissociation Mass Spectrometry. *Proc. Natl. Acad. Sci. U.S.A.* **2004**, 101, 9528-9533.
24. McAlister, G.C., Berggren, W.T., Griep-Raming, J., Horning, S., Makarov, A., Phanstiel, D., Stafford, G., Swaney, D.L., Syka, J.E.P., Zabrouskov, V., Coon, J.J.: A Proteomics Grade Electron Transfer Dissociation-Enabled Hybrid Linear Ion Trap-Orbitrap Mass Spectrometer. *J. Proteome Res.* **2008**, 7, 3127-3136.
25. Coon, J.J., Ueberheide, B., Syka, J.E.P., Dryhurst, D.D., Ausio, J., Shabanowitz, J., Hunt, D.F.: Protein Identification Using Sequential Ion/Ion Reactions and Tandem Mass Spectrometry. *Proc. Natl. Acad. Sci. U.S.A.* **2005**, 102, 9463.
26. Earley, L., Anderson, L.C., Bai, D.L., Mullen, C., Syka, J.E.P., English, A.M., Dunyach, J.-J., Stafford, G.C., Shabanowitz, J., Hunt, D.F., Compton, P.D.: Front-End Electron Transfer Dissociation: A New Ionization Source. *Anal. Chem.* **2013**, 85, 8385-8390.
27. Weisbrod, C.R., Kaiser, N.K., Syka, J.E.P., Early, L., Mullen, C., Dunyach, J.-J., English, A.M., Anderson, L.C., Blakney, G.T., Shabanowitz, J., Hendrickson, C.L., Marshall, A.G., Hunt, D.F.: Front-End Electron Transfer Dissociation Coupled to a 21 Tesla FT-ICR Mass Spectrometer for Intact Protein Sequence Analysis. *J. Am. Soc. Mass. Spectrom.* **2017**, 28, 1787-1795.
28. Williams, J.P., Brown, J.M., Campuzano, I., Sadler, P.J.: Identifying Drug Metallation Sites on Peptides Using Electron Transfer Dissociation (ETD), Collision Induced Dissociation (CID) and Ion Mobility-Mass Spectrometry (IM-MS). *Chem. Commun.* **2010**, 46, 5458-5460.

29. Rand, K.D., Pringle, S.D., Morris, M., Engen, J.R., Brown, J.M.: ETD in a Traveling Wave Ion Guide at Tuned Z-Spray Ion Source Conditions Allows for Site-Specific Hydrogen/Deuterium Exchange Measurements. *J. Am. Soc. Mass. Spectrom.* **2011**, 22, 1784.
30. Lermyte, F., Verschueren, T., Brown, J.M., Williams, J.P., Valkenburg, D., Sobott, F.: Characterization of Top-Down ETD in a Travelling-Wave Ion Guide. *Methods.* **2015**, 89, 22-29.
31. Webb, I.K., Morrison, L.J., Brown, J.: Dueling Electrospray Implemented on a Traveling-Wave Ion Mobility/Time-Of-Flight Mass Spectrometer: Towards a Gas-Phase Workbench for Structural Biology. *Int. J. Mass Spectrom.* **2019**, 444, 116177.
32. Garimella, S.V.B., Webb, I.K., Prabhakaran, A., Attah, I.K., Ibrahim, Y.M., Smith, R.D.: Design of a TW-SLIM Module for Dual Polarity Confinement, Transport, and Reactions. *J. Am. Soc. Mass. Spectrom.* **2017**, 28, 1442-1449.
33. Lee, K.W., Eakins, G.S., Carlsen, M.S., McLuckey, S.A.: Increasing the Upper Mass/Charge Limit of a Quadrupole Ion Trap for Ion/Ion Reaction Product Analysis via Waveform Switching. *J. Am. Soc. Mass. Spectrom.* **2019**, 30, 1126-1132.
34. Rosati, S., Rose, R.J., Thompson, N.J., van Duijn, E., Damoc, E., Denisov, E., Makarov, A., Heck, A.J.R.: Exploring an Orbitrap Analyzer for the Characterization of Intact Antibodies by Native Mass Spectrometry. *Angew. Chem. Int. Ed.* **2012**, 51, 12992-12996.
35. Belov, M.E., Damoc, E., Denisov, E., Compton, P.D., Horning, S., Makarov, A.A., Kelleher, N.L.: From Protein Complexes to Subunit Backbone Fragments: A Multi-stage Approach to Native Mass Spectrometry. *Anal. Chem.* **2013**, 85, 11163-11173.
36. Snijder, J., van de Waterbeemd, M., Damoc, E., Denisov, E., Grinfeld, D., Bennett, A., Agbandje-McKenna, M., Makarov, A., Heck, A.J.R.: Defining the Stoichiometry and Cargo Load of Viral and Bacterial Nanoparticles by Orbitrap Mass Spectrometry. *J. Am. Chem. Soc.* **2014**, 136, 7295-7299.
37. Ben-Nissan, G., Belov, M.E., Morgenstern, D., Levin, Y., Dym, O., Arkind, G., Lipson, C., Makarov, A.A., Sharon, M.: Triple-Stage Mass Spectrometry Unravels the Heterogeneity of an Endogenous Protein Complex. *Anal. Chem.* **2017**, 89, 4708-4715.
38. van de Waterbeemd, M., Fort, K.L., Boll, D., Reinhardt-Szyba, M., Routh, A., Makarov, A., Heck, A.J.R.: High-Fidelity Mass Analysis Unveils Heterogeneity in Intact Ribosomal Particles. *Nature Methods.* **2017**, 14, 283.
39. Fort, K.L., van de Waterbeemd, M., Boll, D., Reinhardt-Szyba, M., Belov, M.E., Sasaki, E., Zschoche, R., Hilvert, D., Makarov, A.A., Heck, A.J.R.: Expanding the Structural Analysis Capabilities on an Orbitrap-Based Mass Spectrometer For Large Macromolecular Complexes. *Analyst.* **2018**, 143, 100-105.

40. Stephenson, J.L., McLuckey, S.A.: Ion/Ion Proton Transfer Reactions for Protein Mixture Analysis. *Anal. Chem.* **1996**, 68, 4026-4032.
41. Reid, G.E., Shang, H., Hogan, J.M., Lee, G.U., McLuckey, S.A.: Gas-Phase Concentration, Purification, and Identification of Whole Proteins from Complex Mixtures. *J. Am. Chem. Soc.* **2002**, 124, 7353-7362.
42. He, M., Reid, G.E., Shang, H., Lee, G.U., McLuckey, S.A.: Dissociation of Multiple Protein Ion Charge States Following a Single Gas-Phase Purification and Concentration Procedure. *Anal. Chem.* **2002**, 74, 4653-4661.
43. Amunugama, R., Hogan, J.M., Newton, K.A., McLuckey, S.A.: Whole Protein Dissociation in a Quadrupole Ion Trap: Identification of an a Priori Unknown Modified Protein. *Anal. Chem.* **2004**, 76, 720-727.
44. Liu, J., Chrisman, P.A., Erickson, D.E., McLuckey, S.A.: Relative Information Content and Top-Down Proteomics by Mass Spectrometry: Utility of Ion/Ion Proton-Transfer Reactions in Electrospray-Based Approaches. *Anal. Chem.* **2007**, 79, 1073-1081.
45. Chi, A., Bai, D.L., Geer, L.Y., Shabanowitz, J., Hunt, D.F.: Analysis of Intact Proteins on a Chromatographic Time Scale by Electron Transfer Dissociation Tandem Mass Spectrometry. *Int. J. Mass Spectrom.* **2007**, 259, 197-203.
46. Drabik, A., Bodzon-Kulakowska, A., Suder, P.: Application of the ETD/PTR Reactions In Top-Down Proteomics as a Faster Alternative to Bottom-Up NanoLC-MS/MS Protein Identification. *J. Mass Spectrom.* **2012**, 47, 1347-1352.
47. Phanstiel, D., Brumbaugh, J., Berggren, W.T., Conard, K., Feng, X., Levenstein, M.E., McAlister, G.C., Thomson, J.A., Coon, J.J.: Mass Spectrometry Identifies and Quantifies 74 Unique Histone H4 Isoforms in Differentiating Human Embryonic Stem Cells. *Proc. Natl. Acad. Sci.* **2008**, 105, 4093.
48. Hartmer, R., Kaplan, D.A., Gebhardt, C.R., Ledertheil, T., Brekenfeld, A.: Multiple Ion/Ion Reactions in the 3D Ion Trap: Selective Reagent Anion Production for ETD and PTR From a Single Compound. *Int. J. Mass Spectrom.* **2008**, 276, 82-90.
49. Anderson, L.C., English, A.M., Wang, W.-H., Bai, D.L., Shabanowitz, J., Hunt, D.F.: Protein Derivatization and Sequential Ion/Ion Reactions to Enhance Sequence Coverage Produced by Electron Transfer Dissociation Mass Spectrometry. *Int. J. Mass Spectrom.* **2015**, 377, 617-624.
50. Zhang, L., English, A.M., Bai, D.L., Ugrin, S.A., Shabanowitz, J., Ross, M.M., Hunt, D.F., Wang, W.-H.: Analysis of Monoclonal Antibody Sequence and Post-Translational Modifications by Time-Controlled Proteolysis and Tandem Mass Spectrometry. *Mol. Cell. Proteomics.* **2016**, 15, 1479.

51. Anderson, L.C., Karch, K.R., Ugrin, S.A., Coradin, M., English, A.M., Sidoli, S., Shabanowitz, J., Garcia, B.A., Hunt, D.F.: Analyses of Histone Proteoforms Using Front-end Electron Transfer Dissociation-enabled Orbitrap Instruments. *Mol. Cell. Proteomics*. **2016**, 15, 975.
52. Bhattacharjee, S., Liu, W., Wang, W.-H., Weitzhandler, I., Li, X., Qi, Y., Liu, J., Pang, Y., Hunt, D.F., Chilkoti, A.: Site-Specific Zwitterionic Polymer Conjugates of a Protein Have Long Plasma Circulation. *ChemBioChem*. **2015**, 16, 2451-2455.
53. Laszlo, K.J., Bush, M.F.: Analysis of Native-Like Proteins and Protein Complexes Using Cation to Anion Proton Transfer Reactions (CAPTR). *J. Am. Soc. Mass. Spectrom.* **2015**, 26, 2152-2161.
54. Wells, J.M., Stephenson, J.L., McLuckey, S.A.: Charge Dependence of Protonated Insulin Decompositions. *Int. J. Mass Spectrom.* **2000**, 203, A1-A9.
55. Reid, G.E., Wu, J., Chrisman, P.A., Wells, J.M., McLuckey, S.A.: Charge-State-Dependent Sequence Analysis of Protonated Ubiquitin Ions via Ion Trap Tandem Mass Spectrometry. *Anal. Chem.* **2001**, 73, 3274-3281.
56. Wells, J.M., Reid, G.E., Engel, B.J., Pan, P., McLuckey, S.A.: Dissociation Reactions of Gaseous Ferri-, Ferri-, and Apo-Cytochrome c Ions. *J. Am. Soc. Mass. Spectrom.* **2001**, 12, 873-876.
57. Newton, K.A., Chrisman, P.A., Reid, G.E., Wells, J.M., McLuckey, S.A.: Gaseous Apomyoglobin Ion Dissociation in a Quadrupole Ion Trap: $[M + 2H]^{2+}$ - $[M + 21H]^{21+}$. *Int. J. Mass Spectrom.* **2001**, 212, 359-376.
58. Engel, B.J., Pan, P., Reid, G.E., Wells, J.M., McLuckey, S.A.: Charge State Dependent Fragmentation of Gaseous Protein Ions in a Quadrupole Ion Trap: Bovine Ferri-, Ferro-, and Apo-Cytochrome c. *Int. J. Mass Spectrom.* **2002**, 219, 171-187.
59. Hogan, J.M., McLuckey, S.A.: Charge State Dependent Collision-Induced Dissociation of Native and Reduced Porcine Elastase. *J. Mass Spectrom.* **2003**, 38, 245-256.
60. Rožman, M., Gaskell, S.J.: Charge State Dependent Top-Down Characterisation Using Electron Transfer Dissociation. *Rapid Commun. Mass Spectrom.* **2012**, 26, 282-286.
61. Holden, D.D., McGee, W.M., Brodbelt, J.S.: Integration of Ultraviolet Photodissociation with Proton Transfer Reactions and Ion Parking for Analysis of Intact Proteins. *Anal. Chem.* **2016**, 88, 1008-1016.
62. Holden, D.D., Brodbelt, J.S.: Ultraviolet Photodissociation of Native Proteins Following Proton Transfer Reactions in the Gas Phase. *Anal. Chem.* **2016**, 88, 12354-12362.

63. Bashyal, A., Sanders, J.D., Holden, D.D., Brodbelt, J.S.: Top-Down Analysis of Proteins in Low Charge States. *J. Am. Soc. Mass. Spectrom.* **2019**, 30, 704-717.
64. Wenger, C.D., Lee, M.V., Hebert, A.S., McAlister, G.C., Phanstiel, D.H., Westphall, M.S., Coon, J.J.: Gas-Phase Purification Enables Accurate, Multiplexed Proteome Quantification with Isobaric Tagging. *Nature Methods.* **2011**, 8, 933.
65. Vincent, C.E., Rensvold, J.W., Westphall, M.S., Pagliarini, D.J., Coon, J.J.: Automated Gas-Phase Purification for Accurate, Multiplexed Quantification on a Stand-Alone Ion-Trap Mass Spectrometer. *Anal. Chem.* **2013**, 85, 2079-2086.
66. McLuckey, S.A., Stephenson, J.L., Asano, K.G.: Ion/Ion Proton-Transfer Kinetics: Implications for Analysis of Ions Derived from Electrospray of Protein Mixtures. *Anal. Chem.* **1998**, 70, 1198-1202.
67. McLuckey, S.A., Reid, G.E., Wells, J.M.: Ion Parking during Ion/Ion Reactions in Electrodynamic Ion Traps. *Anal. Chem.* **2002**, 74, 336-346.
68. Foreman, D.J., Dziekonski, E.T., McLuckey, S.A.: Maximizing Selective Cleavages at Aspartic Acid and Proline Residues for the Identification of Intact Proteins. *J. Am. Soc. Mass. Spectrom.* **2019**, 30, 34-44.
69. Chrisman, P.A., Pitteri, S.J., McLuckey, S.A.: Parallel Ion Parking: Improving Conversion of Parents to First-Generation Products in Electron Transfer Dissociation. *Anal. Chem.* **2005**, 77, 3411-3414.
70. Chrisman, P.A., Pitteri, S.J., McLuckey, S.A.: Parallel Ion Parking of Protein Mixtures. *Anal. Chem.* **2006**, 78, 310-316.
71. Ugrin, S.A., English, A.M., Syka, J.E.P., Bai, D.L., Anderson, L.C., Shabanowitz, J., Hunt, D.F.: Ion-Ion Proton Transfer and Parallel Ion Parking for the Analysis of Mixtures of Intact Proteins on a Modified Orbitrap Mass Analyzer. *J. Am. Soc. Mass. Spectrom.*, **2019**, 30, 2163-2173.
72. Campbell, J.L., Le Blanc, J.C.Y.: Targeted Ion Parking for the Quantitation of Biotherapeutic Proteins: Concepts and Preliminary Data. *J. Am. Soc. Mass. Spectrom.* **2010**, 21, 2011-2022.
73. Frey, B.L., Krusemark, C.J., Ledvina, A.R., Coon, J.J., Belshaw, P.J., Smith, L.M.: Ion-Ion Reactions with Fixed-Charge Modified Proteins to Produce Ions in a Single, Very High Charge State. *Int. J. Mass Spectrom.* **2008**, 276, 136-143.
74. Heuvel, R.H.H.v.d., Heck, A.J.R.: Native Protein Mass Spectrometry: From Intact Oligomers to Functional Machineries. *Curr. Opin. Chem. Biol.* **2004**, 8, 519-526.

75. Sharon, M., Robinson, C.V.: The Role of Mass Spectrometry in Structure Elucidation of Dynamic Protein Complexes. *Annu. Rev. Biochem.* **2007**, 76, 167-193.
76. Sharon, M.: How Far Can We Go with Structural Mass Spectrometry of Protein Complexes? *J. Am. Soc. Mass. Spectrom.* **2010**, 21, 487-500.
77. Leney, A.C., Heck, A.J.R.: Native Mass Spectrometry: What is in the Name? *J. Am. Soc. Mass. Spectrom.* **2017**, 28, 5-13.
78. Zhao, Q., Schieffer, G.M., Soyk, M.W., Anderson, T.J., Houk, R.S., Badman, E.R.: Effects of Ion/Ion Proton Transfer Reactions on Conformation of Gas-Phase Cytochrome c Ions. *J. Am. Soc. Mass. Spectrom.* **2010**, 21, 1208-1217.
79. Laszlo, K.J., Munger, E.B., Bush, M.F.: Folding of Protein Ions in the Gas Phase after Cation-to-Anion Proton-Transfer Reactions. *J. Am. Chem. Soc.* **2016**, 138, 9581-9588.
80. Laszlo, K.J., Buckner, J.H., Munger, E.B., Bush, M.F.: Native-Like and Denatured Cytochrome c Ions Yield Cation-to-Anion Proton Transfer Reaction Products with Similar Collision Cross-Sections. *J. Am. Soc. Mass. Spectrom.* **2017**, 28, 1382-1391.
81. Laszlo, K.J., Bush, M.F.: Interpreting the Collision Cross Sections of Native-like Protein Ions: Insights from Cation-to-Anion Proton-Transfer Reactions. *Anal. Chem.* **2017**, 89, 7607-7614.
82. Laszlo, K.J., Munger, E.B., Bush, M.F.: Effects of Solution Structure on the Folding of Lysozyme Ions in the Gas Phase. *J. Phys. Chem. B.* **2017**, 121, 2759-2766.
83. Gadzuk-Shea, M.M., Bush, M.F.: Effects of Charge State on the Structures of Serum Albumin Ions in the Gas Phase: Insights from Cation-to-Anion Proton-Transfer Reactions, Ion Mobility, and Mass Spectrometry. *J. Phys. Chem. B.* **2018**, 122, 9947-9955.
84. Lermyte, F., Łcki, M.K., Valkenborg, D., Gambin, A., Sobott, F.: Conformational Space and Stability of ETD Charge Reduction Products of Ubiquitin. *J. Am. Soc. Mass. Spectrom.* **2017**, 28, 69-76.
85. Kim, M.-S., Pandey, A.: Electron Transfer Dissociation Mass Spectrometry in Proteomics. *Proteomics.* **2012**, 12, 530-542.
86. Zhurov, K.O., Fornelli, L., Wodrich, M.D., Laskay, U.A., Tsybin, Y.O.: Principles of Electron Capture and Transfer Dissociation Mass Spectrometry Applied to Peptide and Protein Structure Analysis. *Chem. Soc. Rev.* **2013**, 42, 5014-5030.
87. Turek, F., Julian, R.R.: Peptide Radicals and Cation Radicals in the Gas Phase. *Chem. Rev.* **2013**, 113, 6691-6733.

88. Qi, Y., Volmer, D.A.: Electron-Based Fragmentation Methods in Mass Spectrometry: An Overview. *Mass Spectrom. Rev.* **2017**, 36, 4-15.
89. Lermyte, F., Łcki, M.K., Valkenborg, D., Baggerman, G., Gambin, A., Sobott, F.: Understanding Reaction Pathways in Top-Down ETD by Dissecting Isotope Distributions: A Mammoth Task. *Int. J. Mass Spectrom.* **2015**, 390, 146-154.
90. Abzalimov, R.R., Kaltashov, I.A.: Electrospray Ionization Mass Spectrometry of Highly Heterogeneous Protein Systems: Protein Ion Charge State Assignment via Incomplete Charge Reduction. *Anal. Chem.* **2010**, 82, 7523-7526.
91. Zhao, Y., Abzalimov, R.R., Kaltashov, I.A.: Interactions of Intact Unfractionated Heparin with Its Client Proteins Can Be Probed Directly Using Native Electrospray Ionization Mass Spectrometry. *Anal. Chem.* **2016**, 88, 1711-1718.
92. Muneeruddin, K., Bobst, C.E., Frenkel, R., Houde, D., Turyan, I., Sobic, Z., Kaltashov, I.A.: Characterization of a Pegylated Protein Therapeutic by Ion Exchange Chromatography with On-Line Detection by Native ESI MS and MS/MS. *Analyst.* **2017**, 142, 336-344.
93. Minsky, B.B., Abzalimov, R.R., Niu, C., Zhao, Y., Kirsch, Z., Dubin, P.L., Savinov, S.N., Kaltashov, I.A.: Mass Spectrometry Reveals a Multifaceted Role of Glycosaminoglycan Chains in Factor Xa Inactivation by Antithrombin. *Biochemistry.* **2018**, 57, 4880-4890.
94. Wang, G., Johnson, A.J., Kaltashov, I.A.: Evaluation of Electrospray Ionization Mass Spectrometry as a Tool for Characterization of Small Soluble Protein Aggregates. *Anal. Chem.* **2012**, 84, 1718-1724.
95. Abzalimov, R.R., Bobst, C.E., Salinas, P.A., Savickas, P., Thomas, J.J., Kaltashov, I.A.: Studies of pH-Dependent Self-Association of a Recombinant Form of Arylsulfatase A with Electrospray Ionization Mass Spectrometry and Size-Exclusion Chromatography. *Anal. Chem.* **2013**, 85, 1591-1596.
96. Lermyte, F., Williams, J.P., Brown, J.M., Martin, E.M., Sobott, F.: Extensive Charge Reduction and Dissociation of Intact Protein Complexes Following Electron Transfer on a Quadrupole-Ion Mobility-Time-of-Flight MS. *J. Am. Soc. Mass. Spectrom.* **2015**, 26, 1068-1076.
97. Jhingree, J.R., Beveridge, R., Dickinson, E.R., Williams, J.P., Brown, J.M., Bellina, B., Barran, P.E.: Electron Transfer with no Dissociation Ion Mobility–Mass Spectrometry (ETnoD IM-MS). The Effect of Charge Reduction on Protein Conformation. *Int. J. Mass Spectrom.* **2017**, 413, 43-51.

98. Jhingree, J.R., Bellina, B., Pacholarz, K.J., Barran, P.E.: Charge Mediated Compaction and Rearrangement of Gas-Phase Proteins: A Case Study Considering Two Proteins at Opposing Ends of the Structure-Disorder Continuum. *J. Am. Soc. Mass. Spectrom.* **2017**, 28, 1450-1461.
99. Parker, M.L., Gronert, S.: Investigating Reduced Metal Species via Sequential Ion/Ion and Ion/Molecule Reactions: The Reactions of Transition Metal Phenanthrolines with Allyl Iodide. *Int. J. Mass Spectrom.* **2017**, 418, 73-78.
100. Munshi, M.U., Craig, S.M., Berden, G., Martens, J., DeBlase, A.F., Foreman, D.J., McLuckey, S.A., Oomens, J., Johnson, M.A.: Preparation of Labile Ni+(cyclam) Cations in the Gas Phase Using Electron-Transfer Reduction through Ion–Ion Recombination in an Ion Trap and Structural Characterization with Vibrational Spectroscopy. *J. Phys. Chem. Lett.* **2017**, 8, 5047-5052.
101. Munshi, M.U., Martens, J., Berden, G., Oomens, J.: Gas-Phase Infrared Ion Spectroscopy Characterization of Cu(II/I)Cyclam and Cu(II/I)2,2 -Bipyridine Redox Pairs. *J. Phys. Chem. A* **2019**, 123, 4149-4157.
102. Hoffmann, W.D., Jackson, G.P.: Charge Transfer Dissociation (CTD) Mass Spectrometry of Peptide Cations Using Kiloelectronvolt Helium Cations. *J. Am. Soc. Mass. Spectrom.* **2014**, 25, 1939-1943.
103. Li, P., Kreft, I., Jackson, G.P.: Top-Down Charge Transfer Dissociation (CTD) of Gas-Phase Insulin: Evidence of a One-Step, Two-Electron Oxidation Mechanism. *J. Am. Soc. Mass. Spectrom.* **2018**, 29, 284-296.
104. Li, P., Jackson, G.P.: Charge Transfer Dissociation (CTD) Mass Spectrometry of Peptide Cations: Study of Charge State Effects and Side-Chain Losses. *J. Am. Soc. Mass. Spectrom.* **2017**, 28, 1271-1281.
105. Li, P., Jackson, G.P.: Charge Transfer Dissociation of Phosphocholines: Gas-Phase Ion/Ion Reactions between Helium Cations and Phospholipid Cations. *J. Mass Spectrom.* **2017**, 52, 271-282.
106. Ropartz, D., Li, P., Fanuel, M., Giuliani, A., Rogniaux, H., Jackson, G.P.: Charge Transfer Dissociation of Complex Oligosaccharides: Comparison with Collision-Induced Dissociation and Extreme Ultraviolet Dissociative Photoionization. *J. Am. Soc. Mass. Spectrom.* **2016**, 27, 1614-1619.
107. Ropartz, D., Li, P., Jackson, G.P., Rogniaux, H.: Negative Polarity Helium Charge Transfer Dissociation Tandem Mass Spectrometry: Radical-Initiated Fragmentation of Complex Polysulfated Anions. *Anal. Chem.* **2017**, 89, 2017, 3824-3828.
108. Wells, J.M., Chrisman, P.A., McLuckey, S.A.: Formation and Characterization of Protein–Protein Complexes in Vacuo. *J. Am. Chem. Soc.* **2003**, 125, 7238-7249.

109. Bates, D.R., Morgan, W.L.: New Recombination Mechanism: Tidal Termolecular Ionic Recombination. *Phys. Rev. Lett.* **1990**, 64, 2258-2260.
110. Newton, K.A., McLuckey, S.A.: Gas-Phase Peptide/Protein Cationizing Agent Switching via Ion/Ion Reactions. *J. Am. Chem. Soc.* **2003**, 125, 12404-12405.
111. Newton, K.A., McLuckey, S.A.: Generation and Manipulation of Sodium Cationized Peptides in the Gas Phase. *J. Am. Soc. Mass. Spectrom.* **2004**, 15, 607-615.
112. Newton, K.A., Amunugama, R., McLuckey, S.A.: Gas-Phase Ion/Ion Reactions of Multiply Protonated Polypeptides with Metal Containing Anions. *J. Phys. Chem. A.* **2005**, 109, 3608-3616.
113. Hodges, B.D.M., Liang, X., McLuckey, S.A.: Generation of Di-Lithiated Peptide Ions from Multiply Protonated Peptides via Ion/Ion Reactions. *Int. J. Mass Spectrom.* **2007**, 267, 183-189.
114. Barlow, C.K., Hodges, B.D.M., Xia, Y., O'Hair, R.A.J., McLuckey, S.A.: Gas-Phase Ion/Ion Reactions of Transition Metal Complex Cations with Multiply Charged Oligodeoxynucleotide Anions. *J. Am. Soc. Mass. Spectrom.* **2008**, 19, 281-293.
115. Crizer, D.M., Xia, Y., McLuckey, S.A.: Transition Metal Complex Cations as Reagents for Gas-Phase Transformation of Multiply Deprotonated Polypeptides. *J. Am. Soc. Mass. Spectrom.* **2009**, 20, 1718-1722.
116. Gunawardena, H.P., O'Hair, R.A.J., McLuckey, S.A.: Selective Disulfide Bond Cleavage in Gold(I) Cationized Polypeptide Ions Formed via Gas-Phase Ion/Ion Cation Switching. *J. Proteome Res.* **2006**, 5, 2087-2092.
117. Mentinova, M., Han, H., McLuckey, S.A.: Dissociation of Disulfide-Intact Somatostatin Ions: The Roles of Ion Type and Dissociation Method. *Rapid Commun. Mass Spectrom.* **2009**, 23, 2647-2655.
118. Mentinova, M., McLuckey, S.A.: Cleavage of Multiple Disulfide Bonds in Insulin via Gold Cationization and Collision-Induced Dissociation. *Int. J. Mass Spectrom.* **2011**, 308, 133-136.
119. Foreman, D.J., Betancourt, S.K., Pilo, A.L., McLuckey, S.A.: Novel Peptide Ion Chemistry Associated with Gold (I) Cationization: Preferential Cleavage at Lysine Residues. *Int. J. Mass Spectrom.* **2018**, 427, 114-122.
120. Foreman, D.J., Lawler, J.T., Niedrauer, M.L., Hostetler, M.A., McLuckey, S.A.: Gold(I) Cationization Promotes Ring Opening in Lysine-Containing Cyclic Peptides. *J. Am. Soc. Mass. Spectrom.*, **2019**, 30, 1914-1922.

121. Newton, K.A., He, M., Amunugama, R., McLuckey, S.A.: Selective Cation Removal from Gaseous Polypeptide Ions: Proton vs. Sodium Ion Abstraction via Ion/Ion Reactions. *Phys. Chem. Chem. Phys.* **2004**, 6, 2710-2717.
122. Luongo, C.A., Bu, J., Burke, N.L., Gilbert, J.D., Prentice, B.M., Cummings, S., Reed, C.A., McLuckey, S.A.: Selective Removal of Alkali Metal Cations from Multiply-Charged Ions via Gas-Phase Ion/Ion Reactions Using Weakly Coordinating Anions. *J. Am. Soc. Mass. Spectrom.* **2015**, 26, 404-414.
123. Betancourt, S.K., Pilo, A.L., Bu, J., McLuckey, S.A.: Simplification of Electrospray Mass Spectra of Polysorbate 80 via Cation Transfer to Carborane Anions. *J. Mass Spectrom.* **2016**, 51, 453-458.
124. Rojas-Betancourt, S., Stutzman, J.R., Londry, F.A., Blanksby, S.J., McLuckey, S.A.: Gas-Phase Chemical Separation of Phosphatidylcholine and Phosphatidylethanolamine Cations via Charge Inversion Ion/Ion Chemistry. *Anal. Chem.* **2015**, 87, 11255-11262.
125. He, M., Emory, J.F., McLuckey, S.A.: Reagent Anions for Charge Inversion of Polypeptide/Protein Cations in the Gas Phase. *Anal. Chem.* **2005**, 77, 3173-3182.
126. Emory, J.F., McLuckey, S.A.: Charge Inversion of Polypeptide Anions using Protein and Dendrimer Cations as Charge Inversion Reagents. *Int. J. Mass Spectrom.* **2008**, 276, 102-109.
127. Gunawardena, H.P., Emory, J.F., McLuckey, S.A.: Phosphopeptide Anion Characterization via Sequential Charge Inversion and Electron-Transfer Dissociation. *Anal. Chem.* **2006**, 78, 3788-3793.
128. Shih, M., McLuckey, S.A.: Ion/Ion Charge Inversion/Attachment in Conjunction with Dipolar DC Collisional Activation as a Selective Screen for Sulfo- and Phosphopeptides. *Int. J. Mass Spectrom.* **2019**, 444, 116181.
129. Hassell, K.M., LeBlanc, Y., McLuckey, S.A.: Conversion of Multiple Analyte Cation Types to a Single Analyte Anion Type via Ion/Ion Charge Inversion. *Analyst.* **2009**, 134, 2262-2266.
130. Hassell, K.M., LeBlanc, Y.C., McLuckey, S.A.: Chemical Noise Reduction via Mass Spectrometry and Ion/Ion Charge Inversion: Amino Acids. *Anal. Chem.* **2011**, 83, 3252-3255.
131. He, M., McLuckey, S.A.: Two Ion/Ion Charge Inversion Steps To Form a Doubly Protonated Peptide from a Singly Protonated Peptide in the Gas Phase. *J. Am. Chem. Soc.* **2003**, 125, 7756-7757.
132. He, M., McLuckey, S.A.: Increasing the Negative Charge of a Macroanion in the Gas Phase via Sequential Charge Inversion Reactions. *Anal. Chem.* **2004**, 76, 4189-4192.

133. Stutzman, J.R., Blanksby, S.J., McLuckey, S.A.: Gas-Phase Transformation of Phosphatidylcholine Cations to Structurally Informative Anions via Ion/Ion Chemistry. *Anal. Chem.* **2013**, 85, 3752-3757.
134. Betancourt, S.K., Canez, C.R., Shields, S.W.J., Manthorpe, J.M., Smith, J.C., McLuckey, S.A.: Trimethylation Enhancement Using ¹³C-Diazomethane: Gas-Phase Charge Inversion of Modified Phospholipid Cations for Enhanced Structural Characterization. *Anal. Chem.* **2017**, 89, 9452-9458.
135. Franklin, E.T., Betancourt, S.K., Randolph, C.E., McLuckey, S.A., Xia, Y.: In-Depth Structural Characterization of Phospholipids by Pairing Solution Photochemical Reaction with Charge Inversion Ion/Ion Chemistry. *Anal. Bioanal. Chem.* **2019**, 411, 4739-4749.
136. Randolph, C.E., Foreman, D.J., Betancourt, S.K., Blanksby, S.J., McLuckey, S.A.: Gas-Phase Ion/Ion Reactions Involving Tris-Phenanthroline Alkaline Earth Metal Complexes as Charge Inversion Reagents for the Identification of Fatty Acids. *Anal. Chem.* **2018**, 90, 12861-12869.
137. Randolph, C.E., Foreman, D.J., Blanksby, S.J., McLuckey, S.A.: Generating Fatty Acid Profiles in the Gas Phase: Fatty Acid Identification and Relative Quantitation Using Ion/Ion Charge Inversion Chemistry. *Anal. Chem.* **2019**, 91, 9032-9040.
138. Pilo, A.L., McLuckey, S.A.: Oxidation of Methionine Residues in Polypeptide Ions Via Gas-Phase Ion/Ion Chemistry. *J. Am. Soc. Mass. Spectrom.* **2014**, 25, 1049-1057.
139. Pilo, A.L., Zhao, F., McLuckey, S.A.: Selective Gas-Phase Oxidation and Localization of Alkylated Cysteine Residues in Polypeptide Ions via Ion/Ion Chemistry. *J. Proteome Res.* **2016**, 15, 3139-3146.
140. Pilo, A.L., McLuckey, S.A.: Selective Gas-Phase Ion/Ion Reactions: Enabling Disulfide Mapping via Oxidation and Cleavage of Disulfide Bonds in Intermolecularly-Linked Polypeptide Ions. *Anal. Chem.* **2016**, 88, 8972-8979.
141. Pilo, A.L., Bu, J., McLuckey, S.A.: Gas-Phase Oxidation of Neutral Basic Residues in Polypeptide Cations by Periodate. *J. Am. Soc. Mass. Spectrom.* **2016**, 27, 1979-1988.
142. Pilo, A.L., Bu, J., McLuckey, S.A.: Transformation of [M+2H]²⁺ Peptide Cations to [M – H]⁺, [M+H+O]⁺, and M+• Cations via Ion/Ion Reactions: Reagent Anions Derived from Persulfate. *J. Am. Soc. Mass. Spectrom.* **2015**, 26, 1103-1114.
143. Pilo, A.L., Peng, Z., McLuckey, S.A.: The Dehydroalanine Effect in the Fragmentation of Ions Derived from Polypeptides. *J. Mass Spectrom.* **2016**, 51, 857-866.
144. Peng, Z., Bu, J., McLuckey, S.A.: The Generation of Dehydroalanine Residues in Protonated Polypeptides: Ion/Ion Reactions for Introducing Selective Cleavages. *J. Am. Soc. Mass. Spectrom.* **2017**, 28, 1765-1774.

145. Gilbert, J.D., Fisher, C.M., Bu, J., Prentice, B.M., Redwine, J.G., McLuckey, S.A.: Strategies for Generating Peptide Radical Cations via Ion/Ion Reactions. *J. Mass Spectrom.* **2015**, 50, 418-426.
146. Han, H., McLuckey, S.A.: Selective Covalent Bond Formation in Polypeptide Ions via Gas-Phase Ion/Ion Reaction Chemistry. *J. Am. Chem. Soc.* **2009**, 131, 12884-12885.
147. Wang, N., Pilo, A.L., Zhao, F., Bu, J., McLuckey, S.A.: Gas-Phase Rearrangement Reaction of Schiff-Base-Modified Peptide Ions. *Rapid Commun. Mass Spectrom.* **2018**, 32, 2166-2173.
148. Cotham, V.C., McGee, W.M., Brodbelt, J.S.: Modulation of Phosphopeptide Fragmentation via Dual Spray Ion/Ion Reactions Using a Sulfonate-Incorporating Reagent. *Anal. Chem.* **2016**, 88, 8158-8165.
149. Bu, J., Fisher, C.M., Gilbert, J.D., Prentice, B.M., McLuckey, S.A.: Selective Covalent Chemistry via Gas-Phase Ion/ion Reactions: An Exploration of the Energy Surfaces Associated with N-Hydroxysuccinimide Ester Reagents and Primary Amines and Guanidine Groups. *J. Am. Soc. Mass. Spectrom.* **2016**, 27, 1089-1098.
150. Bu, J., Peng, Z., Zhao, F., McLuckey, S.A.: Enhanced Reactivity in Nucleophilic Acyl Substitution Ion/Ion Reactions Using Triazole-Ester Reagents. *J. Am. Soc. Mass. Spectrom.* **2017**, 28, 1254-1261.
151. Peng, Z., McGee, W.M., Bu, J., Barefoot, N.Z., McLuckey, S.A.: Gas Phase Reactivity of Carboxylates with N-Hydroxysuccinimide Esters. *J. Am. Soc. Mass. Spectrom.* **2015**, 26, 174-180.
152. Pitts-McCoy, A.M., Harrilal, C.P., McLuckey, S.A.: Gas-Phase Ion/Ion Chemistry as a Probe for the Presence of Carboxylate Groups in Polypeptide Cations. *J. Am. Soc. Mass. Spectrom.* **2019**, 30, 329-338.
153. Gilbert, J.D., Prentice, B.M., McLuckey, S.A.: Ion/Ion Reactions with “Onium” Reagents: An Approach for the Gas-phase Transfer of Organic Cations to Multiply-Charged Anions. *J. Am. Soc. Mass. Spectrom.* **2015**, 26, 818-825.
154. Bu, J., Pilo, A.L., McLuckey, S.A.: Gas Phase Click Chemistry via Ion/Ion Reactions. *Int. J. Mass Spectrom.* **2015**, 390, 118-123.
155. Peng, Z., Pilo, A.L., Luongo, C.A., McLuckey, S.A.: Gas-Phase Amidation of Carboxylic Acids with Woodward’s Reagent K Ions. *J. Am. Soc. Mass. Spectrom.* **2015**, 26, 1686-1694.
156. Peng, Z., McLuckey, S.A.: C-Terminal Peptide Extension via Gas-Phase Ion/Ion Reactions. *Int. J. Mass Spectrom.* **2015**, 391, 17-23.

157. McGee, W.M., McLuckey, S.A.: Efficient and Directed Peptide Bond Formation in the Gas Phase via Ion/Ion Reactions. *Proc. Natl. Acad. Sci.*, **2014**, 111, 1288-1292.
158. Pitteri, S.J., Chrisman, P.A., Hogan, J.M., McLuckey, S.A.: Electron Transfer Ion/Ion Reactions in a Three-Dimensional Quadrupole Ion Trap: Reactions of Doubly and Triply Protonated Peptides with SO₂[•]. *Anal. Chem.* **2005**, 77, 1831-1839.
159. Liu, J., Gunawardena, H.P., Huang, T.-Y., McLuckey, S.A.: Charge-Dependent Dissociation of Insulin Cations via Ion/Ion Electron Transfer. *Int. J. Mass Spectrom.* **2008**, 276, 160-170.
160. Liu, J., McLuckey, S.A.: Electron Transfer Dissociation: Effects of Cation Charge State on Product Partitioning in Ion/Ion Electron Transfer to Multiply Protonated Polypeptides. *Int. J. Mass Spectrom.* **2012**, 330-332, 174-181.
161. Good, D.M., Wirtala, M., McAlister, G.C., Coon, J.J.: Performance Characteristics of Electron Transfer Dissociation Mass Spectrometry. *Mol. Cell. Proteomics.* **2007**, 6, 1942.
162. Xia, Y., Gunawardena, H.P., Erickson, D.E., McLuckey, S.A.: Effects of Cation Charge-Site Identity and Position on Electron-Transfer Dissociation of Polypeptide Cations. *J. Am. Chem. Soc.* **2007**, 129, 12232-12243.
163. Turek, F., Chung, T.W., Moss, C.L., Wyer, J.A., Ehlerding, A., Holm, A.I.S., Zettergren, H., Nielsen, S.B., Hvelplund, P., Chamot-Rooke, J., Bythell, B., Paizs, B.: The Histidine Effect. Electron Transfer and Capture Cause Different Dissociations and Rearrangements of Histidine Peptide Cation-Radicals. *J. Am. Chem. Soc.* **2010**, 132, 10728-10740.
164. Prentice, B.M., McGee, W.M., Stutzman, J.R., McLuckey, S.A.: Strategies for the Gas Phase Modification of Cationized Arginine via Ion/Ion Reactions. *Int. J. Mass Spectrom.* **2013**, 354-355, 211-218.
165. McLuckey, S.A.: The Emerging Role of Ion/Ion Reactions in Biological Mass Spectrometry: Considerations for Reagent Ion Selection. *Eur. J. Mass Spectrom.* **2010**, 16, 429-436.
166. Coon, J.J., Syka, J.E.P., Schwartz, J.C., Shabanowitz, J., Hunt, D.F.: Anion Dependence in the Partitioning between Proton and Electron Transfer in Ion/Ion Reactions. *Int. J. Mass Spectrom.* **2004**, 236, 33-42.
167. Gunawardena, H.P., He, M., Chrisman, P.A., Pitteri, S.J., Hogan, J.M., Hodges, B.D.M., McLuckey, S.A.: Electron Transfer versus Proton Transfer in Gas-Phase Ion/Ion Reactions of Polyprotonated Peptides. *J. Am. Chem. Soc.* **2005**, 127, 12627-12639.
168. Compton, P.D., Strukl, J.V., Bai, D.L., Shabanowitz, J., Hunt, D.F.: Optimization of Electron Transfer Dissociation via Informed Selection of Reagents and Operating Parameters. *Anal. Chem.* **2012**, 84, 1781-1785.

169. Martens, J., Berden, G., Oomens, J.: Structures of Fluoranthene Reagent Anions Used in Electron Transfer Dissociation and Proton Transfer Reaction Tandem Mass Spectrometry. *Anal. Chem.* **2016**, 88, 6126-6129.
170. Bowers, J.J., Hodges, B.D.M., Saad, O.M., Leary, J.A., McLuckey, S.A.: Proton Hydrates as Soft Ion/Ion Proton Transfer Reagents for Multiply Deprotonated Biomolecules. *Int. J. Mass Spectrom.* **2008**, 276, 153-159.
171. Stephenson, J.L., McLuckey, S.A.: Gaseous Protein Cations Are Amphoteric. *J. Am. Chem. Soc.* **1997**, 119, 1688-1696.
172. Prentice, B.M., Stutzman, J.R., McLuckey, S.A.: Reagent Cluster Anions for Multiple Gas-Phase Covalent Modifications of Peptide and Protein Cations. *J. Am. Soc. Mass. Spectrom.* **2013**, 24, 1045-1052.

CHAPTER 2. NOVEL PEPTIDE ION CHEMISTRY ASSOCIATED WITH GOLD (I) CATIONIZATION: PREFERENTIAL CLEAVAGE AT LYSINE RESIDUES

Adapted from *Int. J. Mass Spectrom.*, Vol. 427, Foreman, D. J.; Betancourt, S. K.; Pilo, A. L.; McLuckey, S. A. Novel Peptide Ion Chemistry Associated with Gold (I) Cationization: Preferential Cleavage at Lysine Residues, pp. 114-122. Copyright 2018, with permission from Elsevier.

2.1 Introduction

The information obtained in a tandem mass spectrometry experiment is highly dependent on the dissociation method and the type of ion subjected to activation.^{1,2} For example, electron capture dissociation (ECD) and electron transfer dissociation (ETD) of protonated peptides primarily result in c and z fragment ions,^{3,4} while collision-induced dissociation (CID) of these same ions typically generates b and y fragment ions.⁵⁻⁷ Collisional activation of protonated peptides and proteins remains the most common approach in MS/MS analysis. However, the structural information obtained when using CID varies with charge state, and activation of the charge state of greatest abundance does not necessarily provide the most sequence coverage.^{8,9} In recognition of the importance of ion-type, much attention has been devoted to the role of the cationizing agent (metal cation, proton, etc.) in influencing the nature and extent of structural information forthcoming from CID. For example, CID of sodiated peptides results in cleavage of the C-terminal residue forming $[b_{n-1} + Na + OH]^+$ fragment ions, where n is the number of residues on the peptide fragment,¹⁰⁻¹² while CID of the protonated peptide tends to result in non-specific cleavages along the peptide backbone. Glish et al. demonstrated that this fragmentation can be repeated in a multistage mass spectrometry experiment. Subsequent activation of $[b_{n-1} + Na + OH]^+$ produces the second generation $[b_{n-2} + Na + OH]^+$ species. This process can be repeated multiple times in favorable cases, thereby allowing for at least partial C-terminal sequencing of sodiated peptides.¹³⁻¹⁵ Competitive fragmentation pathways and the initial abundance of $[b_{n-1} + Na + OH]^+$ limits the extent to which MS^n can be performed, thereby resulting in incomplete sequencing. While the mechanism for $[b_{n-1} + Na + OH]^+$ formation has been the subject of much debate,^{10,16-18} it is evident that the use of sodium as a cationizing agent drastically affects the fragmentation behavior of the peptides.

The gas-phase fragmentation of argentinated primary amines, α , ω -diaminoalkanes, amino acids, and peptides has been extensively characterized.^{19–25} Similar to the sodium cationized peptides, gas-phase fragmentation of the peptide silver complexes affords abundant $[b_n - H + Ag]^+$, $[a^n - H + Ag]^+$, $[y_n - H + Ag]^+$, and $[b_n + Ag + OH]^+$ product ions that can be used to elucidate the primary sequence of the polypeptide.^{17,26,27} In the case of argentinated amines, several unique fragmentation pathways are observed upon collisional activation including the loss of AgH and subsequent loss of NH₃, the loss of one or more molecules H₂, and the loss of H₂ followed by the loss of AgNH₂.^{20,24,25} These observations further reinforce that the cationizing agent plays a crucial role in the observable fragmentation pathways in an MSⁿ experiment.

We have employed gas-phase cation switching ion/ion reactions as a methodology for converting multiply protonated peptides and proteins to metal cationized polypeptides.^{28,29} The use of a quadrupole ion trap mass spectrometer equipped with two ionization sources allows for the generation of multiply protonated peptide cations using one ion source and metal containing anions using another source.³⁰ The ions of opposite polarity are mutually stored in the quadrupole ion trap resulting in the formation of metal containing product ions.³¹ In this approach, the solution and electrospray conditions of the peptide and metal salt are independently optimized, offering greater control and flexibility of solution conditions than the traditional approach of electrospray of peptide/metal salt mixtures. Additionally, this approach allows for the isolation of specific ions of interest to participate in the ion/ion reaction resulting in the selective formation of a desired ion type, whereas electrospray of a peptide/metal salt mixture results in a spectrum containing various ion types with little control of the distribution.

We have previously reported the use of cation switching ion/ion reactions to incorporate gold cations into disulfide linked peptides.^{32–34} In all cases, gold cationization was found to alter the fragmentation behavior of the peptide. For example, CID of singly, doubly, or triply protonated somatostatin-14 provides no evidence for the cleavage of the disulfide bond between Cys-3 and Cys-14, and offers very little structurally informative products. In contrast to protonated somatostatin-14, dissociation of the singly protonated and singly aurated dication, $[M + H + Au]^{2+}$, gave rise to numerous structurally informative fragments corresponding to cleavage of the disulfide bond and an amide bond.³³ Similarly, CID of doubly aurated insulin, which contains three disulfide bonds, results in cleavage of the two inter-chain disulfide bonds and an increase in sequence information compared to ions containing only one gold cation or no gold cations.³⁴ For

both peptides, increased sequence coverage associated with gold cationization can be attributed to the cleavage of the disulfide bonds as well as amide linkages once protected by the disulfide linkage(s).

Herein, multiply protonated peptides lacking disulfide bonds are transformed into aurred peptide cations via cation switching ion/ion reaction with $[\text{AuCl}_2]^-$. Collisional activation of the aurred peptide results in the characteristic loss of 215 Da, which corresponds to the empirical formula NH_4Au . This work demonstrates a newly identified fragmentation channel associated with gold (I) cationization in which the loss of 215 Da generates the $[\text{M} - \text{H} - \text{NH}_3]^+$ oxidized peptide. For some aurred peptides, this loss was observed to be the dominant process upon CID, which motivated this study. We discuss the specificity of this redox chemistry towards lysine and the role of the lysine position on the extent of the reaction. Since the $[\text{M} - \text{H} - \text{NH}_3]^+$ peak is not regularly observed upon collisional activation, its presence could be used as a diagnostic tool to indicate the presence of lysine residues in polypeptides. Subsequent activation of the oxidized species reveals preferential cleavage adjacent to the lysine residues. Thus, the gas-phase oxidation of lysine residues to form the $[\text{M} - \text{H} - \text{NH}_3]^+$ species could be used as a means to introducing a ‘weak spot’ in polypeptides.

2.2 Experimental

2.2.1 Materials

Methanol and HPLC-grade water were purchased from Fisher Scientific (Pittsburgh, PA, USA), glacial acetic acid was purchased from Mallinckrodt (Phillipsburg, NJ, USA), and gold (III) chloride and melittin from honey bee venom were purchased from Sigma-Aldrich (St. Louis, MO, USA). RARARAA was synthesized by NeoBioLab (Cambridge, MA, USA), KAYK was synthesized by CHI Scientific (Maynard, MA, USA), $\text{K}(^{13}\text{C}_6, ^{15}\text{N}_2)\text{-AFK}$, KGAGGHGAGGHL and YGGKFL were synthesized by CPC Scientific (Sunnyvale, CA, USA), and KGAILAGAILR and GAILKGAILR were synthesized by SynPep (Dublin, CA, USA). KAKAKAA, HAHAAHA, HGAGGHGAGGKL, and ARAMAWAKA were synthesized by Pepnome Ltd. (Shenzhen, China). All peptide stock solutions were prepared at a concentration of approximately 1 mg/mL. Spray solution of melittin was made by diluting the stock 40-fold in 49.5/49.5/1 (v/v/v) methanol/water/acetic acid. All other peptide solutions were diluted 100-fold in 49.5/49.5/1 (v/v/v)

methanol/water/acetic acid. Gold (III) chloride was dissolved in water and diluted in water to a final concentration of approximately 5 mM.

2.2.2 Mass Spectrometry

Model peptide data were collected using a QTRAP 4000 hybrid triple quadrupole/linear ion trap mass spectrometer (Sciex, Concord, ON, Canada), previously modified for ion/ion reactions.³¹ Alternatively pulsed nano-electrospray ionization (nESI) allows for sequential injection of reagent anions and analyte cations.³⁰ Negative nESI of the gold chloride solution generated predominantly $[\text{AuCl}_2]^-$ and $[\text{AuCl}_4]^-$. $[\text{AuCl}_2]^-$ was isolated in Q1 and transferred to q2, followed by positive nESI of the peptide/protein solution. Analyte cations, $[\text{M} + 2\text{H}]^{2+}$, were isolated in Q1 prior to injection into q2. The ions were mutually stored in q2 for 200 to 1000 milliseconds. Beam-type CID of the resulting $[\text{M} + \text{AuCl}_2 + 2\text{H}]^+$ complex ions led to two successive HCl losses, producing the $[\text{M} + \text{Au}]^+$ product ion. The aminated peptide ions were then transferred to Q3 where they were dissociated via resonant excitation at a q-value of 0.2 and mass analyzed via mass-selective axial ejection (MSAE).³⁵

Mellitin results were generated using a TripleTOF 5600 System (Sciex, Concord, ON, Canada), modified for ion/ion reactions similarly to the QTRAP 4000. Alternatively pulsed nESI was performed as described above. However, the cations were injected first, followed by the anions. Mutual storage between isolated $[\text{M} + 4\text{H}]^{4+}$ and $[\text{AuCl}_2]^-$ was performed for 30 milliseconds. Products formed during mutual storage were then subjected to broadband excitation by dipolar direct current (DDC) CID.³⁶ DDC excitation of the $[\text{M} + 4\text{H} + 2\text{AuCl}_2]^{2+}$ complex resulted in the loss of four HCl molecules, forming the $[\text{M} + 2\text{Au}]^{2+}$ ion. Subsequent isolation was performed by transferring product ions back to Q1 for RF-DC isolation then transferring the isolated product ions back to q2 for ion-trap CID. Mass analysis was performed using time of flight (TOF).

2.3 Results and Discussion

2.3.1 Formation of $[\text{M} - \text{H} - \text{NH}_3]^+$: Loss of HAuNH_3

The ion/ion reaction between doubly protonated KGAILAGAILR and $[\text{AuCl}_2]^-$ generates a long-lived electrostatic complex, $[\text{M} + 2\text{H} + \text{AuCl}_2]^+$, and, to a lesser extent, the competitive

proton transfer product, $[M + H]^+$ (Figure 2.1a). Figure 2.1b shows the beam-type CID spectrum that results in two successive losses of HCl from the complex, producing the singly aurated peptide, $[M + Au]^+$. The monoisotopic aurated KGAILAGAILR ion was isolated in Q3 and subjected to CID. The resulting spectrum in Figure 2.1c shows the formation of metal ion-containing b and y fragment ions, $[b/y - H + Au]^+$ (i.e. 196 Da greater in mass than the unmodified b/y fragment ions) and are indicated with a green diamond superscript (e.g. y_2 corresponds to $[y_2 - H + Au]^+$). The spectrum suggests that there are multiple gold cation coordination sites as evidenced by the presence of aurated b/y fragment ions. Specifically, y_1 illustrates coordination of the gold cation to the c-terminal arginine residue while b_3 indicates the coordination of the gold cation to the n-terminal lysine, glycine, or alanine residues.

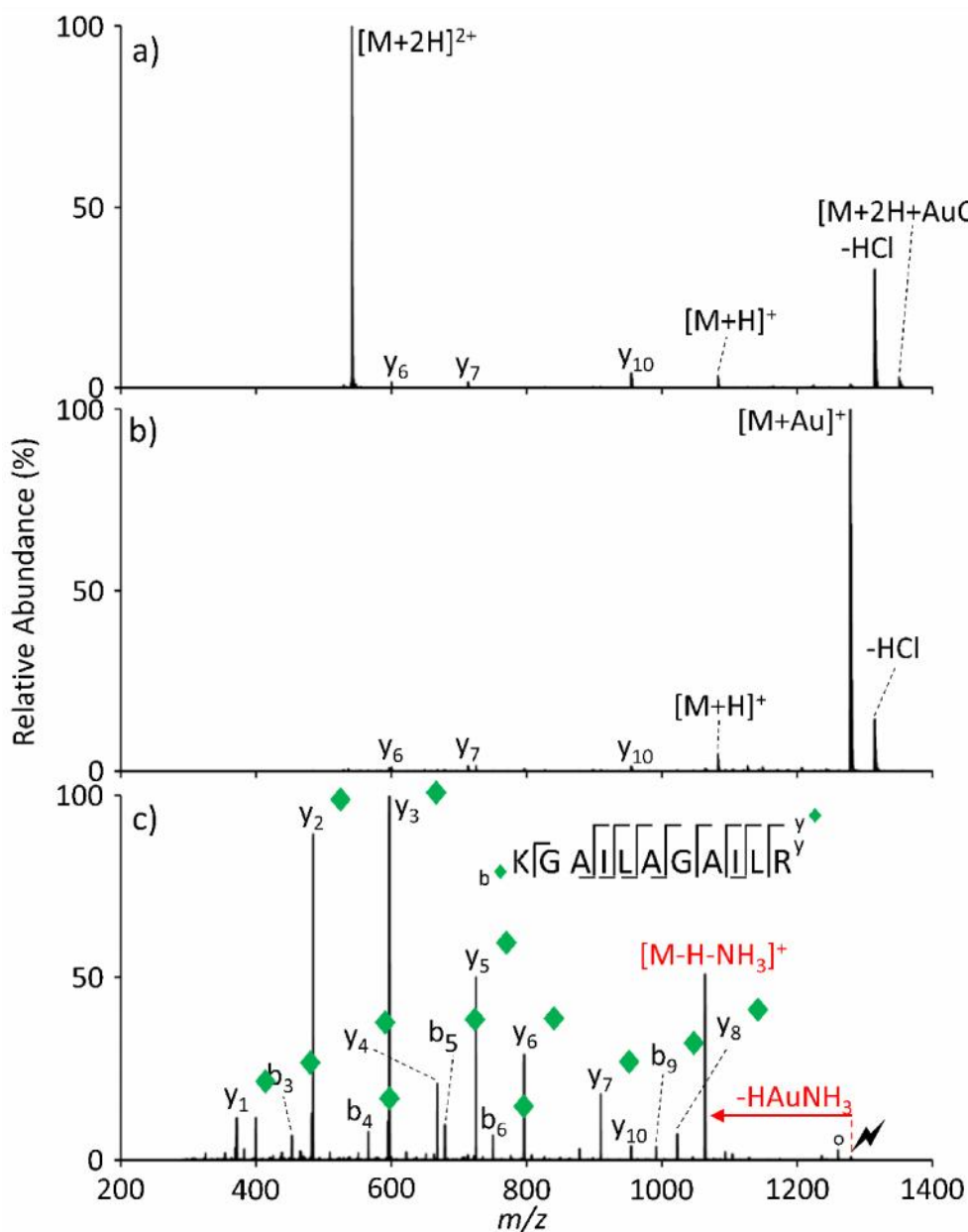


Figure 2.1. a) Post-ion/ion reaction spectrum from the reaction between doubly protonated $M = \text{KGAILLAGAILR}$ and $[\text{AuCl}_2]^-$. b) Beam-type CID of the ion/ion reaction product ions. c) Ion trap CID spectrum of the $[\text{M} + \text{Au}]^+$ ion generated from the process of b). Open circles indicate water loss and the lightning bolt indicates the species subjected to CID. Aurated fragment ions are represented with green diamond superscripts.

While the most abundant peaks in Figure 2.1c are y_2 and y_3 there is an abundant peak at m/z 1064, nominally $[\text{M} - \text{H} - \text{NH}_3]^+$, corresponding to the oxidation of the peptide via the loss of the elements NH_4Au . We note here that the loss of 215 Da likely arises largely, if not exclusively,

from the consecutive losses of gold hydride, AuH, and ammonia, NH₃, in either order (see below). In any case, the net loss of 215 Da will be designated henceforth by the formula H₂AuNH₃. Activation of the [M – H – NH₃]⁺ ion, the CID spectrum of which is shown in Figure 2.2, results in a series of modified a- and b-ions shifted 19 Da lower in mass than their unmodified counterparts (i.e., [b/a – H – NH₃]⁺). Modified fragment ions are indicated by a red square superscript (e.g. b₂[■] corresponds to the [b₂ – H – NH₃]⁺ ion). The fact that only N-terminal fragments are observed to be modified, coupled with the presence of a dominant unmodified y₁₀ fragment, suggests that the oxidation is localized to the lysine residue or N-terminus.

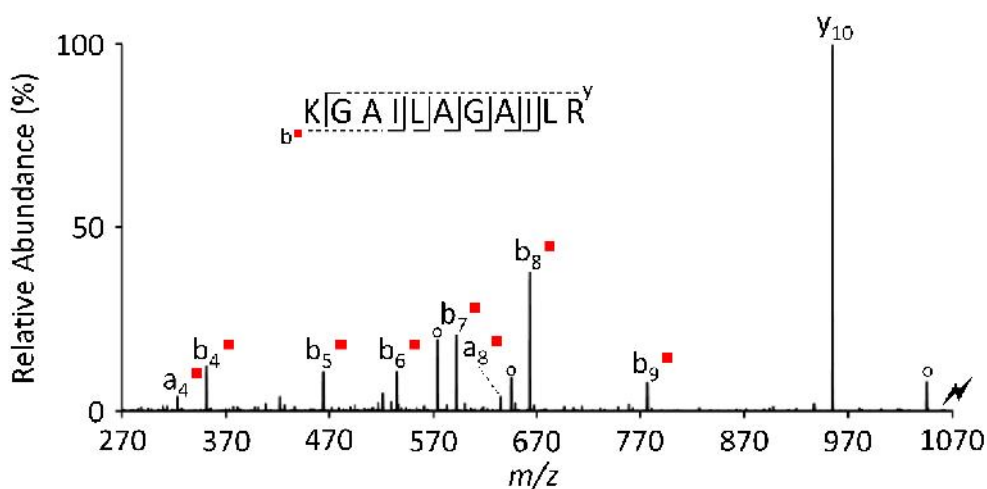


Figure 2.2. Activation of [KGAILAGAILR – H – NH₃]⁺ derived from collisional activation of [M + Au]⁺. Open circles indicate water loss, and the lightning bolt indicates the species subjected to CID. Modified fragment ions are represented with red square superscripts.

2.3.2 Reactivity of Basic Residues

To determine the extent to which basic residues are oxidized in the gas-phase by the gold dichloride reagent anion, a series of basic peptides of the form XAXAXAA (where X = K(lysine), R(arginine), or H(histidine)) were examined. For each peptide, [M + 2H]²⁺ was stored with [AuCl₂][–] after which the product ions were subjected to beam-type CID, resulting in dominant [M + Au]⁺ formation. Figure 2.3a shows the spectrum obtained upon collisional activation of [KAKAKAA + Au]⁺. The spectrum is mainly comprised of aminated b fragment ions with a prominent loss of H₂AuNH₃ to yield [KAKAKAA – H – NH₃]⁺.

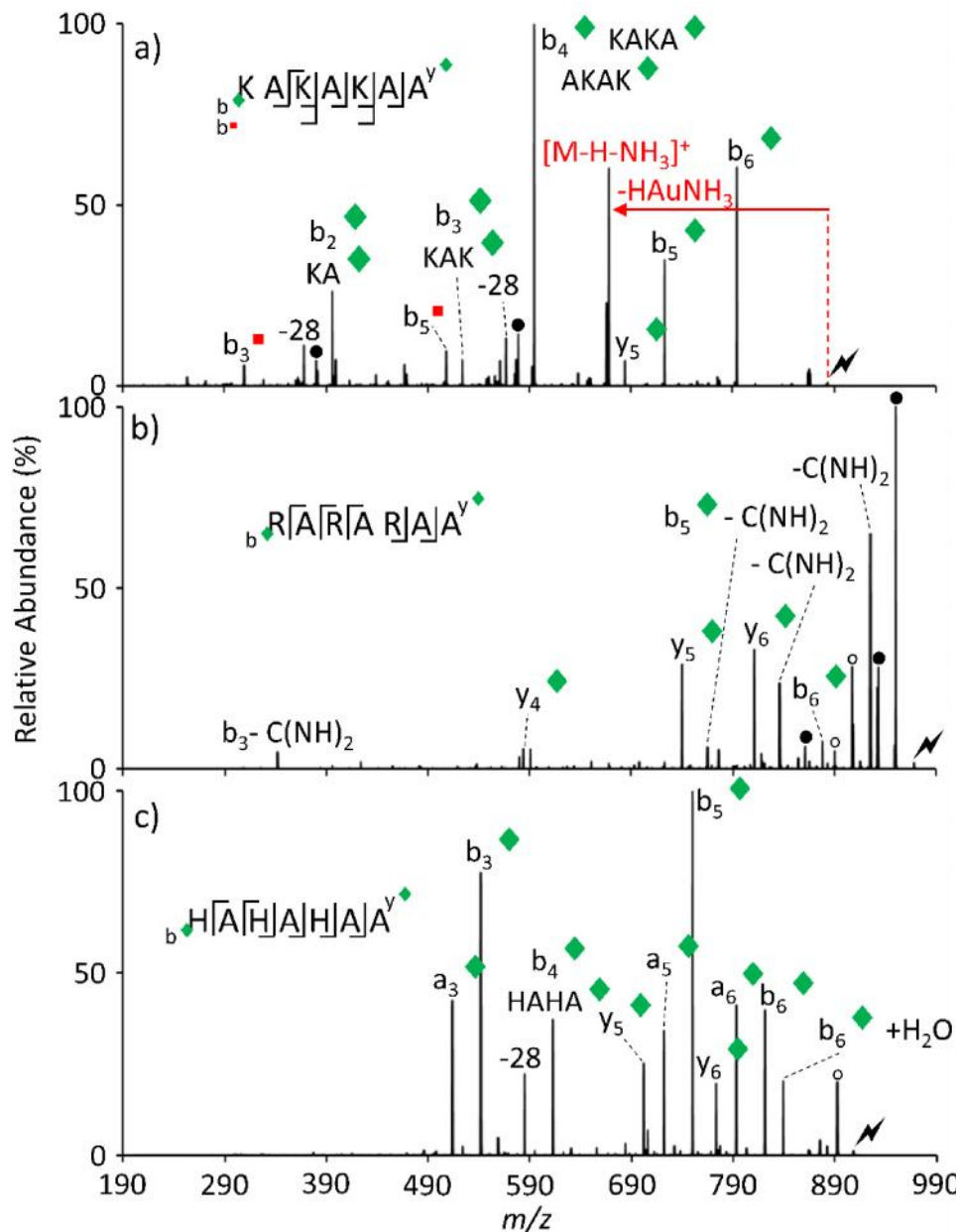


Figure 2.3. Activation of a) $[KAKAKAA + Au]^+$, b) $[RARARAA + Au]^+$, and c) $[HAHAHAA + Au]^+$ ions produced via beam-type CID of the ion/ion reaction products formed between the doubly protonated peptide and the gold dichloride reagent anion. Shaded circles indicate ammonia loss, open circles indicate water loss, and the lightning bolts indicate the species subjected to CID. Aured fragment ions are represented with green diamond superscripts. Modified fragment ions, $[b/y - H - NH_3]^+$, are represented with red square superscripts.

Further interrogation by ion trap CID of the $[KAKAKAA - H - NH_3]^+$ ion, the results of which are shown in Figure 2.4, shows pairs of modified and unmodified b- and y-ions (i.e. b_3 and b_3^\blacksquare), as well as small molecule losses. With the exception of the b_2 fragment ion, the modified b-

ions or modified y-ions are present at greater abundances than the unmodified fragments. Yet the presence of the unmodified fragments reveals the oxidation can occur at any of the neutral lysine residues or N-terminus.

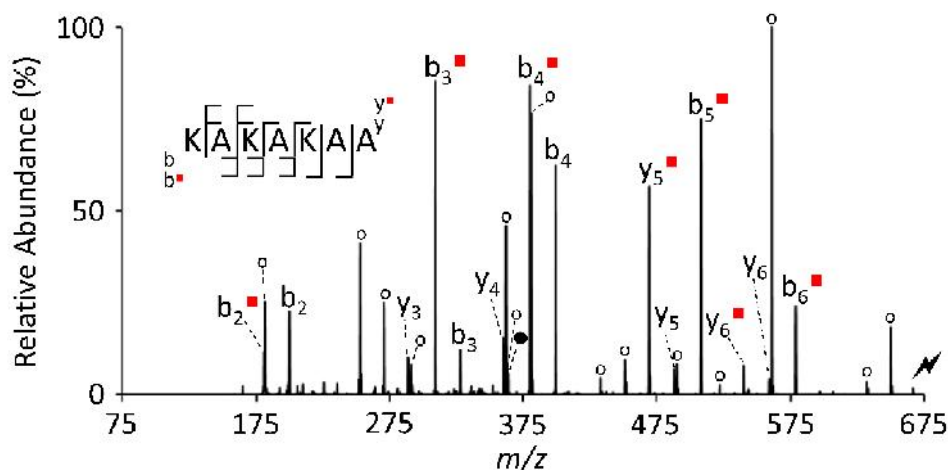


Figure 2.4. Activation of $[KAKAKAA - H - NH_3]^+$ derived from collisional activation of $[M + Au]^+$. Shaded circles indicate ammonia loss, open circles indicate water losses, and the lightning bolt indicates the species subjected to CID. Modified fragment ions are represented with red square superscripts.

Results from the activation of $[RARARAA + Au]^+$ and $[HAHAHAA + Au]^+$ ions are shown in Figures 2.3b and 2.3c, respectively. In the case of RARARAA, activation of the aured peptide results in abundant losses of 42 Da, corresponding to loss of $C(NH)_2$ from the arginine side-chain, as well as some aured b- and y-ions. In the case of HAHAHAA, activation of $[M + Au]^+$ predominantly generates aured b- and a- ions with some aured y-ions also being present. For neither of these two systems is there any evidence for the loss of $HAuNH_3$ suggesting this oxidation chemistry is specific to neutral lysine residues.

2.3.3 Influence of Lysine Position on $HAuNH_3$ Loss

$K(^{13}C_6, ^{15}N_2)$ -AFK, a model peptide containing an isotopically labeled N-terminal lysine and unmodified C-terminal lysine, was used to investigate the influence of lysine position on the extent of $HAuNH_3$ loss. Figure 2.5 shows the CID spectrum of the aured peptide resulting in the loss of both 216 Da and 215 Da, corresponding to the loss of $HAu^{15}NH_3$ from the N-terminal lysine residue and loss of $HAuNH_3$ from the C-terminal lysine residue, respectively. The inset of Figure

2.5 shows the $[M - H - {}^{15}\text{NH}_3]^+$ peak, originating from the loss of $\text{HAu}^{15}\text{NH}_3$ from the isotopically labeled N-terminal lysine, present at approximately four times the abundance than that of the $[M - H - \text{NH}_3]^+$. This observation suggests that oxidation is more favorable on the N-terminus.

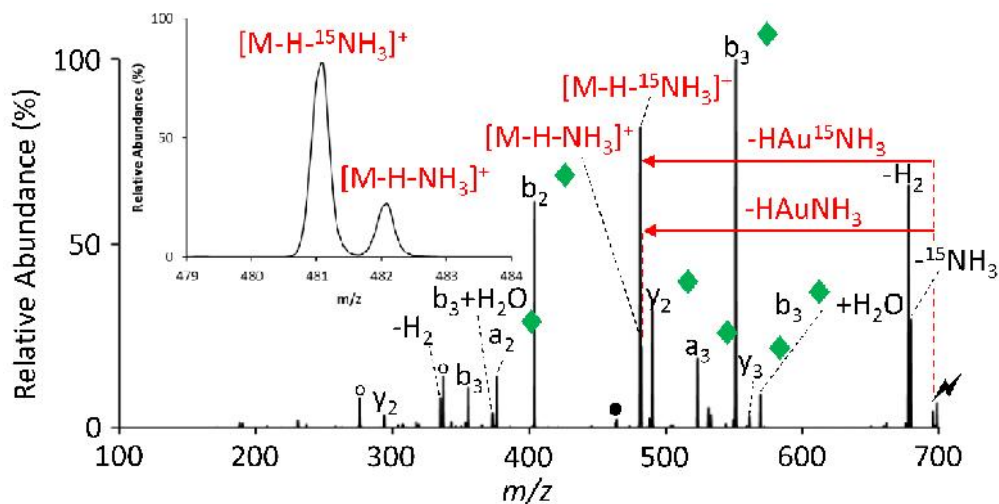


Figure 2.5. Activation of $[\text{K}({}^{13}\text{C}_6, {}^{15}\text{N}_2)\text{-AFK} + \text{Au}]^+$ ion formed via ion/ion reaction. Shaded circles indicate ammonia loss, open circles indicate water loss, and the lightning bolt indicates the species subjected to CID. Aured fragment ions are represented with green diamond superscripts.

Two isomeric peptides varying in the position of the lysine were also examined. Figure 2.6a shows the fragment ions produced by CID of $[\text{KGAGGHHGAGGHL} + \text{Au}]^+$, which results in the dominant formation of the oxidized lysine species, $[M - H - \text{NH}_3]^+$. In contrast, when the lysine residue is located near the C-terminus, as with HGAGGHHGAGGKL , fragmentation of its aured species, depicted in Figure 2.6b, results in little lysine oxidation product. Since both systems are sequence isomers, it can be concluded that lysine oxidation by gold cationization is more prevalent when the lysine is located at the N-terminus, as reflected by the difference in relative abundances of $[M - H - \text{NH}_3]^+$ ions in the two spectra.

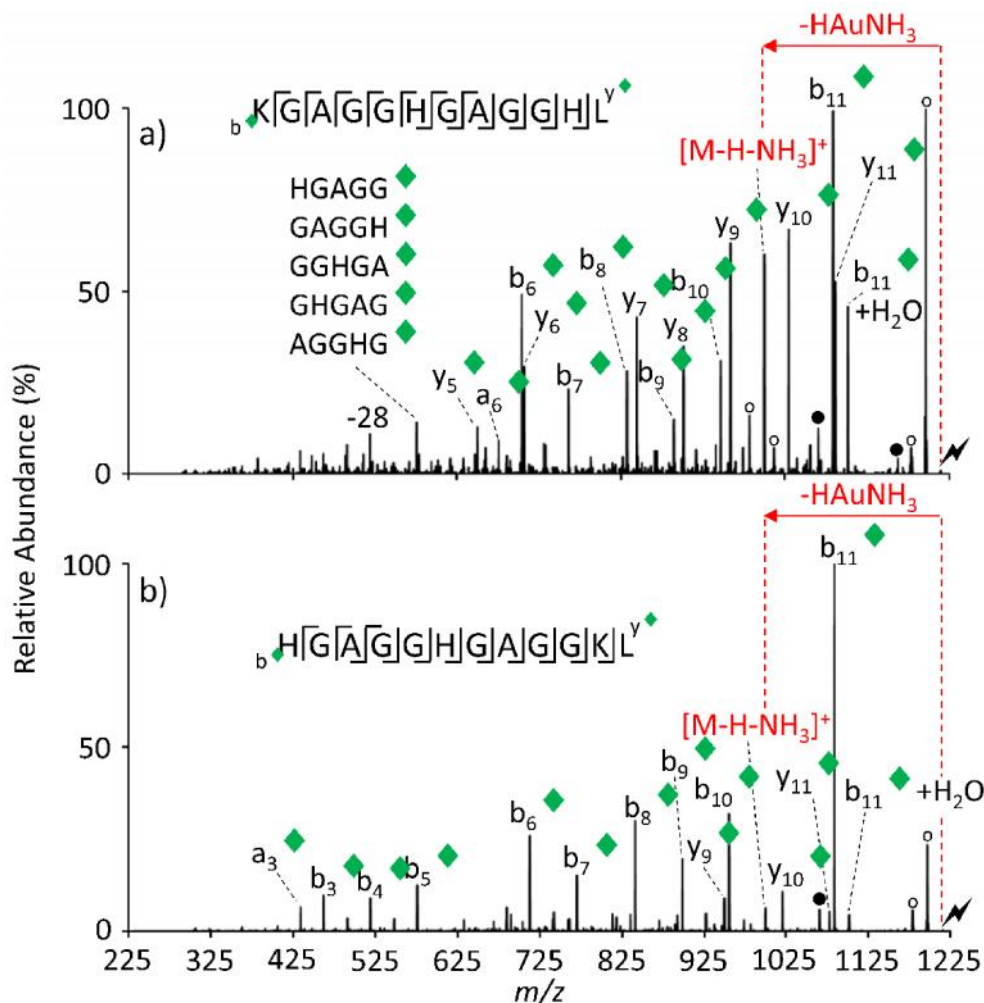


Figure 2.6. Activation of a) aurated KGAGGHGAGGHL and b) aurated HAGGGHGAGGKL formed in the gas-phase. Shaded circles indicate ammonia loss, open circles indicate water losses, and the lightning bolt indicates the species subjected to CID. Aurated fragment ions are represented with green diamond superscripts.

2.3.4 Proposed Mechanisms for the Formation of $[M - H - NH_3]^+$ Ions

As mentioned above, the loss of 215 Da from an aurated peptide likely takes place in a step-wise fashion through the losses of gold hydride and ammonia, in either order. Direct evidence for these two consecutive loss pathways has been observed experimentally. That is, intermediates generated by either loss of ammonia or loss of gold hydride have been observed in some cases, and when such products underwent subsequent activation, the loss of the second small molecule was observed to be a major process. For example, the base peak observed in the ion trap CID of the $[KAYK + Au]^+$ ion (Figure 2.7a) resulted from the loss of $HAuNH_3$. However, there was also

a product at roughly 20% relative abundance corresponding to a loss of 17 Da, which is consistent with ammonia loss. Ion trap CID of this first-generation product ion (Figure 2.7b) showed a dominant loss of 198 Da, which is consistent with loss of gold hydride. Ion trap CID of the $[\text{KAYK} - \text{H} - \text{NH}_3]^+$ ions generated via the two pathways (i.e., via loss of HAuNH_3 directly from $[\text{KAYK} + \text{Au}]^+$ (Figure 2.7a) or via loss of AuH from the $[\text{KAYK} + \text{Au} - \text{NH}_3]^+$ (Figure 2.7b)) generated essentially identical results (compare Figures 2.7c and 2.7d). In the other example, ion trap CID of doubly aurred melittin, $[\text{M} + 2\text{Au}]^{2+}$, results in prominent peaks coinciding with the loss of gold hydride and loss of HAuNH_3 (Figure 2.8a). Isolation and subsequent activation of the gold hydride loss product ion, $[\text{M} - \text{H} + \text{Au}]^{2+}$, solely results in ammonia loss generating $[\text{M} - \text{H} - \text{NH}_3 + \text{Au}]^{2+}$ (Figure 2.9). In either case, the presence of the second generation product ions, $[\text{M} - \text{H} - \text{NH}_3]^+$ or $[\text{M} - \text{H} - \text{NH}_3 + \text{Au}]^{2+}$, suggests a remarkably fast loss of the second small molecule.

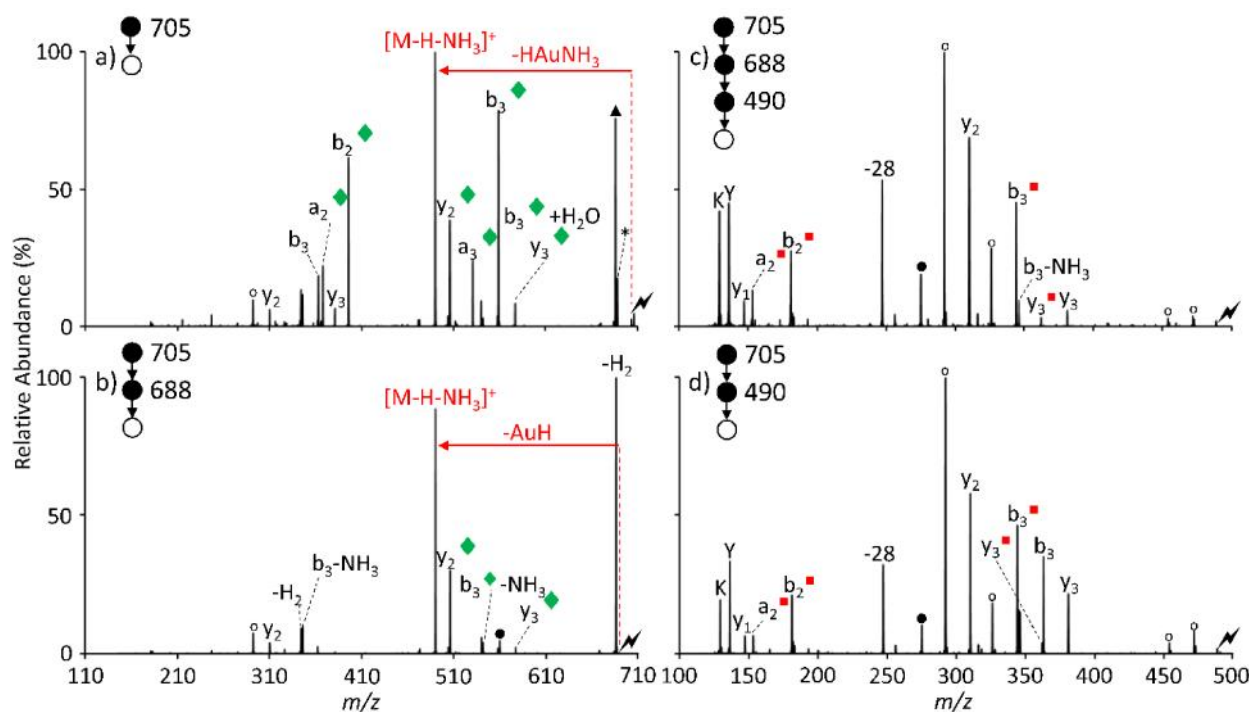


Figure 2.7. Activation of a) $[\text{KAYK} + \text{Au}]^+$, b) $[\text{KAYK} + \text{Au} - \text{NH}_3]^+$, c) $[\text{KAYK} - \text{H} - \text{NH}_3]^+$ produced from sequential NH_3 and HAu loss, and d) $[\text{KAYK} - \text{H} - \text{NH}_3]^+$ produced directly from CID of the post ion/ion product $[\text{M} + \text{Au}]^+$. Shaded circles indicate ammonia loss, open circles indicate water losses, and the lightning bolt indicates the species subjected to CID. Aurred fragment ions are represented with green diamond superscripts. Modified fragment ions are represented with red square superscripts.

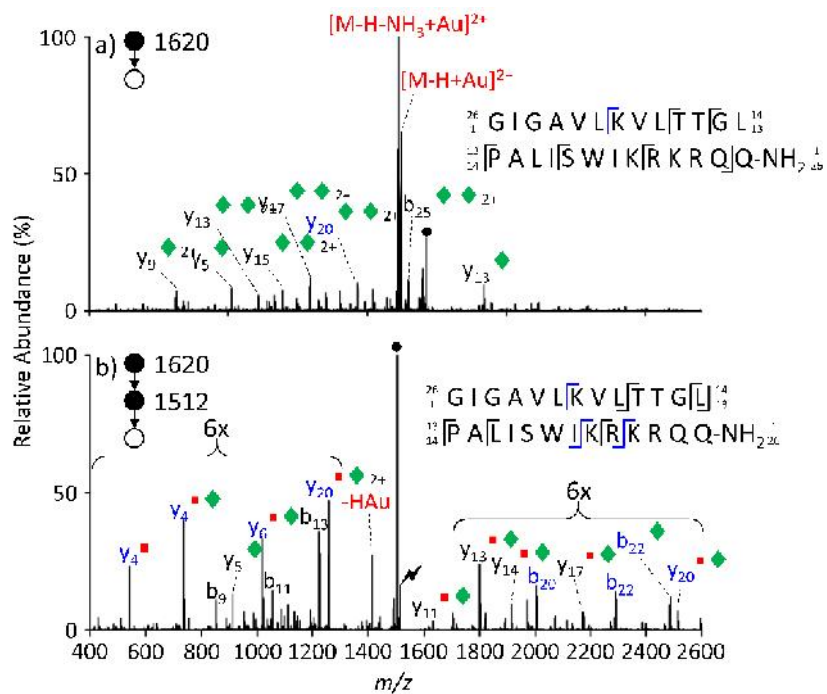


Figure 2.8. a) Activation of doubly aurated melittin, $[M + 2Au]^{2+}$ derived from the ion/ion reaction between quadruply protonated melittin and two gold dichloride reagent anions. b) Activation of oxidized melittin $[M - H - NH_3 + Au]^{2+}$ after the loss of NH_4Au from $[M + 2Au]^{2+}$. Shaded circles indicate ammonia loss and the lightning bolt indicates the species subjected to CID. Aurated fragment ions are represented with green diamond superscripts. Modified fragment ions are represented with red triangle superscripts. Fragment ions corresponding to cleavages N-terminal to oxidized lysine residues are indicated with blue text.

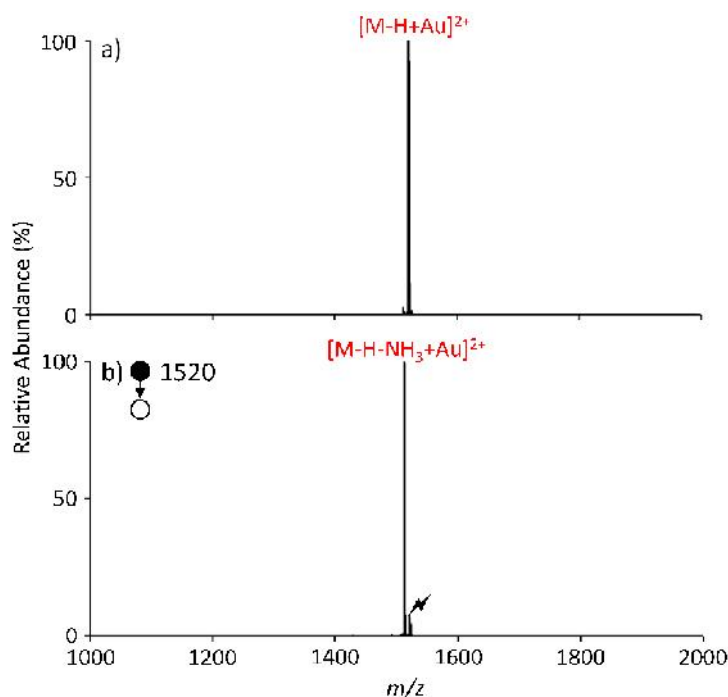
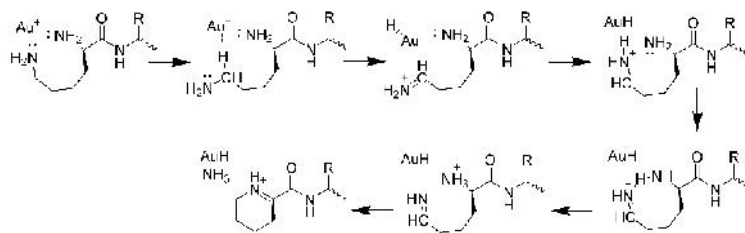


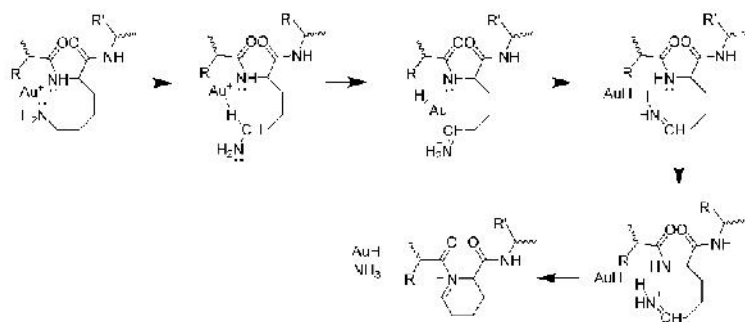
Figure 2.9. a) Q1 isolation of $[\text{melittin} - \text{H} + \text{Au}]^{2+}$. b) q2 CID of $[\text{melittin} - \text{H} + \text{Au}]^{2+}$. The lightning bolt indicates the species subjected to CID.

The generation of $[M - H - \text{NH}_3]^+$ from aminated peptides appears to be highly analogous to the generation of $[M - H - \text{NH}_3]^+$ from argintated amines.^{20,22,24,25} While we have not conducted a detailed mechanistic study, we offer two possible mechanisms (Scheme 2.1 and Scheme 2.2) for the generation $[M - H - \text{NH}_3]^+$ based on the density functional theory (DFT) calculations performed by Hopkinson and Siu.^{20,24} Briefly, in Scheme 2.1, for an N-terminal lysine, the gold cation is coordinated in a tridentate fashion to the N-terminal amine, lysine ϵ -amine, and the carbonyl oxygen.²³ Migration of the gold cation towards the alpha carbon and rotation about the $\text{CH}_2\text{-CH}_2$ bond results in the loss of AuH via hydride abstraction from the alpha carbon and formation of an iminium ion. Finally, a molecule of ammonia can be lost from the N-terminus or lysine sidechain producing a protonated six-membered cyclic iminium ion.



Scheme 2.1. Proposed mechanism for the formation $[M - H - NH_3]^+$ from an N-terminal lysine residue: loss of AuH via hydride abstraction followed by loss of ammonia.

A similar mechanism is proposed for an internal lysine residue or a C-terminal lysine residue (Scheme 2.2). Here, the gold cation coordinates to the lysine amine and a backbone amide nitrogen. The lower nucleophilicity of the amide nitrogen is likely why the redox process appears to be favored when the lysine is the N-terminal residue. Hydride abstraction from the alpha carbon and loss of AuH is followed by loss of a molecule of ammonia from the lysine sidechain. Ultimately, the final structure contains a fixed charge. Analogous mechanisms can be drawn for the loss of ammonia followed by the loss of gold hydride in which a molecule of ammonia is lost prior to hydride abstraction. We note that we have not observed argentinated peptides to lose AgH or HAgNH₃, as is seen from argentinated amines. (See, for example, Figure 2.10, which shows the CID spectrum of [KGAILAGAILR + Ag]⁺. This spectrum should be compared with that of [KGAILAGAILR + Au]⁺, shown in Figure 2.1c).



Scheme 2.2. Proposed mechanism for the formation $[M - H - NH_3]^+$ from an internal lysine residue: loss of AuH via hydride abstraction followed by loss of ammonia.

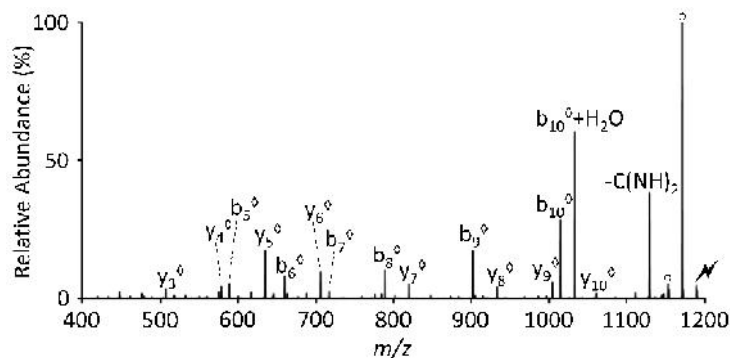
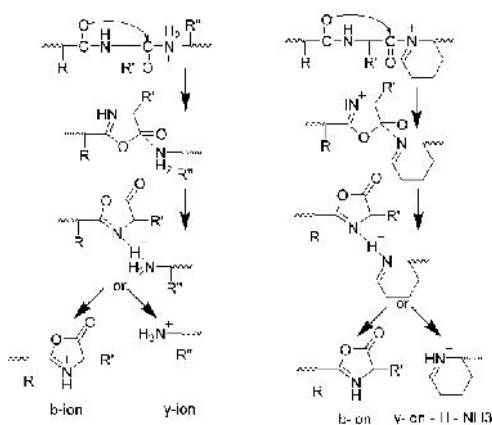


Figure 2.10. Ion trap CID of $[KGAILAGAILR + {}^{107}\text{Ag}]^+$ (Compare to Figure 2.1c – CID of $[KGAILAGAILR + \text{Au}]^+$). Open circles indicate water losses and the lightning bolt indicates the species subjected to CID. Argentinated fragment ions are represented with open diamond superscripts.

2.3.5 MS³ Fragmentation: Preferential Cleavage N-terminal to Oxidized Lysine Residues

CID of protonated peptides form b- and y-ions through either a charge-directed or a charge-remote fragmentation pathway.^{7,37} For the charge-directed fragmentation pathway, the ionizing proton can be mobilized and populate various positions throughout the peptide. Protonation of an amide nitrogen weakens the C-N bond and lowers the energy barrier for dissociation.^{38,39} Nucleophilic attack of an N-terminal neighboring carbonyl oxygen at the carbonyl carbon of the protonated amide ultimately gives rise to a proton-bound dimer that can dissociate into a b or y fragment ion.⁴⁰ The reaction is summarized in Scheme 2.3a.



Scheme 2.3. Fragmentation mechanism for a) $[M + H]^+$ and b) $[M - H - \text{NH}_3]^+$.

The fixed charge cyclic iminium ion formed from CID of an aminated peptide that contains an internal or C-terminal lysine residue, likely withdraws more electron density from the adjacent carbonyl carbon than a protonated amide, resulting in a more electrophilic carbonyl carbon. It is reasonable to suggest this increased electrophilicity produces a weaker C-N bond on the peptide backbone and lowers the energy barrier for dissociation. Therefore, a mechanism similar to that of Scheme 2.3b could rationalize fragmentation at the site associated with HAuNH_3 loss. Nucleophilic attack of the neighboring carbonyl oxygen at the electrophilic carbonyl carbon results in an oxazolone derivative prior to rearrangement to a proton bound dimer. Dissociation of the proton bound dimer would result in either an unmodified b-ion or a modified y-ion, $[\text{y} - \text{H} - \text{NH}_3]^+$.

Figure 2.11 illustrates the preferential cleavage N-terminal to lysine residues upon activation of the oxidized $[\text{M} - \text{H} - \text{NH}_3]^+$ species. The ion trap CID product ion spectrum of $[\text{YGGKFL} - \text{H} - \text{NH}_3]^+$ shown in Figure 2.11a shows dominant y_3^+ and KF^+ formation, both of which entail cleavage N-terminal to the site of HAuNH_3 loss. For GAILKGAILR , activation of the oxidized peptide (Figure 2.11b) generates the b_4 and KGAI^+ fragments as the two most abundant product ions in the spectrum. Additionally, activation of $[\text{ARAMAWAKA} - \text{H} - \text{NH}_3]^+$ in Figure 2.11c further demonstrates the preferential cleavage since the b_7 fragment ion is the most abundant peak in the spectrum. In each case, the most prominent peaks in the spectra correspond to fragments N-terminal to the oxidized lysine residues. These spectra differ significantly from CID of their singly protonated counterparts, in that the N-terminal cleavages mentioned above are observed only as minor fragmentation pathways in the protonated peptides (Figures 2.12, 2.13, and 2.14).

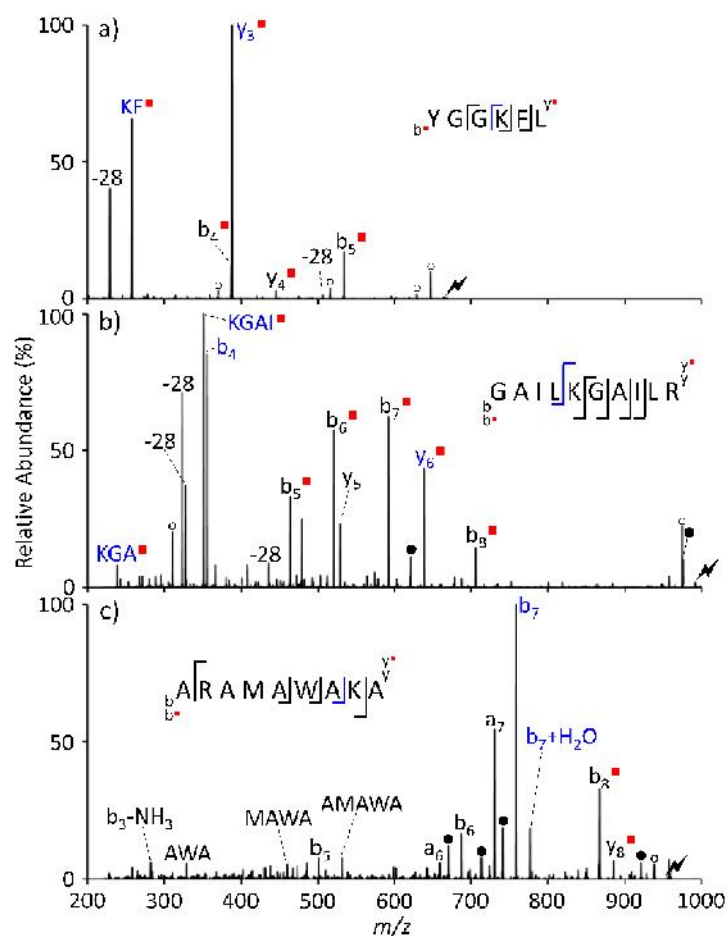


Figure 2.11. Activation of a) $[YGGKFL - H - NH_3]^+$, b) $[GAILKGAILR - H - NH_3]^+$, and c) $[ARAMAWAKA - H - NH_3]^+$ derived from collisional activation of $[M + Au]^+$. Shaded circles indicate ammonia losses, open circles indicate water losses, and the lightning bolt indicates the species subjected to CID. Modified fragment ions, $[b/y - H - NH_3]^+$, are represented with red square superscripts. Fragment ions corresponding to cleavages N-terminal to oxidized lysine residues are indicated with blue text.

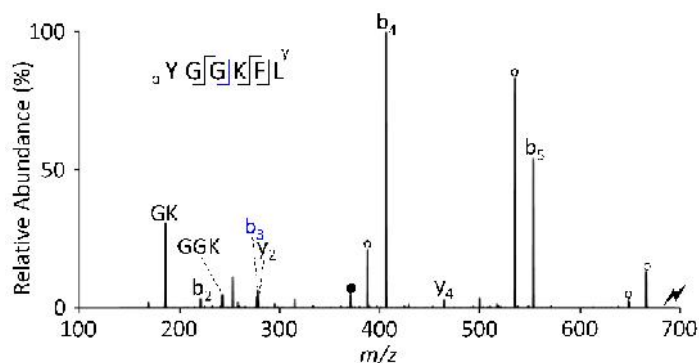


Figure 2.12. Activation of $[YGGKFL + H]^+$. Shaded circles indicate ammonia losses, open circles indicate water losses, and the lightning bolt indicates the species subjected to CID. Fragment ions corresponding to cleavages N-terminal to oxidized lysine residues are indicated with blue text.

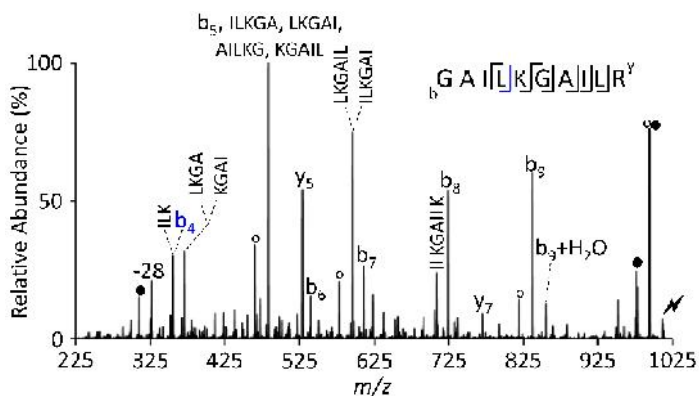


Figure 2.13. Activation of $[GAILKGAAILR + H]^+$. Shaded circles indicate ammonia losses, open circles indicate water losses, and the lightning bolt indicates the species subjected to CID. Fragment ions corresponding to cleavages N-terminal to oxidized lysine residues are indicated with blue text.

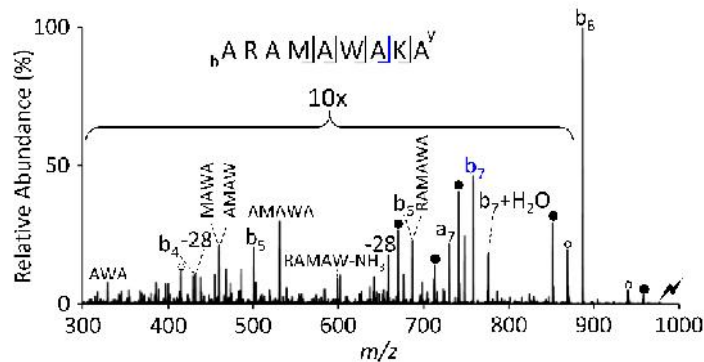


Figure 2.14. Activation of [ARAMAWAKA + H]⁺. Shaded circles indicate ammonia losses, open circles indicate water losses, and the lightning bolt indicates the species subjected to CID. Fragment ions corresponding to cleavages N-terminal to oxidized lysine residues are indicated with blue text.

2.3.6 Oxidation of Melittin

Melittin, the primary toxic constituent of honeybee venom, is a 26 amino acid peptide containing five basic residues – three lysine residues and two arginine residues.^{41–43} Two gold dichloride reagent anions were adducted to quadruply protonated melittin via ion/ion reactions in the gas-phase in order to increase the probability of coordination to lysine residues and to generate a polypeptide cation nominally devoid of excess protons. Figure 2.8a shows results from the ion trap collisional activation of doubly aurated melittin, which results in prominent peaks coinciding with the loss of AuH and loss of H₂AuNH₃.

The oxidized species, [M – H – NH₃ + Au]²⁺ was isolated and subjected to collisional activation (Figure 2.8b). The spectrum shows facile ammonia loss as well as loss of a second AuH moiety. The majority of backbone fragmentation is observed N-terminal to the oxidized lysine residues as evidenced by the highly abundant b₂₀, y₆^{■◆}, b₂₂, y₄^{■◆}, b₂₂, y₄^{■◆}, and y₂₀^{■◆}, fragment ion peaks. The b₁₃ and y₁₃^{■◆} ions are observed at roughly equal abundance as the aforementioned preferential cleavage fragments, indicating that the cleavage N-terminal to the oxidized lysine competes with the proline effect.^{44–46}

2.4 Conclusions

Selective oxidation of lysine residues via ion/ion reactions with gold dichloride reagent anion has been demonstrated using several model peptides. Collisional activation of lysine

containing $[M + Au]^+$ results in loss of $HAuNH_3$ to generate the $[M - H - NH_3]^+$ species via hydride abstraction. Formation of $[M - H - NH_3]^+$ product has been found to be unique to lysine residues as ion/ion reactions between $[AuCl_2]^-$ and the other neutral basic residues (arginine and histidine) show no evidence of oxidation. Two two-step pathways for $[M - H - NH_3]^+$ formation were observed and possible mechanisms are proposed. It is proposed that loss of $HAuNH_3$ from an N-terminal lysine results in a protonated cyclic iminium ion while loss of $HAuNH_3$ from a lysine located elsewhere in the peptide sequence results in a fixed charge cyclic iminium ion. Though N-terminal lysine residues are more readily oxidized than the internal or C-terminal positions, the fixed charge results in a more labile bond N-terminal to oxidized lysine residue and introduces a weak point in the peptide chain. This phenomenon is evidenced by the activation of the $[M - H - NH_3]^+$ ion resulting in preferential cleavage N-terminal to oxidized lysine residues. This chemistry was applied to melittin where activation of the doubly aurred melittin cation resulted in loss of $HAuNH_3$. Activation of the oxidized melittin resulted in preferential cleavage N-terminal to lysine residues that competes with the proline effect. This work demonstrates another unique reaction channel associated with aurred polypeptide ions, in addition to selective cleavage of disulfide bonds.

2.5 References

1. McLuckey, S.A., Mentinova, M.: Ion/Neutral, Ion/Electron, Ion/Photon, and Ion/Ion Interactions in Tandem Mass Spectrometry: Do We Need Them All? Are They Enough? *J. Am. Soc. Mass. Spectrom.* **2011**, 22, 3-12.
2. Prentice, B.M., McLuckey, S.A.: Gas-Phase Ion/Ion Reactions of Peptides and Proteins: Acid/Base, Redox, and Covalent Chemistries. *Chem. Commun.* **2013**, 49, 947-965.
3. Syka, J.E.P., Coon, J.J., Schroeder, M.J., Shabanowitz, J., Hunt, D.F.: Peptide and Protein Sequence Analysis by Electron Transfer Dissociation Mass Spectrometry. *Proc. Natl. Acad. Sci. U.S.A.* **2004**, 101, 9528-9533.
4. Zhurov, K.O., Fornelli, L., Wodrich, M.D., Laskay, U.A., Tsybin, Y.O.: Principles of Electron Capture and Transfer Dissociation Mass Spectrometry Applied to Peptide and Protein Structure Analysis. *Chem. Soc. Rev.* **2013**, 42, 5014-5030.
5. Lin, C., O'Connor, P.: Ion Activation and Mass Analysis in Protein Mass Spectrometry. John Wiley & Sons, Inc., 2011.

6. Dongré, A.R., Jones, J.L., Somogyi, Á., Wysocki, V.H.: Influence of Peptide Composition, Gas-Phase Basicity, and Chemical Modification on Fragmentation Efficiency: Evidence for the Mobile Proton Model. *J. Am. Chem. Soc.* **1996**, 118, 8365-8374.
7. Paizs, B., Suhai, S.: Fragmentation Pathways of Protonated Peptides. *Mass Spectrom. Rev.* **2005**, 24, 508-548.
8. Reid, G.E., Wu, J., Chrisman, P.A., Wells, J.M., McLuckey, S.A.: Charge-State-Dependent Sequence Analysis of Protonated Ubiquitin Ions via Ion Trap Tandem Mass Spectrometry. *Anal. Chem.* **2001**, 73, 3274-3281.
9. Chanthamontri, C., Liu, J., McLuckey, S.A.: Charge State Dependent Fragmentation of Gaseous α -Synuclein Cations via Ion Trap and Beam-Type Collisional Activation. *Int. J. Mass Spectrom.* **2009**, 283, 9-16.
10. Grese, R.P., Cerny, R.L., Gross, M.L.: Metal Ion-Peptide Interactions in the Gas Phase: A Tandem Mass Spectrometry Study of Alkali Metal Cationized Peptides. *J. Am. Chem. Soc.* **1989**, 111, 2835-2842.
11. Renner, D., Spiteller, G.: Linked Scan Investigation of Peptide Degradation Initiated by Liquid Secondary Ion Mass Spectrometry. *Biol. Mass Spectrom.* **1988**, 15, 75-77.
12. Kulik, W., Heerma, W., Terlouw, J.K.: A Novel Fragmentation Process in the Fast-Atom Bombardment/Tandem Mass Spectra of Peptides Cationized with Na^+ , Determining the Identity of the C-Terminal Amino Acid. *Rapid Commun. Mass Spectrom.* **1989**, 3, 276-278.
13. Lin, T., Glish, G.L.: C-Terminal Peptide Sequencing via Multistage Mass Spectrometry. *Anal. Chem.* **1998**, 70, 5162-5165.
14. Payne, A.H., Holly Chelf, J., Glish, G.L.: C-Terminal Peptide Sequencing using Acetylated Peptides with MS in a Quadrupole Ion Trap. *Analyst.* **2000**, 125, 635-640.
15. Lin, T., Payne, A.H., Glish, G.L.: Dissociation Pathways of Alkali-Cationized Peptides: Opportunities for C-Terminal Peptide Sequencing. *J. Am. Soc. Mass. Spectrom.* **2011**, 12, 497-504.
16. Feng, W.Y., Gronert, S., Fletcher, K.A., Warres, A., Lebrilla, C.B.: The Mechanism of C-Terminal Fragmentations in Alkali Metal Ion Complexes of Peptides. *Int. J. Mass Spectrom.* **2003**, 222, 117-134.
17. Tang, X., Ens, W., Standing, K.G., Westmore, J.B.: Daughter Ion Mass Spectra from Cationized Molecules of Small Oligopeptides in a Reflecting Time-Of-Flight Mass Spectrometer. *Anal. Chem.* **1988**, 60, 1791-1799.

18. Lee, S.-W., Kim, H.S., Beauchamp, J.L.: Salt Bridge Chemistry Applied to Gas-Phase Peptide Sequencing: Selective Fragmentation of Sodiated Gas-Phase Peptide Ions Adjacent to Aspartic Acid Residues. *J. Am. Chem. Soc.* **1998**, 120, 3188-3195.
19. Lee, V.W.M., Li, H., Lau, T.-C., Siu, K.W.M.: Structures of b and a Product Ions from the Fragmentation of Argentinated Peptides. *J. Am. Chem. Soc.* **1998**, 120, 7302-7309.
20. Grewal, R.N., Rodriguez, C.F., Shoeib, T., Chu, I.K., Tu, Y.-P., Hopkinson, A.C., Su, K.: Elimination of AgR (R= H, CH₃, C₆H₅) from Collisionally-Activated Argentinated Amines. *Eur. J. Mass Spectrom.* **2000**, 6, 187-192.
21. Chu, I.K., Shoeib, T., Guo, X., Rodriguez, C.F., Hopkinson, A.C., Siu, K.M., Lau, T.-C.: Characterization of the Product Ions from the Collision-Induced Dissociation of Argentinated Peptides. *J. Am. Soc. Mass. Spectrom.* **2001**, 12, 163-175.
22. Talaty, E.R., Perera, B.A., Gallardo, A.L., Barr, J.M., Van Stipdonk, M.J.: Elucidation of Fragmentation Pathways for the Collision-Induced Dissociation of the Binary Ag (I) Complex with Phenylalanine. *J. Phys. Chem. A.* **2001**, 105, 8059-8068.
23. Shoeib, T., Siu, K.M., Hopkinson, A.C.: Silver Ion Binding Energies of Amino Acids: Use of Theory to Assess the Validity of Experimental Silver Ion Basicities Obtained from the Kinetic Method. *J. Phys. Chem. A.* **2002**, 106, 6121-6128.
24. Shi, T., Zhao, J., Shoeib, T., Siu, K., Hopkinson, A.C.: Fragmentation of Singly Charged Silver/ , -Diaminoalkane Complexes: Competition between the Loss of H₂ and Ag Molecules. *Eur. J. Mass Spectrom.* **2004**, 10, 931-940.
25. Schäfer, M., Dreiocker, F., Budzikiewicz, H.: Collision Induced Loss of AgH from Ag⁺ Adducts of Alkylamines, Aminocarboxylic Acids and Alkyl Benzyl Ethers Leads Exclusively to Thermodynamically Favored Product Ions. *J. Mass Spectrom.* **2009**, 44, 278-284.
26. Li, H., Michael Siu, K.W., Guevremont, R., Yves Le Blanc, J.C.: Complexes of Silver(I) with Peptides and Proteins as Produced in Electrospray Mass Spectrometry. *J. Am. Soc. Mass. Spectrom.* **1997**, 8, 781-792.
27. Chu, I.K., Guo, X., Lau, T.-C., Siu, K.W.M.: Sequencing of Argentinated Peptides by Means of Electrospray Tandem Mass Spectrometry. *Anal. Chem.* **1999**, 71, 2364-2372.
28. Newton, K.A., McLuckey, S.A.: Gas-Phase Peptide/Protein Cationizing Agent Switching via Ion/Ion Reactions. *J. Am. Chem. Soc.* **2003**, 125, 12404-12405.
29. Newton, K.A., Amunugama, R., McLuckey, S.A.: Gas-Phase Ion/Ion Reactions of Multiply Protonated Polypeptides with Metal Containing Anions. *J. Phys. Chem. A.* **2005**, 109, 3608-3616.

30. Liang, X., Xia, Y., McLuckey, S.A.: Alternately Pulsed Nanoelectrospray Ionization/Atmospheric Pressure Chemical Ionization for Ion/Ion Reactions in an Electrodynamic Ion Trap. *Anal. Chem.* **2006**, 78, 3208-3212.
31. Xia, Y., Wu, J., McLuckey, S.A., Londry, F.A., Hager, J.W.: Mutual Storage Mode Ion/Ion Reactions in a Hybrid Linear Ion Trap. *J. Am. Soc. Mass. Spectrom.* **2005**, 16, 71-81.
32. Gunawardena, H.P., O'Hair, R.A.J., McLuckey, S.A.: Selective Disulfide Bond Cleavage in Gold(I) Cationized Polypeptide Ions Formed via Gas-Phase Ion/Ion Cation Switching. *J. Proteome Res.* **2006**, 5, 2087-2092.
33. Mentinova, M., Han, H., McLuckey, S.A.: Dissociation of Disulfide-Intact Somatostatin Ions: The Roles of Ion Type and Dissociation Method. *Rapid Commun. Mass Spectrom.* **2009**, 23, 2647-2655.
34. Mentinova, M., McLuckey, S.A.: Cleavage of Multiple Disulfide Bonds in Insulin via Gold Cationization and Collision-Induced Dissociation. *Int. J. Mass Spectrom.* **2011**, 308, 133-136.
35. Londry, F.A., Hager, J.W.: Mass Selective Axial Ion Ejection from a Linear Quadrupole Ion Trap. *J. Am. Soc. Mass. Spectrom.* **2003**, 14, 1130-1147.
36. Webb, I.K., Londry, F.A., McLuckey, S.A.: Implementation of Dipolar Direct Current (DDC) Collision-Induced Dissociation in Storage and Transmission Modes on a Quadrupole/Time-Of-Flight Tandem Mass Spectrometer. *Rapid Commun. Mass Spectrom.* **2011**, 25, 2500-2510.
37. Wysocki, V.H., Cheng, G., Zhang, Q., Herrmann, K.A., Beardsley, R.L., Hilderbrand, A.E.: Peptide Fragmentation Overview. John Wiley & Sons, Inc., 2006.
38. McCormack, A.L., Somogyi, A., Dongre, A.R., Wysocki, V.H.: Fragmentation of Protonated Peptides: Surface-Induced Dissociation in Conjunction with a Quantum Mechanical Approach. *Anal. Chem.* **1993**, 65, 2859-2872.
39. Somogyi, Á., Wysocki, V.H., Mayer, I.: The Effect of Protonation Site on Bond Strengths in Simple Peptides: Application of Ab Initio and Modified Neglect of Differential Overlap Bond Orders and Modified Neglect of Differential Overlap Energy Partitioning. *J. Am. Soc. Mass. Spectrom.* **1994**, 5, 704-717.
40. Paizs, B., Suhai, S.: Combined Quantum Chemical and RRKM Modeling of the Main Fragmentation Pathways of Protonated GGG. II. Formation of b₂, y₁, and y₂ Ions. *Rapid Commun. Mass Spectrom.* **2002**, 16, 375-389.
41. Chen, J., Guan, S.-M., Sun, W., Fu, H.: Melittin, the Major Pain-Producing Substance of Bee Venom. *Neurosci. Bull.* **2016**, 32, 265-272.

42. Terwilliger, T.C., Eisenberg, D.: The Structure of Melittin. II. Interpretation of the Structure. *J. Biol. Chem.* **1982**, 257, 6016-6022.
43. Kreil, G.: The Structure of Apis Dorsata Melittin: Phylogenetic Relationships between Hhoneybees as Deduced from Sequence Data. *FEBS Lett.* **1975**, 54, 100-102.
44. Hunt, D.F., Yates, J.R., Shabanowitz, J., Winston, S., Hauer, C.R.: Protein Sequencing by Tandem Mass Spectrometry. *Proc. Natl. Acad. Sci.* **1986**, 83, 6233-6237.
45. Loo, J.A., Edmonds, C.G., Smith, R.D.: Tandem Mass Spectrometry of Very Large Molecules. 2. Dissociation of Multiply Charged Proline-Containing Proteins from Electrospray Ionization. *Anal. Chem.* **1993**, 65, 425-438.
46. Brechi, L.A., Tabb, D.L., Yates, J.R., Wysocki, V.H.: Cleavage N-Terminal to Proline: Analysis of a Database of Peptide Tandem Mass Spectra. *Anal. Chem.* **2003**, 75, 1963-1971.

CHAPTER 3. GOLD (I) CATIONIZATION PROMOTES RING OPENING IN LYSINE CONTAINING CYCLIC PEPTIDES

Adapted by permission from Springer Nature: Journal of the American Society for Mass Spectrometry, Foreman, D. J.; Lawler, J. T.; Niedrauer, M. L.; Hostetler, M. A.; McLuckey, S. A. *J. Am. Soc. Mass Spectrom.* **2019**, 30, 1914–1922. Copyright 2019.

3.1 Introduction

Cyclic peptides are a class of biomolecules that are more difficult to sequence by mass spectrometry than their linear counterparts. While encountered less often than linear peptides, cyclic peptides represent a body of bioactive natural products and synthetics whose structures must be characterized. Cyclotides, for example, are macrocyclic peptides comprised of a head-to-tail cyclic backbone and three intramolecular disulfide bonds forming a cyclic cysteine knot.^{1,2} This motif instills remarkable thermal, chemical, and enzymatic stability^{3,4} with promising applications in therapeutics and agriculture.^{5–14} Similarly, sunflower trypsin inhibitor (SFTI) analogs, the simplest head-to-tail cyclic peptides containing a single disulfide bond, for example, have been examined as inflammatory bowel disease drug candidates,¹⁵ mammalian melanocortin receptor agonists,¹⁶ autoantibody scavengers,¹⁷ mesotrypsin inhibitors,¹⁸ and plasmin inhibitors.¹⁹

Dating back to the early days of cyclic peptide analysis, nuclear magnetic resonance (NMR) techniques have emerged as, perhaps, the primary means of characterization^{20–22} and remain a popular choice today.^{23–26} However, NMR is not well-suited to sequencing peptides and generally requires multiple milligrams of purified sample. Mass spectrometry-based techniques, on the other hand, are commonly used for peptide sequencing and are attractive for their relatively small sample size and minimal purity requirements. Gross and co-workers first demonstrated the utility of tandem mass spectrometry for cyclic peptide analysis in 1982²⁷ and continued to pioneer MS/MS approaches into the early 2000s. Despite its continued use,^{28–31} tandem mass spectrometry of cyclic peptides remains challenging, particularly regarding data interpretation. Sequence information of a linear peptide is derived via the predictable dissociation of the peptide ion along the amide backbone. Specifically, b- and y-fragment ions are typically generated upon collisional activation of a linear peptide; these fragment ions can be used to elucidate the primary structure.³² MSⁿ of cyclic peptides, on the other hand, requires the cleavage of two amide bonds to generate any

observable fragment ions. In principle, ring opening can occur at any residue creating linear peptide isomers of identical mass complicating the interpretation of the subsequent product ion spectrum. This spectral complexity is exacerbated with UVPD as a-, b-, c- and x-, y-, z-type ions may be formed.^{30,31} It is widely known, however, that backbone cleavages adjacent to particular amino acids can be preferred under some conditions. For example, the facile opening N-terminal to proline residues upon collisional activation has been exploited to aid in structural elucidation of cyclic peptides by mass spectrometry.^{33,34}

The MS/MS sequencing of cyclic peptides can be facilitated through the incorporation of a site-specific ring opening resulting in fragment ions that contain a common N-terminus. For example, several reports of solution-based linearization via enzymatic digestion have appeared.³⁵⁻³⁷ These methods, however, are not universal as cyclic peptides can show remarkable resistance to enzymatic digestion.³ Recently, Brodbelt and co-workers have reported an analogous gas-phase strategy to linearize stapled and cyclic peptides by taking advantage of the “ornithine effect.”^{38,39} Conversion of arginine to ornithine is accomplished through solution-phase deguanidination in the presence of hydrazine. Collisional activation of the ornithine containing cyclic peptide resulted in selective fragmentation C-terminal to the ornithine residue, offering a gas-phase approach to site-selective linearization, enhancing cyclic peptide characterization.

In the present work, we use gold (I) cationization to promote site-specific ring opening of cyclic peptides. Helmut Schwarz is a pioneer in the study of gas-phase organometallic chemistry in general,^{40,41} and he and his co-workers have described many of the unique characteristics of Au(I) chemistry in the gas phase.⁴² The gas-phase organometallic chemistry of gold has been reviewed.⁴³ We have recently noted that collisional activation of $[M + Au]^+$ precursor ions undergo gas-phase oxidation at neutral lysine residues resulting in a weakened C-N bond N-terminal to lysine.⁴⁴ For linear peptides, subsequent activation of the oxidized ion exhibits a facile fragmentation channel competitive with the proline effect. Incorporation of this “weak spot” into cyclic peptide ions via the loss of gold hydride and a molecule of ammonia presents an opportunity to selectively linearize cyclic peptides in the gas phase. Fragment ions containing a common N-terminus upon opening can simplify the MS/MS spectrum and aid in primary structure determination. While competitive ring opening sites can occur, we can further probe the loss of 109 Da to pinpoint the site of linearization at the oxidized lysine residue. This entirely gas-phase approach is demonstrated with sunflower trypsin inhibitor and a model cyclic peptide, -Loop.

3.2 Experimental

3.2.1 Materials and Reagents

Ammonium bicarbonate, dithiothreitol (DTT), iodoacetamide, and gold (III) chloride were purchased from Sigma-Aldrich (St. Louis, MO, USA). HPLC-grade methanol and Optima LC/MS-grade water were purchased from Fisher Scientific (Fair Lawn, NJ, USA), and acetic acid was purchased from Mallinckrodt (Phillipsburg, NJ, USA). Reduced sunflower trypsin inhibitor (SFTI), cyclo-GRCTKSIPPICFPD, was synthesized by Biomatek (Wilmington, DE, USA). - Loop, [45] cyclo-GRWQYV(D-Pro)GKFTVQ(D-Pro), was synthesized by the Gellman Lab of the University of Wisconsin Madison.

3.2.2 Sample Preparation

A gold (III) chloride stock solution was diluted to approximately 5 μM with methanol. - Loop stock solution was prepared at a concentration of 250 $\mu\text{g/mL}$ in an equal mixture of water and methanol. The stock was diluted 20-fold to a concentration of 12.5 $\mu\text{g/mL}$, approximately 7.5 μM , with 49.5:49.5:1, by volume, water/methanol/acetic acid. The sample was used without further purification.

Approximately 1 mg of SFTI was dissolved in 1 mL of reduction buffer (100 mM ammonium bicarbonate, 7 M urea) and incubated at 55 $^{\circ}\text{C}$ for 45 min with 5 mM DTT. After incubation, the solution was cooled to room temperature and then centrifuged briefly to collect any condensation. Fourteen microliters of a freshly prepared 500 mM iodoacetamide solution was added to the mixture and incubated at room temperature in the dark for 30 min. An additional 5 mM of DTT was added. The mixture was then incubated at room temperature for 15 min in the dark. Ten microliters of the reduced and alkylated SFTI was desalted using a TopTip C-18 desalting column (Glygen, Columbia, MD) as per the manufacturer's instructions. The final solution concentration was approximately 6.5 μM .

3.2.3 Mass Spectrometry

All data were collected using a QTRAP 4000 hybrid triple quadrupole/linear ion trap mass spectrometer (Sciex, Concord, ON, Canada), previously modified for ion/ion reactions.⁴⁶ Reagent anions and analyte cations were introduced into the mass spectrometer via alternately pulsed nano-

electrospray ionization (nESI).⁴⁷ Cation switching ion/ion reactions involving gold have been described previously.^{44,48,49} Briefly, the $[\text{AuCl}_2]^-$ reagent anions were isolated in Q1 and transferred to q2, followed immediately by injection of the isolated $[\text{M} + 2\text{H}]^{2+}$ analyte cations. The ions were mutually stored in q2 for up to 1000 ms, forming the $[\text{M} + 2\text{H} + \text{AuCl}_2]^+$ complex. Beam-type CID of the complex from q2 to Q3 resulted in the loss of two neutral HCl molecules, leaving the gold (I) cationized peptide ions, denoted $[\text{M} + \text{Au}]^+$. MS^n experiments were performed in Q3 where aured ions were dissociated via resonance excitation at a q value of 0.2. Product ions were mass analyzed via mass-selective axial ejection (MSAE).⁵⁰ Theoretical product ion masses were generated with CycloBranch and all product ions were verified manually.⁵¹ Figure 3.1 shows the structures of the two cyclic peptides examined in this study.

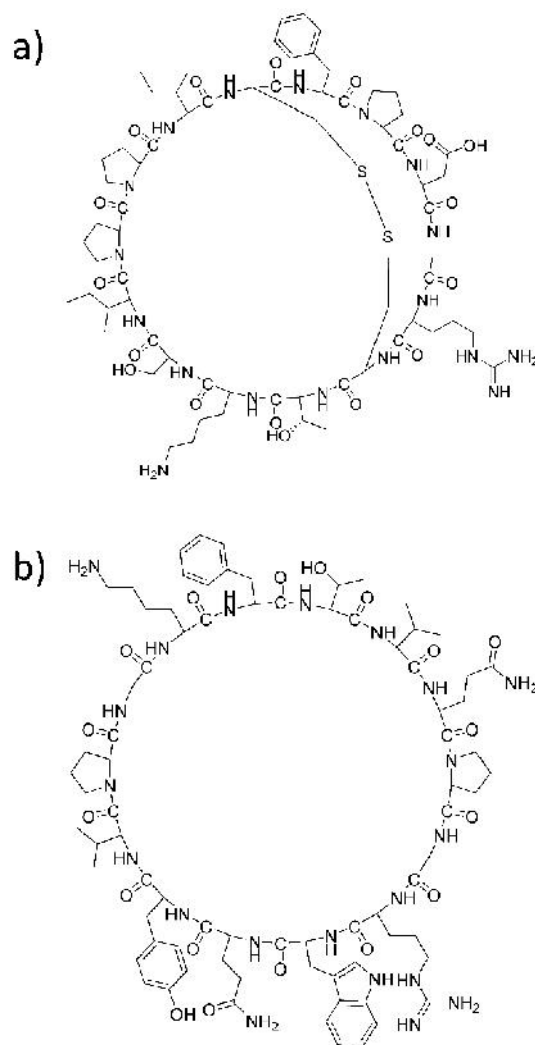
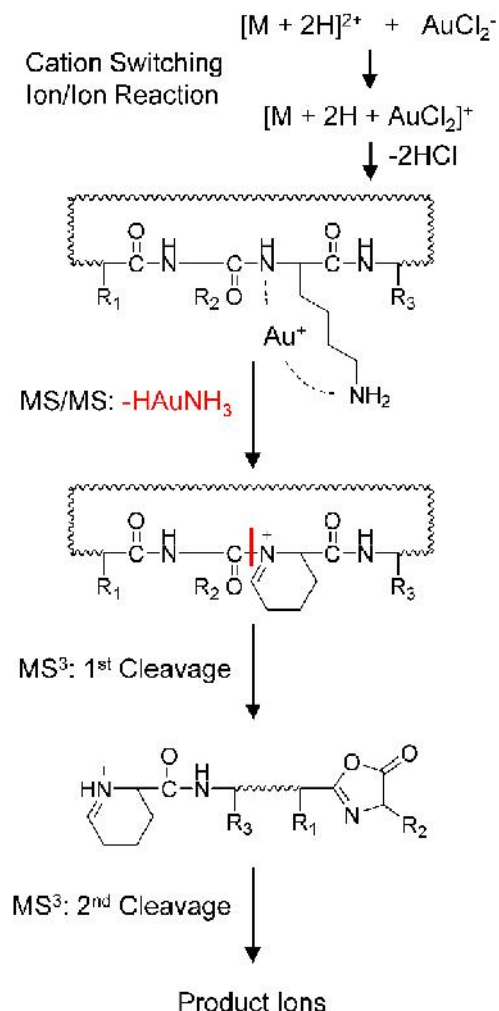


Figure 3.1. Structures of (a) sunflower trypsin inhibitor and (b) -loop. Stereochemistry not shown.

3.3 Results and Discussion

This strategy aims to introduce a weak spot into cyclic peptides by virtue of gas-phase oxidation of neutral lysine residues in gold (I) cationized peptide ions. It has been shown that this oxidation occurs through the consecutive losses of gold hydride and a molecule of ammonia, in either order, generating a cyclic iminium ion and a weaker C-N bond.⁴⁴ Consequently, upon collisional activation, cleavage N-terminal to the oxidized lysine residue is observed as a preferred dissociation pathway. For cyclic peptides, it is expected that activation of the oxidized species, $[M - H - NH_3]^+$, results in the same site-selective fragmentation as their linear counterparts. This initial cleavage converts the cyclic peptide into an acyclic peptide with an imine at the N-terminus and an oxazolone ion, or structural equivalent (e.g., acylium ion) at the C-terminus. Linearization via the initial cleavage of the peptide results in no change in mass-to-charge. Thus, a second cleavage along the peptide backbone is required to form product ions. The described gas-phase ion/ion strategy is illustrated in Scheme 3.1.



Scheme 3.1. General strategy for cyclic peptide analysis via gold (I) cationization utilizing gas-phase ion/ion chemistry.

3.3.1 Sunflower Trypsin Inhibitor

The cation switching ion/ion reaction between doubly protonated reduced and alkylated sunflower trypsin inhibitor and the gold dichloride reagent anion generates the $[M + 2H + AuCl_2]^+$ complex ion. Subsequent beam-type CID of the complex generates a prominent aured peptide ion, $[M + Au]^+$, at m/z 1825.8. As shown in Figure 3.2a, ion trap CID of the monoisotopically isolated $[M + Au]^+$ ion results in dominant losses of 91 Da, likely arising from the even electron side chain loss of C_2H_5NOS (91.01 Da) from the carbamidomethyl cysteine residues to form dehydroalanine. The loss of the carbamidomethyl side chain was found to be a charge remote fragmentation pathway. That is to say the loss of 91 Da is prevalent in systems with limited proton

mobility. Figure 3.3 shows the product ion spectrum resulting from collisional activation of the reduced and alkylated model peptide AACAAACA. In the positive mode with the presence of an ionizing proton, there is no evidence for the loss of 91 Da (Figure 3.3a). Conversely, in the negative mode, in the absence of any protons, the base peak corresponds to the loss of 91 Da (Figure 3.3b).

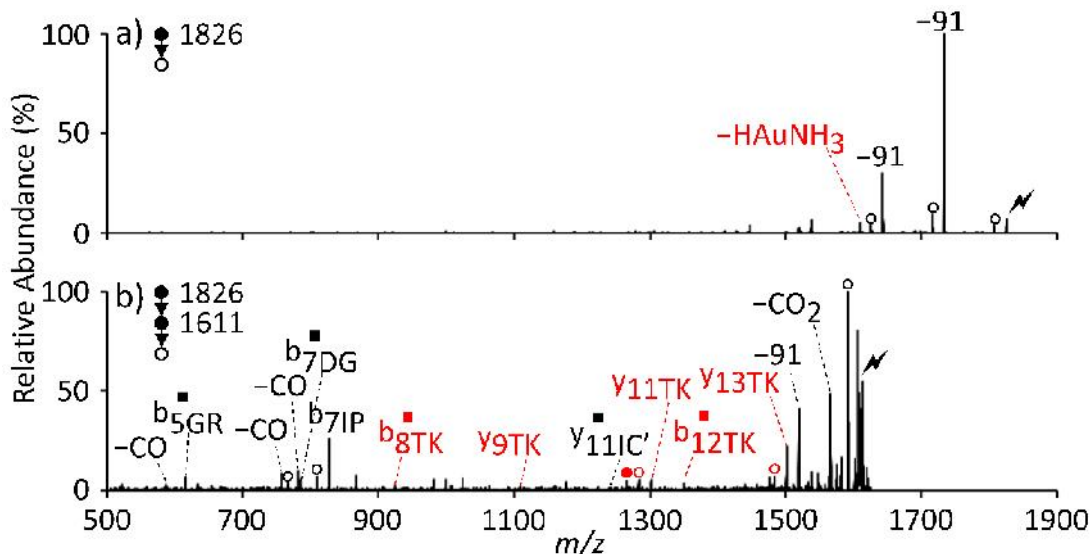


Figure 3.2. Activation of (a) $[M + Au]^+$ and (b) $[M - H - NH_3]^+$ where M = reduced and alkylated sunflower trypsin inhibitor. Open circles indicate water loss and shaded circles indicate ammonia loss. The lightning bolt indicates the species subjected to CID.

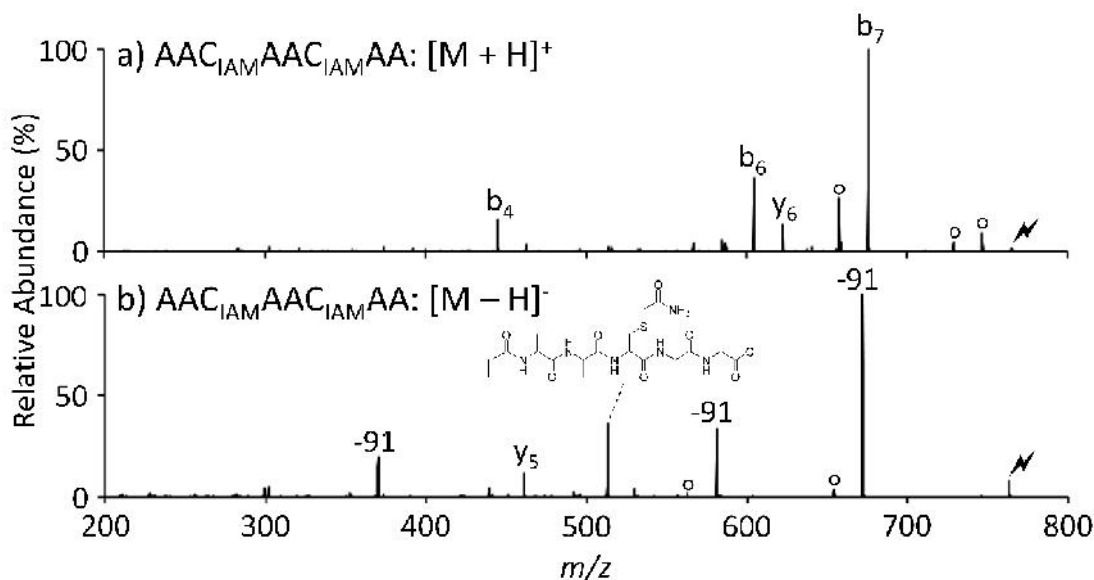


Figure 3.3. Activation of (a) $[M + H]^+$ and (b) $[M - H]^-$ where M = reduced and alkylated AACAAACA. Open circles indicate water loss and the lightning bolt indicates the species subjected to CID.

This charge remote dissociation channel is present with the four common alkylating agents, iodoacetamide, iodoacetic acid, acrylamide, and N-ethylmaleimide. Figure 3.4 shows the product ion spectrum from collisional activation of singly protonated reduced and alkylated KGAILCGAILR. Here, despite the system containing an ionizing proton, the proton is likely sequestered onto the arginine residue, thereby limiting the proton mobility. Activation of the peptide shows a loss of 91 Da, 92 Da, 105 Da, and 159 Da using iodoacetamide, iodoacetic acid, acrylamide, and N-ethylmaleimide, respectively, to alkylate the cysteine. In each case, the loss of the sidechain results in a product ion at m/z 1081. It is thought that the loss of alkyl sidechain generates a dehydroalanine residue.

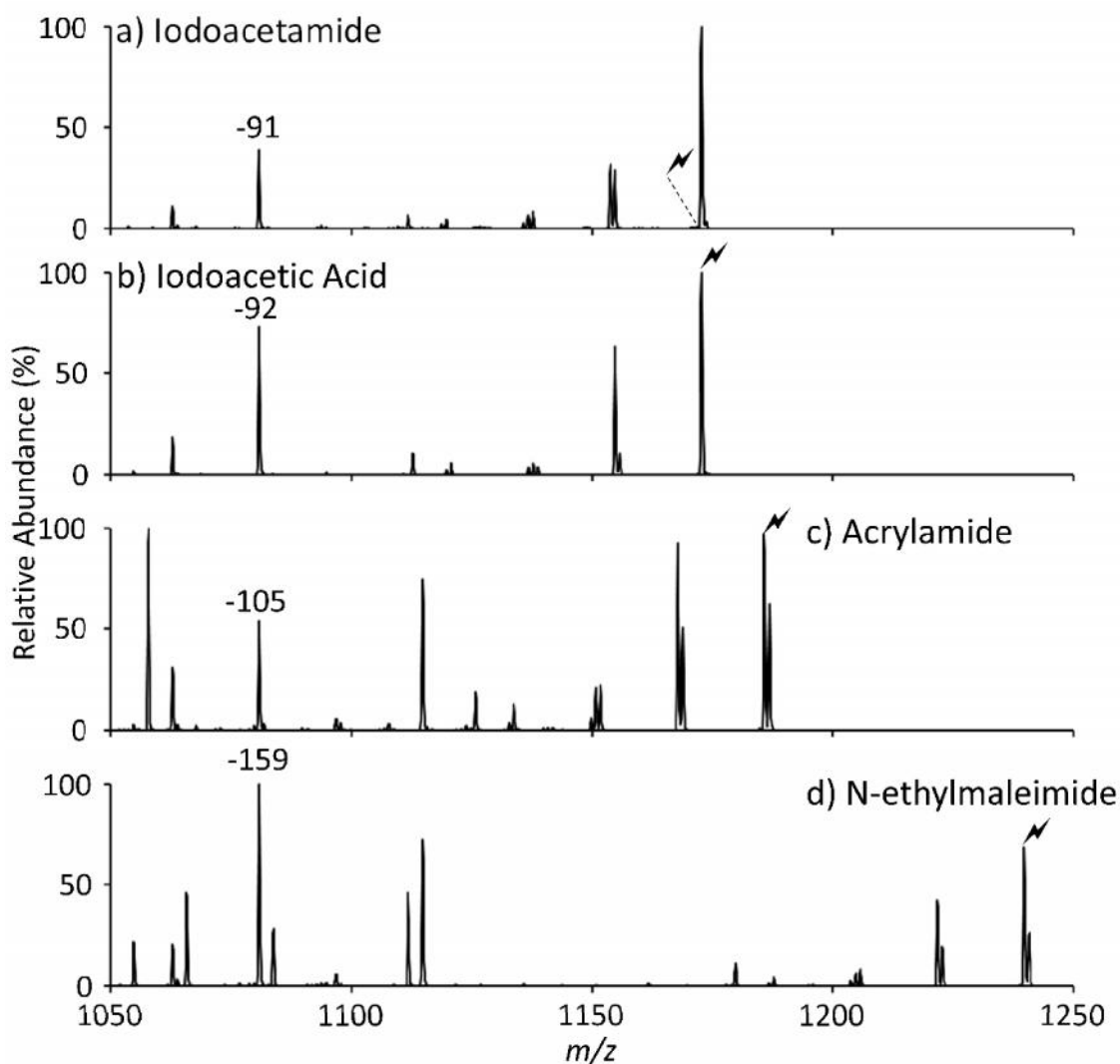


Figure 3.4. Activation of $[M + H]^+$ where M is reduced and alkylated KGAILCGAILR using a) iodoacetamide, b) iodoacetic acid, c) acrylamide, or d) N-ethylmaleimide as the alkylating agent. The lightning bolt indicates the species subjected to CID.

In order to confirm the identity of the product ion at m/z 1081 as a dehydroalanine containing peptide ion, dehydroalanine was introduced into KGAILCGAILR via ion/ion reaction with the periodate anion, IO_4^- .⁵² Briefly, KGAILCGAILR was alkylated with iodoacetic acid using the reduction and alkylation procedure described above. The IO_4^- reagent anions were injected, isolated in Q1 and transferred to q2, followed immediately by injection of the isolated $[\text{M} + 2\text{H}]^{2+}$ analyte cations. The ions were mutually stored in q2 for up to 300 ms, forming the $[\text{M} + 2\text{H} + \text{IO}_4]^+$ complex. The ions were transferred to Q3, where the complex ion was isolated. Ion trap CID of the complex generated the oxidized product ion, $[\text{M} + \text{H} + \text{O}]^+$, at m/z 1189. Subsequent activation of $[\text{M} + \text{H} + \text{O}]^+$, losses 108 Da to form $[\text{KGAILC}_{\text{Dha}}\text{GAILR} + \text{H}]^+$.⁵² The product ion spectrum from CID of the peak at m/z 1081 formed via ion/ion reaction with the periodate anion is identical to the product ion spectrum from CID of the peak at m/z 1081 formed via the loss of 92 Da directly from $[\text{KGAILC}_{\text{N-ethylmaleimide}}\text{GAILR} + \text{H}]^+$ (compare Figure 3.5a, b), confirming the presence of dehydroalanine. Additionally, the product ion spectra contain the c_5 and z_6 fragment ions which are characteristic of dehydroalanine.^{52,53}

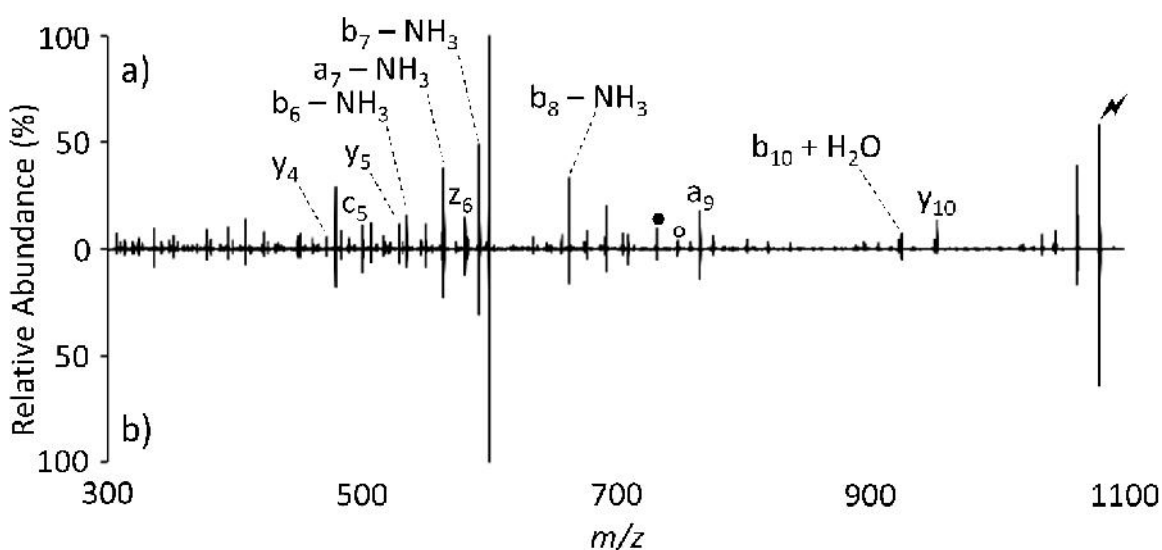


Figure 3.5. Activation of m/z 1081 formed via a) ion/ion reaction with IO_4^- or b) the loss of 159 from $[\text{KGAILC}_{\text{N-ethylmaleimide}}\text{GAILR} + \text{H}]^+$. Open circles indicate water loss and shaded circles indicate ammonia loss. The lightning bolt indicates the species subjected to CID.

Oxidation of lysine is evidenced by the loss of gold hydride and ammonia, designated as HAuNH_3 (215.00 Da), thereby yielding the oxidized product indicated as $[\text{M} - \text{H} - \text{NH}_3]^+$ (Figure

3.2a). The oxidized product ion is present at only 5% relative abundance. Nonetheless, the species was isolated and subjected to additional activation. CID of the $[M - H - NH_3]^+$ species generates the product ion spectrum shown in Figure 3.2b. The spectrum is comprised of sequence informative fragment ions and small molecule losses. Cyclic peptide fragment ions are labeled according to the nomenclature system of Ngoka and Gross.⁵⁴ Briefly, fragment ions are labeled using a four-part descriptor, x_nJZ , where x is the type of backbone fragment ion, n is the number of amino acids in the fragment ion, and J/Z designates the site of ring opening. For example, y_9^{TK} denotes the y_9 fragment ion generated from ring opening between the Thr-Lys bond. We note that a square superscript is associated with fragment ions that are shifted 19 Da lower in mass than their unoxidized counterparts (i.e. $[b_8 - H - NH_3]^+$ versus $[b_8 + H]^+$). Product ions formed through the preferential cleavage at lysine are highlighted in red and designated by the “TK” subscript; they represent approximately half of the structurally informative fragments. Among the other fragment ions are the b_{7IP} and b_{7DG}^{\blacksquare} . These ions are formed from cleavages C-terminal to an aspartic acid and N-terminal to a proline, two selective dissociation channels commonly observed in peptide ion tandem mass spectrometry.⁵⁵⁻⁵⁹

As mentioned above, oxidized SFTI was present at relatively low abundance due in part to the facile side-chain losses of the carbamidomethyl cysteines. While we could perform the MS³ experiment, in some cases, for reduced and alkylated cyclic peptides, the consecutive losses of 91 Da may divert signal from that associated with the oxidation at the lysine residue. We sought to investigate if oxidation occurs once these competitive fragmentation channels are exhausted. Isolation and CID of the ion generated from the first 91 Da loss from auroated SFTI results in, predominantly, a second loss of 91 Da (Figure 3.6b), consistent with the fact that there are two alkylated cysteine residues. Subsequent activation of the ion generated by the second loss of 91 Da, resulting in the spectrum shown in Figure 3.6c, generates the base peak at m/z 1428.8, corresponding to the oxidation of the lysine as indicated by the loss of 215 Da.

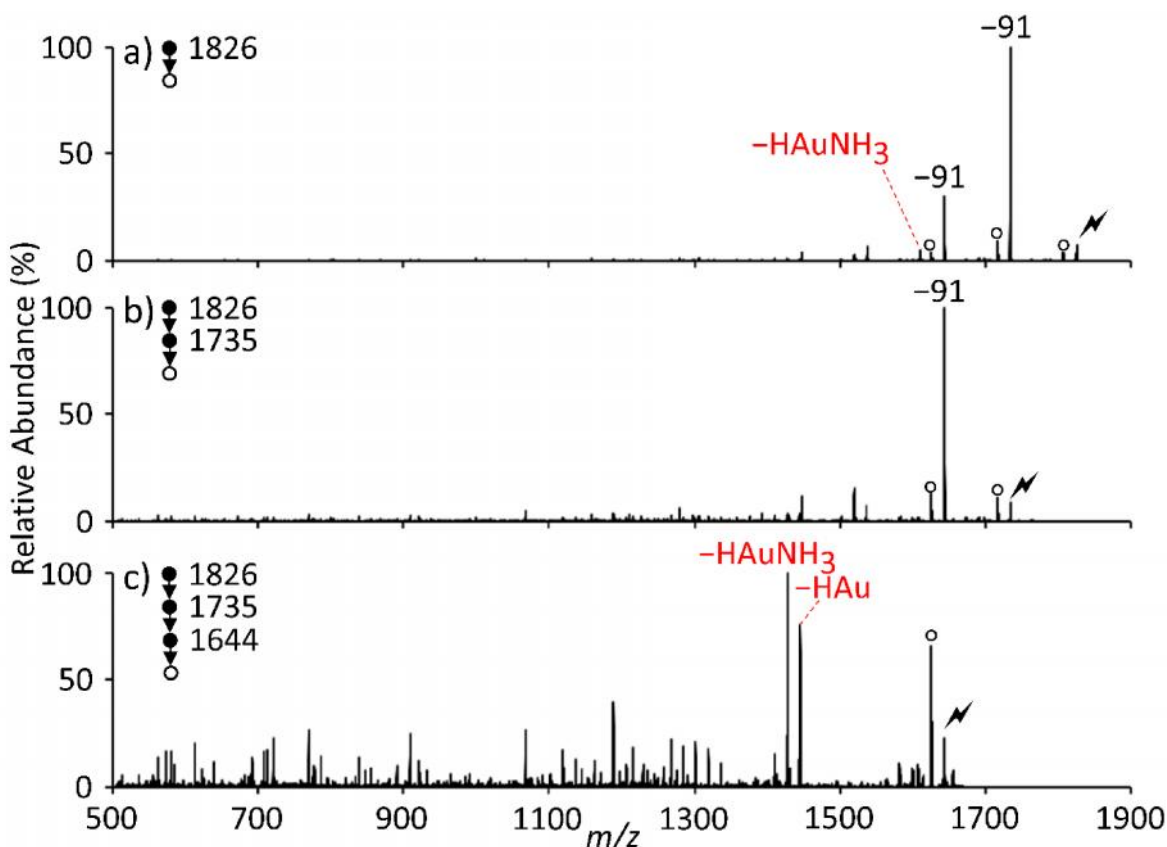
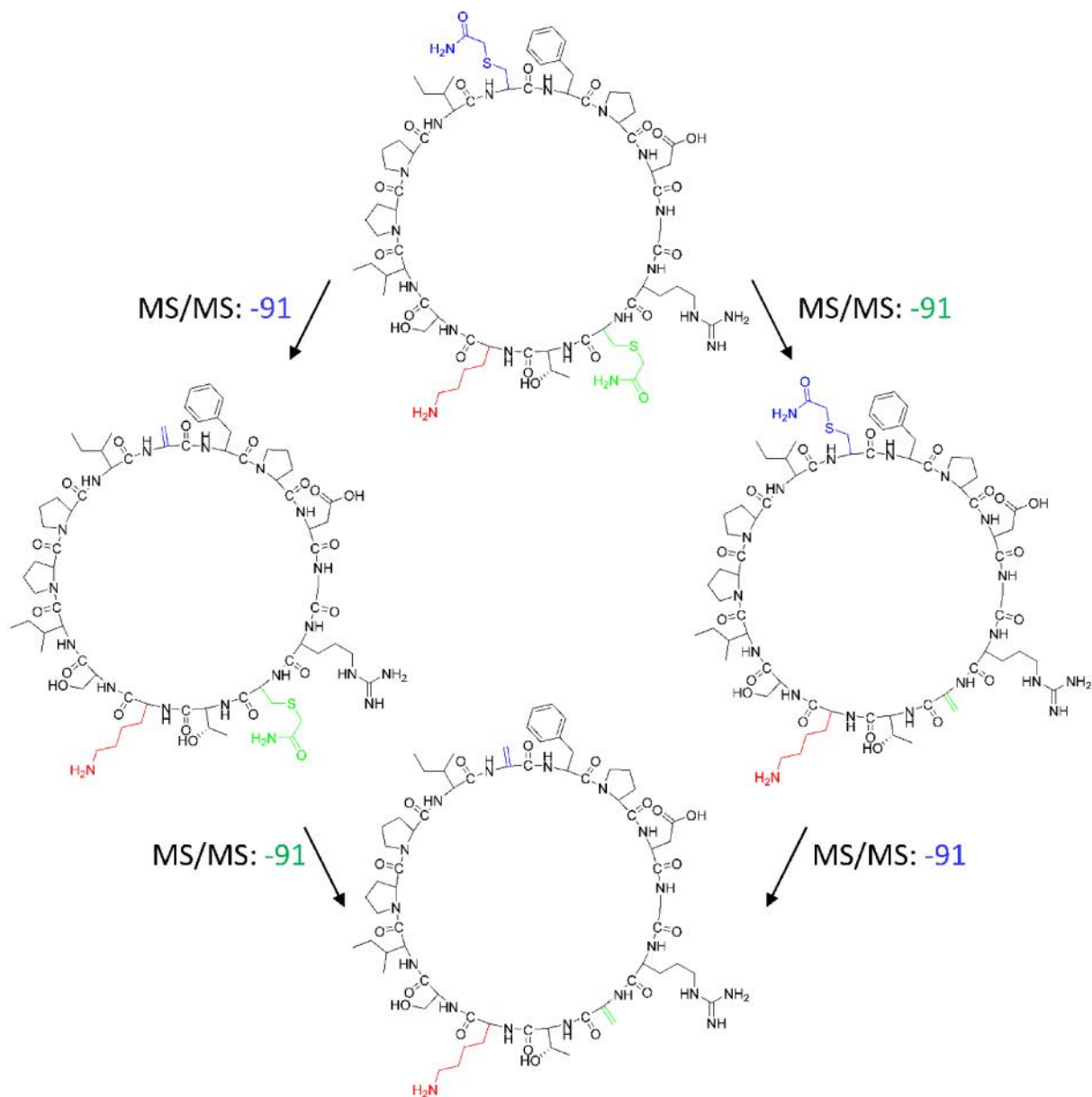


Figure 3.6. Activation of a) $[M + Au]^+$, b) $[M + Au - 91]^+$, and c) $[M + Au - 91 - 91]^+$ where M = reduced and alkylated sunflower trypsin inhibitor. Open circles indicate water loss. The lightning bolt indicates the species subjected to CID.

The consecutive side-chain losses can be viewed as the gas-phase formation of an SFTI analog in which both cysteine residues are converted to dehydroalanine residues (Scheme 3.2) and are indicated with a prime notation (i.e., C'). Figure 3.7 shows the spectrum obtained upon collisional activation of the oxidized dehydroalanine containing cyclic peptide ion. While the most abundant peaks correspond to small molecule loss, there is evidence for ring opening at the lysine residue as indicated by the fragment ions labeled in red. A total of seven ions can be assigned to ring opening at Thr-Lys. Additionally, consistent with the formation of dehydroalanine, there are fragment ions related to an initial *c/z* cleavage adjacent to dehydroalanine.^{52,53} The structures of the acyclic peptides resulting from cleavage at lysine or either dehydroalanine are presented in Figure 3.8.



Scheme 3.2. Generation of the dehydroalanine analog of SFTI via the consecutive losses of 91 Da.

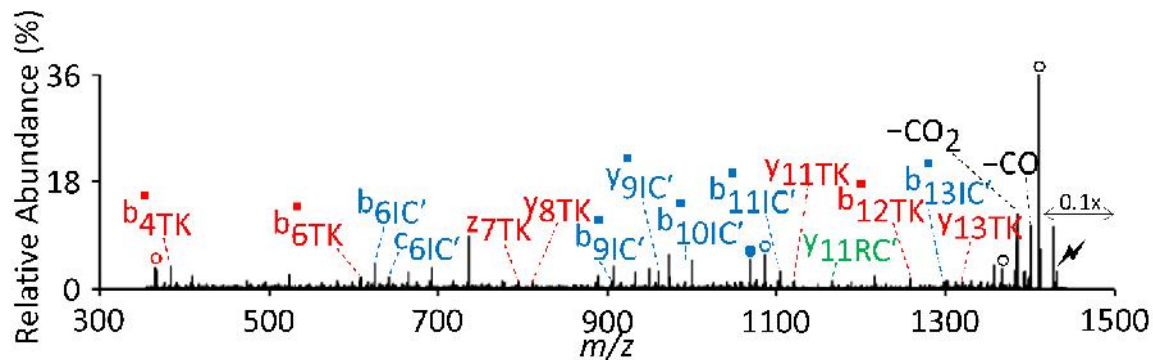


Figure 3.7. MS⁴ product ion spectrum of $[M - H - NH_3 - 91 - 91]^+$ formed via collisional activation as shown in Figure 3.6c. M = reduced and alkylated sunflower trypsin inhibitor. Open circles indicate water loss and shaded circles indicate ammonia loss. The lightning bolt indicates the species subjected to CID. Product ions corresponding to opening at lysine are highlighted in red. Fragment ions corresponding to opening at dehydroalanine are highlighted in blue and green.

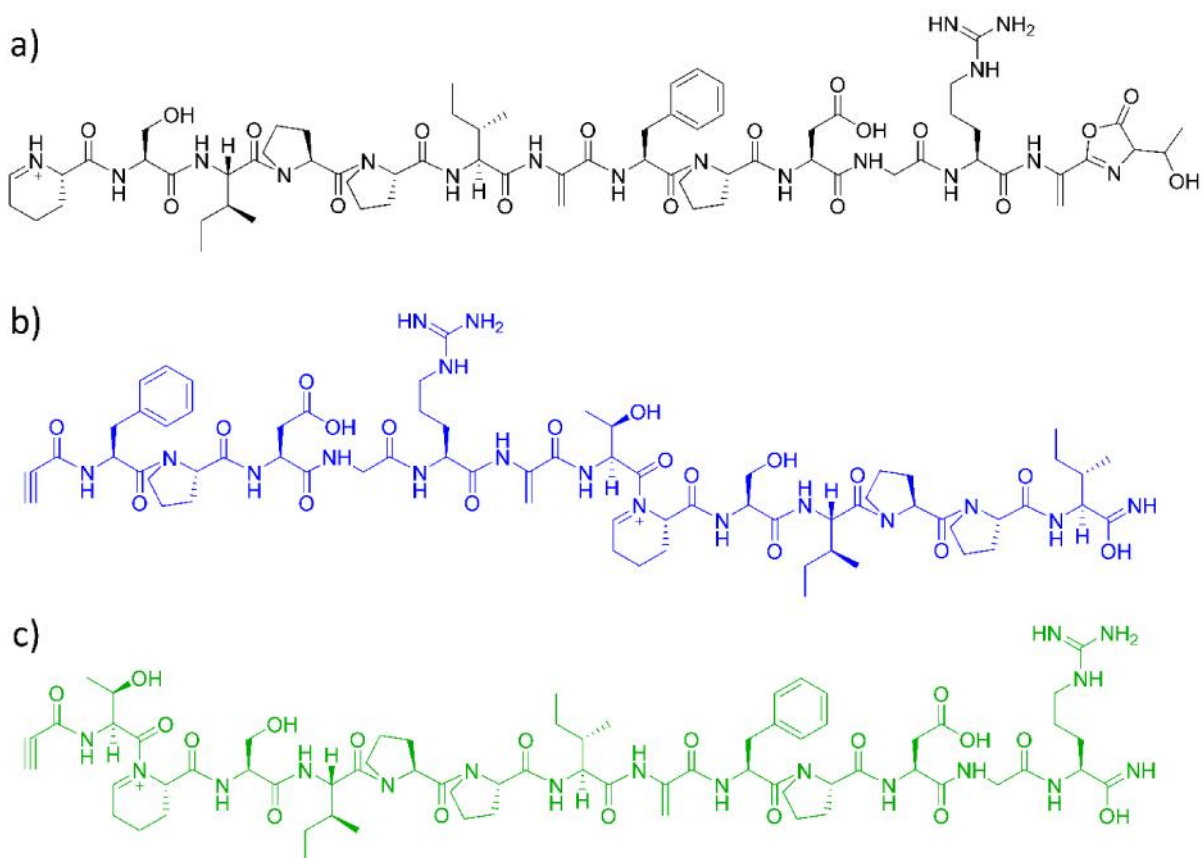


Figure 3.8. Linearized structures of SFTI corresponding to ring opening at a) the oxidized lysine residue, b) dehydroalanine at the 11th position, and c) dehydroalanine at the 3rd position.

Activation of the oxidized product ion, generated via the loss of HAuNH_3 directly from $[\text{M} + \text{Au}]^+$ or via the loss of HAuNH_3 from the $[\text{M} + \text{Au} - 91 - 91]^+$ ion, proved to be an effective ring opening strategy as demonstrated with sunflower trypsin inhibitor. In both cases, when compared to CID of singly and doubly protonated reduced and alkylated SFTI (Figure 3.9), an increase in structurally informative product ions was observed with the described Au (I) cationization approach. While this strategy aims to open cyclic peptides at lysine, competitive ring opening sites are observed at proline, aspartic acid, and dehydroalanine. Nonetheless, in both SFTI cases presented, about half of the product ions can be attributed to ring opening at lysine.

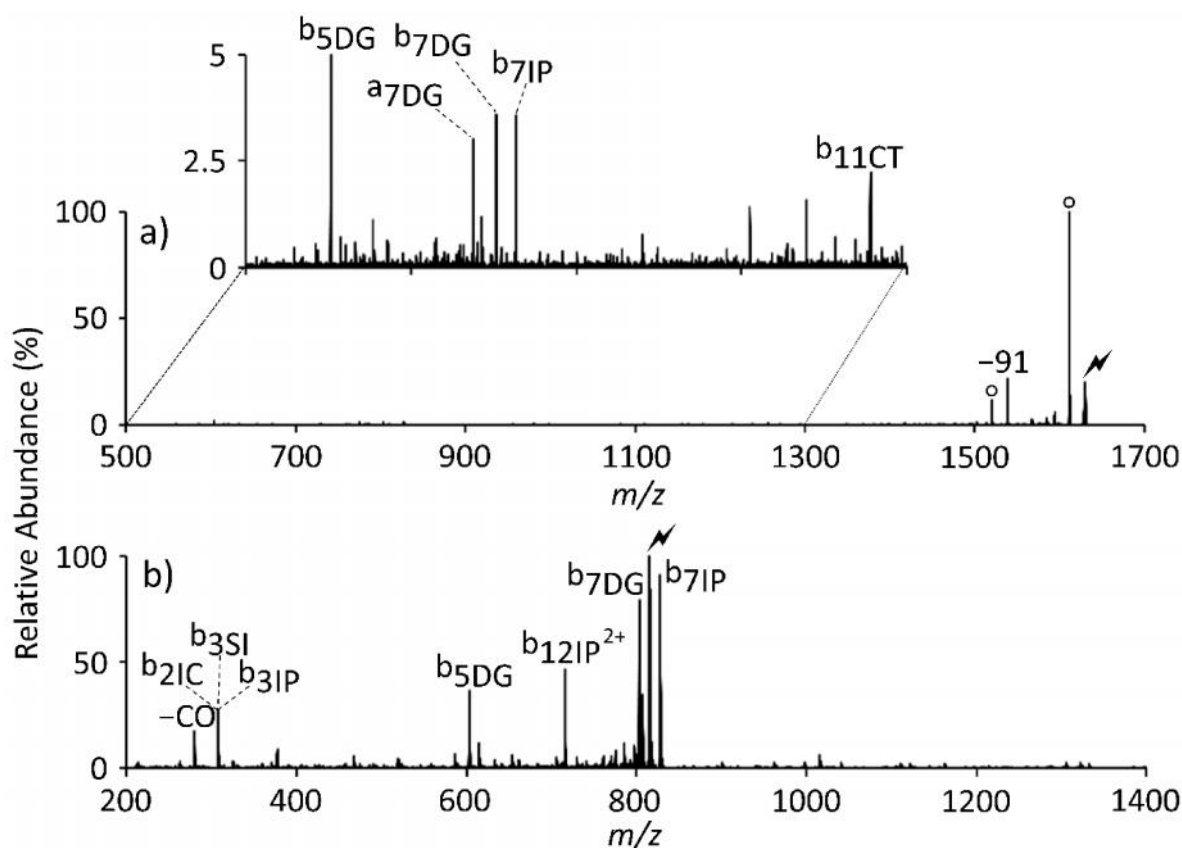


Figure 3.9. Activation of a) singly protonated reduced and alkylated sunflower trypsin inhibitor and b) doubly protonated reduced and alkylated sunflower trypsin inhibitor. Open circles indicate water loss. The lightning bolt indicates the species subjected to CID.

3.3.2 -Loop

Aurated -Loop was generated via the ion/ion chemistry described above. Oxidation of the lysine residue is observed to be the major process upon collisional activation of gold (I) cationized

-Loop (Figure 3.10a). The product ion spectrum also shows several aurred fragment ions. To maximize the abundance of the H_{Au}NH₃ loss, CID of [M + Au]⁺ was immediately followed by CID of the gold hydride loss, without isolation. Activation of the [M - H - NH₃]⁺ ion yields an abundant water loss, CO loss, CO₂ loss, and y_{13GK}, as well as a number of sequence informative fragments between *m/z* 500 and 1500.

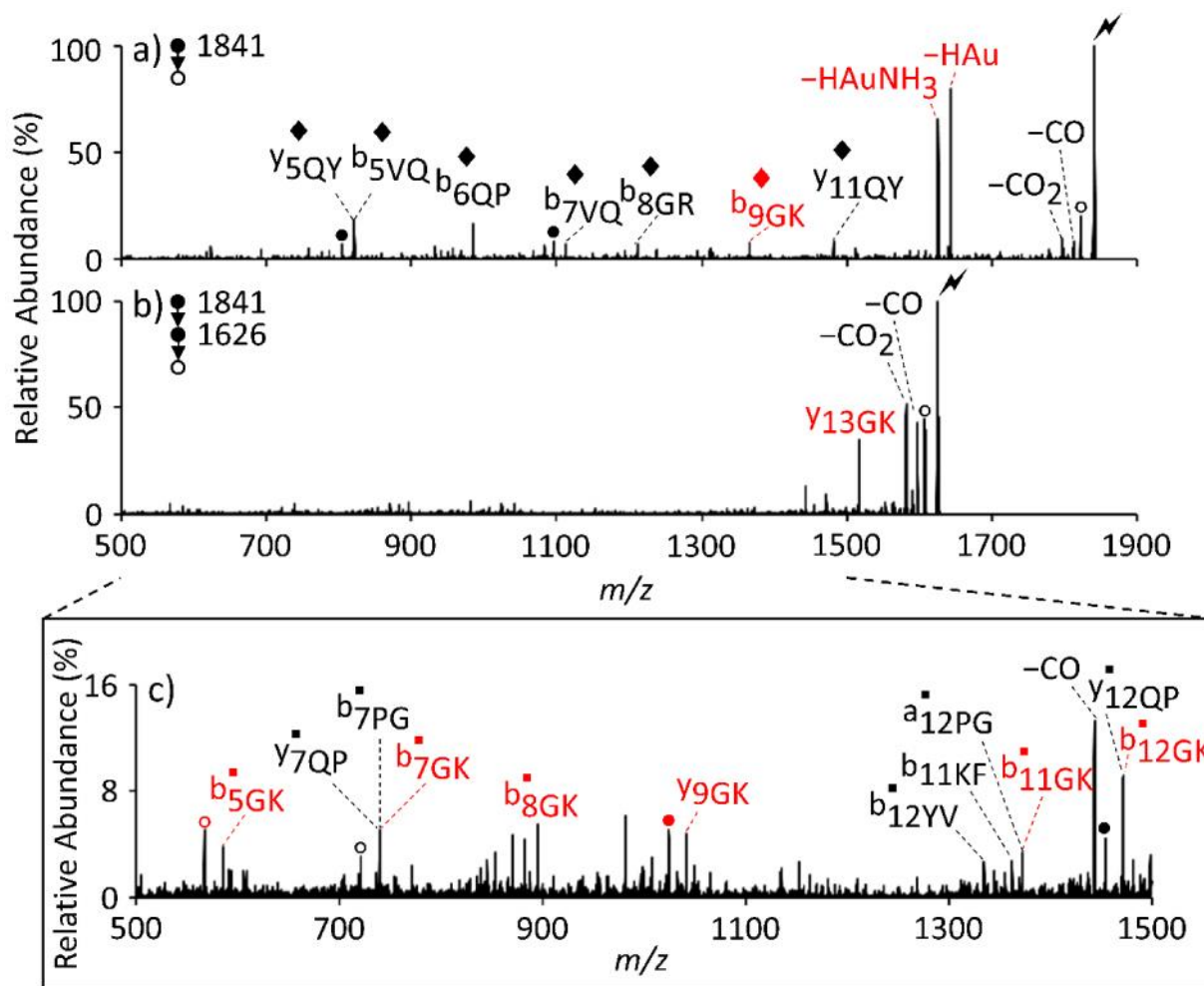


Figure 3.10. Activation of (a) [M + Au]⁺ and (b) [M - H - NH₃]⁺ where M = -loop. (c) Expanded view of (b) between *m/z* 500 and *m/z* 1500. Open circles indicate water loss and shaded circles indicate ammonia loss. The diamond superscript indicates an aurred ion. The lightning bolt indicates the species subjected to CID.

Figure 3.10c is an expanded view of Figure 3.10b over the range of *m/z* 500 to *m/z* 1500. Close examination of the product ions in this range reveals the following low-abundance ions originating from the ring opening at the lysine residue: b_{5GK}, b_{7GK}, b_{8GK}, y_{9GK}, b_{11GK}, and b_{12GK}.

Complicating data interpretation, three of the aforementioned fragment ions are isomeric with other plausible product ions. Specifically, the b_{7GK}^{\blacksquare} is isomeric with b_{7QP}^{\blacksquare} and b_{7PG}^{\blacksquare} , b_{11GK}^{\blacksquare} is isomeric with a_{12PG}^{\blacksquare} , and b_{12GK}^{\blacksquare} is isomeric with y_{12QP}^{\blacksquare} . While it is likely that ring opening occurs primarily N-terminal to lysine, the SFTI data and previous reports suggest that cleavage N-terminal to proline could be a competitive dissociation pathway.^{33,34} Therefore, the y_{7QP}^{\blacksquare} and y_{12QP}^{\blacksquare} fragment ions are plausible products and may therefore contribute to the product ion spectrum.

For unambiguous fragment ion assignment and to pinpoint the site of ring opening at lysine, we further probed the y_{13GK} fragment ion, which is 109 Da lower in mass than the $[M - H - NH_3]^+$ precursor ion. As discussed below, this fragment ion is generated by the loss of the oxidized lysine residue from the N-terminus. The utility of fragmenting the ion generated by consecutive losses of 215 Da and 109 Da is first discussed using the linear peptide KGAILPGAILR for illustration (Figure 3.11). Oxidation of the lysine residue is indicated with the signature loss of 215 Da, $HAuNH_3$ (Figure 3.11a). Activation of the oxidized $[M - H - NH_3]^+$ species is shown in Figure 3.11b. The base peak arises from the loss of 109 Da, producing the y_{10} fragment ion, which, in essence, is singly protonated GAILPGAILR. The fragmentation of the y_{10} fragment ion and fragmentation of singly protonated GAILPGAILR generate identical spectra (compare Figure 3.11c, d), confirming the loss of 109 Da as the loss of the oxidized lysine residue.

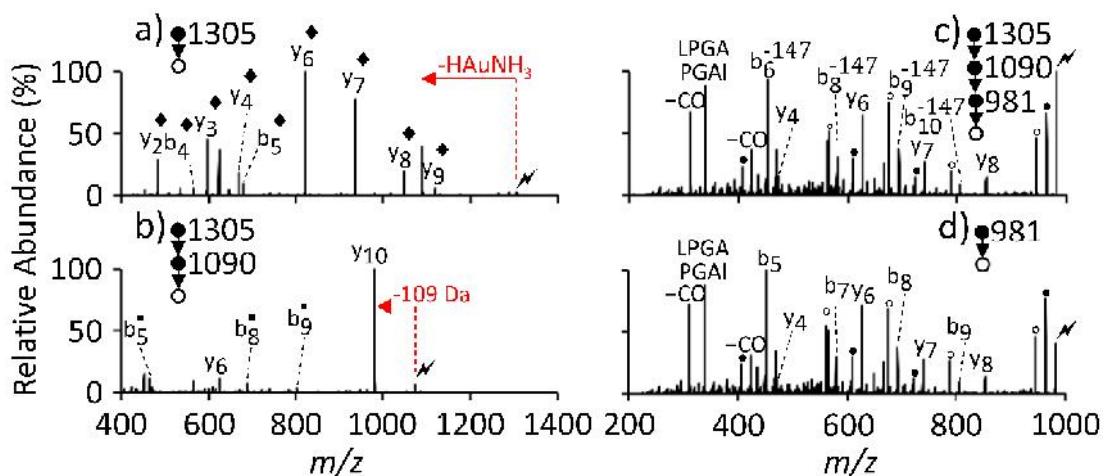


Figure 3.11. Activation of (a) $[M + Au]^+$, (b) $[M - H - NH_3]^+$, and (c) y_{10} where $M = KGAILPGAILR$. Activation of (d) $[GAILPGAILR + H]^+$. Open circles indicate water loss and shaded circles indicate ammonia loss. The lightning bolt indicates the species subjected to CID. Lysine residue loss (i.e., 147 Da lower in mass) is represented with a superscripted “-147.”

Figure 3.12 demonstrates how the loss of 109 Da can be used to obtain unambiguous sequence information for the α -Loop cyclic peptide. The y_{13GK} fragment ion at m/z 1516.8 represents the acyclic peptide ion $[FTVQ(D-Pro)GRWQYV(D-Pro)G + H]^+$. Isolation and CID of y_{13GK} results in a series of 11 b- and y-fragment ions with unambiguous fragment ion structural assignments. This approach to cyclic peptide analysis successfully sequenced greater than 84% of the α -loop cyclic peptide, missing only fragment ions corresponding to cleavage of the Phe-Thr and Pro-Gly amide linkages. We note here that a loss of 109 Da was observed in the sunflower trypsin inhibitor product ion spectrum (Figure 3.2b). However, the signal was too low to perform additional stages of interrogation.

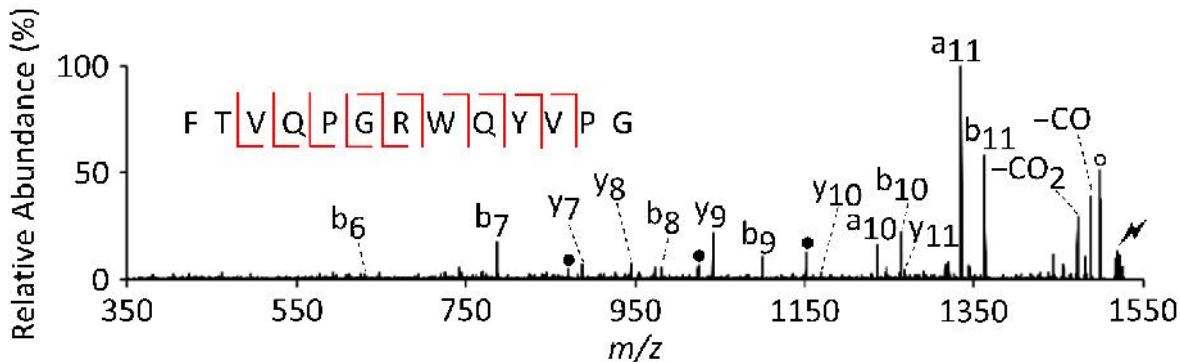


Figure 3.12. Activation of the y_{13GK} fragment ion of Figure 3.7b. Open circles indicate water loss and shaded circles indicate ammonia loss.

3.4 Conclusions

Selective ring opening of two lysine containing cyclic peptides is demonstrated. Ion/ion reactions are used to transform doubly protonated peptides to aurated peptide ions. Oxidation via the loss of $HAuNH_3$ produces a weakened amide bond adjacent to the lysine residue. The unusual redox process that leads to $[M - H - NH_3]^+$ from lysine-containing peptides is a characteristic of gold cationization. Collisional activation of the $[M - H - NH_3]^+$ species generates numerous fragment ions containing a common cyclic imine N-terminus, indicating a highly facile ring opening pathway. This selectivity simplifies the product ion spectrum as ring opening is localized to a few amide bonds.

Other facile cleavage reactions can compete with the process described above. In the case of sunflower trypsin inhibitor, the competitive pathways include openings N-terminal to proline, N-

terminal to dehydroalanine, and C-terminal to aspartic acid as evidenced by the fragment ions annotated DG, IP, IC, and RC. Ions generated via opening at dehydroalanine are more prevalent than ions corresponding to opening at aspartic acid and proline. Incorporation of dehydroalanine may present another strategy to selectively open cyclic peptides upon collisional activation. In the case of the α -Loop peptide ion, linearization at lysine is the major process, yet, linearization at proline is also observed. Additionally, several of the proline related fragment ions are isomeric with product ions opened at lysine. To avoid ambiguities in confident ion assignments arising from possibly isomeric fragments, isolation and activation of the product ion generated by successive losses of 215 Da and 109 Da from the $[M - H - NH_3]^+$ ion ensures that the ions arise from loss of an oxidized lysine residue from the N-terminus (viz., the y_{13GK} ion from α -Loop). CID of y_{13GK} , $[FTVQ(D-Pro)GRWQYV(D-Pro)G + H]^+$, cleaves 10 of the 12 amide bonds. This gas-phase strategy for cyclic peptide analysis offers a convenient means of selectively opening cyclic peptides. In favorable cases, when the abundance of the 109 Da loss does not limit the extent to which MS^4 can be performed, cyclic peptide linearization can be localized to the lysine residue.

3.5 References

1. Craik, D.J., Daly, N.L., Bond, T., Waite, C.: Plant Cyclotides: A Unique Family of Cyclic and Knotted Proteins that Defines the Cyclic Cystine Knot Structural Motif. *J. Mol. Biol.* **1999**, 294, 1327-1336.
2. Craik, D.J.: Discovery and Applications of the Plant Cyclotides. *Toxicon.* **2010**, 56, 1092-1102.
3. Colgrave, M.L., Craik, D.J.: Thermal, Chemical, and Enzymatic Stability of the Cyclotide Kalata B1: The Importance of the Cyclic Cystine Knot. *Biochemistry.* **2004**, 43, 5965-5975.
4. Craik, D.J., Conibear, A.C.: The Chemistry of Cyclotides. *J. Org. Chem.* **2011**, 76, 4805-4817.
5. Pranting, M., Lov, C., Burman, R., Goransson, U., Andersson, D.I.: The Cyclotide Cycloviolacin O2 from *Viola odorata* has Potent Bactericidal Activity Against Gram-Negative Bacteria. *J. Antimicrob. Chemother.* **2010**, 65, 1964-1971.
6. Grundemann, C., Koehbach, J., Huber, R., Gruber, C.W.: Do Plant Cyclotides Have Potential as Immunosuppressant Peptides? *J. Nat. Prod.* **2012**, 75, 167-174.

7. Tang, J., Wang, C.K., Pan, X., Yan, H., Zeng, G., Xu, W., He, W., Daly, N.L., Craik, D.J., Tan, N.: Isolation and Characterization of Cytotoxic Cyclotides from *Viola tricolor*. *Peptides*. **2010**, 31, 1434-1440.
8. Colgrave, M.L., Huang, Y.-H., Craik, D.J., Kotze, A.C.: Cyclotide Interactions with the Nematode External Surface. *Antimicrob. Agents Chemother.* **2010**, 54, 2160.
9. Colgrave, M.L., Kotze, A.C., Kopp, S., McCarthy, J.S., Coleman, G.T., Craik, D.J.: Anthelmintic Activity of Cyclotides: In Vitro Studies with Canine and Human Hookworms. *Acta Tropica*. **2009**, 109, 163-166.
10. Daly, N.L., Koltay, A., Gustafson, K.R., Boyd, M.R., Casas-Finet, J.R., Craik, D.J.: Solution Structure by NMR of Circulin A: A Macrocyclic Knotted Peptide having Anti-HIV Activity. *J. Mol. Biol.* **1999**, 285, 333-345.
11. Hallock, Y.F., Sowder, R.C., Pannell, L.K., Hughes, C.B., Johnson, D.G., Gulakowski, R., Cardellina, J.H., Boyd, M.R.: Cycloviolins A–D, Anti-HIV Macrocyclic Peptides from *Leonia cymosa*. *J. Org. Chem.* **2000**, 65, 124-128.
12. Jennings, C., West, J., Waive, C., Craik, D., Anderson, M.: Biosynthesis and Insecticidal Properties of Plant Cyclotides: The Cyclic Knotted Proteins from *Oldenlandia affinis*. *Proc. Natl. Acad. Sci.* **2001**, 98, 10614.
13. Jennings, C.V., Rosengren, K.J., Daly, N.L., Plan, M., Stevens, J., Scanlon, M.J., Waive, C., Norman, D.G., Anderson, M.A., Craik, D.J.: Isolation, Solution Structure, and Insecticidal Activity of Kalata B2, a Circular Protein with a Twist: Do Möbius Strips Exist in Nature? *Biochemistry*. **2005**, 44, 851-860.
14. Barbata, B.L., Marshall, A.T., Gillon, A.D., Craik, D.J., Anderson, M.A.: Plant Cyclotides Disrupt Epithelial Cells in the Midgut of Lepidopteran Larvae. *Proc. Natl. Acad. Sci.* **2008**, 105, 1221.
15. Caceres, C.C., Bansal, P.S., Navarro, S., Wilson, D., Don, L., Giacomini, P., Loukas, A., Daly, N.L.: An Engineered Cyclic Peptide Alleviates Symptoms of Inflammation in a Murine Model of Inflammatory Bowel Disease. *J. Biol. Chem.* **2017**, 292, 10288-10294.
16. Durek, T., Cromm, P.M., White, A.M., Schroeder, C.I., Kaas, Q., Weidmann, J., Ahmad Fuaad, A., Cheneval, O., Harvey, P.J., Daly, N.L., Zhou, Y., Dellsén, A., Österlund, T., Larsson, N., Knerr, L., Bauer, U., Kessler, H., Cai, M., Hruby, V.J., Plowright, A.T., Craik, D.J.: Development of Novel Melanocortin Receptor Agonists Based on the Cyclic Peptide Framework of Sunflower Trypsin Inhibitor-1. *J. Med. Chem.* **2018**, 61, 3674-3684.
17. Gunasekera, S., Fernandes-Cerqueira, C., Wennmalm, S., Wähämaa, H., Sommarin, Y., Catrina, A.I., Jakobsson, P.-J., Göransson, U.: Stabilized Cyclic Peptides as Scavengers of Autoantibodies: Neutralization of Anticitrullinated Protein/Peptide Antibodies in Rheumatoid Arthritis. *ACS Chem. Biol.* **2018**, 13, 1525-1535.

18. de Veer, S.J., Li, C.Y., Swedberg, J.E., Schroeder, C.I., Craik, D.J.: Engineering Potent Mesotrypsin Inhibitors based on the Plant-Derived Cyclic Peptide, Sunflower Trypsin Inhibitor-1. *Eur. J. Med. Chem.* **2018**, 155, 695-704.
19. Swedberg, J.E., Wu, G., Mahatmanto, T., Durek, T., Caradoc-Davies, T.T., Whisstock, J.C., Law, R.H.P., Craik, D.J.: Highly Potent and Selective Plasmin Inhibitors Based on the Sunflower Trypsin Inhibitor-1 Scaffold Attenuate Fibrinolysis in Plasma. *J. Med. Chem.* **2019**, 62, 552-560.
20. Fesik, S.W., Bolis, G., Sham, H.L., Olejniczak, E.T.: Structure Refinement of a Cyclic Peptide from Two-Dimensional NMR Data and Molecular Modeling. *Biochemistry.* **1987**, 26, 1851-1859.
21. Coles, M., Sowemimo, V., Scanlon, D., Munro, S.L.A., Craik, D.J.: A Conformational Study by Proton NMR of a Cyclic Pentapeptide Antagonist of Endothelin. *J. Med. Chem.* **1993**, 36, 2658-2665.
22. Mazzeo, M., Isernia, C., Rossi, F., Saviano, M., Pedone, C., Paolillo, L., Benedetti, E., Pavone, V.: Conformational Behaviour of a Cyclolinopeptide a Analogue: Two-Dimensional NMR Study of Cyclo(Pro¹-Pro-Phe-Phe-Ac₆c-Ile-Ala-Val⁸). *J. Pept. Sci.* **1995**, 1, 330-340.
23. Porter, C., Wilce, J.: NMR Analysis of G7 18NATE, A Nonphosphorylated Cyclic Peptide Inhibitor of the Grb7 Adapter Protein. *Pept. Sci.* **2007**, 88, 174-181.
24. Johnson, M., Liu, M., Struble, E., Hettiarachchi, K.: Characterization of Cyclic Peptides Containing Disulfide Bonds. *J. Pharm. Biomed. Anal.* **2015**, 109, 112-120.
25. Northfield, S., Wielens, J., Headey, S., Williams-Noonan, B., Mulcair, M., Scanlon, M., Parker, M., Thompson, P., Chalmers, D.: Cyclic Hexapeptide Mimics of the LEDGF Integrase Recognition Loop in Complex with HIV 1 Integrase. *ChemMedChem.* **2018**,
26. Laurencin, M., Simon, M., Fleury, Y., Baudy-Floc'h, M., Bondon, A., Legrand, B.: Selectivity Modulation and Structure of /aza- 3 Cyclic Antimicrobial Peptides. *Chem. Eur. J.* **2018**, 24, 6191-6201.
27. Gross, M.L., McCrery, D., Crow, F., Tomer, K.B., Pope, M.R., Ciuffetti, L.M., Knoche, H.W., Daly, J.M., Dunkle, L.D.: The Structure of the Toxin from *Helminthosporium carbonum*. *Tetrahedron Lett.* **1982**, 23, 5381-5384.
28. Tilvi, S., Naik, C.: Tandem Mass Spectrometry of Kahalalides: Identification of Two New Cyclic Depsipeptides, Kahalalide R and S from *Elysia grandifolia*. *J. Mass Spectrom.* **2007**, 42, 70-80.

29. Mohimani, H., Yang, Y.L., Liu, W.T., Hsieh, P.W., Dorrestein, P.C., Pevzner, P.A.: Sequencing Cyclic Peptides by Multistage Mass Spectrometry. *Proteomics*. **2011**, 11, 3642-3650.
30. Attard, T.J., Carter, M.D., Fang, M., Johnson, R.C., Reid, G.E.: Structural Characterization and Absolute Quantification of Microcystin Peptides Using Collision-Induced and Ultraviolet Photo-Dissociation Tandem Mass Spectrometry. *J. Am. Soc. Mass. Spectrom.* **2018**, 29, 1812-1825.
31. Parsley, N.C., Kirkpatrick, C.L., Crittenden, C.M., Rad, J.G., Hoskin, D.W., Brodbelt, J.S., Hicks, L.M.: PepSAVI-MS Reveals Anticancer and Antifungal Cycloviolacins in *Viola odorata*. *Phytochemistry*. **2018**, 152, 61-70.
32. Paizs, B., Suhai, S.: Fragmentation Pathways of Protonated Peptides. *Mass Spectrom. Rev.* **2005**, 24, 508-548.
33. Tomer, K.B., Crow, F.W., Gross, M.L., Kopple, K.D.: Fast-Atom Bombardment Combined with Tandem Mass Spectrometry for the Determination of Cyclic Peptides. *Anal. Chem.* **1984**, 56, 880-886.
34. Hitzeroth, G., Vater, J., Franke, P., Gebhardt, K., Fiedler, H.-P.: Whole Cell Matrix-Assisted Laser Desorption/Ionization Time-Of-Flight Mass Spectrometry and *In Situ* Structure Analysis of Streptocidins, A Family of Tyrocidine-Like Cyclic Peptides. *Rapid Commun. Mass Spectrom.* **2005**, 19, 2935-2942.
35. Poth, A.G., Colgrave, M.L., Philip, R., Kerenga, B., Daly, N.L., Anderson, M.A., Craik, D.J.: Discovery of Cyclotides in the Fabaceae Plant Family Provides New Insights into the Cyclization, Evolution, and Distribution of Circular Proteins. *ACS Chem. Biol.* **2011**, 6, 345-355.
36. Chan, L.Y., He, W., Tan, N., Zeng, G., Craik, D.J., Daly, N.L.: A New Family of Cystine Knot Peptides from the Seeds of *Momordica cochinchinensis*. *Peptides*. **2013**, 39, 29-35.
37. Narayani, M., Chadha, A., Srivastava, S.: Cyclotides from the Indian Medicinal Plant *Viola odorata* (Banafsha): Identification and Characterization. *J. Nat. Prod.* **2017**, 80, 1972-1980.
38. Crittenden, C.M., Parker, W.R., Jenner, Z.B., Bruns, K.A., Akin, L.D., McGee, W.M., Ciccimaro, E., Brodbelt, J.S.: Exploitation of the Ornithine Effect Enhances Characterization of Stapled and Cyclic Peptides. *J. Am. Soc. Mass. Spectrom.* **2016**, 27, 856-863.
39. McGee, W.M., McLuckey, S.A.: The Ornithine Effect in Peptide Cation Dissociation. *J. Mass Spectrom.* **2013**, 48, 856-861.
40. Eller, K.; Schwarz, H.: Organometallic in the Gas Phase. *Chem. Rev.* **1991**, 91, 1121-1177.

41. Schwarz, H. Relativistic Effects in Gas-Phase Ion Chemistry: An Experimentalist's View. *Angew. Chem. Int. Ed.* **2003**, 42, 4442-4454.
42. Schröder, D., Schwarz, H., Hrušák, J., Pyykkö, P. Cationic Gold (I) Complexes of Xenon and of Ligands Containing the Donor Atoms Oxygen, Nitrogen, Phosphorous, and Sulfur. *Inorg. Chem.* **1998**, 37, 624-632.
43. O'Hair, R.A.J., Mass Spectrometry of Organogold Compounds. In *The Chemistry of Organogold Compounds*; Rappoport, Z.; Liebman, J.F.; Marek, I. Eds.; John Wiley & Sons, Ltd: Chichester, UK, Chapter 4, 2014, 57-105
44. Foreman, D.J., Betancourt, S.K., Pilo, A.L., McLuckey, S.A.: Novel Peptide Ion Chemistry Associated with Gold (I) Cationization: Preferential Cleavage at Lysine Residues. *Int. J. Mass Spectrom.* **2018**, 427, 114-122.
45. Espinosa, J.F., Gellman, S.H. A Designed α -Hairpin Containing a Natural Hydrophobic Cluster. *Angew. Chem. Int. Ed.* **2000**, 39, 2330-2333.
46. Xia, Y., Wu, J., McLuckey, S.A., Londry, F.A., Hager, J.W.: Mutual Storage Mode Ion/Ion Reactions in a Hybrid Linear Ion Trap. *J. Am. Soc. Mass. Spectrom.* **2005**, 16, 71-81.
47. Liang, X., Xia, Y., McLuckey, S.A.: Alternately Pulsed Nanoelectrospray Ionization/Atmospheric Pressure Chemical Ionization for Ion/Ion Reactions in an Electrodynamic Ion Trap. *Anal. Chem.* **2006**, 78, 3208-3212.
48. Gunawardena, H.P., O'Hair, R.A.J., McLuckey, S.A.: Selective Disulfide Bond Cleavage in Gold(I) Cationized Polypeptide Ions Formed via Gas-Phase Ion/Ion Cation Switching. *J. Proteome Res.* **2006**, 5, 2087-2092.
49. Mentinova, M., McLuckey, S.A.: Cleavage of Multiple Disulfide Bonds in Insulin via Gold Cationization and Collision-Induced Dissociation. *Int. J. Mass Spectrom.* **2011**, 308, 133-136.
50. Londry, F.A., Hager, J.W.: Mass Selective Axial Ion Ejection from a Linear Quadrupole Ion Trap. *J. Am. Soc. Mass. Spectrom.* **2003**, 14, 1130-1147.
51. Novák, J., Lemr, K., Schug, K.A., Havlíček, V.: CycloBranch: De Novo Sequencing of Nonribosomal Peptides from Accurate Product Ion Mass Spectra. *J. Am. Soc. Mass. Spectrom.* **2015**, 26, 1780-1786.
52. Pilo, A.L., Peng, Z., McLuckey, S.A.: The Dehydroalanine Effect in the Fragmentation of Ions Derived from Polypeptides. *J. Mass. Spectrom.* **2016**, 51, 857-866.

53. Peng, Z., Bu, J., McLuckey, S.A.: The Generation of Dehydroalanine Residues in Protonated Polypeptides: Ion/Ion Reactions for Introducing Selective Cleavages. *J. Am. Soc. Mass. Spectrom.* **2017**, 28, 1765-1774.
54. Ngoka, L.C., Gross, M.L.: A Nomenclature System for Labeling Cyclic Peptide Fragments. *J. Am. Soc. Mass. Spectrom.* **1999**, 10, 360-363.
55. Yu, W., Vath, J.E., Huberty, M.C., Martin, S.A.: Identification of the Facile Gas-Phase Cleavage of the Asp-Pro and Asp-Xxx Peptide Bonds in Matrix-Assisted Laser Desorption Time-Of-Flight Mass Spectrometry. *Anal. Chem.* **1993**, 65, 3015-3023.
56. Sullivan, A.G., Brancia, F.L., Tyldesley, R., Bateman, R., Sidhu, K., Hubbard, S.J., Oliver, S.G., Gaskell, S.J.: The Exploitation of Selective Cleavage of Singly Protonated Peptide Ions Adjacent to Aspartic Acid Residues using a Quadrupole Orthogonal Time-Of-Flight Mass Spectrometer Equipped with a Matrix-Assisted Laser Desorption/Ionization Source. *Int. J. Mass Spectrom.* **2001**, 210-211, 665-676.
57. Bleiholder, C., Suhai, S., Harrison, A.G., Paizs, B.: Towards Understanding the Tandem Mass Spectra of Protonated Oligopeptides. 2: The Proline Effect in Collision-Induced Dissociation of Protonated Ala-Ala-Xxx-Pro-Ala (Xxx = Ala, Ser, Leu, Val, Phe, and Trp). *J. Am. Soc. Mass. Spectrom.* **2011**, 22, 1032-1039.
58. Schwartz, B.L., Bursey, M.M.: Some Proline Substituent Effects in the Tandem Mass Spectrum of Protonated Pentaalanine. *Biol. Mass Spectrom.* **1992**, 21, 92-96.
59. Vaisar, T., Urban, J.: Probing Proline Effect in CID of Protonated Peptides. *J. Mass Spectrom.* **1996**, 31, 1185-1187.

CHAPTER 4. GAS-PHASE SEQUENCING OF CYCLOTIDES: INTRODUCTION OF SELECTIVE RING OPENING AT DEHYDROALANINE VIA ION/ION REACTION

Adapted with permission from Foreman, D. J.; Parsley, N. C.; Lawler, J. T.; Aryal, U. K.; Hicks, L. M.; McLuckey, S. A. *Anal. Chem.* **2019**, 91, 15608-15616. Copyright 2019 American Chemical Society.

4.1 Introduction

Cyclotides are plant-derived head-to-tail cyclized peptides containing, typically, 28–37 amino acids. In addition to the cyclic backbone, these macrocycles contain six cysteine residues, which all participate in disulfide bonding, forming a cyclic cysteine knot. This motif results in extraordinary thermal, chemical, and enzymatic stability.^{1,2} The regions between the cysteine residues are defined as loops. The general cyclotide motif is provided in Figure 4.1. As a result, this motif has garnered great interest in biotechnological applications (e.g., drug delivery).^{3–7} Naturally occurring cyclotides exhibit diverse biological properties including, but not limited to, uterotonic activity to accelerate childbirth,^{8,9} anti-HIV activity,^{10–13} cytotoxicity,^{14,15} trypsin inhibitory activity,¹⁶ and insecticidal activity.^{17–19}

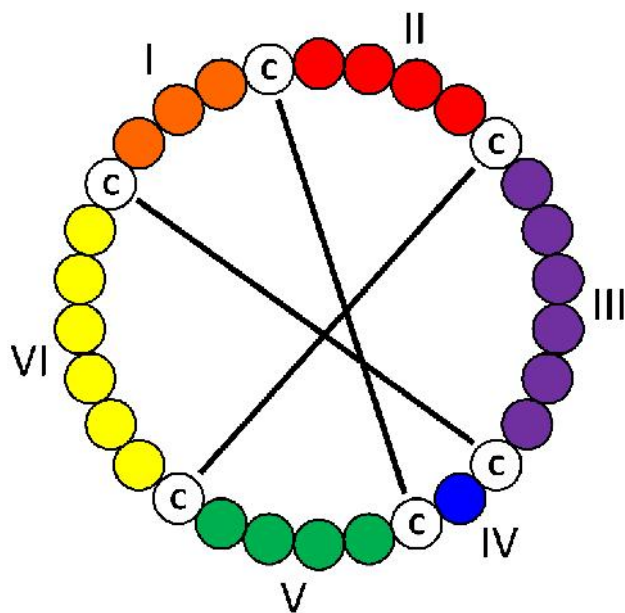


Figure 4.1. General cyclotide structure showing the head-to-tail cyclic backbone and three disulfide bonds forming the cyclic cysteine knot.

In addition to the diversity of biological activity, there exists great sequence diversity among cyclotides. Recent reports estimate a range of 30,000–150,000 different sequences in a single plant family.^{20–22} While the number of unique cyclotides is unknown, these macrocycles have been found in hundreds of plant species from five major plant families, Rubiaceae, Violaceae, Curcubitaceae, Solanaceae, and Fabaceae.^{23,24} Typically, anywhere from tens to hundreds of cyclotides are found in a single plant.²⁵ The sheer volume of sequenced and predicted cyclotides across plant families led to the development of CyBase (<http://www.cybase.org.au>), a database of cyclotides and cyclic peptides.^{26,27} However, to date, CyBase contains only 433 cyclotide sequences. Therefore, it is critical that additional efforts to identify cyclotide sequences must be undertaken to advance the fundamental knowledge of their function.

Nuclear magnetic resonance (NMR) techniques have historically been the primary means of cyclotide structural characterization, revealing important three-dimensional characteristics such as disulfide connectivity and structure–activity relationships between the cyclotide and molecular targets.^{28–32} NMR, however, is not well-suited for peptide sequencing. Cyclotides present a number of unique analytical challenges in primary structure elucidation. For example, the innate cyclic motif and high sequence homology between cyclotides present in the same plant species are

problematic for sequence characterization. Several analytical approaches have been used for the primary structural analysis of cyclotides that have been able to overcome such challenges.³³

Mass spectrometry has played vital roles in cyclotide characterization. In the earliest studies, Edman degradation was used to determine sequence identity while mass spectrometry was used to confirm the peptide mass.^{10,34,35} Tandem mass spectrometry (MS/MS) approaches have emerged as the primary analytical technique in cyclotide sequencing, yet not without associated challenges. Unlike their linear counterparts, MS/MS of cyclic peptides requires the cleavage of two amide bonds to observe any fragment ions. Thus, due to the presence of the cyclic cysteine knot, native cyclotides do not readily fragment.³⁶ As such, tandem mass spectrometry-based techniques employ reduction and alkylation of cysteine residues and proteolytic digestion to induce ring opening prior to MS analysis.

Conventional tandem mass spectrometry techniques for primary structure elucidation of cyclotides heavily rely on certain characteristics unique to this family of peptides. First, putative cyclotides are identified via a mass shift of 348.17 Da between the wild-type and reduced/alkylated samples, corresponding to the addition of 58.02 Da for each of the six cysteine residues present in cyclotides. Additionally, cyclotides contain a highly conserved glutamic acid residue that is often exploited for proteolytic digestion.^{37–39} This residue is often the only glutamic acid residue present in cyclotides. Digestion with endoproteinase Glu-C cleaves the peptide C-terminal to glutamic acid and aspartic acid. While several cyclotides contain aspartic acid residues, the differences in digestion kinetics of glutamic acid and aspartic acid (approximately 10× slower for aspartic acid) results in predominantly a single acyclic peptide linearized at the single glutamic acid residue. This linear peptide can be fragmented and sequenced. Digestion-based methods, however, are not amenable to low-abundance cyclotides; sample loss related to reduction, alkylation, and Glu-C digestion of the less abundant species hinders MS/MS analysis, where the precursor is no longer abundant enough to sequence via liquid chromatography–tandem mass spectrometry (LC–MS/MS) analysis.^{38,40} Additionally, complete sequence coverage is not always achieved with a single digestion. Oftentimes, further digestion with enzymes such as pepsin, trypsin, and chymotrypsin is required, leading to increased analysis times.

An alternative approach to cyclic peptide analysis via solution-based linearization is site-selective ring opening in the gas phase. In one example, the highly selective cleavage N-terminal to proline has been used to facilitate ring opening in the gas phase.^{41,42} More recently, solution-

phase conversion of arginine to ornithine was performed to selectively open cyclic peptides C-terminal to ornithine in the gas phase.^{43,44} Finally, it has been shown that gold (I) cationization promotes ring opening N-terminal to oxidized lysine residues in the gas phase. The location of ring opening can be pinpointed to the lysine residue upon MS⁴, offering a convenient means to cyclic peptide sequencing.⁴⁵ Of note, competitive ring opening at dehydroalanine was observed in addition to ring opening at lysine.

Herein, we report the site-selective linearization of cyclotides at dehydroalanine residues and its application to cyclotide sequencing. In this approach, alkylated cysteine residues are transformed into dehydroalanine residues via gas-phase ion/ion reactions. The selective cleavage of dehydroalanine in linear polypeptides has been described.^{46,47} Upon collisional activation, abundant c- and z-type fragment ions are formed N-terminal to dehydroalanine. Triply protonated cyclotide ions are transformed into radical cations via gas-phase ion/ion reaction with the sulfate radical anion. Activation of the radical-containing cyclotides leads to predominantly the odd-electron side-chain loss of carbamidomethyl cysteines and generation of dehydroalanine. Other odd-electron side-chain losses from leucine, asparagine, lysine, and glutamic acid to produce dehydroalanine are observed. In the case of the four cyclotides examined, the abundance of these losses is considerably lower than that of the alkylated cysteine residues and are, therefore, not the primary focus of this study. Subsequent collisional activation produces rich fragmentation corresponding to ring opening at dehydroalanine. This methodology is demonstrated with four known cyclotides of varying abundance, showing, in all cases, cumulative sequence coverage of greater than 93%. Finally, we demonstrate the utility of this method by partial sequencing of an unknown cyclotide found in *Viola inconspicua*.

4.2 Experimental

4.2.1 Materials

Ammonium bicarbonate, dithiothreitol (DTT), iodoacetamide, urea, sodium persulfate, and endoproteinase Glu-C enzyme were purchased from Sigma-Aldrich (St. Louis, MO, U.S.A.). HPLC grade methanol and acetonitrile and Optima LC-MS grade water were purchased from Fisher Scientific (Fair Lawn, NJ, U.S.A.). Acetic acid and formic acid were purchased from Mallinckrodt (Phillipsburg, NJ, U.S.A.).

4.2.2 Sample Preparation

Detailed preparation and extraction procedures have been described previously.⁴⁸ Isolated cyI4 and the complex cyclotide-containing fractions were reconstituted in 1 mL of water. The cyI4 wild-type sample was prepared by diluting 10 μ L of the stock to 1000 μ L with a final composition of 49.5/49.5/1 (by volume) water/methanol/acetic acid. For the early LC fraction, wild-type sample was prepared by diluting 100 μ L of the stock to 1000 μ L with a final composition of 49.5/ 49.5/1 (by volume) water/methanol/acetic acid.

4.2.3 Reduction and Alkylation

10 μ L amounts of cyI4 stock and 100 μ L of complex fraction stock were diluted 100 \times and 10 \times , respectively, in reduction buffer (100 mM ammonium bicarbonate, 7 M urea). To each vial, 10 μ L of DTT stock (500 mM in 100 mM ammonium bicarbonate) was added, and the samples were incubated at 55 $^{\circ}$ C for 45 min. An amount of 14 μ L of freshly prepared iodoacetamide stock (500 mM in 100 mM ammonium bicarbonate) was added to the cooled solutions. The samples were incubated for 30 min in the dark. The reaction was quenched with the addition of another 10 μ L of DTT stock, and the mixture was allowed to incubate for 15 min in the dark. Samples were immediately desalted using TopTip C-18 desalting columns (Glygen, Columbia, MD, U.S.A.) per the manufacturer's instructions.

4.2.4 Ion/Ion Mass Spectrometry

All ion/ion reaction experiments were performed on a TripleTOF 5600 quadrupole/time-of-flight mass spectrometer (SCIEX, Concord, ON, Canada) with modifications for ion/ion reactions and dipolar direct current (DDC) collisional activation analogous to those previously described.^{49,50} Alternately pulsed nanoelectrospray ionization (nESI) allows for the sequential injection of cations and radical anions.⁵¹ Triply protonated peptide cations, $[M + 3H]^{3+}$, were isolated in Q1 and transferred to q2. The sulfate radical anion, $[SO_4]^{-\bullet}$, was isolated in Q1 and transferred to q2 where the two ion populations were mutually stored for 10 ms resulting in the formation of the $[M + 3H + SO_4]^{2+\bullet}$ complex. Beam-type collision-induced dissociation (CID) of the isolated complex from Q1 to q2 or DDC collisional activation in q2 both lead to the consecutive losses of H_2SO_4 and $\bullet SCH_2CONH_2$ (90 Da), in either order, generating $[M + H - 90]^{2+}$. The $[M +$

H – 90]²⁺ ion was back transferred to Q1, isolated, and transferred to q2. Ion trap CID was performed in q2 at a q value of 0.2. Product ions were mass analyzed via time of flight.

4.2.5 LC-MS/MS Analysis

The reduction, alkylation, and Glu-C digestion of the complex fraction has been described.⁴⁸ For collisional activation experiments, approximately 1 µg of acidified reduced/alkylated/glu-C digested *V. inconspicua* sample was injected onto a nano-LC–ESI-MS/MS platform consisting of a NanoAcquity (Waters, Milford, MA, U.S.A.) coupled to a TripleTOF5600 MS (AB Sciex, Framingham, MA). Front-end UPLC separation of peptides was achieved on an HSS T3C18 column (100 Å, 1.8 µm, 75 µm × 250 mm, Waters), after passing a Symmetry C18 trap column (100 Å, 5 µm, 180 µm × 20 mm, Waters), with a flow rate of 0.3 µL/min and a 30 min linear ramp of 5%–50% B (mobile phase A, 1% formic acid in water; mobile phase B, 1% formic acid in acetonitrile). The TripleTOF5600 MS was operated in positive-ion, high-sensitivity mode with the MS survey spectrum using a mass range of 350–1600 Da in 250 ms. Targeted CID MS/MS data was acquired for 3319 Da using reduced/alkylated and Glu-C digested samples and a collision energy (CE) of 40.

For electron transfer dissociation (ETD) experiments, the material was analyzed using a Dionex UltiMate 3000 RSLC Nano system (Thermo Fisher Scientific, Odense, Denmark) coupled online to an ETD-enabled Orbitrap Fusion Lumos mass spectrometer (Thermo Fisher Scientific, Waltham, MA, U.S.A.). Reversed-phase peptide separation was accomplished using a trap column (300 mm i.d. × 5 mm) packed with 5 mm 100 Å PepMap C18 medium coupled to a 50 cm long × 75 µm inner diameter analytical column packed with 2 µm 100 Å PepMap C18 silica (Thermo Fisher Scientific). The column temperature was maintained at 50 °C. Mobile phase solvent A consisted of purified water and 0.1% formic acid (FA), and mobile phase solvent B consisted of 80% acetonitrile and 0.1% FA. Sample was loaded to the trap column in a loading buffer (3% acetonitrile, 0.1% FA) at a flow rate of 5 µL/min for 5 min and eluted from the analytical column at a flow rate of 300 nL/min using a 90 min LC gradient as follows: linear gradient of 6.5–27% of solvent B in 55 min, 27–40% of B in the next 8 min, 40–100% of B in 7 min, at which point the gradient was held at 100% of B for 5 min before reverting back to 2% of B. The mobile phase gradient was held at 2% of B for the next 15 min for column equilibration. All data were acquired in the Orbitrap mass analyzer, and data were collected using an EThcD fragmentation scheme. For

MS scans, the scan range was from m/z 350 to 1600 at a resolution of 120 000, the automatic gain control (AGC) target was set at 4×10^5 , maximum injection time was 50 ms, dynamic exclusion was 30 s, and intensity threshold was 5.0×10^4 . MS data were acquired in data-dependent mode with cycle time of 5 s/scan. For ddMS², the EThCD method was used with parallelizable time activation checked, Orbitrap resolution set at 60 000, the AGC target set at 2×10^5 , the ETD reaction time set at 50 ms, and the HCD-normalized collision energy set at 15%. Targeted EThCD MS/MS spectra were also acquired for m/z 922.3968, 922.6982, 922.8982, and 922.1483.

4.3 Results and Discussion

4.3.1 Generation of Dehydroalanine via Ion/Ion Reaction

The odd-electron side-chain losses of radical-containing polypeptides and polypeptide fragment ions, $z_n^{+\bullet}$, have been extensively studied.^{52–56} For several amino acids, this odd-electron loss results in the generation of dehydroalanine.⁵⁰ In this report, we first generate cyclotide radical cations via ion/ion reaction with the sulfate radical anion, $[\text{SO}_4]^{-\bullet}$. Then, dehydroalanine was generated via odd-electron side-chain losses upon collisional activation of the cyclotide radical cation, $[\text{M} + \text{H}]^{2+\bullet}$. The incorporation of dehydroalanine into cyclotides provides a facile gas-phase linearization pathway, the utility of which is demonstrated with extensive sequence coverage of cyclotides with both known and unknown sequences. This methodology is first demonstrated with the cyclotide cyI4 (Figure 4.2).

Ion/ion reaction between triply protonated reduced and alkylated cyI4 and $[\text{SO}_4]^{-\bullet}$ results in the formation of the $[\text{M} + 3\text{H} + \text{SO}_4]^{2+\bullet}$ complex ion and, to a lesser extent, the $[\text{M} + 3\text{H} + 2\text{SO}_4]^{+\bullet\bullet}$ product ion (Figure 4.2a). Ions were transferred back into Q1, where $[\text{M} + 3\text{H} + \text{SO}_4]^{2+\bullet}$ was isolated. Beam-type CID from Q1 to q2 generates a spectrum that shows the major fragmentation pathway to be the loss of sulfuric acid forming the $[\text{M} + \text{H}]^{2+\bullet}$ radical cation (Figure 4.2b). Isolation and ion trap CID of $[\text{M} + \text{H}]^{2+\bullet}$ shows abundant small-molecule loss as well as the ejection of $\bullet\text{SCH}_2\text{CONH}_2$ from a carbamidomethyl side chain,^{57,58} generating dehydroalanine at one of the six cysteine residues (Figure 4.2c). DDC-CID can be used to generate the product ion of interest, $[\text{M} + \text{H} - 90]^{2+}$, ultimately eliminating the need for multiple back-transfer and isolation steps (Figure 4.2d). Interestingly, we also observe that DDC-CID reduces the extent of water and ammonia loss.

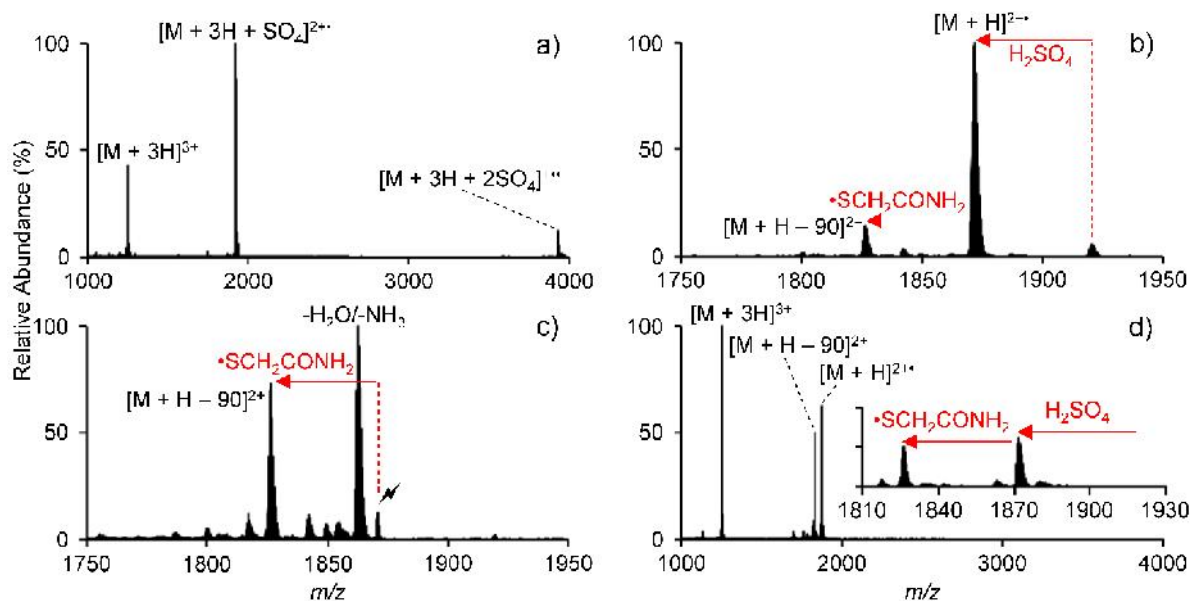


Figure 4.2. Ion/ion reaction between triply protonated cyI4 and sulfate radical anion: a) post ion/ion reaction spectrum, b) beam-type CID of $[M + 3H + SO_4]^{2+*}$, c) ion trap CID of $[M + H]^{2+*}$, and d) DDC-CID of the ion/ion reaction products of panel a.

It is worth noting that collisional activation also results in the odd-electron side-chain losses from leucine, asparagine, lysine, and glutamic acid residues as minor products (<10% relative abundance). Probing these lower level fragment ions could produce a simpler product ion spectrum (i.e., ring opening at one leucine residue, or three asparagine residues, or three lysine residues, or one glutamic acid residue vs the six cysteine residues). However, for this method to be applicable to sequencing low-abundance cyclotides, the loss of $\bullet\text{SCH}_2\text{CONH}_2$ to introduce dehydroalanine was solely explored as this fragmentation pathway was always observed to be the most abundant odd-electron side-chain loss.

4.3.2 Opening CyI4 at Dehydroalanine

As cyclotides are head-to-tail cyclic peptides, two backbone cleavages are needed to observe a change in m/z in MS^n workflows. An initial c/z cleavage N-terminal to the dehydroalanine generates a linear peptide with an alkyne at the N-terminus and a primary ketimine at the C-terminus. A second backbone cleavage would generate sequence-informative fragment ions. The observed loss of 90 Da from $[M + H]^{2+*}$ signifies dehydroalanine formation at a single carbamidomethyl cysteine residue. That is to say, the loss of 90 Da generates six structural isomers

of identical mass in which the side chain can be lost from any of the six cysteines. Activation of $[M + H - 90]^{2+}$ represents a strategy to selectively open the cyclotide at dehydroalanine from any of the isomers.

The product ion spectrum from collisional activation of $[M + H - 90]^{2+}$ derived from ion/ion reaction and subsequent DDC collisional activation is shown to contain high-abundance small molecule losses and numerous low-abundance fragment ions (Figure 4.3). The preponderance of the latter corresponds to band y-type fragment ions from ring opening at dehydroalanine and are indicated with colored circles (Figure 4.3). Fragment ions originating from ring opening at dehydroalanine formed at the first, second, third, fourth, fifth, and sixth cysteine are highlighted in black, red, green, blue, orange, and purple, respectively (Figure 4.3, Figure 4.4, and Table 4.1). Please note that a series of product ions originating from an initial b/y cleavage N-terminal to proline is also observed.

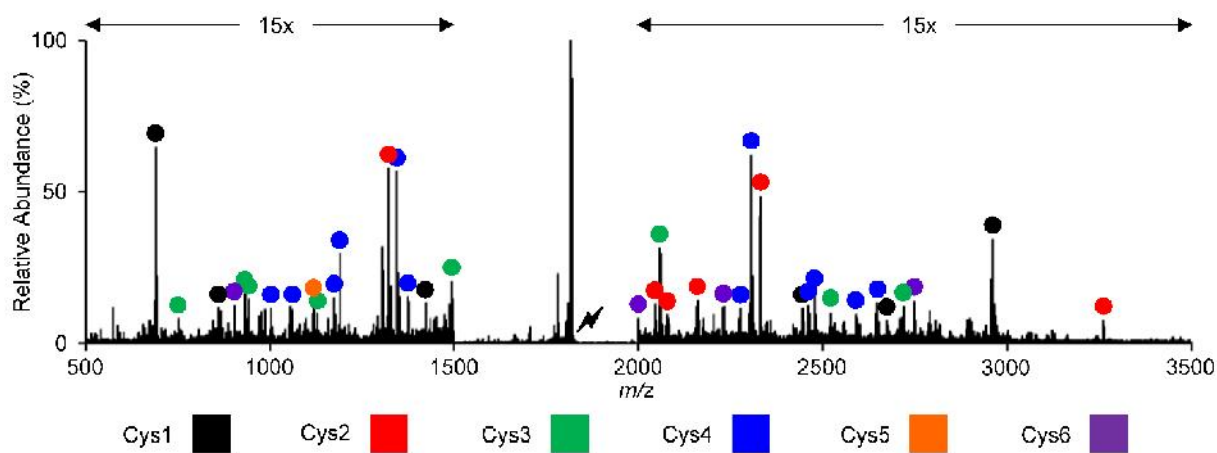


Figure 4.3. Product ion spectrum from the collisional activation of dehydroalanine containing cyI4, $[M + H - 90]^{2+}$. The lightning bolt corresponds to the species CID.

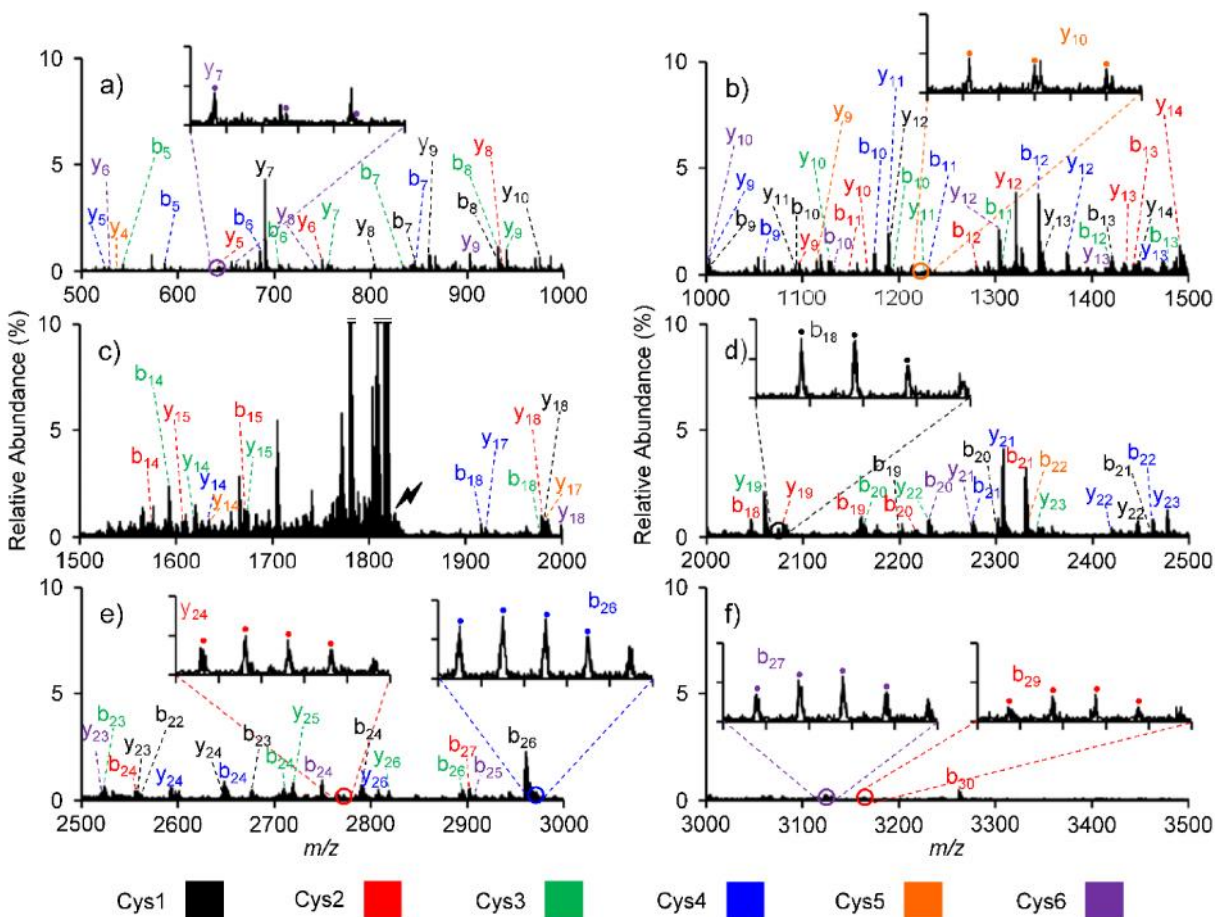


Figure 4.4. 500 m/z wide zoomed views from the collisional activation of cyI4 $[M + H - 90]^{2+}$. a) m/z 500-1000, b) m/z 1000-1500, c) m/z 1500-2000, d) m/z 2000-2500, e) m/z 2500-3000, and f) m/z 3000-3500. The lightning bolt corresponds to the species subjected to CID.

Table 4.1. List of assignments, measured isotopic masses, theoretical isotopic masses, and mass differences for the cyI4 data of Figure 4.4.

Assignment	Theoretical	Observed	Mass Difference	Mass Error (ppm)
b7	846.35867	846.35686	-0.00181	-2.14
b8	933.39070	933.36685	-0.02385	-25.55
b9	1004.42781	1004.39077	-0.03704	-36.88
b10	1091.45984	1091.44600	-0.01384	-12.68
b13	1421.59437	1421.60974	0.01537	10.81
b18	2073.85663	2073.83695	-0.01968	-9.49
b19	2201.95160	2201.93060	-0.02099	-9.53
b20	2301.02001	2300.99350	-0.02651	-11.52
b21	2461.04901	2461.01206	-0.03695	-15.01
b22	2562.09668	2562.07709	-0.01959	-7.65
b23	2675.18075	2675.15432	-0.02643	-9.88

Table 4.1 Continued

Assignment	Theoretical	Observed	Mass Difference	Mass Error (ppm)
b24	2789.22369	2789.18203	-0.04166	-14.93
b25	2960.28808	2960.25684	-0.03124	-10.55
y5	536.21002	536.20212	-0.00790	-14.74
y7	690.28425	690.27917	-0.00508	-7.37
y8	804.32719	804.32175	-0.00544	-6.76
y9	861.34865	861.34192	-0.00673	-7.81
y10	975.39158	975.38399	-0.00759	-7.78
y11	1088.47565	1088.46785	-0.00780	-7.17
y12	1189.52333	1189.50486	-0.01847	-15.53
y13	1349.55233	1349.54452	-0.00781	-5.78
y14	1448.62074	1448.61094	-0.00980	-6.77
y18	1981.91694	1981.83700	-0.07993	-40.33
y22	2446.02842	2446.00144	-0.02698	-11.03
y23	2559.11249	2559.08910	-0.02339	-9.14
y24	2646.14452	2646.10343	-0.04109	-15.53
b11	1152.40518	1152.50780	0.10262	89.05
b12	1280.50015	1280.49139	-0.00876	-6.84
b13	1443.56348	1443.54907	-0.01441	-9.98
b14	1571.65845	1571.64600	-0.01245	-7.92
b15	1670.72686	1670.71208	-0.01478	-8.85
b18	2044.88761	2044.86538	-0.02223	-10.87
b19	2158.93054	2158.90288	-0.02766	-12.81
b20	2215.95200	2215.92744	-0.02456	-11.08
b21	2329.99493	2329.96849	-0.02644	-11.35
b23	2484.06916	2484.03893	-0.03023	-12.17
b24	2555.10627	2555.07307	-0.03320	-13.00
b27	2901.19933	2901.17373	-0.02560	-8.82
b29	3162.27601	3162.22588	-0.05013	-15.85
b30	3261.34442	3261.30995	-0.03447	-10.57
y5	648.32533	648.32282	-0.00251	-3.87
y6	749.37300	749.36664	-0.00636	-8.49
y8	935.43706	935.42784	-0.00922	-9.86
y9	1095.46606	1095.45937	-0.00669	-6.11
y10	1166.50317	1166.48879	-0.01438	-12.33
y12	1320.57740	1320.56817	-0.00923	-6.99
y13	1434.62033	1434.60748	-0.01285	-8.96
y14	1491.64180	1491.63028	-0.01152	-7.72
y15	1605.68473	1605.67022	-0.01451	-9.04
y18	1979.84547	1979.82790	-0.01757	-8.88
y19	2078.91389	2078.89765	-0.01624	-7.81

Table 4.1 Continued

Assignment	Theoretical	Observed	Mass Difference	Mass Error (ppm)
y24	2772.23908	2772.11802	-0.12106	-43.67
b5	542.20112	542.19728	-0.00384	-7.07
b6	705.26445	705.26029	-0.00416	-5.90
b7	833.35941	833.35196	-0.00745	-8.94
b8	932.42783	932.41736	-0.01047	-11.23
b9	1092.45682	1092.44841	-0.00841	-7.70
b10	1193.50450	1193.49600	-0.00850	-7.12
b11	1306.58857	1306.57130	-0.01727	-13.22
b12	1420.63150	1420.61567	-0.01583	-11.15
b13	1477.65297	1477.63145	-0.02152	-14.56
b14	1591.69590	1591.67952	-0.01638	-10.29
b18	1976.83624	1976.81161	-0.02463	-12.46
b20	2162.90030	2162.89153	-0.00877	-4.05
b23	2523.04539	2523.00658	-0.03881	-15.38
b24	2709.12470	2709.09528	-0.02941	-10.86
b26	2894.24112	2894.21091	-0.03021	-10.44
y7	756.33121	756.33219	0.00098	1.29
y9	941.44764	941.43975	-0.00789	-8.38
y10	1127.52695	1127.51563	-0.01132	-10.04
y11	1226.59536	1226.58633	-0.00903	-7.36
y12	1386.62436	1386.61723	-0.00713	-5.14
y13	1487.67204	1487.65389	-0.01815	-12.20
y14	1616.71464	1616.67431	-0.04032	-24.94
y15	1673.73610	1673.71473	-0.02137	-12.77
y19	2058.87644	2058.85995	-0.01649	-8.01
y21	2229.94083	2229.92303	-0.01780	-7.98
y22	2343.98376	2343.96240	-0.02136	-9.11
y25	2718.14451	2718.12905	-0.01546	-5.69
y26	2817.21292	2817.18647	-0.02645	-9.39
b5	586.298386	586.29359	-0.00480	-8.18
b6	685.3668	685.35962	-0.00718	-10.48
b7	845.395797	845.38696	-0.00884	-10.45
b8	946.443475	946.43344	-0.01004	-10.60
b9	1059.527545	1059.5178	-0.00975	-9.20
b10	1173.570477	1173.55788	-0.01260	-10.73
b11	1230.59194	1230.57734	-0.01460	-11.86
b12	1344.634872	1344.62029	-0.01458	-10.84
b16	1729.77521	1729.75367	-0.02154	-12.45
b18	1915.83927	1915.82007	-0.01920	-10.02
b21	2275.984359	2275.96138	-0.02298	-10.10

Table 4.1 Continued

Assignment	Theoretical	Observed	Mass Difference	Mass Error (ppm)
b22	2462.063668	2462.03359	-0.03008	-12.22
b24	2647.180096	2647.14073	-0.03937	-14.87
b26	2970.272426	2970.22687	-0.04556	-15.34
y5	522.230768	522.23902	0.00825	15.80
y7	680.299909	680.29464	-0.00527	-7.75
y8	843.363242	843.35479	-0.00845	-10.02
y9	1003.392239	1003.38569	-0.00655	-6.53
y10	1131.487204	1131.47984	-0.00736	-6.51
y11	1188.508667	1188.50056	-0.00811	-6.82
y12	1374.587976	1374.57547	-0.01251	-9.10
y13	1473.65639	1473.64402	-0.01237	-8.39
y14	1633.685387	1633.67288	-0.01251	-7.66
y15	1734.733065	1734.72279	-0.01028	-5.92
y17	1920.797125	1920.78023	-0.01689	-8.80
y21	2305.937463	2305.91893	-0.01853	-8.04
y22	2419.980395	2419.95709	-0.02331	-9.63
y23	2477.001858	2476.98031	-0.02155	-8.70
y24	2591.04479	2591.01911	-0.02568	-9.91
y26	2805.176538	2805.15737	-0.01917	-6.83
b22	2335.94796	2335.94117	-0.00679	-2.91
y4	536.35386	536.35280	-0.00106	-1.97
y9	1114.50827	1114.49866	-0.00961	-8.63
y10	1227.59234	1227.58632	-0.00602	-4.91
y11	1314.62437	1314.61179	-0.01258	-9.57
y13	1472.69352	1472.65733	-0.03618	-24.57
y14	1635.75685	1635.67551	-0.08134	-49.72
y17	1980.90227	1980.83443	-0.06784	-34.25
b9	970.40708	970.39888	-0.00820	-8.45
b10	1130.43607	1130.42227	-0.01380	-12.21
b12	1380.53144	1380.51374	-0.01770	-12.82
b20	2229.83907	2229.92303	0.08396	37.65
b23	2649.09233	2649.12006	0.02773	10.47
b24	2748.16074	2748.13013	-0.03061	-11.14
b25	2908.18974	2908.18065	-0.00909	-3.13
b27	3122.32149	3122.28725	-0.03424	-10.97
y6	528.25085	528.24728	-0.00357	-6.75
y7	641.33492	641.33055	-0.00437	-6.81
y8	742.38259	742.37804	-0.00455	-6.13
y9	902.41159	902.40438	-0.00721	-7.99
y10	1001.48001	1001.47287	-0.00714	-7.12

Table 4.1 Continued

Assignment	Theoretical	Observed	Mass Difference	Mass Error (ppm)
y11	1129.57497	1129.56297	-0.01200	-10.62
y12	1292.63830	1292.62800	-0.01030	-7.97
y13	1420.73327	1420.71462	-0.01865	-13.13
y18	1998.88769	1998.86991	-0.01778	-8.89
y21	2270.04090	2270.00526	-0.03564	-15.70
y23	2520.13626	2520.15664	0.02038	8.09
y25	2808.26022	2808.16871	-0.09151	-32.59

As mentioned above, the $[M + H - 90]^{2+}$ precursor ion is composed of six isomers differing only in the position of dehydroalanine. Product ions derived from the linearization of each isomer are observed (Figure 4.5a–f). Four of the six peptides show greater than 50% sequence coverage – ring opening at the first, second, third, and fourth cysteine results in 53.1%, 53.1%, 56.3%, and 59.4% sequence coverage, respectively. Individually, no single location of ring opening generated sufficient fragmentation to completely sequence cyI4. Cumulatively, however, cleavage at 31 of 33 amide linkages (93.9%) is observed, only lacking fragment ions from the Gly-Cys and Pro-Gly bonds (Figure 4.5g).

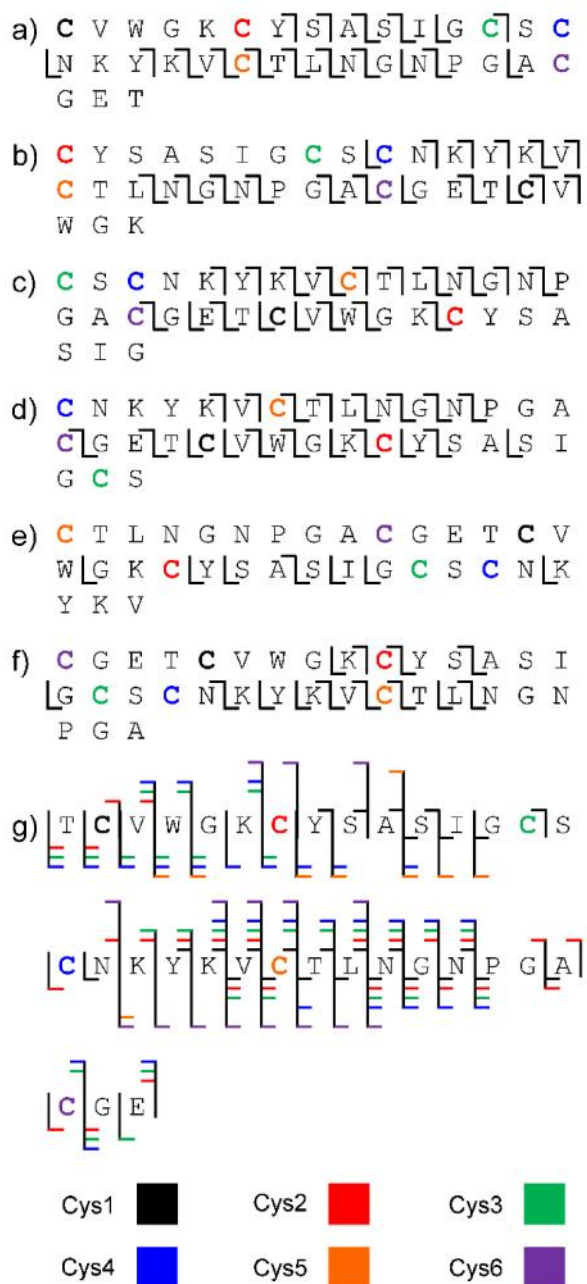


Figure 4.5. Individual fragmentation maps of cyI4 opened at a) Cys1, b) Cys2, c) Cys3, d) Cys4, e) Cys5, and f) Cys6. g) Cumulative fragmentation map from all ring openings.

The cumulative sequence coverage is attributed to the complementary sequence information on individual locations of linearization. Examination of the fragmentation maps depicted in Figure 4.5 reveals that fragmentation is generally localized to the interior of the linearized peptide. As cysteine residues in cyclotides are spaced by as little as one amino acid and

as many as 10 amino acids, interior fragment ions of the linear peptides can sequence unique portions of the cyclotide (Figure 4.6). Cysteines in close proximity to one another display several common fragment ions, while distant cysteines share few, if any, common fragments. Additionally, Cys1, Cys2, Cys3, Cys4, and Cys5 all show unique fragment ions, where cysteine residues are labeled in sequential order in the Glu-C linearized peptide, TCVWGKCYSASIGCSCNKYKVCTLNGNPGACGE. The combination of overlapped regions and unique regions is a characteristic of selectively opening cyclotides at cysteine residues and aids in the de novo sequencing of unknown cyclotides, which will be demonstrated below.

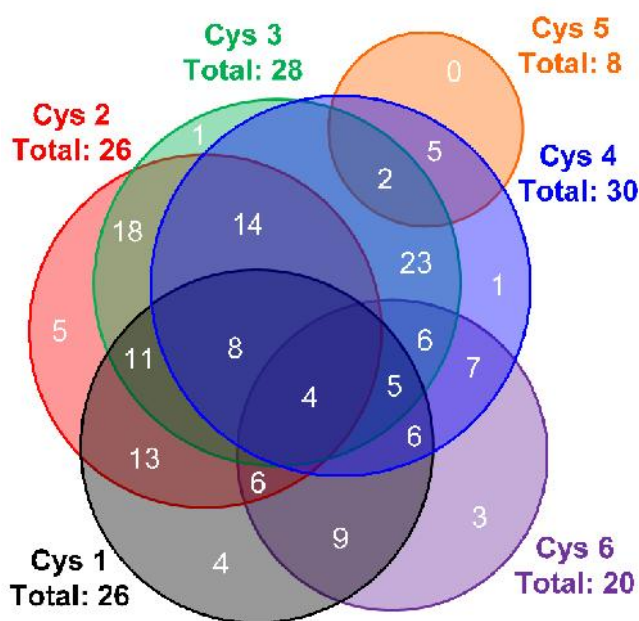


Figure 4.6. Venn diagram showing the unique and overlapping fragment ions from activation of the cyI4 $[M + H - 90]^{2+}$ ion.

4.3.3 Sequencing Known Cyclotides in a Complex Fraction

Positive nESI of the wild-type complex fraction from *V. inconspicua* shows triply charged peaks at m/z 1037.1236, 1076.1441, and 1087.4729 corresponding to the known cyclotides viba11, cyO8, and cyI2 (Figure 4.7a). CyO8 is observed to be the base peak, cyI2 is observed at approximately 65% relative abundance, and viba11 is observed at approximately 15% relative abundance. Their identities as cyclotides are confirmed by the mass shift of 348.2 Da upon

reduction with DTT and alkylation with iodoacetamide (Figure 4.7b). The three peptides were selected for further interrogation through the gas-phase linearization as described with cyI4.

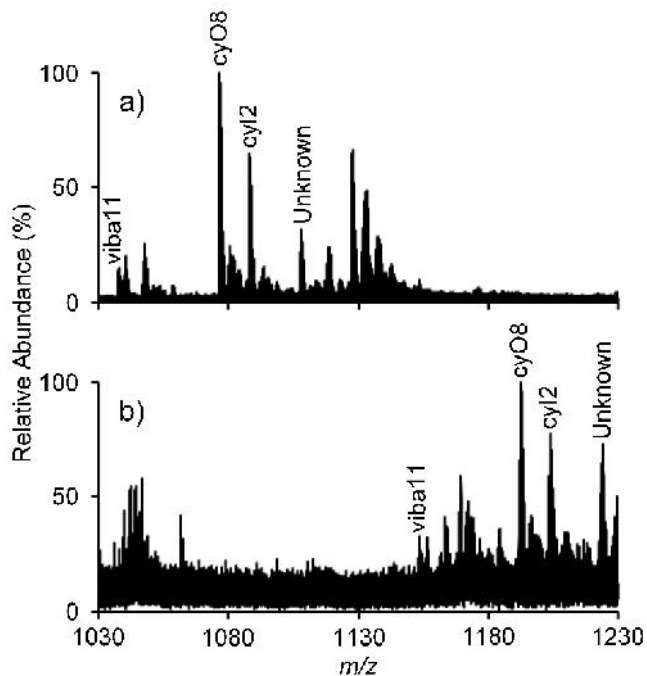


Figure 4.7. Positive nESI of a) wild type early LC fraction and b) reduced and alkylated early LC fraction.

CyO8, cyI2, and viba11 were subjected to the same ion/ion reaction workflow described above. Briefly, ion/ion reaction of the triply protonated species with the sulfate radical anion produces the $[M + 3H + SO_4]^{2+}$ complex. DDC of the ion/ion reaction products results in successive losses of H_2SO_4 and $\bullet SCH_2CONH_2$. Subsequent activation of $[M + H - 90]^{2+}$ for each of the aforementioned cyclotides generates the product ion spectra with greater than 96% total sequence coverage (Figures 4.8 – 4.11). Similar to cyI4, there are regions of fragment ion overlap as well as fragment ions unique to specific ring-opening sites. In the case of viba11, the fewest number of fragment ions corresponding to ring opening induced by dehydroalanine was observed when compared to cyI4, cyO8, and cyI2. This is likely due, in part, to viba11 being the lowest abundance of the four cyclotides examined and the smallest cyclotide examined, with 29 amino acids versus the 31 amino acids of cyO8 and cyI2 and the 33 amino acids of cyI4. Nonetheless, extensive sequence coverage was still observed.

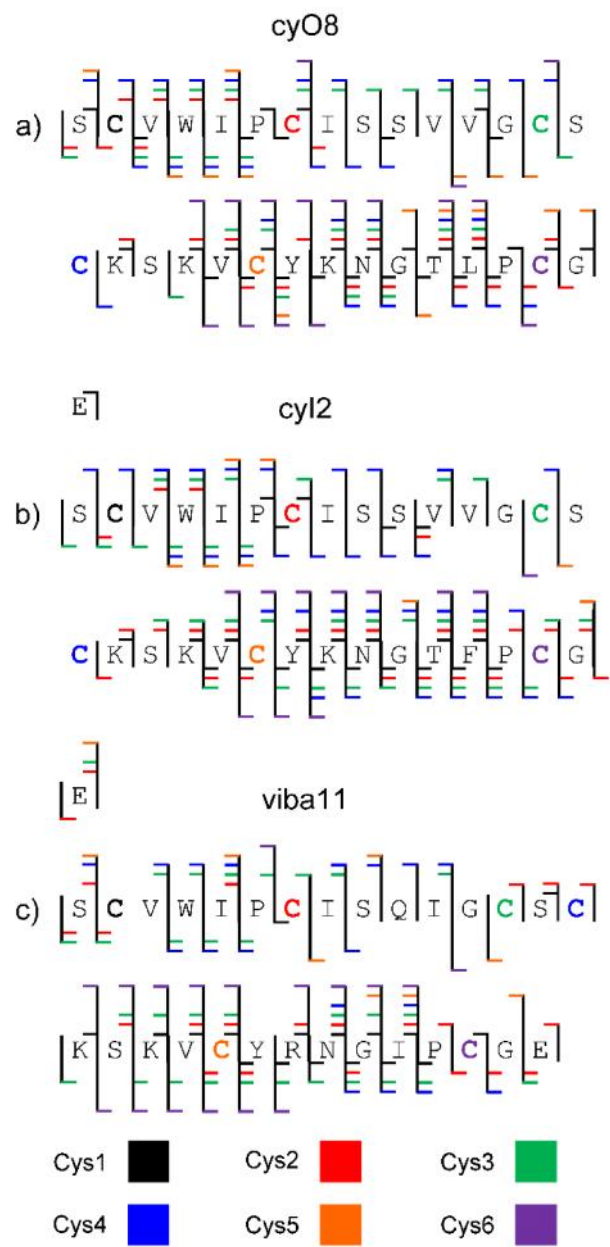


Figure 4.8. Cumulative fragmentation maps of a) cyO8, b) cyl2, and c) viba11.

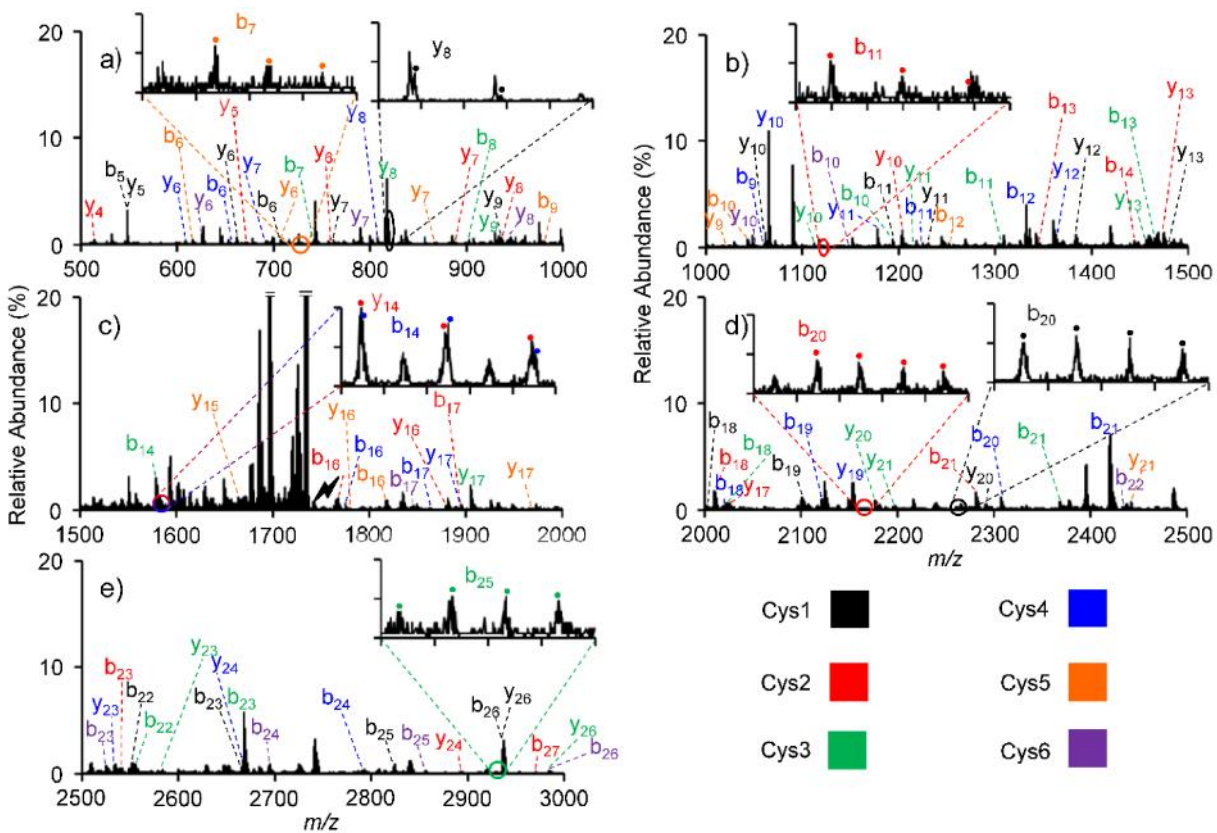


Figure 4.9. 500 m/z wide zoomed views from the collisional activation of cy8 $[M + H - 90]^{2+}$. a) m/z 500-1000, b) m/z 1000-1500, c) m/z 1500-2000, d) m/z 2000-2500, and e) m/z 2500- 3000. The lightning bolt corresponds to the species subjected to CID.

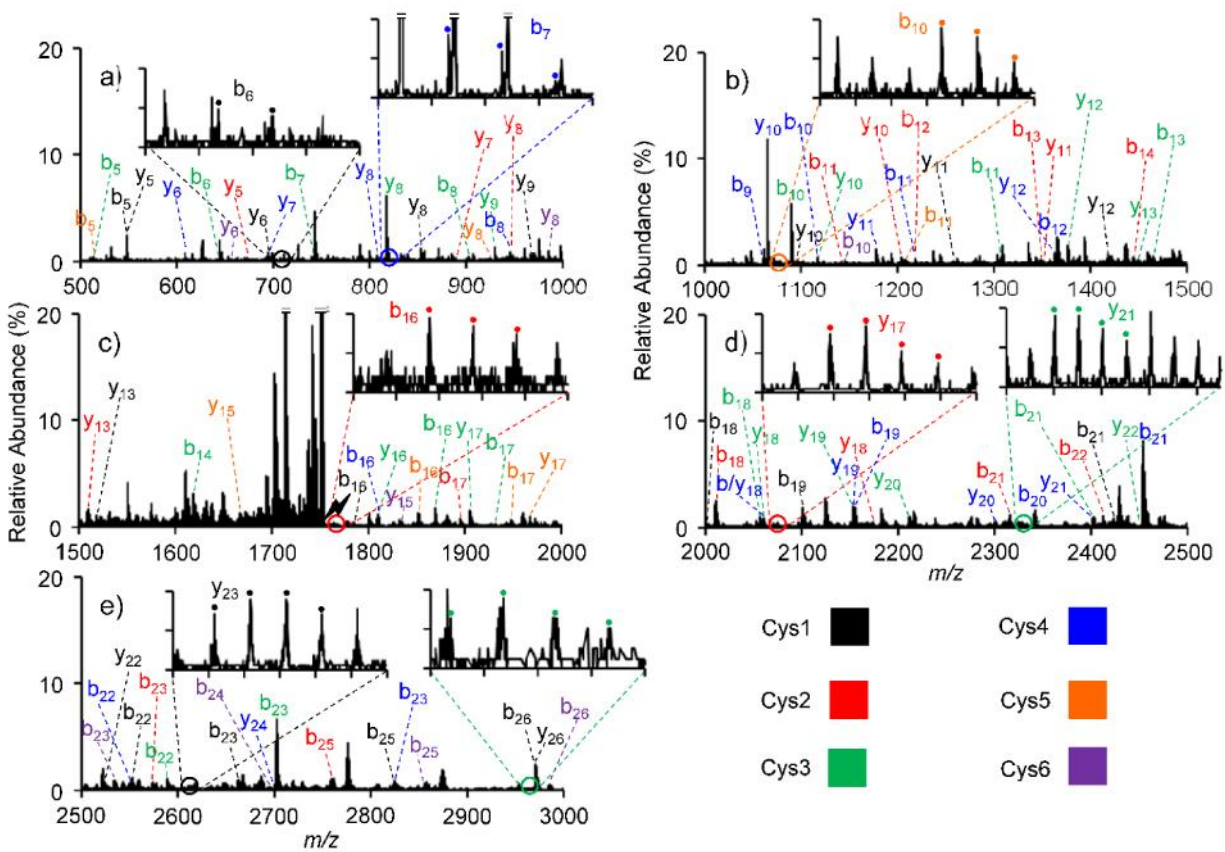


Figure 4.10. 500 m/z wide zoomed views from the collisional activation of cyI2 $[M + H - 90]^{2+}$. a) m/z 500-1000, b) m/z 1000-1500, c) m/z 1500-2000, d) m/z 2000-2500, and e) m/z 2500- 3000. The lightning bolt corresponds to the species subjected to CID.

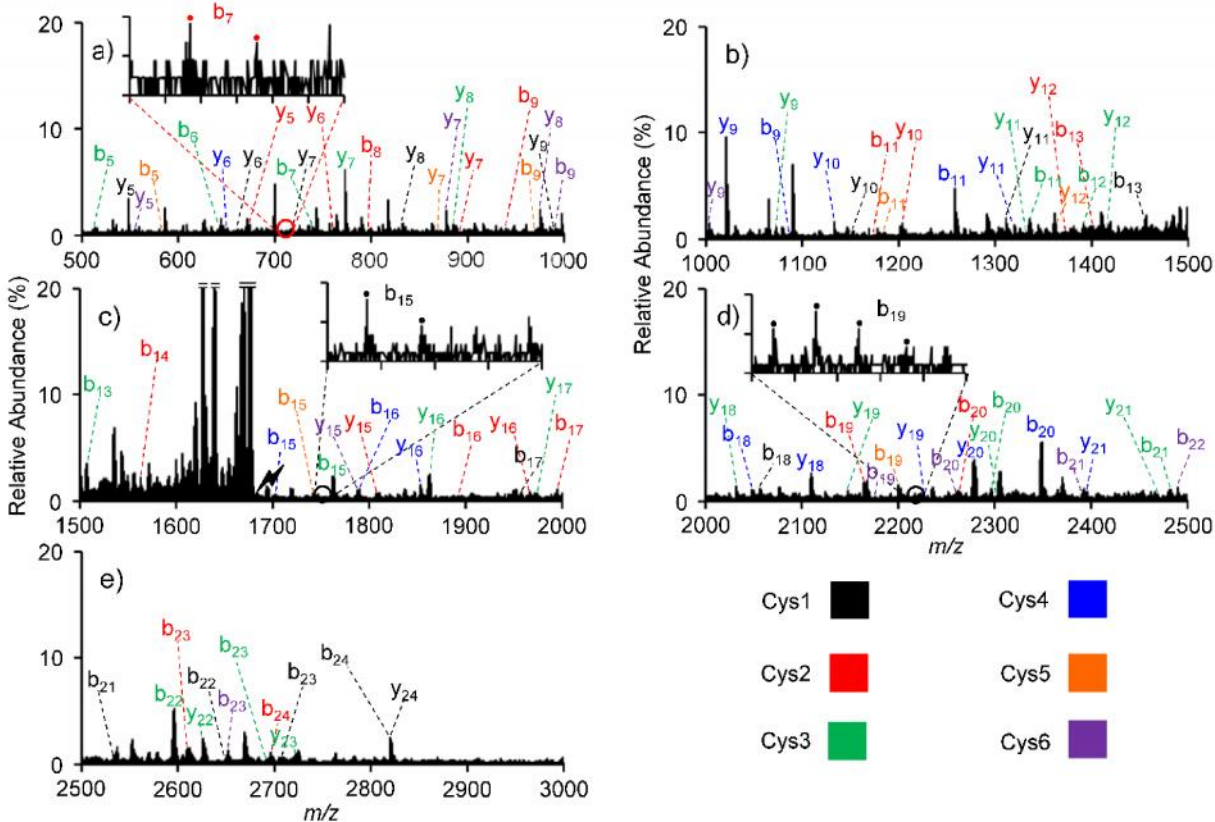


Figure 4.11. 500 m/z wide zoomed views from the collisional activation of viba11 $[M + H - 90]^{2+}$. a) m/z 500-1000, b) m/z 1000-1500, c) m/z 1500-2000, d) m/z 2000-2500, and e) m/z 2500-3000. The lightning bolt corresponds to the species subjected to CID.

4.3.4 Partial de Novo Sequencing of an Unknown Cyclotide

Inspection of the MS^1 spectrum of the complex mixture reveals a putative cyclotide (3319.3445 Da) indicated by the 348.2 Da mass shift (Figure 4.7). To our knowledge, this cyclotide represents an unknown that has not been previously sequenced. Dehydroalanine was introduced at a single cysteine residue, and the $[M + H - 90]^{2+}$ was subjected to collisional activation. Analogous to the known sequences above, activation of this species results in the selective ring opening at the dehydroalanine. The resulting product ion spectrum shows numerous fragment ions of ample signal-to-noise ratio that can be used for de novo sequencing. Specifically, the region between m/z 400 and m/z 1700 shows well-resolved fragment ions with little chemical noise.

The de novo sequencing was performed according to the general procedure provided in Figure 4.12. To summarize, first, a product ion of low m/z is selected, and then the peak-to-peak masses for each amino acid are calculated. That is to say, from the chosen product ion new masses

are calculated by the addition of the 20 different amino acid residue masses. Next, product ions with an appropriate mass error (less than 100 ppm) and the appropriate isotopic distribution are identified. If there is a peak that corresponds to the addition of an amino acid, this process is repeated until no additional amino acid residues can be identified, generating a partial primary sequence. If no product ions corresponding to an amino acid residue are identified, a new initiating product ion of low m/z is identified, and the process is repeated. This partial sequence generation process is repeated with all potential initiating product ions of low m/z until no initiating ions remain. Here, this workflow was performed via manual data interpretation. Yet, one could imagine this process could be automated if a large number of product ion spectra were to be analyzed.

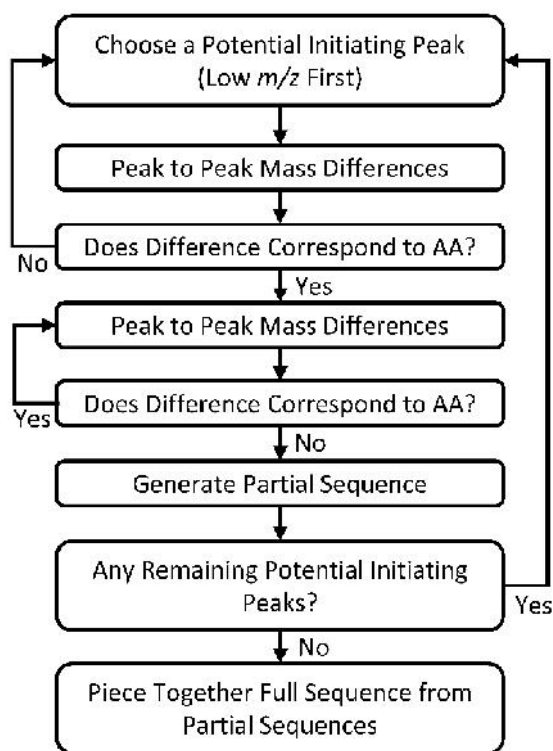


Figure 4.12. General procedure for de novo sequencing.

Manual interpretation of the product ion spectrum revealed 10 distinct partial sequences, referred to here as ion series (Figures 4.13–4.23). The aligned partial sequences are displayed in Figure 4.24. As mentioned previously, the sequence information from different locations of linearization is complementary. This characteristic is reinforced in Figure 4.24 where each ion series overlaps with at least one other ion series. In many cases, the overlap serves as an “anchor”

point to which the sequence of one ion series can be extended with the sequence of another ion series. For example, the sixth ion series overlaps with the seventh ion series at the glycine and asparagine residues. In the sixth series, six additional residues are identified, while in the seventh series, seven additional residues are identified. The combined information results in the partial cyclotide sequence of YKVCT(I/L)NGNPGACGE.

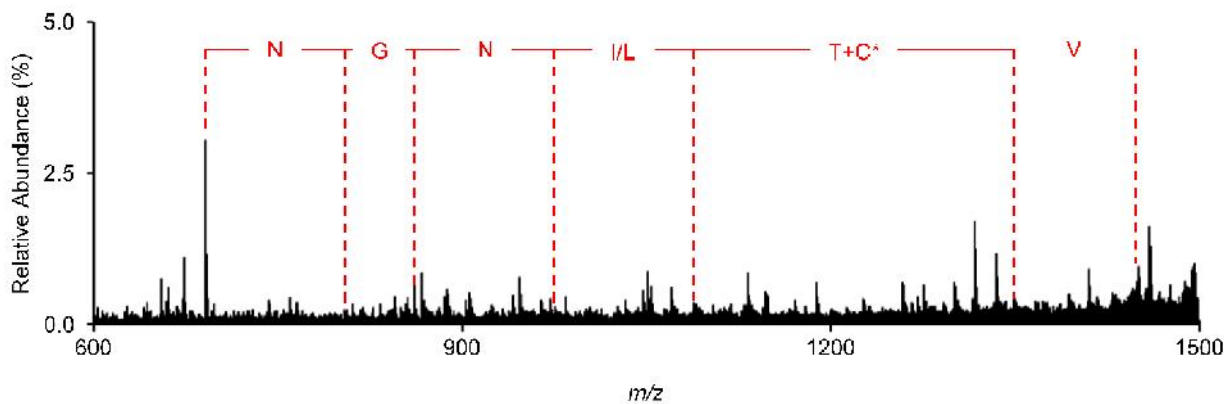


Figure 4.13. De novo sequencing of ion series 1.

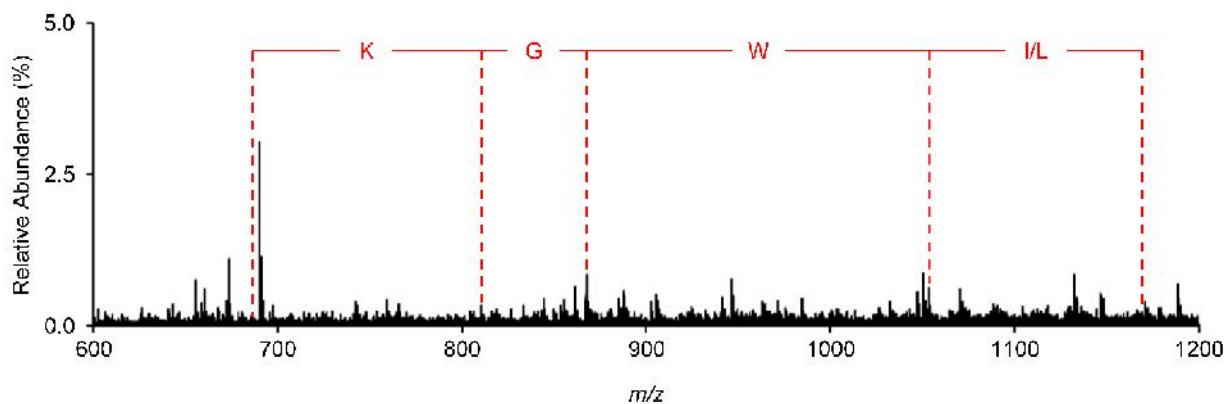


Figure 4.14. De novo sequencing of ion series 2.

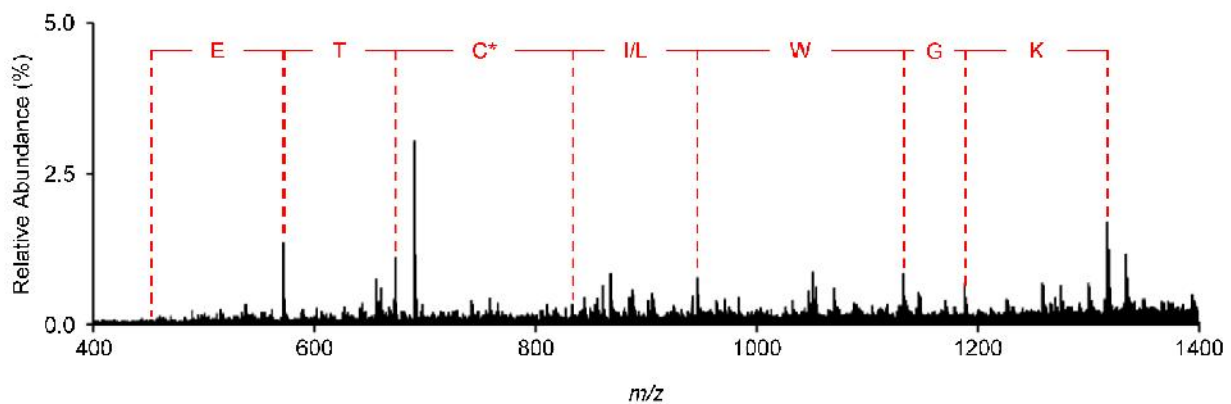


Figure 4.15. De novo sequencing of ion series 3.

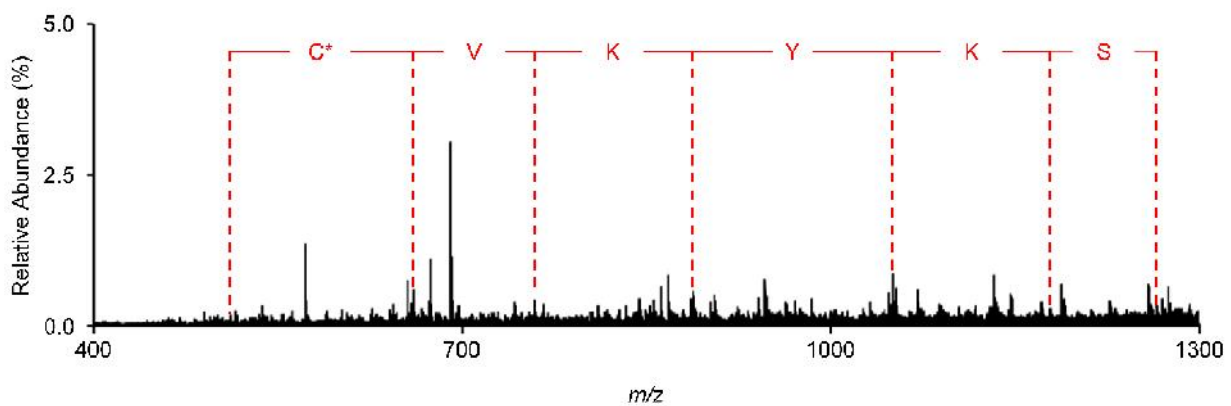


Figure 4.16. De novo sequencing of ion series 4.

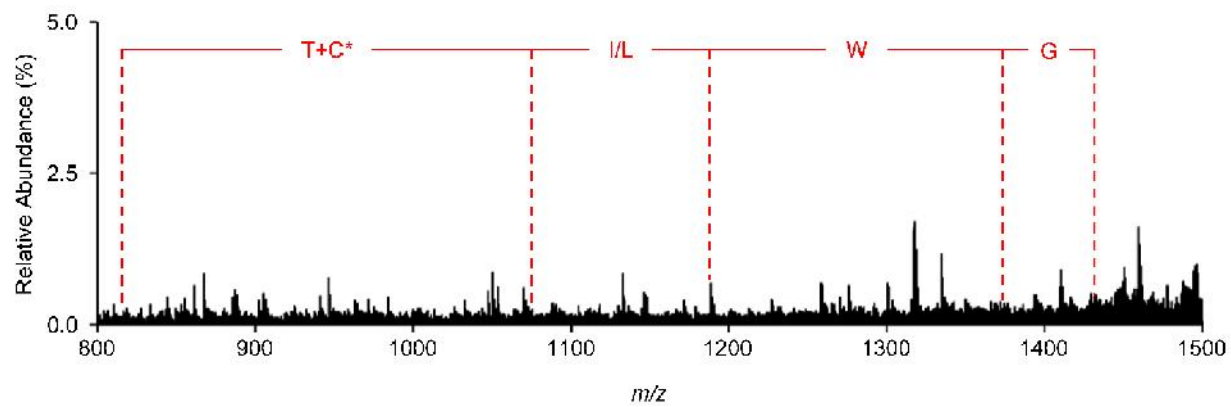


Figure 4.17. De novo sequencing of ion series 5.

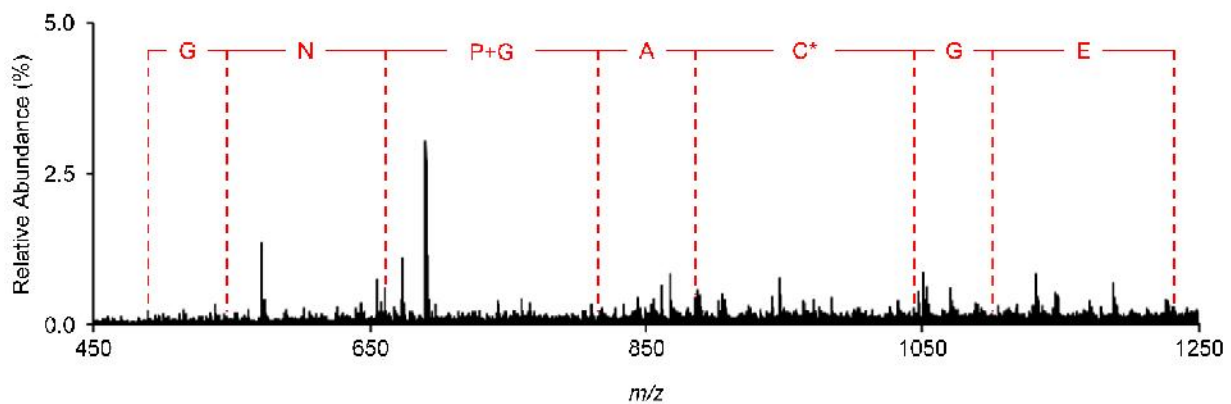


Figure 4.18. De novo sequencing of ion series 6.

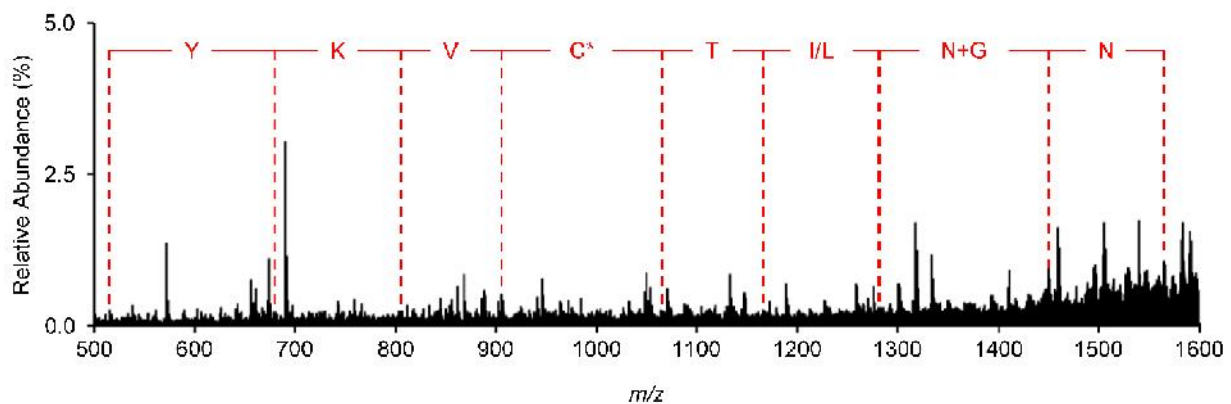


Figure 4.19. De novo sequencing of ion series 7.

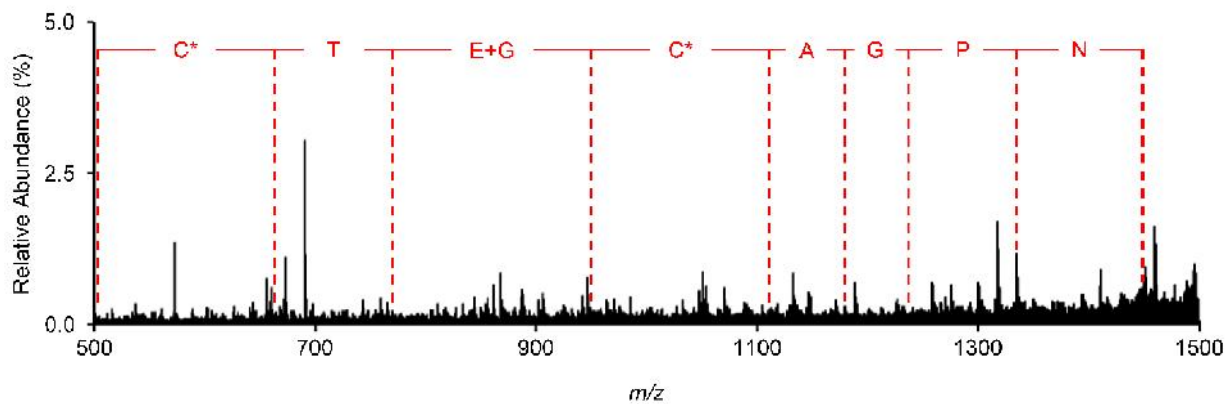


Figure 4.20. De novo sequencing of ion series 8.

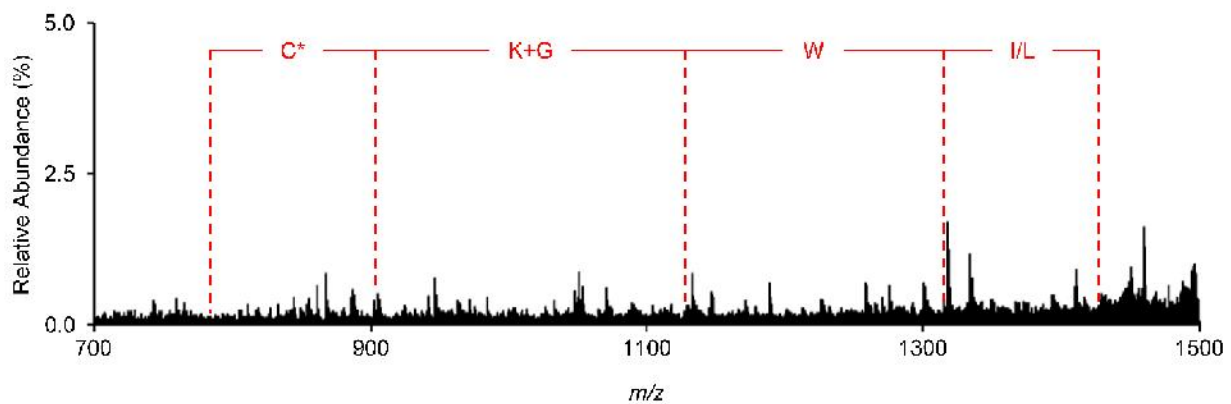


Figure 4.21. De novo sequencing of ion series 9.

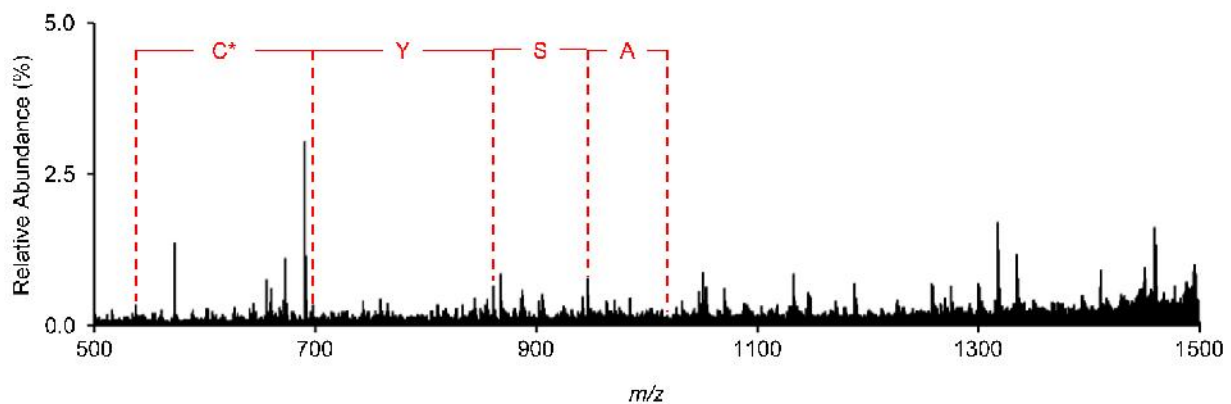


Figure 4.22. De novo sequencing of ion series 10.

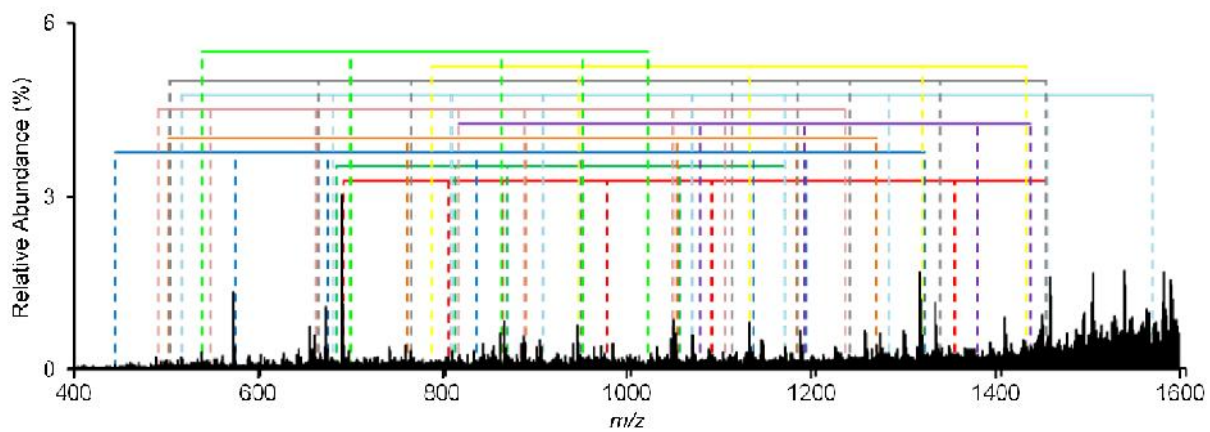


Figure 4.23. All identified ion series overlaid in one spectrum. Ion series are stacked in chronological order, with Ion Series 1 on the bottom and Ion Series 10 on the top.

	1	2	3	4	5	6
1	- - - - -	- - - - -	- - - - -	- - - - -	- - - - - V C - I/L N G N - - - - -	- - - - -
2	- - - /L W G K - - - - -	- - - - -	- - - - -	- - - - -	- - - - -	- - - - -
3	- C - /L W G K - - - - -	- - - - -	- - - - -	- - - - -	- - - - -	- - - - - E
4	- - - - -	- - - - -	- - - - -	- - - S K Y K V C - - - - -	- - - - -	- - - - -
5	- C - /L W G - - - - -	- - - - -	- - - - -	- - - - -	- - - - -	- - - - -
6	- - - - -	- - - - -	- - - - -	- - - - -	- - - - -	- - - G N P G A C G E
7	- - - - -	- - - - -	- - - - -	- - - - -	- - - Y K V C - I/L N G N - - - - -	- - - - -
8	- C - - - - -	- - - - -	- - - - -	- - - - -	- - - - -	- - - N P G A C G E
9	- - - /L W G K C - - - - -	- - - - -	- - - - -	- - - - -	- - - - -	- - - - -
10	- - - - - C Y S A - - - - -	- - - - -	- - - - -	- - - - -	- - - - -	- - - - -
	- C - /L W G K C Y S A	- - - - -	- - - - -	- - - S K Y K V C - I/L N G N P G A C G E	- - - - -	- - - - -

Figure 4.24. Aligned sequences for the ten ion series identified during de novo sequencing.

The process of extending the sequence of the unknown cyclotide can be repeated with all 10 ion series, yielding a partial sequence of TC(I/L)WGKCYSA – – – – – SKYKVCT(I/L)-GNPGACGE. The dashes indicate unknown amino acid residues of the cyclotide that could not be sequenced based on peak-to-peak mass differences. However, the identities of the unknown amino acids can be deduced. For the seventh ion series, using the overlap between the fourth ion series and the seventh ion series, the identity of the two amino acids N-terminal to the tyrosine are lysine and serine. Additionally, this workflow selectively opens the cyclotide from a c/z cleavage at dehydroalanine, forming a linear peptide with an alkyne as the new N-terminus.^{45–47} Subtraction of the alkyne moiety (51.9949 Da), lysine (128.0950 Da), serine (87.0320 Da), and an ionizing proton (1.007276 Da) from the initiating peak of the seventh series at m/z 515.1336 accounts for all but 247.0644 Da. The remaining mass suggests two or three amino acids are missing. An analysis of all possible two/three amino acid combinations reveals only two sequences ± 0.1 Da of 247.0644 Da, an alkylated cysteine and serine, in either order. This analysis suggests a sequence of CSC with a serine in loop 4. This is consistent with the fact that 73% of the cyclotides in CyBase contain a Ser in loop 4. Additionally, the deduction of serine in this position suggests the seventh ion series originates from ring opening at Cys3. The theoretical b_5 product ion mass is calculated to be m/z 515.1902, and the first product ion of the seventh series is observed experimentally at m/z 515.1936 (6.5 ppm).

The provisional assignment of serine above now generates a partial cyclotide sequence of TC(I/L)WGKCYSA – – CSCSKYKVCT(I/L)NGNPGACGE, where, again, the dashes indicate unknown amino acid residues. The mass of the partial sequence is 3121.2683 Da, accounting for all but 198.0762 Da from the intact unknown. Again, the remaining mass suggests two or three

amino acids are missing. An analysis of all possible two/three amino acid combinations reveal only three sequences ± 0.1 Da of 198.0762 Da – PT, TP, and VV. Assignment of leucine/isoleucine based on homology, while not ideal, has been used within the cyclotide community in cases where chymotrypsin digestion cannot be performed due to an adjacent proline residue or in cases where the amount of isolated protein is insufficient for amino acid analysis.^{59–61} On the basis of sequence homology to other known cyclotides from the same plant species, the two amino acids would likely be VV.⁴⁸ However, based on mass, the identity of the unknown residues are likely TP or PT rather than VV (compare 198.1004 to 198.1368 Da). The ETD product ion spectrum, as shown in Figure 4.25b, of the Glu-C digested unknown suggests TP rather than PT as c_{10} and c_{12} ions are observed. Given that ETD does not result in an observable fragment ion N-terminal to proline, no c_{10} ion would be observed if the order of these amino acids were PT.

To summarize, the direct evidence from the de novo sequencing using the ring-opening approach described here results in TC(I/L)WGKCYSA – – – – SKYKVCT(I/L)-NGNPGACGE, accounting for all but five residues. The identities of the remaining residues can be inferred on the basis of mass, as demonstrated above, resulting in a provisional assignment of TC(I/L)WGKCYSA(T/P)(P/T)CSCSKYKVCT(I/L)NGNPGACGE. It is noted here that we cannot distinguish between the isomeric leucine and isoleucine. Additionally, while the mass analysis suggests a threonine and proline at the end of loop 3, there is insufficient evidence in the product ion spectrum to distinguish between TP or PT. The observed experimental mass of the unknown (3319.3445 Da) is in good agreement with the theoretical mass of the provisional sequence (3319.3687 Da) showing a mass accuracy of 7.3 ppm.

To validate the utility of the described approach to sequencing cyclotides, we compare the results of the gas-phase ring opening at dehydroalanine to the conventional condensed-phase approach. CID and ETD of the Glu-C digested $[M + 4H]^{4+}$ generates the product ion spectra shown in Figure 4.25, parts a and b, respectively. For CID, 21 fragment ions are assigned with high confidence, accounting for cleavages at 17 of 31 amide linkages (54.8%). For ETD, 28 fragment ions are assigned with high confidence, accounting for cleavages at 19 of 31 amide linkages (61.3%). The fragmentation maps are overlaid in Figure 4.25c. Cumulatively, CID and ETD results in 77.4% sequence coverage. Particularly noteworthy is the stretch of five amino acids, KVCT(I/L) where no fragment ions are observed. Comparison of the two approaches (i.e., ring opening in the gas phase vs ring opening in the condensed phase) demonstrates a situation where both approaches

can sequence all but five residues. With the conventional digestion approach, however, CID and ETD were needed to generate extensive coverage of the unknown. Additionally, while many cyclotides are abundant enough to be fully sequenced with digestion-based methods, many low-abundance cyclotides remain uncharacterized. Here, the ability to reduce sample loss with the gas-phase linearization is demonstrated by eliminating the need for proteolytic digestion.

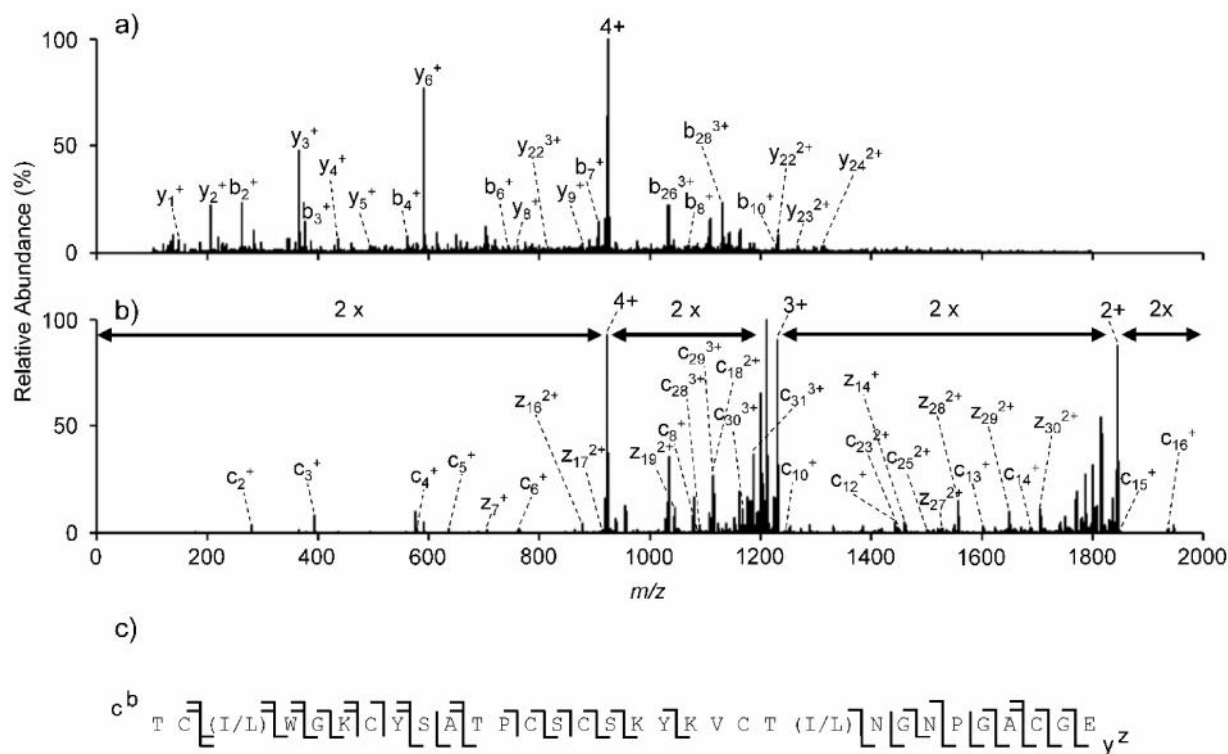


Figure 4.25. LC-MS/MS analysis of reduced and alkylated Glu-C digested $[unknown + 4H]^{4+}$ using a) targeted CID or b) targeted EThcD as an activation method. c) The combined fragmentation maps of panels a and b.

4.4 Conclusions

In this work, we demonstrated the site-selective ring opening of cyclotides at dehydroalanine residues formed via gas-phase ion/ion reaction. Transformation of a single carbamidomethyl cysteine residue to a dehydroalanine residue occurs through the odd-electron loss of $\bullet\text{SCH}_2\text{CONH}_2$. Dehydroalanine can be formed at any of the six alkylated cysteine residues, generating six isomers of identical mass. Collisional activation of $[M + H - 90]^{2+}$ leads to an initial c/z cleavage N-terminal to dehydroalanine and a second backbone cleavage to produce fragment

ions indicative the cyclotide sequence. Linearization from ring opening at all cysteine residues is observed, with sequence coverages of up to 58% observed for individual linearization sites. The fragmentation from each ring opening is highly complementary, which enables extensive sequence coverage to be obtained. For the four known cyclotide sequences examined, cumulative sequence coverages of no less than 93% was observed. This complementarity proved extremely important in the de novo sequencing of an unknown cyclotide from *V. inconspicua*. Using this novel approach, a partial sequence of TC(I/L)WGKCYSA – – – – SKYKVCT(I/L)NGNPGACGE is obtained. Interestingly, MS/MS of Glu-C digested unknown resulted in much lower sequence coverage, using solely CID or EThcD, demonstrating further the utility of the described gas-phase sequencing approach.

4.5 References

1. Craik, D.J., Daly, N.L., Bond, T., Waine, C.: Plant Cyclotides: A Unique Family of Cyclic and Knotted Proteins that Defines the Cyclic Cystine Knot Structural Motif. *J. Mol. Biol.* **1999**, 294, 1327-1336.
2. Colgrave, M.L., Craik, D.J.: Thermal, Chemical, and Enzymatic Stability of the Cyclotide Kalata B1: The Importance of the Cyclic Cystine Knot. *Biochemistry.* **2004**, 43, 5965-5975.
3. Jagadish, K., Camarero, J.A.: Cyclotides, A Promising Molecular Scaffold for Peptide-Based Therapeutics. *Biopolymers.* **2010**, 94, 611-616.
4. Henriques, S.T., Craik, D.J.: Cyclotides as Templates in Drug Design. *Drug Discovery Today.* **2010**, 15, 57-64.
5. Poth, A.G., Chan, L.Y., Craik, D.J.: Cyclotides as Grafting Frameworks for Protein Engineering and Drug Design Applications. *Biopolymers.* **2013**, 100, 480-491.
6. Burman, R., Gunasekera, S., Strömstedt, A.A., Göransson, U.: Chemistry and Biology of Cyclotides: Circular Plant Peptides Outside the Box. *J. Nat. Prod.* **2014**, 77, 724-736.
7. Gould, A., Camarero, J.A.: Cyclotides: Overview and Biotechnological Applications. *ChemBioChem.* **2017**, 18, 1350-1363.
8. Gran, L.: Oxytocic Principles of *Oldenlandia affinis*. *Lloydia.* **1973**, 36, 174-178.
9. Gran, L.: On the Effect of a Polypeptide Isolated from “Kalata Kalata” (*Oldenlandia affinis* DC) on the Oestrogen Dominated Uterus. *Acta Pharmacol. Toxicol.* **1973**, 33, 400-408.

10. Gustafson, K.R., Sowder, R.C., Henderson, L.E., Parsons, I.C., Kashman, Y., Cardellina, J.H., McMahon, J.B., Buckheit, R.W., Pannell, L.K., Boyd, M.R.: Circulins A and B. Novel Human Immunodeficiency Virus (HIV)-Inhibitory Macrocyclic Peptides from the Tropical Tree *Chassalia parvifolia*. *J. Am. Chem. Soc.* **1994**, 116, 9337-9338.
11. Gustafson, K.R., Walton, L.K., Sowder, R.C., Johnson, D.G., Pannell, L.K., Cardellina, J.H., Boyd, M.R.: New Circulin Macrocyclic Polypeptides from *Chassalia parvifolia*. *J. Nat. Prod.* **2000**, 63, 176-178.
12. Chen, B., Colgrave, M.L., Daly, N.L., Rosengren, K.J., Gustafson, K.R., Craik, D.J.: Isolation and Characterization of Novel Cyclotides from *Viola hederaceae*: Solution Structure and Anti-HIV Activity of vhl-1, A Leaf-Specific Expressed Cyclotide. *J. Biol. Chem.* **2005**, 280, 22395-22405.
13. Wang, C.K.L., Colgrave, M.L., Gustafson, K.R., Ireland, D.C., Göransson, U., Craik, D.J.: Anti-HIV Cyclotides from the Chinese Medicinal Herb *Viola yedoensis*. *J. Nat. Prod.* **2008**, 71, 47-52.
14. Lindholm, P., Göransson, U., Johansson, S., Claeson, P., Gullbo, J., Larsson, R., Bohlin, L., Backlund, A.: Cyclotides: A Novel Type of Cytotoxic Agents. *Mol. Cancer Ther.* **2002**, 1, 365-369.
15. Svängård, E., Göransson, U., Hocaoglu, Z., Gullbo, J., Larsson, R., Claeson, P., Bohlin, L.: Cytotoxic Cyclotides from *Viola tricolor*. *J. Nat. Prod.* **2004**, 67, 144-147.
16. Hernandez, J.-F., Gagnon, J., Chiche, L., Nguyen, T.M., Andrieu, J.-P., Heitz, A., Trinh Hong, T., Pham, T.T.C., Le Nguyen, D.: Squash Trypsin Inhibitors from *Momordica cochinchinensis* Exhibit an Atypical Macrocyclic Structure. *Biochemistry.* **2000**, 39, 5722-5730.
17. Jennings, C., West, J., Waine, C., Craik, D., Anderson, M.: Biosynthesis and Insecticidal Properties of Plant Cyclotides: The Cyclic Knotted Proteins from *Oldenlandia affinis*. *Proc. Natl. Acad. Sci.* **2001**, 98, 10614.
18. Jennings, C.V., Rosengren, K.J., Daly, N.L., Plan, M., Stevens, J., Scanlon, M.J., Waine, C., Norman, D.G., Anderson, M.A., Craik, D.J.: Isolation, Solution Structure, and Insecticidal Activity of Kalata B2, a Circular Protein with a Twist: Do Möbius Strips Exist in Nature? *Biochemistry.* **2005**, 44, 851-860.
19. Barbeta, B.L., Marshall, A.T., Gillon, A.D., Craik, D.J., Anderson, M.A.: Plant Cyclotides Disrupt Epithelial Cells in the Midgut of Lepidopteran Larvae. *Proc. Natl. Acad. Sci.* **2008**, 105, 1221.
20. Gruber, C.W., Elliott, A.G., Ireland, D.C., Delprete, P.G., Dessen, S., Göransson, U., Trabi, M., Wang, C.K., Kinghorn, A.B., Robbrecht, E., Craik, D.J.: Distribution and Evolution of Circular Miniproteins in Flowering Plants. *Plant Cell.* **2008**, 20, 2471-2483.

21. Zhang, J., Li, J., Huang, Z., Yang, B., Zhang, X., Li, D., Craik, D.J., Baker, A.J.M., Shu, W., Liao, B.: Transcriptomic Screening for Cyclotides and Other Cysteine-Rich Proteins in the Metallophyte *Viola baoshanensis*. *J. Plant Physiol.* **2015**, 178, 17-26.
22. Hellinger, R., Koehbach, J., Soltis, D.E., Carpenter, E.J., Wong, G.K.-S., Gruber, C.W.: Peptidomics of Circular Cysteine-Rich Plant Peptides: Analysis of the Diversity of Cyclotides from *Viola tricolor* by Transcriptome and Proteome Mining. *J. Proteome Res.* **2015**, 14, 4851-4862.
23. de Veer, S.J., Weidmann, J., Craik, D.J.: Cyclotides as Tools in Chemical Biology. *Acc. Chem. Res.* **2017**, 50, 1557-1565.
24. Burman, R., Yeshak, M.Y., Larsson, S., Craik, D.J., Rosengren, K.J., Göransson, U.: Distribution of Circular Proteins in Plants: Large-Scale Mapping of Cyclotides in the Violaceae. *Front. Plant Sci.* **2015**, 6, 855.
25. Trabi, M., Svängård, E., Herrmann, A., Göransson, U., Claeson, P., Craik, D.J., Bohlin, L.: Variations in Cyclotide Expression in *Viola* Species. *J. Nat. Prod.* **2004**, 67, 806-810.
26. Mulvenna, J.P., Wang, C., Craik, D.J.: Cybase: A Database of Cyclic Protein Sequence and Structure. *Nucleic Acids Res.* **2006**, 34, D192-D194.
27. Wang, C.K.L., Kaas, Q., Chiche, L., Craik, D.J.: Cybase: A Database of Cyclic Protein Sequences and Structures, with Applications in Protein Discovery and Engineering. *Nucleic Acids Res.* **2007**, 36, D206-D210.
28. Craik, D.J., Daly, N.L.: NMR as a Tool for Elucidating the Structures of Circular and Knotted Proteins. *Mol. Biosyst.* **2007**, 3, 257-265.
29. Rosengren, K.J., Daly, N.L., Plan, M.R., Waine, C., Craik, D.J.: Twists, Knots, and Rings in Proteins: Structural Definition of the Cyclotide Framework. *J. Biol. Chem.* **2003**, 278, 8606-8616.
30. Göransson, U., Craik, D.J.: Disulfide Mapping of the Cyclotide Kalata B1: Chemical Proof of the Cyclic Cysteine Knot Motif. *J. Biol. Chem.* **2003**, 278, 48188-48196.
31. Ji, Y.; Majumder, S.; Millard, M.; Borra, R.; Bi, T.; Elnagar, A. Y.; Neamati, N.; Shekhtman, A.; Camarero, J. A. In Vivo Activation of the p53 Tumor Suppressor Pathway by an Engineered Cyclotide. *J. Am. Chem. Soc.* **2013**, 135, 11623-11633.
32. Li, Y., Gould, A., Aboye, T., Bi, T., Breindel, L., Shekhtman, A., Camarero, J.A.: Full Sequence Amino Acid Scanning of α -Defensin RTD-1 Yields a Potent Anthrax Lethal Factor Protease Inhibitor. *J. Med. Chem.* **2017**, 60, 1916-1927.
33. Colgrave, M. L. Primary Structural Analysis of Cyclotides. In *Advances in Botanical Research: Plant Cyclotides*; Craik, D. J., Ed.; Academic Press: London, 2015

34. Witherup, K.M., Bogusky, M.J., Anderson, P.S., Ramjit, H., Ransom, R.W., Wood, T., Sardana, M.: Cyclopsychotride A, a Biologically Active, 31-Residue Cyclic Peptide Isolated from *Psychotria longipes*. *J. Nat. Prod.* **1994**, 57, 1619-1625.
35. Saether, O., Craik, D.J., Campbell, I.D., Sletten, K., Juul, J., Norman, D.G.: Elucidation of the Primary and Three-Dimensional Structure of the Uterotonic Polypeptide Kalata B1. *Biochemistry.* **1995**, 34, 4147-4158.
36. Poth, A.G., Colgrave, M.L., Philip, R., Kerenga, B., Daly, N.L., Anderson, M.A., Craik, D.J.: Discovery of Cyclotides in the Fabaceae Plant Family Provides New Insights into the Cyclization, Evolution, and Distribution of Circular Proteins. *ACS Chem. Biol.* **2011**, 6, 345-355.
37. Pinto, M.E.F., Najas, J.Z.G., Magalhães, L.G., Bobey, A.F., Mendonça, J.N., Lopes, N.P., Leme, F.M., Teixeira, S.P., Trovó, M., Andricopulo, A.D., Koehbach, J., Gruber, C.W., Cilli, E.M., Bolzani, V.S.: Inhibition of Breast Cancer Cell Migration by Cyclotides Isolated from *Pombalia calceolaria*. *J. Nat. Prod.* **2018**, 81, 1203-1208.
38. Parsley, N.C., Kirkpatrick, C.L., Crittenden, C.M., Rad, J.G., Hoskin, D.W., Brodbelt, J.S., Hicks, L.M.: PepSAVI-MS Reveals Anticancer and Antifungal Cycloviolacins in *Viola odorata*. *Phytochemistry.* **2018**, 152, 61-70.
39. Narayani, M., Sai Varsha, M.K.N., Potunuru, U.R., Sofi Beaula, W., Rayala, S.K., Dixit, M., Chadha, A., Srivastava, S.: Production of Bioactive Cyclotides in Somatic Embryos of *Viola odorata*. *Phytochemistry.* **2018**, 156, 135-141.
40. Niyomploy, P., Chan, L.Y., Harvey, P.J., Poth, A.G., Colgrave, M.L., Craik, D.J.: Discovery and Characterization of Cyclotides from *Rinorea* Species. *J. Nat. Prod.* **2018**, 81, 2512-2520.
41. Tomer, K.B., Crow, F.W., Gross, M.L., Kopple, K.D.: Fast-Atom Bombardment Combined with Tandem Mass Spectrometry for the Determination of Cyclic Peptides. *Anal. Chem.* **1984**, 56, 880-886.
42. Hitzeroth, G., Vater, J., Franke, P., Gebhardt, K., Fiedler, H.-P.: Whole Cell Matrix-Assisted Laser Desorption/Ionization Time-Of-Flight Mass Spectrometry and In Situ Structure Analysis of Streptocidins, A Family of Tyrocidine-Like Cyclic Peptides. *Rapid Commun. Mass Spectrom.* **2005**, 19, 2935-2942.
43. Crittenden, C.M., Parker, W.R., Jenner, Z.B., Bruns, K.A., Akin, L.D., McGee, W.M., Ciccimaro, E., Brodbelt, J.S.: Exploitation of the Ornithine Effect Enhances Characterization of Stapled and Cyclic Peptides. *J. Am. Soc. Mass. Spectrom.* **2016**, 27, 856-863.
44. McGee, W.M., McLuckey, S.A.: The Ornithine Effect in Peptide Cation Dissociation. *J. Mass Spectrom.* **2013**, 48, 856-861.

45. Foreman, D.J., Lawler, J.T., Niedrauer, M.L., Hostetler, M.A., McLuckey, S.A.: Gold(I) Cationization Promotes Ring Opening in Lysine-Containing Cyclic Peptides. *J. Am. Soc. Mass. Spectrom.* **2019**, 30, 1914-1922.
46. Pilo, A.L., Peng, Z., McLuckey, S.A.: The Dehydroalanine Effect in the Fragmentation of Ions Derived from Polypeptides. *J. Mass Spectrom.* **2016**, 51, 857-866.
47. Peng, Z., Bu, J., McLuckey, S.A.: The Generation of Dehydroalanine Residues in Protonated Polypeptides: Ion/Ion Reactions for Introducing Selective Cleavages. *J. Am. Soc. Mass. Spectrom.* **2017**, 28, 1765-1774.
48. Parsley, N.C., Sadecki, P.W., Hartmann, C.J., Hicks, L.M.: *Viola* “inconspicua” No More: An Analysis of Antibacterial Cyclotides. *J. Nat. Prod.* **2019**, 82, 2537-2543.
49. Xia, Y., Chrisman, P.A., Erickson, D.E., Liu, J., Liang, X., Londry, F.A., Yang, M.J., McLuckey, S.A.: Implementation of Ion/Ion Reactions in a Quadrupole/Time-of-Flight Tandem Mass Spectrometer. *Anal. Chem.* **2006**, 78, 4146-4154.
50. Webb, I.K., Londry, F.A., McLuckey, S.A.: Implementation of Dipolar Direct Current (DDC) Collision-Induced Dissociation in Storage and Transmission Modes on a Quadrupole/Time-Of-Flight Tandem Mass Spectrometer. *Rapid Commun. Mass Spectrom.* **2011**, 25, 2500-2510.
51. Liang, X., Xia, Y., McLuckey, S.A.: Alternately Pulsed Nanoelectrospray Ionization/Atmospheric Pressure Chemical Ionization for Ion/Ion Reactions in an Electrodynamic Ion Trap. *Anal. Chem.* **2006**, 78, 3208-3212.
52. Turek, F., Julian, R.R.: Peptide Radicals and Cation Radicals in the Gas Phase. *Chem. Rev.* **2013**, 113, 6691-6733.
53. Wee, S., O’Hair, R.A.J., McFadyen, W.D.: Comparing the Gas-Phase Fragmentation Reactions of Protonated and Radical Cations of the Tripeptides GXR. *Int. J. Mass Spectrom.* **2004**, 234, 101-122.
54. Chung, T.W., Turek, F.: Backbone and Side-Chain Specific Dissociations of z Ions from Non-Tryptic Peptides. *J. Am. Soc. Mass. Spectrom.* **2010**, 21, 1279-1295.
55. Eva Fung, Y.M., Chan, T.-W.D.: Experimental and Theoretical Investigations of the Loss of Amino Acid Side Chains in Electron Capture Dissociation of Model Peptides. *J. Am. Soc. Mass. Spectrom.* **2005**, 16, 1523-1535.
56. Han, H., Xia, Y., McLuckey, S.A.: Ion Trap Collisional Activation of c and z• Ions Formed via Gas-Phase Ion/Ion Electron-Transfer Dissociation. *J. Proteome Res.* **2007**, 6, 3062-3069.

57. Chalkley, R.J., Brinkworth, C.S., Burlingame, A.L.: Side-Chain Fragmentation of Alkylated Cysteine Residues in Electron Capture Dissociation Mass Spectrometry. *J. Am. Soc. Mass. Spectrom.* **2006**, 17, 1271-1274.
58. Sun, R.-X., Dong, M.-Q., Song, C.-Q., Chi, H., Yang, B., Xiu, L.-Y., Tao, L., Jing, Z.-Y., Liu, C., Wang, L.-H., Fu, Y., He, S.-M.: Improved Peptide Identification for Proteomic Analysis Based on Comprehensive Characterization of Electron Transfer Dissociation Spectra. *J. Proteome Res.* **2010**, 9, 6354-6367.
59. Ireland, D. C., Colgrave, M. L., Craik, D. J.: A Novel Suite of Cyclotides from *Viola odorata*: Sequence Variation and the Implications for Structure, Function and Stability. *Biochem. J.* **2006**, 400, 1-12.
60. Herrmann, A., Burman, R., Mylne, J.S., Karlsson, G., Gullbo, J., Craik, D.J., Clark, R.J., Göransson, U.: The Alpine Violet, *Viola biflora*, is a Rich Source of Cyclotides with Potent Cytotoxicity. *Phytochemistry.* **2008**, 69, 939-952.
61. He, W., Chan, L.Y., Zeng, G., Daly, N.L., Craik, D.J., Tan, N.: Isolation and Characterization of Cytotoxic Cyclotides from *Viola philippica*. *Peptides.* **2011**, 32, 1719-172

CHAPTER 5. MAXIMIZING SELECTIVE CLEAVAGES AT ASPARTIC ACID AND PROLINE RESIDUES FOR THE IDENTIFICATION OF INTACT PROTEINS

Adapted by permission from Springer Nature: Journal of the American Society for Mass Spectrometry, Foreman, D. J.; Dziekonski, E. T.; McLuckey, S. A. *J. Am. Soc. Mass Spectrom.* **2018**, 30, 34-44. Copyright 2018.

5.1 Introduction

The notion of using collision-induced dissociation (CID) to elucidate the primary structure of intact proteins was first presented in 1990,¹ and formed the basis for the development of “top-down” tandem mass spectrometry of proteins. Today, collisional activation remains one of the most common techniques for the identification of proteins in top-down workflows.²⁻⁶ Other dissociation approaches, such as electron capture dissociation,⁷ electron transfer dissociation,⁸ and UV photodissociation (UVPD)⁹ have subsequently been applied to whole protein ions with a common objective of maximizing the number of sequence informative products. With this objective in mind, it is desirable that fragmentation be non-selective. However, as the number of different product ions increase, the overall product ion signal is dispersed among the many fragmentation channels.¹⁰ There is merit, therefore, in having the option to maximize selective cleavages that tend to concentrate product ion signal into fewer channels. Scenarios that might benefit from this capability include, for example, the identification of low level proteins in cases when the dispersal of product ion signal among many channels limits dynamic range and in single (or multiple) reaction monitoring workflows. We note here a distinction between “identification” of a protein or “proteoform”¹¹ and complete “characterization.” Maximizing the number of cleavages is a priority for the latter objective in spite of the fact that this might limit detection limits and dynamic range.

The generation of almost exclusively b- and y-type fragment ions upon CID of multiply protonated proteins is commonly observed and is consistent with the mobile proton model.¹²⁻¹⁴ Collisional activation of a peptide or protein leads to mobilization of the excess protons along the polypeptide backbone that can initiate a charge-directed fragmentation process to produce b- and y-fragment ions.¹⁵ While a number of non-specific fragmentation pathways are observed when using collisional activation, particularly at intermediate charge states, several site-specific

fragmentation pathways have been reported.^{16–20} Specifically, under favorable conditions, cleavages at aspartic acid residues and proline residues have been shown to be the dominant pathways.^{16,19,21–24} Despite both fragmentation pathways resulting in highly selective cleavages, the underlying mechanism regarding both cleavages differs. The higher basicity of the proline amide bond, relative to those of other amino acids, leads to preferential localization of a mobilized proton at the proline amide bond, initiating the charge-directed fragmentation N-terminal to the proline residue. The favorable cleavage at aspartic acid residues C-terminal to the acidic side chain does not require a mobile proton and can become prominent when the ionizing protons are sequestered by arginine residues.²⁵

Numerous studies have been performed to characterize the gas-phase fragmentation behavior of intact proteins,^{26–32} revealing that the information obtained in a CID experiment is highly dependent on the charge state subjected to activation as well as the number of basic residues present in the protein sequence.^{33,34} Fragmentation patterns can be rationalized on the basis of three major precursor ion types: high charge states, intermediate charge states, and low charge states. Activation of high charge states, where the large intramolecular Coulomb field tends to minimize proton mobilization, leads to fragmentation patterns that are difficult to predict a priori. Activation of intermediate charge states typically results in a high degree of sequence coverage and extensive non-specific fragmentation due to maximum proton mobility. Collisional activation of low charge state proteins, where protein mobility is hindered by solvation of a proton by multiple basic residues or where protons are sequestered onto mostly arginine residues, generates prominent small molecule loss and cleavage C-terminal to aspartic acid residues.

Recently, in recognition of the differences observed between the product ion spectra of protein ions generated under denaturing conditions versus those generated under native conditions,^{26–29,35} the Kelleher group examined the gas-phase fragmentation propensities of native intact proteins.³⁶ In this study, a statistical analysis of 5311 matched fragments from 165 different experiments revealed striking differences in fragmentation propensities for native conditions when compared to denatured conditions. Most notably, under native conditions, fragmentation C-terminal to aspartic acid residues and N-terminal to proline residues showed significant enhancement in fragmentation tendency when compared to their denatured counterparts. This observation suggests that the CID of protein ions generated under native conditions could constitute a strategy for maximizing selective fragmentation at aspartic acid and proline residues.

However, protein ion signals tend to be less intense using native conditions relative to denaturing conditions (e.g., low pH and, perhaps, some fraction of organic solvent) and the extent of sodium and potassium ion adduction tends to be greater due to differences in ionization mechanism.³⁷

Here, we present a methodology for the identification of intact proteins that maximizes the selective cleavages at aspartic acid and proline residues while retaining the advantages in signal levels and lower metal ion adduction afforded by generating ions under denaturing conditions.^{38–}

⁴¹ A drawback associated with protein ionization under denaturing conditions is that the precursor ion signal is divided among many relatively high charge states. We therefore use a sequence of proton transfer ion/ion reactions within the mass spectrometer to, first, concentrate the precursor ion charge state distribution largely into one charge state prior to ion isolation and, second, to move the precursor ion charges into a range (i.e., m/z 1500– 2500) that is most likely to lead to selective cleavages. This methodology is demonstrated here with four standard proteins often used by the National Resource for Translational and Developmental Proteomics in optimizing top-down workflows: ubiquitin (8.6 kDa), myoglobin (16.9 kDa), trypsinogen (24.0 kDa), and carbonic anhydrase (29.0 kDa).⁴²

5.2 Experimental

5.2.1 Sample Preparation

Ubiquitin from bovine erythrocytes, myoglobin from equine skeletal muscle, trypsinogen from bovine pancreas, carbonic anhydrase from bovine erythrocytes, 2,2,3,3,4,4,5,5,6,6,7,7,8,8,8-pentadecafluoro-1-octanol (PFO), ammonium bicarbonate, dithiothreitol (DTT), iodoacetamide, and formic acid were purchased from Sigma-Aldrich (St. Louis, MO, USA). Optima-grade acetonitrile, HPLC-grade methanol, and Optima LC/MS-grade water were purchased from Fisher Scientific (Fair Lawn, NJ, USA). Chloroform was purchased from Mallinckrodt (Phillipsburg, NJ, USA) and urea was purchased from Pierce Chemical (Rockford, IL, USA). PFO was made at a concentration of 200 μ M in a methanol solution containing 2% ammonium hydroxide.

Stock solutions of ubiquitin, myoglobin, and carbonic anhydrase were prepared at approximately 2 mg/mL in water. Fifty microliters of the ubiquitin stock, 80 μ L of the myoglobin stock, and 80 μ L of the carbonic anhydrase stock were combined and precipitated using 1:1:4:3 protein/chloroform/methanol/water.⁴³ The dried precipitated protein mixture was reconstituted in

100 μ L of mobile phase A. The proteins were then separated via reverse-phase HPLC using an Agilent 1200 series with manual injector (Palo Alto, CA, USA) using an Agilent Zorbax 300SB-C3 4.6 \times 150 mm, 5 μ m (Palo Alto, CA, USA) analytical HPLC column. The HPLC method consisted of a linear gradient from 5% mobile phase B to 50% mobile phase B over 60 min (mobile phase A: 95% water, 5% acetonitrile, and 0.2% formic acid, mobile phase B: 5% water, 95% acetonitrile, 0.2% formic acid) at flow rate of 1 mL/min and a detection wavelength of 215 nm.

A total of four 20 μ L injections were made. For each injection, each protein was collected into a separate Eppendorf tube for a total of four fractions for each protein. The first three fractions were dried under vacuum and reconstituted in the fourth sample. The concentrations of the working samples are approximately 9, 8, and 4 μ M for ubiquitin, myoglobin, and carbonic anhydrase, respectively.

5.2.2 Reduction and Alkylation of Trypsinogen

Approximately 2 mg of trypsinogen was dissolved in 1 mL of reduction buffer (100 mM ammonium bicarbonate, 7 M urea). DTT was added from a 500 mM stock to a final concentration of 5 mM and was incubated for 45 min at 55 $^{\circ}$ C. The solution was cooled to room temperature and centrifuged briefly. Iodoacetamide was added to a final concentration of 14 mM, from a 500 mM freshly prepared stock solution. The solution was incubated at room temperature in the dark for 30 min. Unreacted iodoacetamide was quenched with addition of another 5 mM of DTT and incubated at room temperature for 15 min in the dark. One hundred microliters of the reduced and alkylated trypsinogen was subjected to the precipitation and HPLC procedures as described above. The final trypsinogen concentration is estimated to be approximately 6 μ M.

5.2.3 Mass Spectrometry

All data were collected using a modified TripleTOF 5600 quadrupole/time-of-flight mass spectrometer (SCIEX, Concord, ON, Canada), modified to perform ion/ion reactions.⁴⁴ Alternatively pulsed nano-electrospray (nESI) ionization allows for sequential injection of multiply protonated proteins and singly deprotonated pentadecafluoro-1-octanol dimer (PFO).⁴⁵ Analyte cations were injected into the mass spectrometer and trapped in q0 followed immediately by injection of the reagent anions. Instrument parameters were tuned such that PFO dimer was

injected and transmitted through q0 while still trapping protein cations, resulting in consecutive proton transfer ion/ion reactions.^{46,47} During the reaction, the period which anions are passing through q0, an excitation voltage was applied at a slightly higher frequency than the desired ion's fundamental frequency.⁴⁸ This process is referred to as ion parking. Application of the excitation voltage slows the ion/ion reaction rate of a specific mass-to-charge, allowing concentration of signal into a single, lower charge state. Ion parking was performed at the charge state immediately prior to m/z 1500. Reaction times varied from 100 to 300 ms.

Next, the charge reduced protein was isolated in Q1 and transferred to q2. PFO dimer was once again generated via negative nESI and transferred to q2. The ions were mutually stored for a reaction time optimized to generate a distribution of charge states between m/z 1500 and m/z 2500 (10–30 ms).⁴⁹ Application of two high amplitude frequency sweeps were used to eject any low m/z ions ($< m/z$ 1500) and any high m/z ions ($> m/z$ 2500). All charge states between m/z 1500 and 2500 were isolated and subjected to dipolar direct current (DDC) collisional activation.⁵⁰ Mass analysis was performed using time of flight (TOF).

5.2.4 Database Search

Database searches were performed using a program written in MATLAB (MathWorks®, Natick, MA, USA). All entries of the SWISS-PROT database (556,197 entries) were processed to create separate entries for the cleavage of the N-terminal initiator methionine residue and cleavage into individual protein chains.⁵¹ The processing of the SWISS-PROT entries resulted in a database of 624,084 entries across all species.

Uninterpreted MS/MS spectra were processed using a zero-charge THRASH deconvolution algorithm written in MATLAB, using a S/N threshold of three.⁵² The output contained a list of monoisotopic zero-charge masses as well the total area under each fragment's isotopic distribution. Theoretical zero-charge b- and y-fragment masses for each protein, within a ± 100 Da window of the experimentally derived protein mass, were compared to the masses of the deconvoluted peak list with a fragmentation tolerance of ± 15 ppm. A McLuckey Score, with modified coefficients for native-like protein charge states, was calculated for each protein within the 200-Da mass window as shown below,

$$\text{Score} = (5 \times nD \times \sum D_A) + (3 \times nP \times \sum P_A) + (nX \times \sum X_A) \quad (5.1)$$

where n and A are, respectively, the number of matched fragments and summation of fragment area (where the smallest area is normalized to an area of 1) for either D (aspartic acid), P (proline), or X (non-specific) cleavages.⁵³ These coefficients are based qualitatively off our understanding of the well-known aspartic acid effect and the fragmentation propensities of native intact proteins as determined by Kelleher and coworkers.³⁶ This scoring system accounts for the preferential cleavage at aspartic acid and proline observed with native-like protein charge states.

5.3 Results and Discussion

5.3.1 Experimental Design and Rationale

The approach to intact protein analysis as described here exploits the highly selective cleavages C-terminal to aspartic acid residues and N-terminal to proline residues upon collisional activation, resulting in fewer, more abundant fragment ions, when compared to conventional top-down protocols where complete sequence coverage is desirable. Using a 27-residue polypeptide represented schematically in Figure 5.1 as an example, cleavage at every residue would result in a minimum of 26 fragments ions, inherently dispersing the precursor ion intensity across 26 different fragmentation channels. Realistically, the resulting tandem mass spectrum will likely contain more than 26 fragment ions as both complementary fragments from a single cleavage often appear in the spectrum, as do products from small molecule losses, amino acid side chain losses, and from multiple backbone cleavages (i.e., internal fragment ions). As an alternative to complete sequence coverage, one could manipulate the protein charge state distribution to produce abundant aspartic acid cleavages. As shown in Figure 5.1, cleavage at aspartic acid residues, as represented by the red amino acids, generates six fragment ions. Consequently, the precursor ion intensity is divided into only six fragments of higher abundance. In principle, this approach can lead to an extension of the lower limit of the dynamic range for top-down protein analysis.

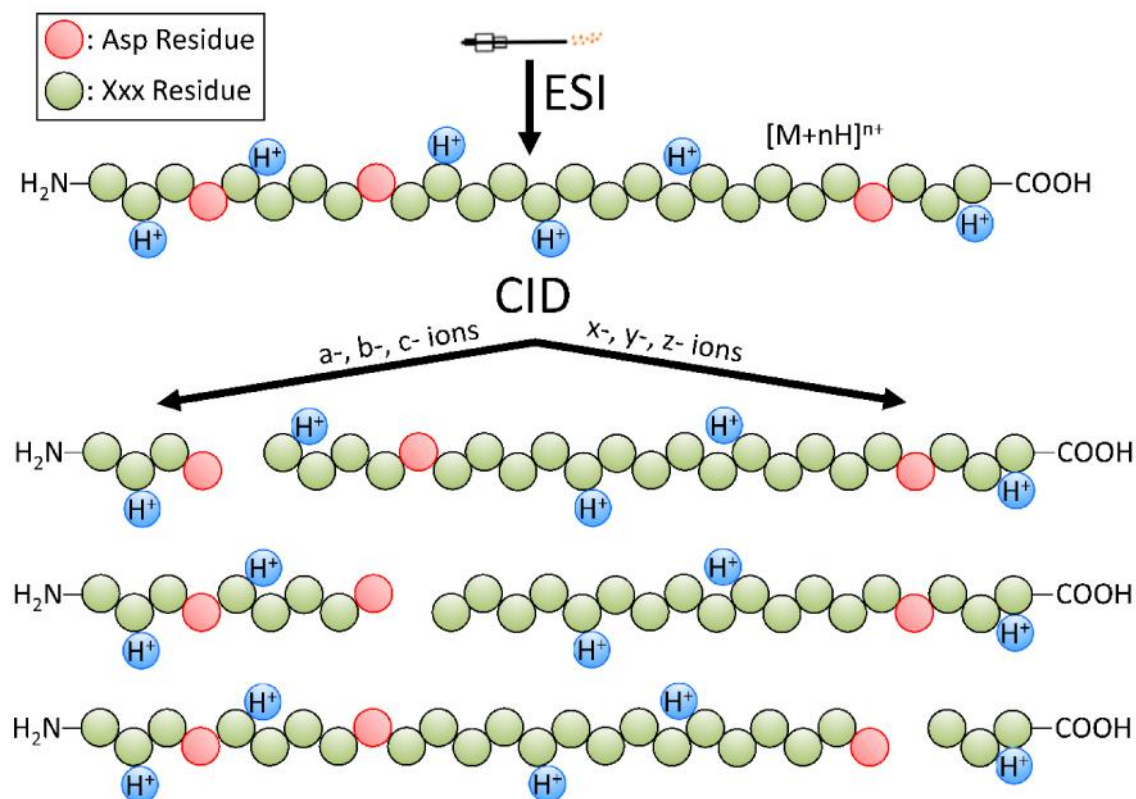


Figure 5.1. Illustration of selective cleavages upon collisional activation.

The influence of precursor ion charge state on the gas-phase fragmentation behavior of multiply charged proteins is illustrated by ubiquitin (Figure 5.2). The ion trap CID product ion spectra of $[M + 8H]^{8+}$, $[M + 7H]^{7+}$, $[M + 6H]^{6+}$, and $[M + 5H]^{5+}$ precursor ions show drastic differences in both fragment ion identities and abundances. At intermediate charge states, as shown in Figure 5.2a, b, extensive nonspecific cleavage was observed. For lower charge states, fragmentation at aspartic acid residues becomes more prominent. Activation of the $[M + 6H]^{6+}$ ion, the spectrum of which is shown in Figure 5.2c, shows a base peak corresponding to the doubly charged y_{18} fragment (aspartic acid channel), and activation of the $[M + 5H]^{5+}$ ion (Figure 5.2d) produces almost exclusively cleavages at aspartic acid residues. These results are consistent with fragmentation characterization studies of ubiquitin and are consistent with the mobile proton model for peptide and protein dissociation.^{26,32} For ubiquitin, a small protein containing four arginine residues, the number of ionizing protons for the $[M + 6H]^{6+}$ and $[M + 5H]^{5+}$ ions begins to approach the number of arginine residues. The arginine residues, which have the highest gas-phase basicity of any amino acid,^{54,55} sequester the protons allowing for processes that do not

require proton mobilization (e.g., cleavage at aspartic acid residues and small molecule loss) to dominate the spectrum. These processes are also observed for the $[M + 4H]^{4+}$ precursor ions, where the number of ionizing protons is equal to the number of arginine residues. The ion trap CID spectrum, as shown in Figure 5.3, shows a dominant water loss as well as cleavages C-terminal to aspartic acid residues.

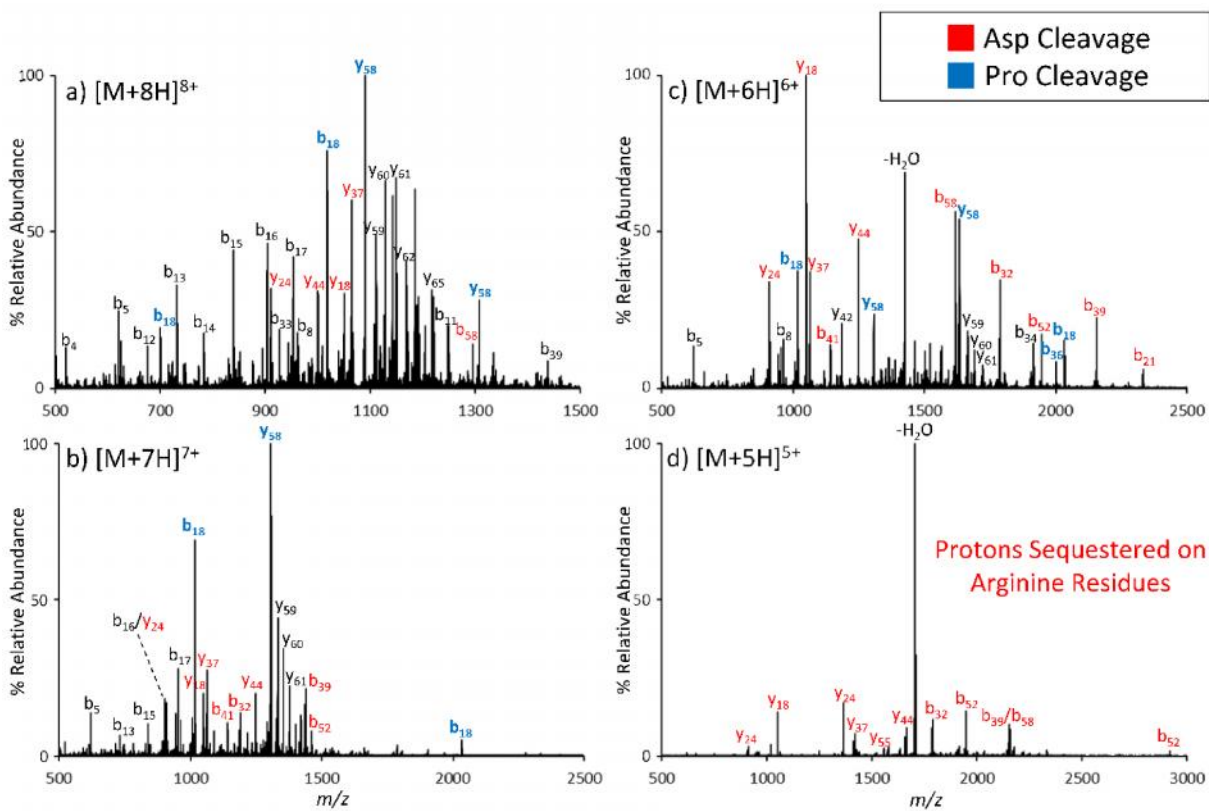


Figure 5.2. Ion trap CID spectrum of ubiquitin for a) $[M + 8H]^{8+}$, b) $[M + 7H]^{7+}$, c) $[M + 6H]^{6+}$, and d) $[M + 5H]^{5+}$ precursor ions. Cleavages C-terminal to aspartic acid residues are labeled in red, cleavages N-terminal to proline residues are labeled in blue, and non-specific cleavages are labeled in black.

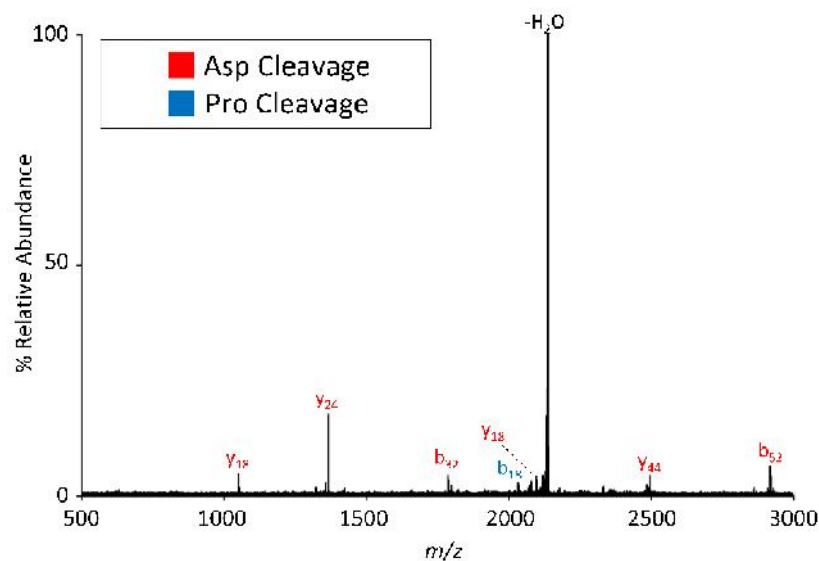


Figure 5.3. Ion trap CID spectrum of ubiquitin $[M + 4H]^{4+}$. Cleavages C-terminal to aspartic acid residues are labeled in red, cleavages N-terminal to proline residues are labeled in blue, and non-specific cleavages are labeled in black.

Based on the assumption that proton mobility in protein ions is inhibited when the number of excess protons is roughly equal to the number of arginine residues in the protein, we sought to determine the m/z range within which most protein ions with limited proton mobility are likely to fall. A program written in MATLAB was used to count the number of arginine residues and calculate the mass of each protein 250,000 Da in the SWISS-PROT database. Linear regression of mass versus arginine count was used to predict the number of arginine residues for each entry (Figure 5.4a). Next, the true count, the actual number of arginine residues present in the protein sequence, was compared to the predicted count, the number of arginine residues predicted by the linear model. For any sequence ± 3 arginine residues to the true count, seven mass-to-charge ratios were generated from $[M + n_{(PR-3)}H]^{n+}$ to $[M + n_{(PR+3)}H]^{n+}$, where PR is the number of predicted arginine residues. Inspection of the histogram plot of these mass-to-charge ratios provided in Figure 5.4b reveals that greater than 75% of the charge states fall between m/z 1500 and m/z 2500.

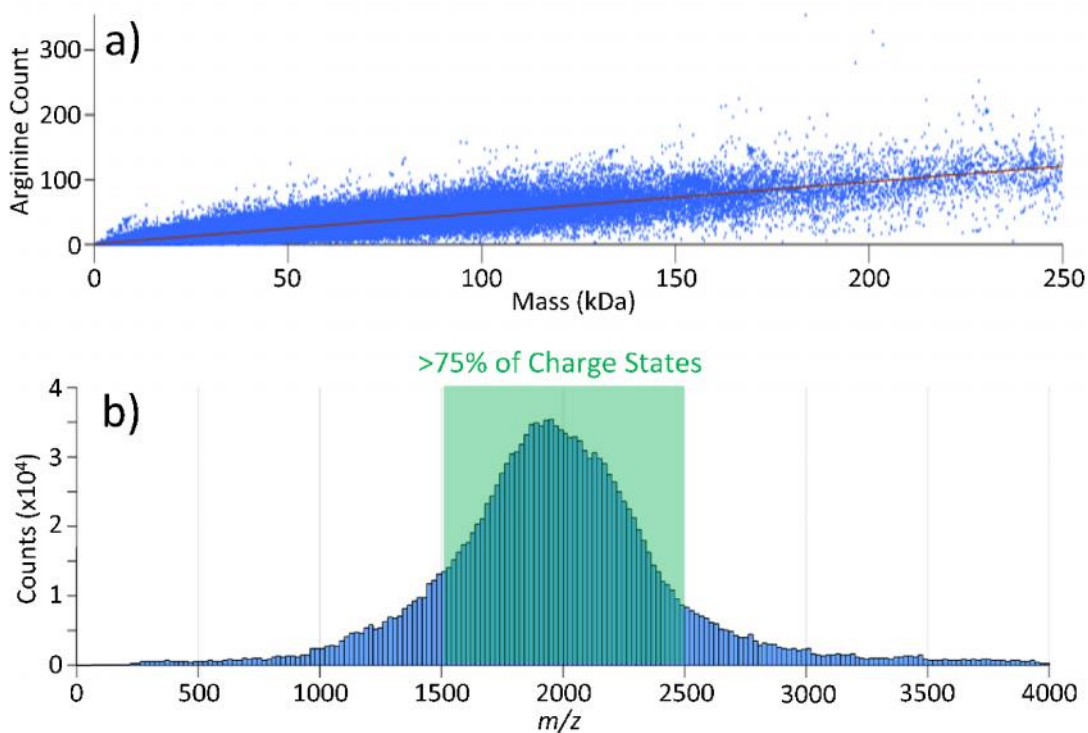


Figure 5.4. a) Scatter plot of arginine count versus protein mass. b) Histogram of mass-to-charge ratios calculated using ± 3 the predicted number of arginine residues.

5.3.2 Protocol Demonstration Using Reduced and Alkylated Trypsinogen

Positive nESI of the reduced and alkylated trypsinogen sample under acidic denaturing conditions generates a broad and bi-modal distribution of charge states (Figure 5.5a) with the highest and lowest observable charge states being the $[M + 33H]^{33+}$ and $[M + 9H]^{9+}$ species, respectively. Much of the protein signal at the highest charge states was concentrated into a single lower charge state, $[M + 17H]^{17+}$, via a series of q0 transmission mode proton transfer ion/ion reactions and ion parking (Figure 5.5c). Signal enhancement is evidenced by the ion abundance of the $[M + 17H]^{17+}$ species (compare Figure 5.5c to Figure 5.5a, b). Figure 5.5b demonstrates that there is no signal enhancement in the absence of ion parking, as no auxiliary excitation voltage is applied to inhibit the ion/ion reaction of the $[M + 17H]^{17+}$ species in that experiment.

The concentrated $[M + 17H]^{17+}$ ion was isolated in Q1 (Figure 5.5d) and transferred to q2 where it was subjected to a second set of proton transfer ion/ion reactions. Reaction conditions were tuned such that the reduced charge states fell largely into the m/z 1500–2500 window. This region is highlighted in green in Figure 5.5e. Two high amplitude frequency sweeps were applied

to q2, one using a frequency to eject ions lower in m/z than 1500, and one using a frequency to eject ions higher in m/z than 2500. The resulting spectrum is shown in Figure 5.5e.

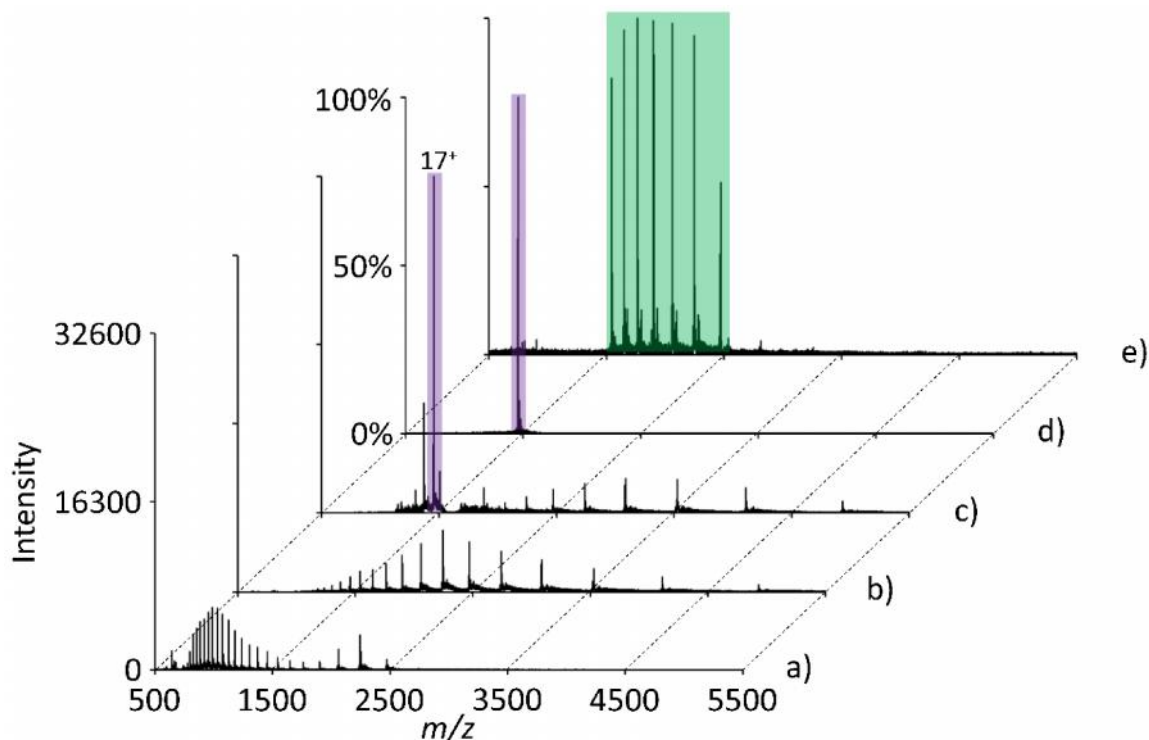


Figure 5.5. a) Nano-electrospray mass spectrum of reduced and alkylated trypsinogen. b) Post ion/ion spectrum from reaction of a with PFO dimer. c) q0 ion parking of the $[M + 17H]^{17+}$ ion under the same reaction conditions as b. d) Q1 isolation of c). e) Post ion/ion spectrum and isolation of m/z 1500 to m/z 2500 from the reaction of d) with PFO dimer. ^aa, b, and c are plotted on the same absolute intensity scale while ^bd and e are plotted on a scale of percent relative abundance.

In the case of reduced and alkylated trypsinogen, m/z 1500 to m/z 2500 contains seven charge states, ranging from the $[M + 16H]^{16+}$ ion to the $[M + 10H]^{10+}$ ion. These charge states were subjected to broadband DDC collisional activation, maximizing the chances of observing the preferential cleavage at aspartic acid and proline residues. The MS/MS spectrum is provided in Figure 5.6. Only b- and y-type fragment ions, matched within a ± 15 ppm tolerance, are labeled. As summarized in Table 5.1, a total of 12 fragments were identified, 6 coinciding with selective fragmentation, 3 at aspartic acid, and 3 at proline. Visually, it is evident proline fragment ions are among the most abundant peaks in the spectrum.

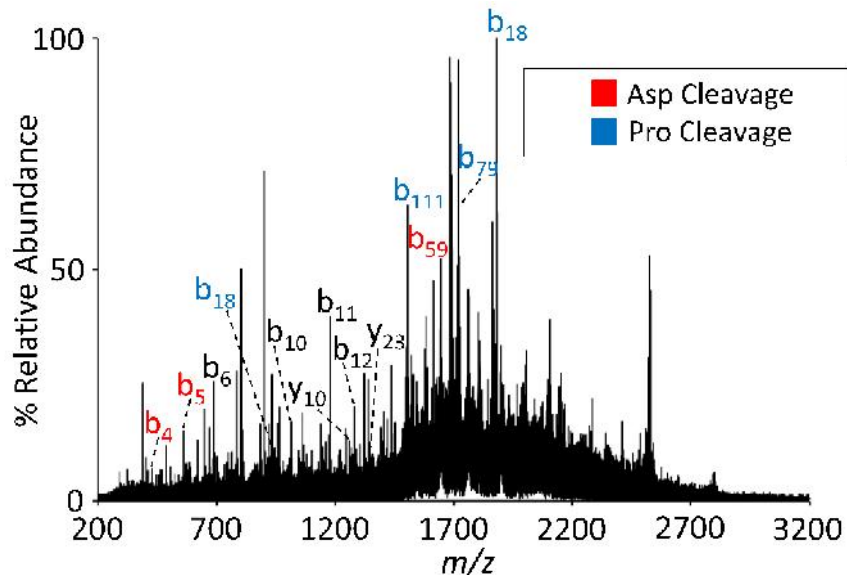


Figure 5.6. Simultaneous activation of the $[M + 16H]^{16+}$ to $[M + 10H]^{10+}$ charge states of reduced and alkylated trypsinogen via DDC collisional activation. Only peaks matched to ± 15 ppm of theoretical b- and y-fragment ions are labeled.

Table 5.1. Summary of Database Search Results.

Observed Mass (Monoisotopic)	8559.72
Theoretical Mass (Monoisotopic)	8559.62
Mass Difference (ppm)	12.08
Identity	Ubiquitin
Species	Various
Sequence	MQIFVKTLTGKTITLEVEPSDTIENVKAKIQDKEGIP PDQQRLLIFAGKQLEDGRTLSDYNIQKESTLHLVLR RGG
Matches	22 of 100 (22 of 100) ^a
McLuckey Score	100719.97 (76750.99) ^b
P-Score	3.8e-29 (3.8e-29) ^c
Matched Fragments	b ₇ , b ₈ , b ₉ , b ₁₁ , b ₁₃ , b ₁₆ , b ₁₈ , b ₂₁ , b ₃₂ , b ₃₆ , b ₃₉ , b ₅₂ , y ₉ , y ₁₂ , y ₁₃ , y ₁₆ , y ₁₈ , y ₂₄ , y ₂₅ , y ₃₇ , y ₅₅
Observed Mass (Monoisotopic)	16941.02
Theoretical Mass (Monoisotopic)	16940.96
Mass Difference (ppm)	3.27
Identity	Myoglobin
Species	Equus caballus (Horse)

Table 5.1 Continued

Sequence	GLSDGEWQQVLNVWGKVEADIAGHGQEVLRIRLFT GHPETLEKFDKFKHLKTEAEMKASEDLKKHGTVVV TALGGILKKKGHHEAELKPLAQSHATKHKIPIKYLE FISDAIHVLHSHKHPGDFGADAQGAMTKALELFRND IAAKYKELGFQG
Matches	24 of 45 (11 of 45) ^a
McLucky Score	36787.9 (5729.11) ^b
P-Score	6.1e-34 (9.9e-13) ^c
Matched Fragments	b ₂₀ , b ₄₁ , b ₄₄ , b ₄₇ , b ₆₃ , b ₇₈ , b ₇₉ , b ₉₆ , b ₁₁₈ , b ₁₂₂ , y ₇ , y ₈ , y ₉ , y ₁₀ , y ₁₁ , y ₁₂ , y ₁₃ , y ₂₇ , y ₃₁ , y ₃₄ , y ₄₄ , y ₇₄ , y ₉₀
Observed Mass (Monoisotopic)	24662.18
Theoretical Mass (Monoisotopic)	24661.82
Mass Difference (ppm)	14.43
Identity	Trypsinogen
Species	Bos taurus (Bovine)
Sequence	VDDDDKIVGGYTCGANTVPYQVSLNSGYHFCGGS LINSQWVVSAAHCYKSGIQVRLGEDNINVVEGNEQ FISASKSIVHPSYNSNTLNNDIMLIKLSAASLNSRV ASISLPTSCASAGTQCLISGWGNTKSSGTSYPDVLK CLKAPILSDSSCKSAYPGQITSNMFCAGYLEGGKDS CQGDSGGPVVCSGKLGQIVSWGSGCAQKNKPGVY TKVCNYVSWIKQTIASN
Matches	12 of 143 (2 of 143) ^a
McLucky Score	129384.11 (12828.84) ^b
P-Score	3.7e-10 (0.24) ^c
Matched Fragments	b ₄ , b ₅ , b ₆ , b ₁₀ , b ₁₁ , b ₁₂ , b ₁₈ , b ₅₉ , b ₇₉ , b ₁₁₁ , y ₁₀ , y ₂₃
Observed Mass (Average)	29024.55
Theoretical Mass (Average)	29024.63
Mass Difference (ppm)	-2.83
Identity	Carbonic anhydrase 2
Species	Bos taurus (Bovine)
Sequence	Ac-SHHWGYGKHNGPEHWHKDFPIANGERQSPVD IDTKAVVQDPALKPLALVYGEATSRRMVNNHGSFN VEYDDSQDKAVLKDGPLTGTYRLVQFHFHWGSSD DQGSEHTVDRKKYAAELHLVHWNTKYGDFGTAA QQPDGLAVVGVFLKVGDNALQKVLDAALDSIKT KGKSTDFPNFDPGSLLPNVLDYWYTPGSLTTPPLLE SVTWIVLKEPISVSSQQMLKFRTLNFNAEGPELLM LANWRPAQPLKNRQVRGFPK

Table 5.1 Continued

Matches	21 of 69 (2 of 69) ^a
McLucky Score	183239.01 (12439.74) ^b
P-Score	1.6e-28 (0.047) ^c
Matched Fragments	b ₃ , b ₆ , b ₈ , b ₁₇ , b ₁₈ , b ₃₁ , b ₃₃ , b ₃₈ , b ₄₀ , b ₄₀ , b ₇₀ , y ₁₇ , y ₂₇ , y ₄₇ , y ₄₈ , y ₆₁ , y ₆₂ , y ₆₃ , y ₆₄ , y ₆₇ , y ₆₈

5.3.3 Identification of Model Proteins

For each protein, database searching was initiated by retrieval of all proteins within the user-defined precursor tolerance. In all cases, this tolerance was set to ± 100 Da of the experimentally derived precursor mass, obtained from deconvolution based on Bayesian statistics within the PeakView Software (SCIEX, Concord, ON, Canada). Theoretical b- and y-fragment zero-charge masses were calculated for each protein in the retrieved list and compared to the experimental zero-charge masses. Proteins were ranked according to their McLucky Score.

In the case of ubiquitin, 2350 proteins were retrieved and scored in the database search. The top 153 scores were identical and, upon inspection, all 153 were correctly identified as ubiquitin. This is an artifact of the database creation as there are several parent proteins, across all species, in the SWISS-PROT database containing ubiquitin chains. Of the 100 fragment masses obtained by the THRASH deconvolution algorithm, 22 corresponded to b- and y-fragments of ubiquitin. The results of the top scoring protein are summarized in Table 5.1. By concentrating the precursor signal via proton transfer ion/ion reaction in conjunction with ion parking, and moving the charge state distribution to a region which maximizes selective cleavages, we observed greater than 90% of the matched fragment ion signal corresponding to cleavage at aspartic acid and proline residues. Specifically, 86.4% of the total matched fragment area was contained in seven unique aspartic acid fragments and 5.5% was contained in two proline fragment ions (Figure 5.7).

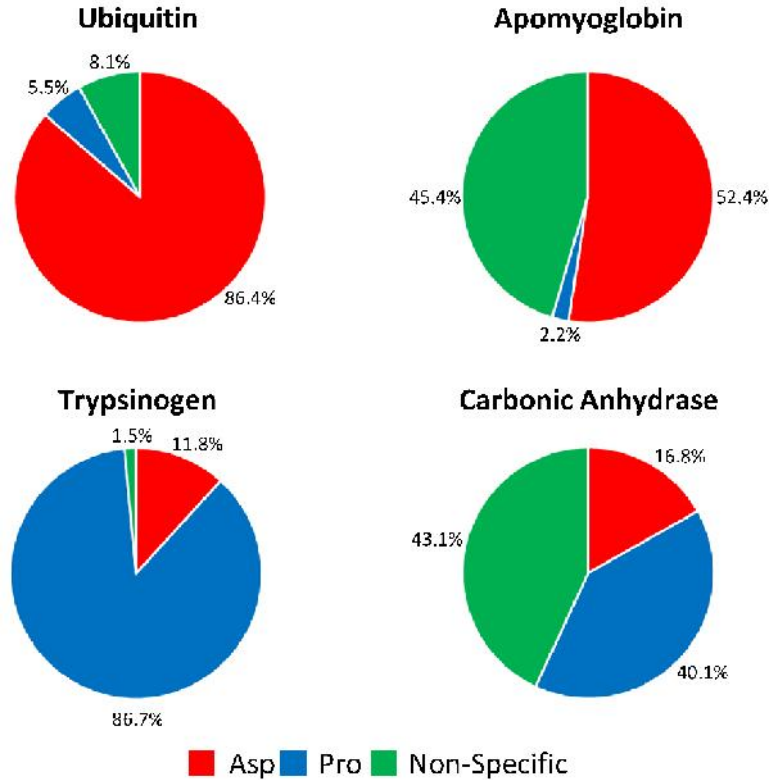


Figure 5.7. Percentage of the total matched fragment area for (red) cleavages C-terminal to aspartic acid residues, (blue) cleavages N-terminal to proline residues, or (green) nonspecific cleavages.

ProSight Lite was used to calculate a P-Score for each of the top five ranked proteins.⁵⁶ While the output of the database search ranked according to the McLuckey Score does not necessarily coincide with ranking based on P-Score, in the case of ubiquitin, the top five unique protein sequences based on P-Score were identical to the top five unique protein sequences ranked according to their McLuckey Score. As shown in Table 5.1 and Table 5.2, the top two ranked proteins each matched 22 fragment masses of the 100 experimental fragment masses, resulting in equivalent P-Scores.⁵⁷ In our approach, three specific aspartic acid fragments, b₅₂, y₃₇, and y₅₅, provided sufficient information to distinguish between ubiquitin and ubiquitin-related proteins (Table 5.3). These results demonstrate the utility of using a scoring system that is weighted both by abundance and cleavage site as the conventional approach was unable to distinguish between ubiquitin and the ubiquitin-related protein.

Table 5.2. Summary of the Top Five Proteins Ranked According to P-Score for Ubiquitin MS/MS Data.

Identity	Species	P-Score	Matches
1 Ubiquitin	Various	3.8e-29	22 of 100
2 Ubiquitin-related	Various	3.8e-29	22 of 100
3 Ubiquitin-related	Equus caballus (Horse)	3.3e-24	19 of 100
4 Ubiquitin-related 1	Cricetulus griseus (Chinese hamster)	1.3e-22	18 of 100
5 Ubiquitin-related 1	Dictyostelium discoideum (Slime mold)	5.2e-21	17 of 100

For apomyoglobin, the database search returned 2446 results. The highest scoring protein was correctly identified as myoglobin from *Equus caballus*, while the second and third scoring proteins, as shown in supplementary Table 5.4, were found to be myoglobin from different species. Here, greater than 50% of the matched fragment area is comprised of seven aspartic acid fragments (Figure 5.7). While equine myoglobin contains only two arginine residues, there are 19 lysine residues and 11 histidine residues in addition to the N-terminus, for a total of 33 nominal basic sites. When the charge state distribution is moved to the m/z 1500 to m/z 2500 region, $[M + 11H]^{11+}$ to $[M + 7H]^{7+}$, the ionizing protons may well be solvated by multiple basic residues, thereby reducing the proton mobility and thereby allowing for prominent cleavage at the aspartic acid residues

Table 5.3. Summary of the top five ranked proteins of the ubiquitin MS/MS database search.

	Identity	Species	Theoretical Mass (Monoisotopic)	Mass Difference (ppm)	Score	Matches
1	Ubiquitin	Various	8559.62	12.08	100719.97	22 of 100
2	Ubiquitin-related	Various	8559.62	12.08	76750.99	22 of 100
3	Ubiquitin-related	Equus caballus (Horse)	8593.60	-3942.5	52363.35	19 of 100
4	Ubiquitin-related 1	Cricetulus griseus (Chinese hamster)	8558.63	127.06	47774.16	18 of 100
5	Ubiquitin-related 1	Dictyostelium discoideum (Slime mold)	8562.59	-335.31	32432.08	17 of 100

Table 5.4. Summary of the top five ranked proteins of the apomyoglobin MS/MS database search.

	Identity	Species	Theoretical Mass (Monoisotopic)	Mass Difference (ppm)	Score	Matches
1	Myoglobin	Equus caballus (Horse)	16940.96	3.27	36787.9	24 of 45
2	Myoglobin	Lagostomus maximus (Plains viscacha)	16868.93	4273.5	5729.11	11 of 45
3	Myoglobin	Tupaia glis (Tree shrew)	16959.97	-940.58	5729.11	11 of 45
4	50S ribosomal protein L15	Methanopyrus kandleri	17030.04	-5227.2	3851.36	1 of 45
5	Lipopolysaccharide-induced tumor necrosis factor-alpha factor homolog	Mus musculus (Mouse)	16934.06	410.81	912.79	3 of 45

Like equine myoglobin, trypsinogen is another protein containing only two arginine residues. The database search, which included carbamidomethylation (+ 57.0198 Da) of cysteine residues, successfully identified trypsinogen, matching only 12 fragment masses (Table 5.5). Despite the lowest number of matched fragments, there remains a factor 10 difference in the score between trypsinogen and the second ranking protein (Table 5.1). Unlike apomyoglobin, where the majority of information was comprised of aspartic acid fragment ions, activation of trypsinogen resulted in cleavage at three proline residues, accounting for 86.7% of the matched fragment area (Figure 5.7). The differences between the two systems arise from the total number of basic residues. Trypsinogen contains only 20 basic residues compared to myoglobin's 32. As previously stated, the m/z region subjected to DDC excitation for trypsinogen contains the $[M + 16H]^{16+}$ to $[M + 10H]^{10+}$ charge states. While some protons may be solvated by two basic residues, a sufficient number of mobile protons remain to initiate cleavage at proline residues.

Lastly, two database searches for carbonic anhydrase were performed. The first search was performed with no N-terminal modifications while the second accounted for N-terminal acetylation (+ 42.0095 Da). The results of the former are summarized in supplementary Table 5.6. As shown in Table 5.6, the top two proteins exhibit the same score and the same number of matched fragments. The two sequences were identified as bovine carbonic anhydrase II, where the sequences differ only by the cleavage of the initiator methionine residue. In both cases, the 10 matched fragments were identical (y-type fragments). It was observed that the experimentally derived average mass of the precursor was 89 Da lower in mass than carbonic anhydrase with the N-terminal methionine, whereas the average mass of the precursor was 42 Da greater in mass than the sequence lacking the initiator methionine.

Table 5.5. Summary of the top five ranked proteins of the trypsinogen MS/MS database search.

	Identity	Species	Theoretical Mass (Monoisotopic)	Mass Difference (ppm)	Score	Matches
1	Trypsinogen	Bos taurus (Bovine)	24661.82	14.43	129384.11	12 of 143
2	Vesicle-associated protein 2-1	Arabidopsis thaliana (Mouse-ear cress)	24707.83	-1847.6	12828.84	2 of 143
3	Deoxyribose-phosphate aldolase	Aeropyrum pernix	24628.30	1375.7	9525.58	1 of 143
4	Elongation factor 1-delta	Beta vulgaris (Sugar beet)	24587.33	3044.3	9525.58	1 of 143
5	Interleukin-37	Homo sapiens (Human)	24566.99	3874.7	9525.58	1 of 143

Table 5.6. Summary of the top five ranked proteins for carbonic anhydrase without N-terminal acetylation.

	Identity	Species	Theoretical Mass (Monoisotopic)	Mass Difference (ppm)	Score	Matches
1	Carbonic anhydrase 2 (with methionine)	Bos taurus (Bovine)	29113.78	-3064.9	108768.64	10 of 69
2	Carbonic anhydrase 2 (without methionine)	Bos taurus (Bovine)	28982.59	1447.8	108768.64	10 of 69
3	2,3,4,5-tetrahydropyridine-2,6-dicarboxylate N-succinyltransferase	Aeropyrum pernix	29108.13	-2871.4	16713.59	3 of 69
4	Uncharacterized protein UL10	Beta vulgaris (Sugar beet)	29023.47	37.2	15790.58	2 of 69
5	4-hydroxy-tetrahydrodipicolinate reductase	Homo sapiens (Human)	28955.85	2372.6	10481.54	2 of 69

While it is possible to deduce the correct sequence based on mass, a second search was performed with N-terminal acetylation. Here, the top scoring protein was, again, correctly identified as carbonic anhydrase II lacking the initiator methionine with N-terminal acetylation. Note that the results of the top five proteins, as shown in Table 5.7, do not include carbonic anhydrase II with the initiator methionine since addition of the N-terminal modification puts this sequence outside of the ± 100 -Da retrieval window. When comparing the two searches, N-terminal acetylation matched 11 additional fragments (b-type fragments), for a total of 21 matched fragments (Table 5.1). Despite being the largest protein examined in this study, selective cleavages are still observed, with 56.9% of the total matched fragment area held in aspartic acid and proline cleavages (Figure 5.7).

Table 5.7. Summary of the top five ranked proteins for carbonic anhydrase with N-terminal acetylation.

	Identity	Species	Theoretical Mass (Monoisotopic)	Mass Difference (ppm)	Score	Matches
1	Carbonic anhydrase 2	Bos taurus (Bovine)	29024.63	-2.83	183239.01	21 of 69
2	4-hydroxy- tetrahydrodipicolinate reductase	Methanococcus vannielii	29028.36	-131.12	12439.74	2 of 69
3	4-hydroxy- tetrahydrodipicolinate reductase	Synechococcus sp.	28997.89	919.45	10481.54	2 of 69
4	Uncharacterized protein UL10	Human cytomegalovirus	29065.51	-1409.2	10481.54	2 of 69
5	ATP synthase subunit a	Pseudarthrobacter chlorophenicus	29008.84	541.41	10236.76	2 of 69

5.4 Conclusions

Proof-of-concept is presented here for a protein top-down tandem mass spectrometry methodology that exploits the advantages of ionization under denaturing conditions while also maximizing the likelihood for selective cleavages at aspartic acid and proline residues. The generation of precursor ions under denaturing conditions and the relatively short reaction times are amenable to an online LC-MS workflow, though demonstration of an online LC-MS workflow was outside the scope of the present work. Ion/ion reactions are used both to concentrate ions of interest into a single charge state for ion isolation and to generate subsequently precursor ions within a mass-to-charge range most likely to yield selective cleavages under collisional activation conditions. The objective is to generate sufficient fragmentation for identification while concentrating product ion signals into a relatively limited number of channels. This approach is not intended to compete with strategies that maximize the number of backbone cleavages for characterization purposes. Rather, it is a complementary approach that is effective in protein identification that offers advantages in dynamic range and quantitation via single- or multiple-reaction monitoring due to the fact that product ion signal is not distributed among a large number of product channels.

Broadband collisional activation using DDC of precursor ions within the targeted m/z window for all proteins studied here resulted in greater than 50% of the total matched fragment area arising from aspartic acid and proline cleavages (up to 91.9% for ubiquitin). While the conventional scoring system based on matching predicted and observed product masses can be used with this approach yielding respectable P-Scores, a scoring system that weights most heavily C-terminal aspartic acid and N-terminal proline cleavages can add discriminatory power to an approach like this that is intended to maximize such cleavages. The combination of the ion processing workflow described here with an abundance-weighted scoring system lead to the successful identification of four model proteins, ranging in mass from 8.5 to 29.0 kDa. In the case of trypsinogen, successful identification was achieved with only 12 matched fragments (3 aspartic acid, 3 proline, and 6 non-specific cleavages), demonstrating the utility of maximizing selective fragmentation pathways. Interestingly, two of the selected model proteins contain an unusually low number of arginine residues. Nevertheless, selective cleavage at either proline or aspartic acid residues was noted. In addition to the application of intact protein identification, it stands to reason this workflow may be useful in multiple-reaction monitoring, particularly of low level proteins.

5.5 References

1. Loo, J., Edmonds, C., Smith, R.: Primary Sequence Information from Intact Proteins by Electrospray Ionization Tandem Mass Spectrometry. *Science*. **1990**, 248, 201-204.
2. Schaffer, L.V., Shortreed, M.R., Cesnik, A.J., Frey, B.L., Solntsev, S.K., Scalf, M., Smith, L.M.: Expanding Proteoform Identifications in Top-Down Proteomic Analyses by Constructing Proteoform Families. *Anal. Chem.* **2018**, 90, 1325-1333.
3. Khan, A., Eikani, C.K., Khan, H., Iavarone, A.T., Pesavento, J.J.: Characterization of *Chlamydomonas reinhardtii* Core Histones by Top-Down Mass Spectrometry Reveals Unique Algae-Specific Variants and Post-Translational Modifications. *J. Proteome Res.* **2018**, 17, 23-32.
4. Lubeckyj, R.A., McCool, E.N., Shen, X., Kou, Q., Liu, X., Sun, L.: Single-Shot Top-Down Proteomics with Capillary Zone Electrophoresis-Electrospray Ionization-Tandem Mass Spectrometry for Identification of Nearly 600 Escherichia coli Proteoforms. *Anal. Chem.* **2017**, 89, 12059-12067.
5. Cai, W., Tucholski, T., Chen, B., Alpert, A.J., McIlwain, S., Kohmoto, T., Jin, S., Ge, Y.: Top-Down Proteomics of Large Proteins up to 223 kDa Enabled by Serial Size Exclusion Chromatography Strategy. *Anal. Chem.* **2017**, 89, 5467-5475.
6. Kilpatrick, L.E., Kilpatrick, E.L.: Optimizing High-Resolution Mass Spectrometry for the Identification of Low-Abundance Post-Translational Modifications of Intact Proteins. *J. Proteome Res.* **2017**, 16, 3255-3265.
7. Zubarev, R.A., Kelleher, N.L., McLafferty, F.W.: Electron Capture Dissociation of Multiply Charged Protein Cations. A Nonergodic Process. *J. Am. Chem. Soc.* **1998**, 120, 3265-3266.
8. Syka, J.E.P., Coon, J.J., Schroeder, M.J., Shabanowitz, J., Hunt, D.F.: Peptide and Protein Sequence Analysis by Electron Transfer Dissociation Mass Spectrometry. *Proc. Natl. Acad. Sci. U.S.A.* **2004**, 101, 9528-9533.
9. Brodbelt, J.S.: Photodissociation Mass Spectrometry: New Tools for Characterization of Biological Molecules. *Chem. Soc. Rev.* **2014**, 43, 2757-2783.
10. Compton, P.D., Zamdborg, L., Thomas, P.M., Kelleher, N.L.: On the Scalability and Requirements of Whole Protein Mass Spectrometry. *Anal. Chem.* **2011**, 83, 6868-6874.
11. Smith, L.M., Kelleher, N.L., The Consortium for Top Down, P.: Proteoform: A Single Term Describing Protein Complexity. *Nature Methods*. **2013**, 10, 186.
12. McCormack, A.L., Somogyi, A., Dongre, A.R., Wysocki, V.H.: Fragmentation of Protonated Peptides: Surface-Induced Dissociation in Conjunction with A Quantum Mechanical Approach. *Anal. Chem.* **1993**, 65, 2859-2872.

13. Dongré, A.R., Somogyi, Á., Wysocki, V.H.: Surface-induced Dissociation: An Effective Tool to Probe Structure, Energetics and Fragmentation Mechanisms of Protonated Peptides. *J. Mass Spectrom.* **1996**, 31, 339-350.
14. Paizs, B., Suhai, S.: Fragmentation Pathways of Protonated Peptides. *Mass Spectrom. Rev.* **2005**, 24, 508-548.
15. Paizs, B., Suhai, S.: Towards Understanding the Tandem Mass Spectra of Protonated Oligopeptides. 1: Mechanism of Amide Bond Cleavage. *J. Am. Soc. Mass. Spectrom.* **2004**, 15, 103-113.
16. Yu, W., Vath, J.E., Huberty, M.C., Martin, S.A.: Identification of the Facile Gas-Phase Cleavage of the Asp-Pro and Asp-Xxx Peptide Bonds in Matrix-Assisted Laser Desorption Time-Of-Flight Mass Spectrometry. *Anal. Chem.* **1993**, 65, 3015-3023.
17. Kish, M.M., Wesdemiotis, C.: Selective Cleavage at Internal Lysine Residues in Protonated vs. Metalated Peptides. *Int. J. Mass Spectrom.* **2003**, 227, 191-203.
18. Gehrig, P.M., Roschitzki, B., Rutishauser, D., Reiland, S., Schlapbach, R.: Phosphorylated Serine and Threonine Residues Promote Site-Specific Fragmentation of Singly Charged, Arginine-Containing Peptide Ions. *Rapid Commun. Mass Spectrom.* **2009**, 23, 1435-1445.
19. Bleiholder, C., Suhai, S., Harrison, A.G., Paizs, B.: Towards Understanding the Tandem Mass Spectra of Protonated Oligopeptides. 2: The Proline Effect in Collision-Induced Dissociation of Protonated Ala-Ala-Xxx-Pro-Ala (Xxx = Ala, Ser, Leu, Val, Phe, and Trp). *J. Am. Soc. Mass. Spectrom.* **2011**, 22, 1032-1039.
20. McGee, W.M., McLuckey, S.A.: The Ornithine Effect in Peptide Cation Dissociation. *J. Mass Spectrom.* **2013**, 48, 856-861.
21. Schwartz, B.L., Bursey, M.M.: Some Proline Substituent Effects in the Tandem Mass Spectrum of Protonated Pentaalanine. *Biol. Mass Spectrom.* **1992**, 21, 92-96.
22. Vaisar, T., Urban, J.: Probing Proline Effect in CID of Protonated Peptides. *J. Mass Spectrom.* **1996**, 31, 1185-1187.
23. Tsaprailis, G., Somogyi, Á., Nikolaev, E.N., Wysocki, V.H.: Refining the Model for Selective Cleavage at Acidic Residues in Arginine-Containing Protonated Peptides. *Int. J. Mass Spectrom.* **2000**, 195-196, 467-479.
24. Sullivan, A.G., Brancia, F.L., Tyldesley, R., Bateman, R., Sidhu, K., Hubbard, S.J., Oliver, S.G., Gaskell, S.J.: The Exploitation of Selective Cleavage of Singly Protonated Peptide Ions Adjacent to Aspartic Acid Residues using a Quadrupole Orthogonal Time-Of-Flight Mass Spectrometer Equipped with a Matrix-Assisted Laser Desorption/Ionization Source. *Int. J. Mass Spectrom.* **2001**, 210-211, 665-676.

25. Gu, C., Tsaprailis, G., Brechi, L., Wysocki, V.H.: Selective Gas-Phase Cleavage at the Peptide Bond C-Terminal to Aspartic Acid in Fixed-Charge Derivatives of Asp-Containing Peptides. *Anal. Chem.* **2000**, 72, 5804-5813.
26. Reid, G.E., Wu, J., Chrisman, P.A., Wells, J.M., McLuckey, S.A.: Charge-State-Dependent Sequence Analysis of Protonated Ubiquitin Ions via Ion Trap Tandem Mass Spectrometry. *Anal. Chem.* **2001**, 73, 3274-3281.
27. Newton, K.A., Chrisman, P.A., Reid, G.E., Wells, J.M., McLuckey, S.A.: Gaseous Apomyoglobin Ion Dissociation in a Quadrupole Ion Trap: $[M + 2H]^{2+}$ - $[M + 21H]^{21+}$. *Int. J. Mass Spectrom.* **2001**, 212, 359-376.
28. Engel, B.J., Pan, P., Reid, G.E., Wells, J.M., McLuckey, S.A.: Charge State Dependent Fragmentation of Gaseous Protein Ions in a Quadrupole Ion Trap: Bovine Ferri-, Ferro-, and Apo-Cytochrome *c*. *Int. J. Mass Spectrom.* **2002**, 219, 171-187.
29. Hogan, J.M., McLuckey, S.A.: Charge State Dependent Collision-Induced Dissociation of Native and Reduced Porcine Elastase. *J. Mass Spectrom.* **2003**, 38, 245-256.
30. Huang, Y., Triscari, J.M., Tseng, G.C., Pasa-Tolic, L., Lipton, M.S., Smith, R.D., Wysocki, V.H.: Statistical Characterization of the Charge State and Residue Dependence of Low-Energy CID Peptide Dissociation Patterns. *Anal. Chem.* **2005**, 77, 5800-5813.
31. Huang, Y., Tseng, G.C., Yuan, S., Pasa-Tolic, L., Lipton, M.S., Smith, R.D., Wysocki, V.H.: A Data-Mining Scheme for Identifying Peptide Structural Motifs Responsible for Different MS/MS Fragmentation Intensity Patterns. *J. Proteome Res.* **2008**, 7, 70-79.
32. Cobb, J.S., Easterling, M.L., Agar, J.N.: Structural Characterization of Intact Proteins is Enhanced by Prevalent Fragmentation Pathways Rarely Observed for Peptides. *J. Am. Soc. Mass. Spectrom.* **2010**, 21, 949-959.
33. Newton, K.A., Pitteri, S.J., Laskowski, M., McLuckey, S.A.: Effects of Single Amino Acid Substitution on the Collision-Induced Dissociation of Intact Protein Ions: Turkey Ovomuroid Third Domain. *J. Proteome Res.* **2004**, 3, 1033-1041.
34. Dongré, A.R., Jones, J.L., Somogyi, Á., Wysocki, V.H.: Influence of Peptide Composition, Gas-Phase Basicity, and Chemical Modification on Fragmentation Efficiency: Evidence for the Mobile Proton Model. *J. Am. Chem. Soc.* **1996**, 118, 8365-8374.
35. Loo, J.A., Loo, R.R.O., Udseth, H.R., Edmonds, C.G., Smith, R.D.: Solvent-Induced Conformational Changes of Polypeptides Probed by Electrospray-Ionization Mass Spectrometry. *Rapid Commun. Mass Spectrom.* **1991**, 5, 101-105.

36. Haverland, N.A., Skinner, O.S., Fellers, R.T., Tariq, A.A., Early, B.P., LeDuc, R.D., Fornelli, L., Compton, P.D., Kelleher, N.L.: Defining Gas-Phase Fragmentation Propensities of Intact Proteins During Native Top-Down Mass Spectrometry. *J. Am. Soc. Mass. Spectrom.* **2017**, 28, 1203-1215.
37. Ahadi, E., Konermann, L.: Modeling the Behavior of Coarse-Grained Polymer Chains in Charged Water Droplets: Implications for the Mechanism of Electrospray Ionization. *J. Phys. Chem. B.* **2012**, 116, 104-112.
38. Wang, G., Cole, R.B.: Effect of Solution Ionic Strength on Analyte Charge State Distributions in Positive and Negative Ion Electrospray Mass Spectrometry. *Anal. Chem.* **1994**, 66, 3702-3708.
39. Pan, P., McLuckey, S.A.: Electrospray Ionization of Protein Mixtures at Low pH. *Anal. Chem.* **2003**, 75, 1491-1499.
40. Pan, P., Gunawardena, H.P., Xia, Y., McLuckey, S.A.: Nanoelectrospray Ionization of Protein Mixtures: Solution pH and Protein pI. *Anal. Chem.* **2004**, 76, 1165-1174.
41. Yue, X., Vahidi, S., Konermann, L.: Insights into the Mechanism of Protein Electrospray Ionization from Salt Adduction Measurements. *J. Am. Soc. Mass. Spectrom.* **2014**, 25, 1322-1331.
42. National Resource for Translational and Developmental Proteomics Home Page. <http://nrtdp.northwestern.edu/> (Accessed Mar 3, 2018).
43. Wessel, D., Flügge, U.I.: A Method for the Quantitative Recovery of Protein in Dilute Solution in the Presence of Detergents and Lipids. *Anal. Biochem.* **1984**, 138, 141-143.
44. Xia, Y., Chrisman, P.A., Erickson, D.E., Liu, J., Liang, X., Londry, F.A., Yang, M.J., McLuckey, S.A.: Implementation of Ion/Ion Reactions in a Quadrupole/Time-of-Flight Tandem Mass Spectrometer. *Anal. Chem.* **2006**, 78, 4146-4154.
45. Liang, X., Xia, Y., McLuckey, S.A.: Alternately Pulsed Nanoelectrospray Ionization/Atmospheric Pressure Chemical Ionization for Ion/Ion Reactions in an Electrodynamic Ion Trap. *Anal. Chem.* **2006**, 78, 3208-3212.
46. Liang, X., McLuckey, S.A.: Transmission Mode Ion/Ion Proton Transfer Reactions in a Linear Ion Trap. *J. Am. Soc. Mass. Spectrom.* **2007**, 18, 882-890.
47. Emory, J.F., Hassell, K.H., Londry, F.A., McLuckey, S.A.: Transmission Mode Ion/Ion Reactions in the Radiofrequency-Only Ion Guide of Hybrid Tandem Mass Spectrometers. *Rapid Commun. Mass Spectrom.* **2009**, 23, 409-418.
48. McLuckey, S.A., Reid, G.E., Wells, J.M.: Ion Parking during Ion/Ion Reactions in Electrodynamic Ion Traps. *Anal. Chem.* **2002**, 74, 336-346.

49. Xia, Y., Wu, J., McLuckey, S.A., Londry, F.A., Hager, J.W.: Mutual Storage Mode Ion/Ion Reactions in a Hybrid Linear Ion Trap. *J. Am. Soc. Mass. Spectrom.* **2005**, 16, 71-81.
50. Webb, I.K., Londry, F.A., McLuckey, S.A.: Implementation of Dipolar Direct Current (DDC) Collision-Induced Dissociation in Storage and Transmission Modes on a Quadrupole/Time-Of-Flight Tandem Mass Spectrometer. *Rapid Commun. Mass Spectrom.* **2011**, 25, 2500-2510.
51. Giglione, C., Boularot, A., Meinel, T.: Protein N-Terminal Methionine Excision. *Cell. Mol. Life Sci.* **2004**, 61, 1455-1474.
52. Horn, D.M., Zubarev, R.A., McLafferty, F.W.: Automated Reduction and Interpretation of High Resolution Electrospray Mass Spectra of Large Molecules. *J. Am. Soc. Mass. Spectrom.* **2000**, 11, 320-332.
53. Reid, G.E., Shang, H., Hogan, J.M., Lee, G.U., McLuckey, S.A.: Gas-Phase Concentration, Purification, and Identification of Whole Proteins from Complex Mixtures. *J. Am. Chem. Soc.* **2002**, 124, 7353-7362.
54. Gorman, G.S., Speir, J.P., Turner, C.A., Amster, I.J.: Proton Affinities of the 20 Common Amino Acids. *J. Am. Chem. Soc.* **1992**, 114, 3986-3988.
55. Harrison, A.G.: The Gas-Phase Basicities and Proton Affinities of Amino Acids and Peptides. *Mass Spectrom. Rev.* **1997**, 16, 201-217.
56. Fellers, R.T., Greer, J.B., Early, B.P., Yu, X., LeDuc, R.D., Kelleher, N.L., Thomas, P.M.: ProSight Lite: Graphical Software to Analyze Top-Down Mass Spectrometry Data. *Proteomics.* **2015**, 15, 1235-1238.
57. Meng, F., Cargile, B.J., Miller, L.M., Forbes, A.J., Johnson, J.R., Kelleher, N.L.: Informatics and Multiplexing of Intact Protein Identification in Bacteria and the Archaea. *Nat. Biotechnol.* **2001**, 19, 952.

CHAPTER 6. VALET PARKING FOR PROTEIN ION CHARGE STATE CONCENTRATION: ION/MOLECULE REACTIONS IN LINEAR ION TRAPS

6.1 Introduction

Electrospray ionization (ESI) is a soft ionization technique capable of generating large intact bio-ion and bio-ion complexes.^{1,2} As ESI generates ions directly from solution, it is readily coupled to liquid chromatography and is compatible with all commonly used mass analyzers due to its propensity for generating a distribution of multiply charged ions in a modest and relatively narrow mass-to-charge range. For these and other reasons, ESI has become widely used in bioanalytical mass spectrometry. While the multiplicity of charge states can be beneficial for accurate mass measurement and for generating a range of precursor ions to be subjected to various fragmentation techniques, there are several scenarios in which it is desirable to manipulate the precursor ion distribution. Such scenarios include the generation of charge states not directly formed under normal operating conditions, reduction in spectral complexity, the concentration of ion signal into a single charge state, or a combination of the latter two for increased sensitivity.

Changes in charge state distributions in an electrospray mass spectrum resulting from changes in solution conditions can be dramatic, particularly when the conformational states of the analytes are altered.³ However, precise control over charge states via alteration in solution conditions is generally limited. Both gas-phase ion/ion and gas-phase ion/molecule proton transfer reactions, on the other hand, can be used to precisely manipulate ion charge. These approaches are relatively mature in terms of their analytical utility. Some examples of early work involving gas-phase proton transfer reactions include, but are not limited to, the improved mass determination of protein ions,^{4,5} the determination of product ion charge,⁶⁻⁸ and charge state purification.^{9,10} In recent years, there has been an extension of proton transfer ion/ion reactions to higher resolution instruments,¹¹⁻¹⁴ due, in part, to an increase in the complexity of protein mixtures subjected to analysis and to an increase in the number of instruments equipped to perform such experiments. On the other hand, proton transfer ion/molecule reactions are less widespread in modern workflows. Rather, functional group specific reactions constitute the majority of recent literature in the field of analytical ion/molecule reactions.¹⁵⁻¹⁷ Nonetheless, proton transfer ion/molecule reactions are easy to implement across multiple instrument platforms as they require only the

controlled admission of a gaseous reagent into a reaction region. In most cases, this can be accomplished by tapping the existing bath gas line.

Previous work from our group involving ion/ion reactions has demonstrated that the kinetics, and the extent of reactant ion population overlap, can be affected to impede the progress of the reaction in a process referred to as “ion parking.”¹⁸ This is accomplished by the application of an auxiliary RF signal at the secular frequency of an ion/ion reaction product ion. Application of auxiliary RF serves to excite ions of a particular mass-to-charge ratio such that the velocity of the ions is increased and, consequently, the ion/ion capture cross section is decreased. Additionally, the excitation leads to a slight decrease in ion cloud overlap as one population of ions is excited away from the center of the trap while the other is retained in the center of the trap. This decrease in cross section and in ion cloud overlap is the basis for ion parking. In this approach, only a narrow band of m/z values are affected. Similarly, a broad range of frequencies can be applied to park a broad range of m/z values in “parallel ion parking.”^{19,20}

To our knowledge, there is no equivalent technique to mass selectively inhibit ion/molecule reactions. This report demonstrates the mass selective inhibition of ion/molecule reactions denoted, herein, as “valet parking.” Valet parking uses mass selective axial ejection, MSAE,²¹ to axially eject ion/molecule product ions, as they are formed, into a separate region of the mass spectrometer where no further ion/molecule reaction products are formed. Proof-of-concept data is presented for three model proteins, ubiquitin, cytochrome *c*, and myoglobin. Additionally, valet parking has been applied to a simple two component mixture of cytochrome *c* and myoglobin.

6.2 Experimental

6.2.1 Materials and Sample Preparation

Ubiquitin from bovine erythrocytes, cytochrome *c* from equine heart, and myoglobin from equine heart were purchased from Sigma-Aldrich (St. Louis, MO, USA). Trimethylamine was purchased from EMD Chemicals (Gibbstown, NJ, USA). HPLC-grade methanol and Optima LC/MS-grade water were purchased from Fisher Scientific (Fair Lawn, NJ, USA), and acetic acid was purchased from Mallinckrodt (Phillipsburg, NJ, USA). Protein stock solutions were prepared at a concentration of approximately 1 mg/mL. Stocks were diluted to a concentration of 1 μ M, 2 μ M, and 2 μ M for ubiquitin, cytochrome *c*, and myoglobin, respectively, in 49.5/49.5/1, by volume,

water/methanol/acetic acid. A simple protein mixture of 1 μ M cytochrome c and 1 μ M myoglobin was prepared in 49.5/49.5/1, by volume, water/methanol/acetic acid.

6.2.2 Mass Spectrometry

All experiments were performed on a modified QTRAP 4000 hybrid triple quadrupole/linear ion trap mass spectrometer (Sciex, Concord, ON, Canada). The ion path is depicted in Figure 6.1. The major components of the ion path relevant to valet parking include a QStar collision cell (q2) equipped with a LINAC (LN) followed by an RF/DC quadrupole array (Q3). The collision cell has an inscribed radius of 4.17 millimeters and is enclosed by IQ2 and IQ3. The RF used to drive q2 was transferred from the 816 kHz Q3 power supply through a capacitive coupling network at 58%.

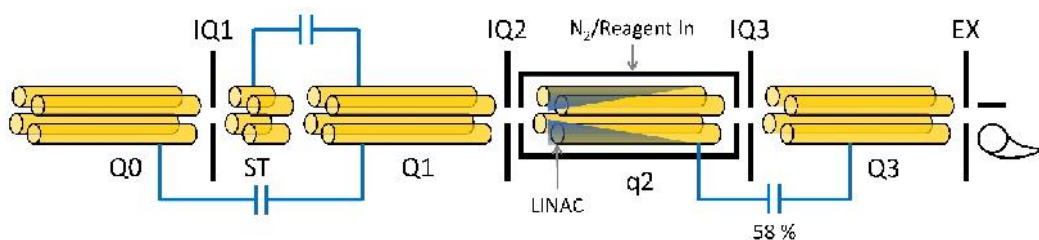


Figure 6.1. Ion optics and essential elements of the QTRAP 4000 ion path.

The bath gas supply line of q2 was modified ex-vacuo with an external reagent mixing manifold similar to those described by Gronert and Kenttämäa (Figure 6.2).^{22,23} The supply line was split using a tee connector with the mixing manifold on one side and a pure nitrogen gas supply on the other. To perform ion/molecule reactions, the needle valve of the pure nitrogen gas supply line was closed, and the needle valve of the manifold was opened. Initially, the variable leak valve (Granville-Phillips, Series 203, Boulder, CO, USA) was fully closed; the valve was slowly opened until the pressure in the main vacuum chamber was approximately 3.5×10^{-5} Torr, corresponding to a pressure of approximately 6.67 mTorr in q2. The neutral reagent (trimethylamine) was introduced into the nitrogen flow by opening the ultra-high precision leak valve (Kurt J. Lesker, VZLVM263R, Jefferson Hills, PA, USA). For all experiments, admittance of trimethylamine into q2 did not result in a change in the ion gauge reading, and, therefore, the exact concentration of trimethylamine is unknown. However, based on the sensitivity of the ion gauge, the concentration

of neutral reagent can be deduced as less than 0.3% of the total pressure. The instrument was allowed to equilibrate for approximately 20 minutes prior to data collection.

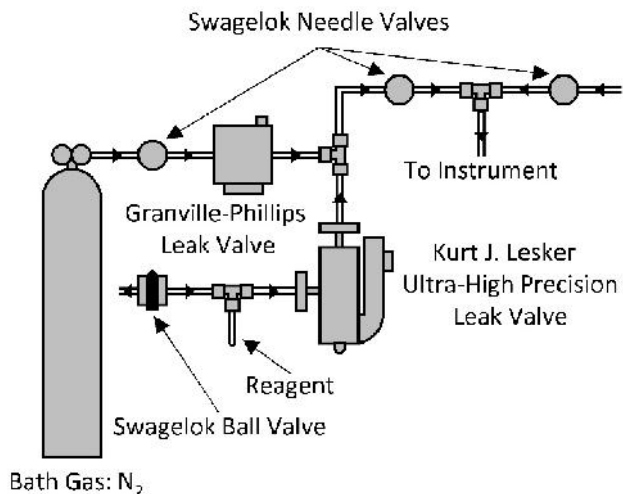


Figure 6.2. Schematic of the external manifold used to introduce reagent in q2 for ion/molecule reactions.

During valet parking experiments, q2 and Q3 were both operated as linear ion traps. Analyte cations were generated via electrospray ionization and injected into q2. During injection, the LINAC voltage was set to 20 V and the ions were trapped axially in q2 by DC barriers applied to IQ2 and IQ3. After injection, the DC voltage of IQ3 was lowered and ions were bunched in q2 near the fringing-field of IQ3 using a LINAC voltage of 200 V. The amplitude of the RF applied to Q3 was adjusted to place the desired ion/molecule product ion at $q = 0.4$ in q2. The ions were allowed to react with the neutral reagent for up to 900 ms, during which, an auxiliary sinusoidal waveform was applied to q2 in a dipolar fashion at $q = 0.4$ (calculated). The auxiliary waveform was generated using the buffered and amplified output of an Agilent 33220A waveform generator which was monitored using an oscilloscope (Tektronix, TDS 2014C, Beaverton, OR, USA). The frequency of the auxiliary waveform was tuned to be on resonance with the secular frequency of the desired ion/molecule product ion. After the reaction period, the auxiliary waveform was switched off and any product ions that were transferred into Q3 during valet parking were mass analyzed via MSAE. After detection, the voltages of the ion path were adjusted to eject the remaining ions in q2.

6.3 Results and Discussion

6.3.1 Valet Parking Premise and Theory

Unlike ion/ion reactions, where the reaction rates follow a v^{-3} dependence, the reaction rates for ion/molecule reactions under accessible conditions are not strongly dependent upon ion velocity. Therefore, ion/molecule reaction rates cannot be significantly affected by simply applying auxiliary RF to excite the product ion of interest. Rather, to halt ion/molecule reactions, product ions must be transferred from the reaction cell to a region of the instrument where no further reactive ion/molecule collisions occur. Here, the inhibition of ion/molecule reactions via the shuttling of a reaction product of interest to a location where no reactions occur is referred to here as “valet parking”. The premise for valet parking is the physical separation of product ions from the neutral reagent, which can be accomplished via MSAE.

With MSAE, ions can be axially ejected from a linear ion trap in a mass selective fashion as a consequence of the electric fields near the fringing region. In the fringing region, there is a diminishing quadrupolar potential where an ion’s radial motion is coupled to axial motion. Superposition of a repulsive DC potential of the endcap lens with the diminishing quadrupolar potential generates a cone of reflection.²¹ The cone of reflection is a conical shaped barrier that separates a region of reflection and a region of ejection (i.e. ions inside the cone are reflected back into the quadrupole while ions outside of the cone are axially ejected). In the absence of an auxiliary signal, ions will remain trapped. The ions, however, can be selectively excited on the basis of mass-to-charge.

The mass dependent frequencies of ion motion are described by the equations:

$$\omega_{n,u} = \frac{2n \pm u}{2} \omega_u \quad (6.1)$$

$$\omega_u \cong \sqrt{a_u + \frac{q_u^2}{2}} \quad (6.2)$$

where u represents the x - or y -dimension, n is an integer, ω_u is the angular frequency of the drive RF, and a and q parameters are the Mathieu dimensionless parameters given by:

$$a_u = \frac{C_1 e U}{m r_0^2 \omega^2} \quad (6.3)$$

$$q_u = \frac{C_2 e V}{m r_0^2 \omega^2} \quad (6.4)$$

where C1 and C2 are constants that vary depending on the operating mode of the ion trap, U is the amplitude of DC, V is the amplitude of RF used to trap the ions, r_o is the radius of the quadrupole array, m is the mass of the ion, and e is the charge of the ion. In the special case where n is equal to zero, we obtain the ion's fundamental frequency written as:

$$\omega_{0,u} = \frac{u}{2} \quad (6.5)$$

Equation 6.5 contains $\omega_{0,u}$, which, as shown in Equation 6.2 is dependent on a_u and q_u . As the cone of reflection is only present in the fringing regions, ions can be bunched into the fringing region using the LINAC. Application of auxiliary RF at the fundamental frequency increases the radial displacement of the desired product ion. Once the ion's radial displacement passes the cone of reflection barrier, the ion is axially ejected into Q3.

6.3.2 Demonstration of Valet Parking

For valet parking to effectively inhibit ion/molecule reactions, ions must be transferred to a region of the mass spectrometer where no further ion/molecule reaction occurs. Figure 6.3 establishes the fact that the number density of neutral reagent in Q3 is sufficiently low such that there is no observable ion/molecule reaction over an extended period. Electrospray ionization of ubiquitin prior to introduction of trimethylamine generates the mass spectrum shown in Figure 6.3a. The abundance weighted average charge state was calculated to be 10.48 and is shown in red. After a 400 ms reaction with trimethylamine in q2, the abundance weighted average charge states shifts to 5.58 (Figure 6.3b). Conversely, when the ubiquitin ions are injected through q2 and trapped in Q3 for 400 ms, the abundance weighted average charge state is identical to that of the pre ion/molecule reaction spectrum (Figure 6.3c).

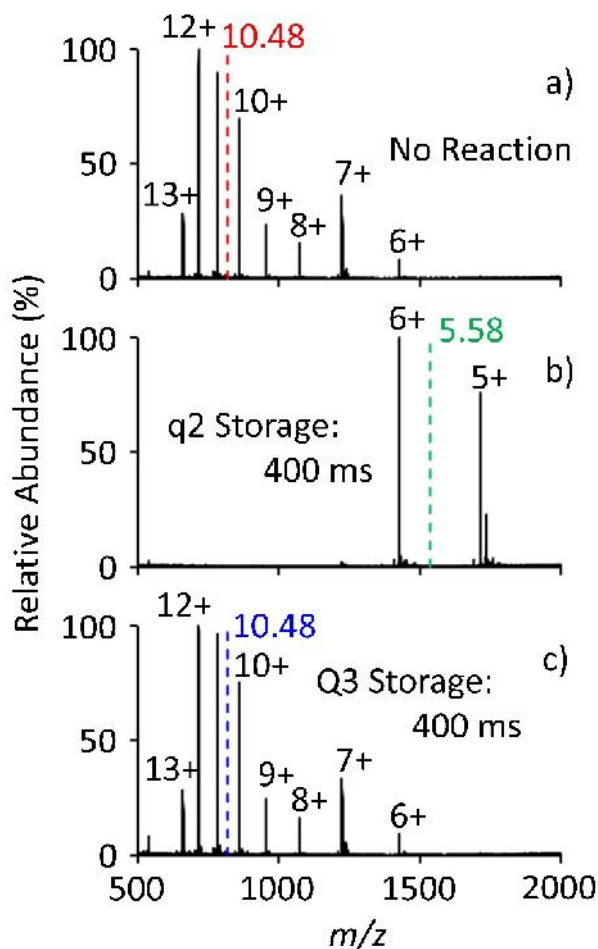


Figure 6.3. Positive electrospray mass spectrum of ubiquitin with a) no additional storage time in q2 or Q3, b) 400 ms storage in q2 (i.e. 400 ms ion/molecule reaction), and c) 400 ms storage in Q3 prior to mass analysis. The abundance weighted average charge state is represented with the colored dashed line.

Valet parking is first demonstrated using ubiquitin ions. Figure 6.4a shows the electrospray mass spectrum of ubiquitin under denaturing conditions. Here, ubiquitin ions were transmitted through q2, trapped and stored in Q3 for 900 ms, and subsequently mass analyzed. Akin to a normal electrospray mass spectrum with no neutral admitted into q2, the spectrum shows a bimodal distribution spanning the 13+ to the 6+ charge states (compare Figure 6.3a to Figure 6.4a). Figure 6.4b shows the mass spectrum after the ubiquitin cations were stored in q2, with trimethylamine, for 900 ms prior to being transferred to Q3 and subsequently mass analyzed. Under these conditions, the ubiquitin distribution shifts to lower charge states. The base peak in the post ion/molecule reaction spectrum is the 6+.

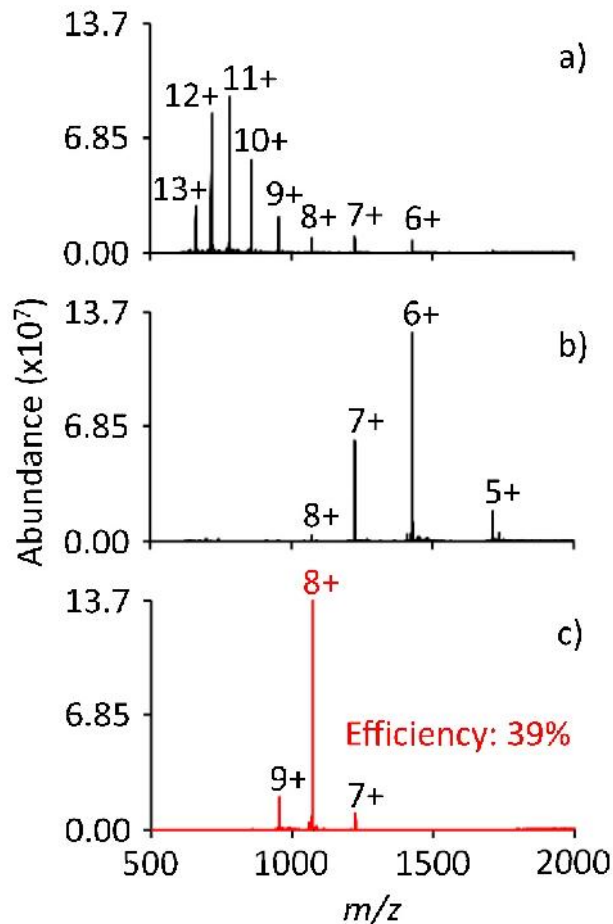


Figure 6.4. Positive electrospray mass spectrum of ubiquitin a) pre-ion/molecule reaction, b) post ion/molecule reaction, and c) valet parking of the 8+ charge state. The ion/molecule reaction time is 900 ms, the IQ3 barrier was set to 1.5 V, and a valet parking waveform of 1.9 V at 114.367 kHz was used.

Figure 6.4c displays the resulting mass spectrum after valet parking, where the reagent concentration and the ion/molecule reaction duration is identical to Figure 6.4b. In this experiment, however, the Q3 low mass cut off (LMCO) was set to m/z 876.5, which places the 8+ charge state of ubiquitin at approximately $q = 0.4$ in q_2 . Additionally, during the reaction period, a 1.9 V auxiliary signal was applied to q_2 at a frequency of 114.367 kHz. By applying a dipolar sine wave at a frequency corresponding to $q = 0.4$, and by judiciously lowering the IQ3 barrier to 1.5 V, any ions at $q = 0.4$ will be axially transferred from q_2 to Q3 as a consequence of their radial displacement in response to the auxiliary signal.

The progression of the ion/molecule proton transfer reaction is significantly affected in the valet parking experiment as evidenced by the abundance of 8+ ion in Figure 6.4c relative to that

depicted in Figure 6.4b. Transferring the 8+ ions to Q3 as they are formed halts the reactions and concentrates the ion signal into largely the 8+ charge state. In fact, when comparing the area of the parked 8+ to the area of the 8+ in the pre ion/molecule spectrum, there is a 16x increase in signal. Additionally, the efficiency of valet parking can be quantified as a percentage of the summed charge state area for all charge states prior to, and including, the 8+ from the pre ion/molecule spectrum. In the case of ubiquitin 8+, valet parking showed an efficiency of 39%. In other words, 39% of the signal preceding, and including ubiquitin 8+, in the pre ion/molecule spectrum was concentrated into ubiquitin 8+ during valet parking.

Valet parking was also successfully demonstrated with cytochrome *c* and myoglobin with efficiencies ranging from 27% to 32% (Figures 6.5 and 6.6, respectively). In the case of cytochrome *c*, separate valet parking experiments were performed on three charge states during a 900 ms ion/molecule reaction. The Q3 LMCO was set to m/z 843.8, 919.8, and 1011.4 to place cytochrome *c* 12+, 11+, and 10+, respectively, at $q = 0.4$. For parking, the IQ3 barrier was set to 1.8 V and a 1.8 V resonance excitation waveform at 114.367 kHz was applied to q2. Similarly, for myoglobin, valet parking was performed on the 16+, 15+, and 14+ charge states using an IQ3 barrier of 2.0 V and a 2.0 V sine wave at 114.367 kHz. In all cases, the progression of the ion/molecule reaction is largely inhibited in a mass selective fashion. There is, however, a small degree of undesired charge states that are also transferred to Q3 during valet parking that are likely due to limitations of the current apparatus, as discussed further below.

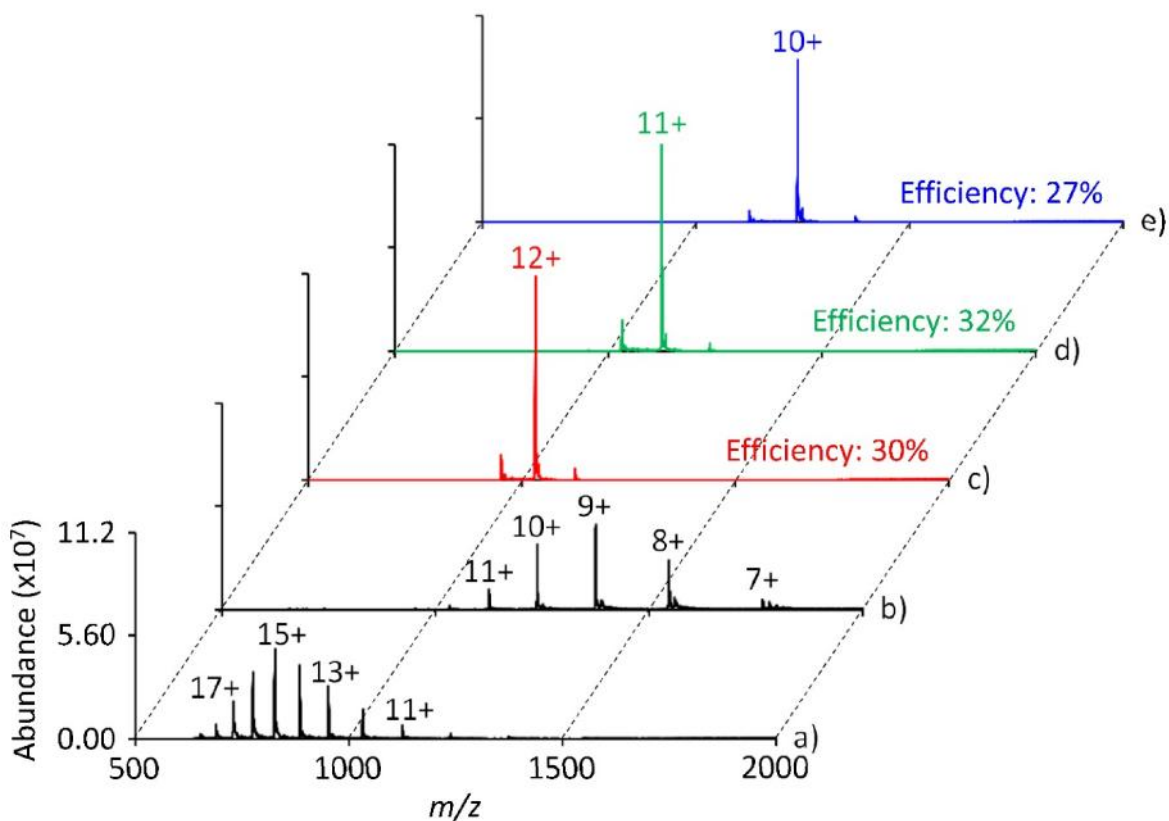


Figure 6.5. Positive electrospray mass spectrum of cytochrome c a) pre-ion/molecule reaction, b) post ion/molecule reaction, and valet parking of the c) 12+, d) 11+, or e) 10+ charge state. The ion/molecule reaction time is 900 ms, the IQ3 barrier was set to 1.8 V, and a valet parking waveform of 1.8 V at 114.367 kHz was used.

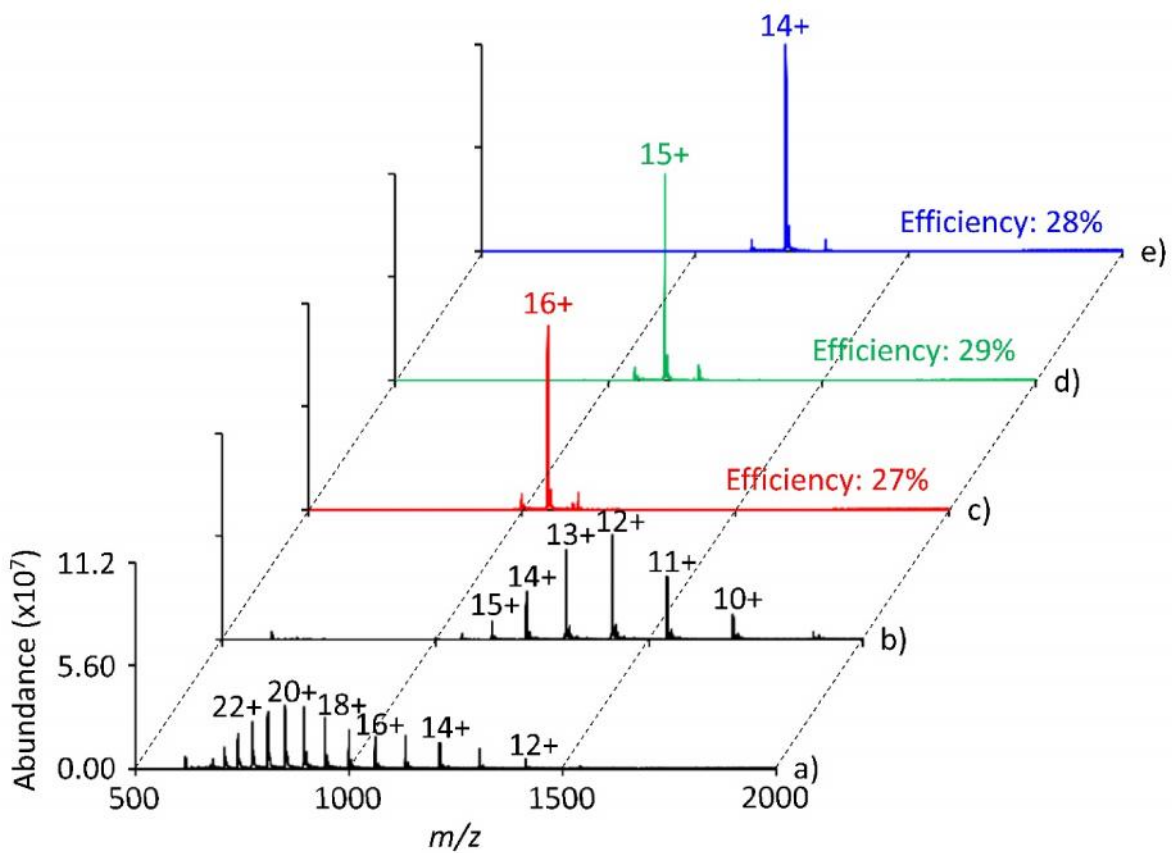


Figure 6.6. Positive electrospray mass spectrum of myoglobin a) pre-ion/molecule reaction, b) post ion/molecule reaction, and valet parking of the c) 16+, d) 15+, or e) 14+ charge state. The ion/molecule reaction time is 600 ms, the IQ3 barrier was set to 2.0 V, and a valet parking waveform of 2.0 V at 114.367 kHz was used.

6.3.3 Valet Parking of a Simple Mixture

The utility of using ion parking during ion/ion reactions has been demonstrated with applications that have included precursor ion charge state concentration,^{24,25} enhancements in selectivity during protein quantitation,²⁶ and gas-phase charge state purification.^{8,27} Similar applications for valet parking can be envisioned. Perhaps the simplest application of valet parking is the charge state purification of a simple two protein mixture. This scenario is demonstrated in Figure 6.7.

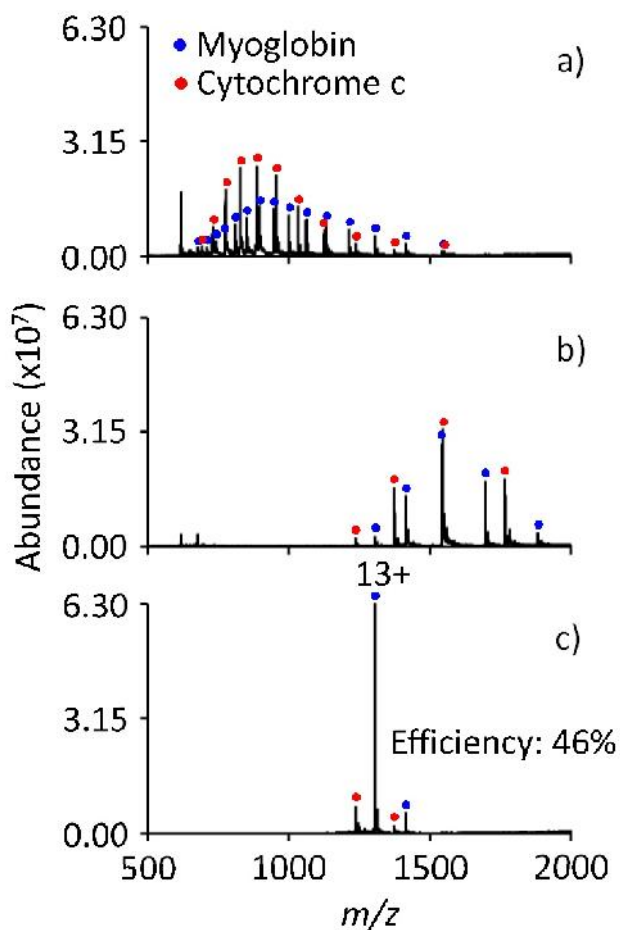


Figure 6.7. Positive electrospray mass spectrum of a cytochrome *c* and myoglobin mixture a) pre-ion/molecule reaction, b) post ion/molecule reaction, and c) valet parking of the myoglobin 13+ charge state. The ion/molecule reaction time is 900 ms, the IQ3 barrier was set to 2.0 V, and a valet parking waveform of 2.0 V at 114.367 kHz was used.

Figure 6.7a shows the electrospray mass spectrum from a mixture of ions derived from cytochrome *c* and myoglobin. There are several cases where cytochrome *c* and myoglobin ions are

close in m/z . For example, the most abundant charge state of myoglobin, $[M + 19H]^{19+}$, is only 2 units higher in nominal m/z than a sodium adducted cytochrome c ion at m/z 892. A 900 ms ion/molecule reaction results in the spectrum shown in Figure 6.7b. Here, the majority of charge states are well resolved. A valet parking experiment allows for the concentration of one protein component while discriminating against the other component as demonstrated in the comparison of Figures 6.7b and 6.7c. Figure 6.7c shows the post ion/molecule reaction spectrum using the same conditions as Figure 6.7b except a valet parking waveform (114.367 kHz, 2.0 V) was used to park myoglobin 13+. Much of the myoglobin population is concentrated into the 13+, showing an efficiency of 46% while most of the cytochrome c ions remain in q_2 for subsequent removal.

6.3.4 Potential Improvements

As mentioned above, during valet parking in this work, some undesired charge states are also admitted into Q3. Additionally, less than half of the potential signal is actually concentrated. While the degrees of selectivity and concentration can be maximized, to some extent, by tuning the IQ3 barrier and auxiliary waveform parameters (i.e. amplitude and frequency), these figures of merit are largely limited by the q -value at which valet parking is performed. With the current setup, q_2 is capacitively coupled to Q3 at 58%, which limits the q -value in q_2 to $q = 0.4$ before the mass of the desired ion becomes lower in m/z than the Q3 LMCO. For example, a Q3 LMCO of m/z 843.2 is needed to place the 12+ charge state of cytochrome c (m/z 1031) at $q = 0.4$ in q_2 while a Q3 LMCO of m/z 1054.0 is needed to place the same ion at $q = 0.5$ in q_2 . It is clear that if valet parking were performed at $q = 0.5$ the desired ion would be transferred to but not trapped in Q3 on the basis of m/z .

Londry and Hager have demonstrated that the sensitivity and resolution of MSAE increases as a function of q -value.^{21,28,29} The increase in ion signal (i.e. sensitivity) is due to the changes in the shape of the cone of reflection; at higher q -values, the cone of reflection penetrates further into the quadrupole and, consequently, increases the volume in which axial ejection can occur. Therefore, it is expected that if q_2 and Q3 were decoupled, valet parking could be performed at a higher q -value with greater efficiency resulting in higher percentages of concentration.

Increasing the q -value for MSAE is also expected to improve the valet parking selectivity. Figure 6.8 shows the calculated secular frequency dispersion between three consecutive charge states of cytochrome c . When cytochrome c 12+ is placed at $q = 0.4$, there is a 10.74 kHz difference

between the 13+ and 12+ ions and a 10.50 kHz difference between the 12+ and 11+ ions. Yet, when cytochrome *c* 12+ is placed at $q = 0.8$, there is a 48.72 kHz difference between the 13+ and 12+ ions and a 35.47 kHz difference between the 12+ and 11+ ions. Additionally, since ions at higher q require less radial displacement to overcome the repulsive barrier of the cone of reflection, lower amplitude waveforms can be used for resonance excitation leading to less off-resonance power absorption by ions of nearby m/z . When combining the increased frequency spacing between consecutive charges states with the ability to use lower amplitude auxiliary signals, the resolution of the MSAE, and hence the selectivity of valet parking, should increase. Further improvements to valet parking may be accomplished with phase synchronous RF applied to IQ3.³⁰

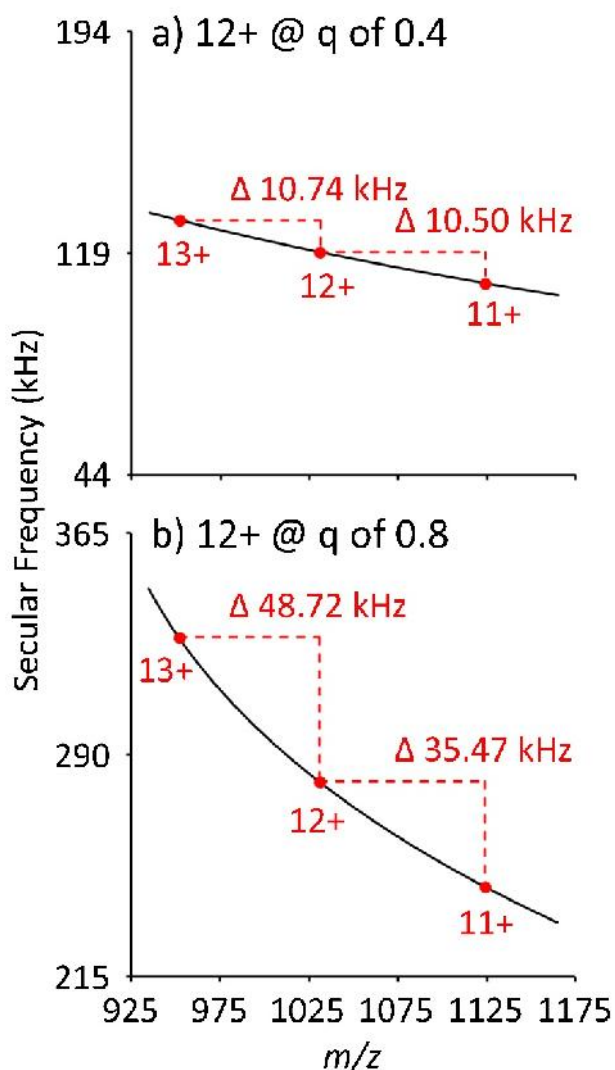


Figure 6.8. Calculated ion frequencies and ion frequency dispersion for consecutive charge states of cytochrome *c* when cytochrome *c* 12+ is placed at a) $q = 0.4$ and b) $q = 0.8$.

6.4 Conclusions

Proof-of-concept data is presented for protein ion charge state concentration via ion/molecule reactions. Ions of a selected mass-to-charge ratio are transferred from the reaction cell to a region of the mass spectrometer where no ion/molecule reaction is observed. We have demonstrated valet parking on a hybrid triple quadrupole/linear ion trap mass spectrometer using MSAE, yet one could envision the technique to be implemented on other ion trapping instruments with consecutive trapping regions. For instance, valet parking could be implemented using a 3D ion trap using resonance ejection, provided that ions could be transferred and trapped in another trapping device. Additionally, valet parking could be coupled to higher resolution mass analysis techniques. Valet parking efficiencies up to 46% were demonstrated here, though the RF coupling between quadrupoles in the platform used here limited performance. The gas-phase purification and concentration of a simple protein mixture demonstrates one application of valet parking. Implementation of valet parking is attractive for several applications and offers a means to impede ion/molecule reaction progression in a mass selective fashion.

6.5 References

1. Wilm, M.: Principles of Electrospray Ionization. *Mol. Cell. Proteom.* **2011**, 10, M111.009407.
2. Banerjee, S., Mazumdar, S.: Electrospray Ionization Mass Spectrometry: A Technique to Access the Information beyond the Molecular Weight of the Analyte. *Int. J. Anal. Chem.* **2012**, Article ID 282574.
3. Ogorzalek Loo, R.R., Lakshmanan, R., Loo, J.A.: What Protein Charging (and Supercharging) Reveal about the Mechanism of Electrospray. *J. Am. Soc. Mass Spectrom.* **2014**, 25, 1675-1693.
4. McLuckey, S.A., Goeringer, D.E.: Ion/Molecule Reactions for Improved Effective Mass Resolution in Electrospray Mass Spectrometry. *Anal. Chem.* **1995**, 67, 2493-2497.
5. Stephenson Jr, J.L., McLuckey, S.A.: Charge Manipulation for Improved Mass Determination of High-Mass Species and Mixture Components by Electrospray Mass Spectrometry. *J. Mass Spectrom.* **1998**, 33, 664-672.
6. McLuckey, S.A., Glish, G.L., Van Berkel, G.J.: Charge Determination of Product Ions Formed from Collision-Induced Dissociation of Multiply Protonated Molecules via Ion/Molecule Reactions. *Anal. Chem.* **1991**, 63, 1971-1978.

7. Herron, W.J., Goeringer, D.E., McLuckey, S.A.: Product Ion Charge State Determination via Ion/Ion Proton Transfer Reactions. *Anal. Chem.* **1996**, 68, 257-262.
8. Coon, J.J., Ueberheide, B., Syka, J.E.P., Dryhurst, D.D., Ausio, J., Shabanowitz, J., Hunt, D.F.: Protein Identification using Sequential Ion/Ion Reactions and Tandem Mass Spectrometry. *Proc. Natl. Acad. Sci. U.S.A.* **2005**, 102, 9463 (2005)
9. Reid, G.E., Shang, H., Hogan, J.M., Lee, G.U., McLuckey, S.A.: Gas-Phase Concentration, Purification, and Identification of Whole Proteins from Complex Mixtures. *J. Am. Chem. Soc.* **2002**, 124, 7353-7362.
10. He, M., Reid, G.E., Shang, H., Lee, G.U., McLuckey, S.A.: Dissociation of Multiple Protein Ion Charge States Following a Single Gas-Phase Purification and Concentration Procedure. *Anal. Chem.* **2002**, 74, 4653-4661.
11. Wenger, C.D., Lee, M.V., Hebert, A.S., McAlister, G.C., Phanstiel, D.H., Westphall, M.S., Coon, J.J.: Gas-Phase Purification Enables Accurate, Multiplexed Proteome Quantification with Isobaric Tagging. *Nature Methods.* **2011**, 8, 933-935.
12. Anderson, L.C., English, A.M., Wang, W.-H., Bai, D.L., Shabanowitz, J., Hunt, D.F.: Protein Derivatization and Sequential Ion/Ion Reactions to Enhance Sequence Coverage Produced by Electron Transfer Dissociation Mass Spectrometry. *Int. J. Mass Spectrom.* **2015**, 377, 617-624.
13. Huguet, R., Mullen, C., Szrenti, K., Greer, J.B., Fellers, R.T., Zabrouskov, V., Syka, J.E.P., Kelleher, N.L., Fornelli, L.: Proton Transfer Charge Reduction Enables High-Throughput Top-Down Analysis of Large Proteoforms. *Anal. Chem.* **2019**, 91, 15732-15739.
14. Sanders, J.D., Mullen, C., Watts, E., Holden, D.D., Syka, J.E.P., Schwartz, J.C., Brodbelt, J.S.: Enhanced Sequence Coverage of Large Proteins by Combining Ultraviolet Photodissociation with Proton Transfer Reactions. *Anal. Chem.* **2020**, 92, 1041-1049.
15. Osburn, S., Ryzhov, V.: Ion-Molecule Reactions: Analytical and Structural Tool. *Anal. Chem.* **2013**, 85, 769-778.
16. Kong, J.Y., Hilger, R.T., Jin, C., Yerabolu, R., Zimmerman, J.R., Replogle, R.W., Jarrell, T.M., Easterling, L., Kumar, R., Kenttämä, H.I.: Integration of a Multichannel Pulsed-Valve Inlet System to a Linear Quadrupole Ion Trap Mass Spectrometer for the Rapid Consecutive Introduction of Nine Reagents for Diagnostic Ion/Molecule Reactions. *Anal. Chem.* **2019**, 91, 15652-15660.
17. Poad, B.L.J., Marshall, D.L., Harazim, E., Gupta, R., Narreddula, V.R., Young, R.S.E., Duchoslav, E., Campbell, J.L., Broadbent, J.A., Cvačka, J., Mitchell, T.W., Blanksby, S.J.: Combining Charge-Switch Derivatization with Ozone-Induced Dissociation for Fatty Acid Analysis. *J. Am. Soc. Mass. Spectrom.* **2019**, 30, 2135-2143.

18. McLuckey, S.A., Reid, G.E., Wells, J.M.: Ion Parking during Ion/Ion Reactions in Electrodynamic Ion Traps. *Anal. Chem.* **2002**, 74, 336-346.
19. Chrisman, P.A., Pitteri, S.J., McLuckey, S.A.: Parallel Ion Parking: Improving Conversion of Parents to First-Generation Products in Electron Transfer Dissociation. *Anal. Chem.* **2005**, 77, 3411-3414.
20. Chrisman, P.A., Pitteri, S.J., McLuckey, S.A.: Parallel Ion Parking of Protein Mixtures. *Anal. Chem.* **2006**, 78, 310-316.
21. Londry, F.A., Hager, J.W.: Mass Selective Axial Ion Ejection from a Linear Quadrupole Ion Trap. *J. Am. Soc. Mass. Spectrom.* **2003**, 14, 1130-1147.
22. Gronert, S.: Estimation of Effective Ion Temperatures in a Quadrupole Ion Trap. *J. Am. Soc. Mass. Spectrom.* **1998**, 9, 845-848.
23. Habicht, S.C., Vinueza, N.R., Archibold, E.F., Duan, P., Kenttämäa, H.I.: Identification of the Carboxylic Acid Functionality by Using Electrospray Ionization and Ion-Molecule Reactions in a Modified Linear Quadrupole Ion Trap Mass Spectrometer. *Anal. Chem.* **2008**, 80, 3416-3421.
24. Foreman, D.J., Dziekonski, E.T., McLuckey, S.A.: Maximizing Selective Cleavages at Aspartic Acid and Proline Residues for the Identification of Intact Proteins. *J. Am. Soc. Mass. Spectrom.* **2019**, 30, 34-44.
25. Holden, D.D., McGee, W.M., Brodbelt, J.S.: Integration of Ultraviolet Photodissociation with Proton Transfer Reactions and Ion Parking for Analysis of Intact Proteins. *Anal. Chem.* **2016**, 88, 1008-1016.
26. Campbell, J.L., Le Blanc, J.C.Y.: Targeted Ion Parking for the Quantitation of Biotherapeutic Proteins: Concepts and Preliminary Data. *J. Am. Soc. Mass. Spectrom.* **2010**, 21, 2011-2022.
27. Anderson, L.C., Karch, K.R., Ugrin, S.A., Coradin, M., English, A.M., Sidoli, S., Shabanowitz, J., Garcia, B.A., Hunt, D.F.: Analyses of Histone Proteoforms Using Front-end Electron Transfer Dissociation-enabled Orbitrap Instruments. *Mol. Cell. Proteom.* **2016**, 15, 975-988.
28. Hager, J.W.: A New Linear Ion Trap Mass Spectrometer. *Rapid Commun. Mass Spectrom.* **2002**, 16, 512-526.
29. Hager, J.W.: Linear Ion Trap Mass Spectrometry with Mass-Selective Axial Ejection. In *Practical Aspects of Trapped Ion Mass Spectrometry Volume IV Theory and Instrumentation*; March, R.E.; Todd, J.F.J. Eds. CRC Press, Boca Raton, 2010.

30. Guna, M., Biesenthal, T.A.: Performance Enhancements of Mass Selective Axial Ejection from a Linear Ion Trap. *J. Am. Soc. Mass. Spectrom.* **2009**, 20, 1132-1140.

VITA

David John Foreman was born on August 13, 1989 in Malden, MA and is the youngest of John and Maire Foreman's two children. After graduating from Malden Catholic in 2007, he enrolled at Merrimack College. In his freshman year, David was awarded the McGravey-Werman Scholarship Award, a faculty nominated award given to a student for outstanding laboratory work in analytical chemistry. Beginning in the spring of his junior year, David began his undergraduate research in the area of sustainable organic chemistry utilizing microwave reaction vessels. Following his junior year, he spent the summer as a process chemistry intern at ArQule, Inc. During David's time at Merrimack, he played rugby for four years, serving as the captain during his senior season, and was a resident assistant for three years. David graduated from Merrimack College in 2011 and spent four years working in the pharmaceutical industry prior to beginning his graduate studies at Purdue University in 2015. In November of 2015, he joined the research group of Dr. Scott A McLuckey, where his research was primarily focused on introducing selective dissociation channels into bio-ions following gas-phase ion/ion reactions. David was awarded the W. Brooks Fortune Analytical Chemistry Fellowship in 2016 and the American Society for Mass Spectrometry Fall Workshop Student Stipend Award in 2017. He defended his Ph.D. in February of 2020.

PUBLICATIONS

1. Foreman, D.J.; McLuckey, S.A.: Recent Developments in Gas-Phase Ion/Ion Reactions for Analytical Mass Spectrometry. *Anal. Chem.* **2020**, 92, 252-266.
2. Foreman, D.J.; Parsley, N.C.; Lawler, J.T.; Aryal, U.K.; Hicks, L.M.; McLuckey, S.A.: Gas-Phase Sequencing of Cyclotides: Introduction of Selective Ring Opening at Dehydroalanine via Ion/Ion Reaction. *Anal. Chem.* **2019**, 91, 15608-15616.
3. Foreman, D.J.; Lawler, J.T.; Niedrauer, M.L.; Hostetler, M.A.; McLuckey, S.A.: Gold (I) Cationization Promotes Ring Opening in Lysine-Containing Cyclic Peptides. *J. Am. Soc. Mass Spectrom.* **2019**, 30, 1914-1922.
4. Randolph, C.E.; Foreman, D.J.; Blanksby, S.J.; McLuckey, S.A.: Generating Fatty Acid Profiles in the Gas Phase: Fatty Acid Identification and Relative Quantitation Using Ion/Ion Charge Inversion Chemistry. *Anal. Chem.* **2019**, 91, 9032-9040.
5. Foreman, D.J.; Dziekonski, E.T.; McLuckey, S.A.: Maximizing Selective Cleavages at Aspartic Acid and Proline Residues for the Identification of Intact Proteins. *J. Am. Soc. Mass Spectrom.* **2019**, 30, 34-44.
6. Randolph, C.E.; Foreman, D.J.; Betancourt, S.K.; Blanksby, S.J.; McLuckey, S.A.: Gas-Phase Ion/Ion Reactions Involving Tris-Phenanthroline Alkaline Earth Metal Complexes as Charge Inversion Reagents for the Identification of Fatty Acids. *Anal. Chem.* **2018**, 90, 12861-12869.
7. Foreman, D.J.; Betancourt, S.K.; Pilo, A.L.; McLuckey, S.A.: Novel Peptide Ion Chemistry Associated with Gold(I) Cationization: Preferential Cleavage at Lysine Residues. *Int. J. Mass Spectrom.* **2018**, 427, 114-122.
8. Munshi, M.U.; Craig, S.M.; Berden, G.; Martens, J.; DeBlase, A.F.; Foreman, D.J.; McLuckey, S.A.; Oomens, J.; Johnson, M.A.: Preparation of Labile Ni⁺(cyclam) Cations in the Gas Phase Using Electron Transfer Reduction Through Ion-Ion Recombination in an Ion Trap and Structural Characterization with Vibrational Spectroscopy. *J. Phys. Chem. Lett.* **2017**, 8, 20, 5047-5052.